INVESTIGATIONS ON MULTI-LEVEL INVERTER FED PERMANENT MAGNET SYNCHRONOUS MOTOR DRIVE

Ph.D. THESIS

by

SUKANTA HALDER

DEPARTMENT OF ELECTRICAL ENGINEERING
INDIAN INSTITUTE OF TECHNOLOGY ROORKEE
ROORKEE – 247667 (INDIA)
JUNE, 2017

INVESTIGATIONS ON MULTI-LEVEL INVERTER FED PERMANENT MAGNET SYNCHRONOUS MOTOR DRIVE

A THESIS

Submitted in partial fulfilment of the requirements for the award of the degree

of

DOCTOR OF PHILOSOPHY

in

ELECTRICAL ENGINEERING

by

SUKANTA HALDER

DEPARTMENT OF ELECTRICAL ENGINEERING
INDIAN INSTITUTE OF TECHNOLOGY ROORKEE
ROORKEE – 247667 (INDIA)
JUNE, 2017

INDIAN INSTITUTE OF TECHNOLOGY ROORKEE
ROORKEE

CANDIDATE'S DECLARATION

I hereby certify that the work which is being presented in this thesis entitled "**INVESTIGATIONS ON MULTI-LEVEL INVERTER FED PERMANENT MAGNET SYNCHRONOUS MOTOR DRIVE**" in partial fulfilment of the requirements for the award of the Degree of Doctor of Philosophy and submitted in the Department of Electrical Engineering of Indian Institute of Technology Roorkee, Roorkee is an authentic record of my own work carried out during a period from December, 2011 to June, 2017 under the supervision of Dr. Pramod Agarwal, Professor and Dr. S.P.Srivastava, Professor, Department of Electrical Engineering, Indian Institute of Technology Roorkee, Roorkee.

The matter presented in this thesis has not been submitted by me for the award of any other degree of this or any other Institute.

(SUKANTA HALDER)

This is to certify that the above statement made by the candidate is correct to the best of our knowledge.

(Pramod Agarwal)
Supervisor

(S.P.Srivastava)
Supervisor

Dated: _____

The Ph.D. Viva-Voce Examination of Mr. Sukanta Halder, Research Scholar, has been held on ……

Chairman, SRC

Signature of External Examiner

This is to certify that the student has made all the correction in the thesis.

Signature of Supervisor(s)

Head of the Department

ABSTRACT

Electric motors are the prime mover of the growing industries. Motion control with electric drives is always a challenge for researchers and technologists. According to the technological progress adjustable speed drives are preferred over constant speed drives because of several reasons like energy saving, velocity or position control for good transient response etc. DC motors have been used widely in variable speed drive systems for many decades. On the other hand, due to some of the disadvantages, like recurrent maintenance, increased cost due to commutators and brush, motivated researchers to develop AC motors. Although Induction Motors (IM) have been widely used and considered as a workhorse in the industry but slip power loss and lagging power factor limits the use of induction motor drives. Synchronous motor attracts researcher to overcome these limitations. However, the conventional wire wound synchronous motors suffers from necessity of extra power supply for field excitation. To meet the increasing application demand of adjustable speed drive researchers and technologist have been persistent in their efforts to develop new machines like Brushless DC (BLDC) motor, Switched Reluctance Motor (SRM), and Permanent Magnet Synchronous Motor (PMSM). With the advancement of permanent magnet material PMSM becomes the most promising and fastest growing machine for variable speed drive.

Permanent magnet synchronous motors gained wide spread popularity and acceptance in adjustable speed drive due to its interesting characteristics like high efficiency, high air gap flux density, high torque-to-inertia ratio, high power density, high acceleration and deceleration rates, lower maintenance cost, simplicity and ruggedness. In a PMSM the excitation is provided by the permanent magnets on rotor which eliminates the external excitation requirements. The elimination of excitation winding reduces the cost and power loss. Compared to DC motor PMSM has some advantages, which includes compact size, less maintenance, longer life. On the other hand it also has some advantages over induction motor in terms of high efficiency, small size and wide range of power factor.

The rapid development of power electronic devices and converter topology in the last few decades has made possible to develop energy efficient adjustable speed PMSM drive. In industrial drives, two-level inverters are mostly used to fed the PMSM due to their simple structure, control, reliability as well as cheaper parts. However, in case of two-level inverter, the switching frequency is one of the main concerns regarding to the size of passive

components, superior control of electric drives and to proliferation power density of inverter. Higher switching frequencies operation reduces the size of the passive components. On contradictory, the higher switching frequencies may lead to have higher switching losses, which cause inferior inverter efficiency. Compare to two-level inverter, Multi-Level Inverter (MLI) produce lower switching losses at higher switching frequencies to get the same dc-link voltage. The other attracting feature is reduction in total harmonic distortion. Lower dv/dt also reduces the voltage stress across the power switches. To increase the fundamental output voltage and corresponding power level of the inverter, the DC link voltage also need to be increased substantially. However, high frequency semiconductors have a limitation in the maximum voltage and very high voltage jump will lead to terrible electromagnetic interference and high windings insulation stress. So for the high performance of AC drive systems at increased power level, high quality inverter output with low harmonic loss and generating low torque fluctuation is necessary. The significant reduction in the torque ripple is achieved with use of three-level inverter. Multi-level topology provides some additional benefits compared to conventional two-level inverter which includes superior harmonic spectrums for a given gate switching frequency, a lower over voltage stress at cables and end windings of motors, a lower common-mode voltage, and substantially lower semiconductor switching losses. Satisfying the application demand, PMSM bring the keen attention of the researchers and technologist. The combination of MLI and PMSM allow to operate at increase dc bus voltage. Multi-level inverter is an emerging technology used in efficient permanent magnet synchronous motor drive system with low harmonic distortion, low torque fluctuations and avoid the limitations of two-level Voltage Source Inverter. To drive the machine, multi-level inverter becomes the most preferred choice replacing the conventional two-level VSI.

The vector controlled PMSM drives brought renaissance in the variable speed drives, replacing the traditional scalar-controlled drives. In order to overcome the inherent coupling effect and the sluggish response of scalar control and to achieve the high performance, the vector control is employed. To implement the vector control the accurate position sensing is required. The rotor position information is usually obtained by encoders or resolvers attached to rotor shaft. However, the use of these position sensors reduces the noise immunity, and increase the size, cost and weight of the system. Elimination of these position sensors is highly encouraged to increase the reliability and robustness and also reduce the cost of drive.

The present work is carried out to improve the performance of PMSM drive. The drive mainly consists of four major components, PMSM, inverter, position sensor and a controller. An

extensive literature review is carried out which starts with the basic motor modelling and covers speed control in vector controlled drive, possible inverters and control techniques, and different sensorless control of the PMSM drive. Extensive efforts have been made by researchers to meet the challenges associated with PMSM drive. However, software based position sensing approach from the resolver without using Resolver to Digital Converter (RDC), attract attention to reduce the cost of the drive. Vector-control of resolver based RDC less PMSM drive fed by two-level VSI is taken as the investigative objective initially. Then problems associated with conventional two-level voltage source PWM (Pulse Width Modulation) inverter fed PMSM drive is addressed. Their possible solution and recent trends attract further attention to improve the performance of the drive system using MLI topology. Sensorless control motivates to reduce the hardware complexity, increase the mechanical robustness and reliability and also reduce the maintenance requirements.

The design of an accurate control system requires the mathematical model of actual system being controlled. In this thesis, complete mathematical model of the PMSM drive is developed in MATLAB/Simulink environment. PMSM, inverters, position sensor and controller are the four main constituents of the drive model. A Mathematical model of PMSM with saliency and without saliency in synchronously rotating reference frame is developed. This model consists of dynamic equations of PMSM in terms of the actual parameters and load performance. The equation relating to switching states of the two-level inverter devices with the d-axis and q-axis voltage of the PMSM are derived. The initial step to implement the different control strategies is to simulate the system and to find out the response of the system. To obtain a closed loop operation of PMSM drive mathematical model of resolver sensor, speed controller and load are also developed.

The basic idea of the vector control algorithm is to decompose a stator current into a magnetic field-producing component and a torque-producing component. After decomposition both components can be separately controlled like dc machine. The vector control scheme is developed for PMSM drive in MATLAB/ Simulink environment. Implementation of vector control needs accurate position and speed estimation. In usual practice Resolver to Digital Converter (RDC) are used for position and speed estimation from resolver. But a software based position estimation using the output signal of the resolver has been implemented to eliminate the RDC, which reduce the cost of the drive. In addition, a demodulation based algorithm is implemented to calculate the speed and rotor position. Depending on the placement of the permanent magnet PMSM can be categories as Interior Permanent Magnet Synchronous Motor (IPMSM) and Surface Permanent Magnet Motor (SPMSM). Extensive

simulation study is carried out in MATLAB/ Simulink environment to investigate both type of PMSM. Vector control in terms zero d-axis current control and Maximum Torque Per Ampere (MTPA) control is investigated in IPMSM. A comparative analysis also has been presented for both the control techniques. Further to achieve the wide speed range of operation, a MTPA based flux-weakening control algorithm is developed for IPMSM drive. SPMSM drive with zero d-axis current control and its performance is investigated. Simulation study is carried out in MATLAB/ Simulink environment. The effects of load variation and speed change on the performance of drive are extensively studied.

To achieve the high performance of PMSM drive systems at increased power levels the multi-level inverter fed drive is considered. The analytical model of the multilevel inverter is presented. Mathematical models are based on the determination of state equations for dynamic variables. These models are conspicuous by their extreme simplicity in front of other previous analytical models presented in the literature. Cost effective RDC less software based position estimation is implemented for proposed PMSM drive. A detailed study on Neutral Point Clamped (NPC) three-level inverter fed PMSM drive with vector control is presented. But the disadvantage with this inverter is capacitor voltage balancing. To maintain the voltage across the capacitor, a capacitor voltage balancing technique using Three-Level Boost Converter (TLBC) is developed for the proposed drive. The additional advantage of this balancing circuit as compared to the other carrier based PWM technique or SVM technique is the boosting feature, which is most demanding now a day for the electric vehicle application. This proposed MLI fed PMSM drive reduces the voltage THD and torque pulsation. Moreover, performance of the proposed balancing scheme is examined by carrying out extensive simulations studies on a surface-mounted permanent magnet synchronous machine with vector control in terms of zero d-axis current control. The exhaustive simulation study is carried out in MATLAB/ Simulink environment for the proposed drive system. The comparative study between a conventional two-level PMSM drive and proposed drive is also presented. The enhanced performance is achieved with the proposed drive.

Furthermore the proposed drive is also investigated for sensorless control operation. Sensorless controls in terms back-EMF based position estimation and Model Reference Adaptive System (MRAS) based estimation have been implemented. Back-EMF based estimation of rotor speed and angular position ensure accurate speed regulation. This method is satisfactory at medium and high-speed. Among the existing sensorless approaches adaptive control seems to be the most promising. The MRAS based estimators provide the desired state from two different models, one is reference and the other one is adjustable. The MRAS is

simple and easier to implement. Exhaustive simulation is carried out using MATLAB/ Simulink and the performance results are obtained under different operating condition to verify the effectiveness and feasibility of the MRAS based estimator in proposed PMSM drive system.

In order to validate the simulation, the following prototypes have been developed in the laboratory and experimentation is performed: (i)two-level VSI fed PMSM drive system, (ii) three-level NPC inverter fed PMSM drive system and (iii) capacitor voltage balancing circuit with three-level boost converter. The different hardware component as required for the proper operation of experimental set up such as driver circuit, isolation and dead band circuit, dc power supply, voltage and current sensor circuits designed, developed and interfaced with dSPACE controller. A DSP DS1104 of dSPACE has been used for the real-time implementation of control algorithms of two different inverters topology in MATLAB/ Simulink environment. Extensive experimentation has been carried out to investigate the performance of the drive.

Software based RDC less position estimation is implemented using the resolver based position estimation algorithm to estimate the accurate speed and position. The experimental results show the complete 360^{o} rotation of the drive. The accurate position and speed estimation is achieved. In the second part of the experimental work, a two-level inverter fed PMSM drive system is tested in different operating conditions. The vector control in terms of zero d-axis current control is implemented. Further experimentation is carried out in three-level NPC inverter fed PMSM drive. To maintain the voltage across the two dc-link capacitors in three-level NPC inverter a TLBC circuit is used. The exhaustive experimentation is carried out on the proposed drive in different operating condition. The experimental results show the validity and effectiveness of the proposed drive in accordance with the simulation results. A comparative analysis is made between two-level inverter and three-level NPC inverter fed PMSM drive. Further, the experimentation is also carried out in sensorless control mode with three-level NPC inverter fed drive. The MRAS based estimation is implemented and the results show the validity of the drive under different operating conditions.

ACKNOWLEDGEMENTS

With GOD's grace I have got this opportunity to thanks all those who have supported me all through this course of work. First and foremost, I would like to express my deepest sense of gratitude towards my supervisors Dr. Pramod Agarwal, Professor, Department of Electrical Engineering and Dr. S.P.Srivastava, Professor, Department of Electrical Engineering of Indian Institute of Technology Roorkee, Roorkee, for their patience, inspiring guidance, constant encouragement, moral support, and keen interest in minute details of the work. I am sincerely indebted to them for their pronounced individuality, humanistic and warm personal approach, and excellent facility provided to me in the laboratory to carry out this research.

I also express my sincere gratitude towards my research committee members Dr. G.K.Singh (Professor EED & Chairmen SRC), Dr. M.K. Pathak, (Associate Professor, EED) Dr. R.P.Saini, (Professor, Department of AHEC) for their invaluable direction, encouragement and support, and above all the noblest treatment extended by them during the course of my studies at IIT Roorkee.

I heartily extend my gratitude to Head of the Department of Electrical Engineering, and all faculty members of the department for their help, moral support, and providing the excellent infrastructure, laboratory and computing facility for the research work.

My heartfelt thanks to Dr. Chandan Chakraborty (Professor, EED, IIT KGP) Dr. K. Gopakumar (Professor, CEDT, IISC Bangalore), Dr. Bhim Singh (Professor, EED, IITD) for their valuable suggestion and inspiration during their visit at IIT Roorkee.

I acknowledge my sincere gratitude to the Ministry of Human Resources and Development (MHRD), Government of India for providing financial support during my doctoral research work.

I express my sincere thanks to all seniors especially to Dr. Malay Jana, Dr. J.P.Misra, Mr. Manojit Samanta, Mr. Soumitra Maity, Mr. Mousam Ghosh, Dr. Aurobinda Panda, Dr. P.K.Mishra, Dr. Soumya Ghosh, Dr. Atanu Bhattacharya, Dr. Pratul Arvind, Dr. Sanjiv kumar, Dr. Ambrish Mishra, Dr. Jignesh Makhwana, Dr. K.S. Sajan for supporting me during the whole period. I extend my sincere thanks to my colleagues Mr. Anubhav Agrawal, Mr. Nagendra Gautam, Mr. Shailendra Kumar Bhasker, Dr. Ashoke Manori, Mr. Janardana

Kotturu, Mr. Srinivasa Rao, Mr. Vadtiya Jagan, Mr. Santosh Kumar for sharing and supporting me during my research work. I will never forget my friends Dr. Rahul Barman, Debojit Biswas, Arnab Saw, Pradeep Sanodiya, Rahul Patil, Anil Gambhir, Jayveer Singh for kept me motivated by their caring words and whole hearted supports during the research work.

I would also like to thank all the administrative &technical staff of the department of Electrical Engineering, Indian Institute of Technology Roorkee, Roorkee for their cooperation and necessary facility provided to me to carry out this research work. My special thanks to Mr. Amir Ahmed, Mr. Gautam Singh and Mr. Rakesh Kumar, who helped me to prepare experimental setup of my research work.

I owe a debt of gratitude to my parents, Late Sukesh Chandra Halder and Smt. Minati Halder, my brother Shantanu Halder, Sumanta Ch. Halder, sister-in law Annesha Halder, Sister Sujata Sur, brother- in-law Uttam Sur and nephew Utsa Sur and Swarna Deep Halder nieces Udita Sur, for their endless support, encouragement, patience and care.

I sincerely acknowledge the ethical support from my Father-in-law Shri Bhubaneswar Dutta and Mother-in-law Smt. Nivedita Dutta.

No words can adequately express my deepest gratitude and love to my wife Smt. Mousumi Dutta Halder for her unconditional support, encouragement, love and inspiration and always being there for good and bad times. I express my deepest love to my cute daughter Snaya, whose smiling faces always refresh me.

May all praise be to the Almighty, the most beneficent, and the most merciful.

(Sukanta Halder)

CONTENTS

LIST OF FIGURES

LIST OF TABLES

LIST OF SYMBOLS

Symbols	Meaning
L_d	Direct axis inductance
L_q	Quadrature axis inductance
L_s	Stator phase winding inductance
L_{ls}	Leakage inductance
L_{0s} and L_{2s}	Components of magnetizing inductance of stator winding
L_{aa}, L_{bb}, L_{cc},	Magnitude of self-inductance of stator phase windings
L_{ab}, L_{bc}, L_{ca},	Magnitude of mutual-inductance of stator phase windings
r_s	Stator phase winding resistance
δ	Torque angle
V_a,V_b,V_c	Three-phase input voltage to the PMSM
I_a,I_b,I_c	Three-phase input current to the PMSM
λ_{as} , λ_{bs} , λ_{cs}	Three-phase flux linkage
λ_{ds} , λ_{qs}	Direct axis and quadrature axis flux linkage
λ_m	Rotor magnetic flux
θ_r	Rotor position angle
P	No of poles
T_e	Electromagnetic torque
T_l	Load torque
B	Damping friction
J	Moment of inertia
ω_m	Mechanical rotor speed
ω_r	Angular velocity of rotor (electrical)
K_P	Proportional gain of PI speed controller
K_I	Integral gain of PI speed controller
V_{in}	Input voltage to resolver primary winding
V_{01},V_{02}	Output voltage of resolver secondary winding
V_{dc}	Input voltage to the inverter
V_{c1},V_{c2}	Capacitor voltage

i_{qs}^{r} and i_{ds}^{r}	d-axis and q-axis components of stator current
V_{qs}^{r} and V_{ds}^{r}	Quadrature and direct-axis voltage in the rotor reference frame
r_q and r_d	Quadrature and direct-axis winding resistance
T_{SW}	Switching period of the conventional BC
D	Duty ratio
ΔI	Current ripple of boost converter
L	Inductance of TLBC
e_s	Back-emf space vector components for a balanced three-phase system
$e_{s\alpha}$ and $e_{s\beta}$	real and imaginary axes component of the back-emf e_s
v_a , v_b	A phase and B phase voltage
i_a and i_b	Phase current
$\vec{i}_s$	Stator currents space vector
x and x	State variables of reference and adjustable model
θ_m	Mechanical angle
θ_e	Electrical angle

LIST OF ABBREVIATIONS

Abbreviations	Meaning
PMSM	Permanent Magnet Synchronous Motor
IPMSM	Interior Permanent Magnet Synchronous Motor
SPMSM	Surface Permanent Magnet Synchronous Motor
PM	Permanent Magnet
BLDC	Brushless DC
SRM	Switched Reluctance Machine
ZDAC	Zero d-axis Current control
MTPA	Maximum Torque Per Ampere control
FW	Field Weakening
RDC	Resolver to Digital Converter
VSI	Voltage Source Inverter
CSI	Current Source Inverter
MLI	Multi-Level Inverter
NPC	Neutral Point Clamped
DCMLI	Diode Clamped Multi-Level Inverter
TLBC	Three-Level Boost Converter
THD	Total Harmonic Distortion
CMLI	Cascaded Multi-Level Inverter
CHB	Cascaded H-Bridge
FCMLI	Flying Capacitor Multi-Level Inverter
ASD	Adjustable speed drives
IM	Induction Motor
DC	Direct Current
AC	Alternating Current
PWM	Pulse Width Modulation
CPWM	Carrier Pulse Width Modulation
SPWM	Sinusoidal Pulse Width Modulation
SVM	Space Vector Modulation
SVPWM	Space Vector Pulse Width Modulation
SHE	Selective Harmonic Elimination

SHM	Selective Harmonic Mitigation
GA	Genetic Algorithm
AI	Artificial Intelligent
ANN	Artificial Neural Network
MRAS	Model Reference Adaptive System
SMO	Sliding Mode Observer
EKF	Extended Kalman Filter
DSP	Digital Signal Processor
RTW	Real-Time Workshop
RTI	Real-Time Interface
ADC	Analog to Digital Converters
DAC	Digital to Analog Converters
MOSFET	Metal-Oxide Semiconductor Field-Effect Transistor
MOV	Metal-Oxide Varistor

CHAPTER 1: INTRODUCTION

[This chapter describes introduction to the research work. It starts with a brief background on permanent magnet synchronous motor drive system and the challenges associated with it. Then the solutions to the problems have been discussed. Next, scope of work, author's contribution and thesis outlines are explained.]

1.1 Overview

Electric motors are the key of the industrial development. Motion control with electric drive is always a challenge for researchers and technologists. According to the technological progress adjustable speed drives are preferred over constant speed drives because of several reasons like energy saving, velocity or position control for good transient response etc. DC motors have been used broadly for adjustable speed drive systems for many decades. But due to some of the disadvantages, like frequent maintenance as well as high cost due to brush-gear, and commutators motivated researchers to develop AC motors. Among the AC motors induction motors (IM) have been extensively used and considered as a workhorse in the industrial application. But slip power loss and lagging power factor limits the use of induction motor drives. Synchronous motor attracts researcher to overcome these limitation. However, the conventional wire wound excited synchronous motors suffers from some of the disadvantages which include the necessity of additional power supply for the field excitation. To meet the growing application demand of adjustable speed drive researchers and technologist have been persistent in their efforts to develop and advance new machines such as Brushless DC (BLDC) motor, Switched Reluctance Motor (SRM), and Permanent Magnet Synchronous Motor (PMSM). With the advancement of permanent magnet material PMSM becomes the most promising and fastest growing machine for variable speed drive. The permanent magnet synchronous motor gained wide spread popularity and acceptance in adjustable speed drive due to some of its advantageous features:

- High efficiency
- High torque to volume ratio
- High torque to inertia ratio
- High air gap flux density
- High power factor

- High acceleration and deceleration rates
- Less maintenance cost
- Simplicity and ruggedness
- Compact structure

In a PMSM, permanent provide the excitation to the rotor. The elimination of excitation windings reduces the cost and power losses. The advantages of PMSM as compared to dc motor are compact size, less maintenance and over induction motor are high efficiency, small size and wide range of power factor.

1.2 Motivation of Research Work

The primitive model of the electric motor was constructed by Michael Faraday in 1821, which was a dc motor. This motor was developed and commercially viable in 1870s. Faraday paved the way towards the creation of ac motors. The concept behind this innovation was electromagnetic induction. Induction motor was the first AC motor which was invented by Nikolai Tesla [1]. Tesla also invented other AC motor namely synchronous motor. However, inaccessibility of commercial ac power restricts the frequent use of these motors. Finally the flexibility of AC power provides the commercial success of the AC motors after a long power battle. Conventional direct current (DC), induction and synchronous machines are the three basic electric machines that serve daily needs, from small household appliances to large industrial plants, year after year. Due to simple decoupled control (field and armature), dc machine are vastly used in variable speed drive application. However, the drawback in DC motor such as necessity of frequent maintenance, power loss and high cost due to commutators and brush-gear restricts its application. Researchers provide potential solution towards robustness and maintenance free operations and also developed AC motors for high performance variable speed drives.

Among the AC motors, induction motors (IM) gain widespread popularity due to its inherent advantages like good efficiency, low cost, reliability and ruggedness. However the drawback such as lagging power factor and slip power loss in these motors initiates the necessity of the use of synchronous motors for easier control in high performance variable speed drives. The advantageous feature of synchronous machines are it runs at synchronous speed, wide power factor operation, less complex control, and remove the slip power loss problem. However, the conventional wire wound synchronous motors suffers from necessity of excitation requirements and corresponding losses. The exhaustive research paved the creation of new

special machine. Permanent Magnet Synchronous Motor (PMSM) is one of the finest creations of the researchers [2], [3] .

The development of permanent-magnet synchronous motor was described by F.W.Merril. According to the author, PMSM combines the good starting and accelerating characteristics of the induction motor with the high efficiency and power factor obtained in d-c excited synchronous motors [4]. The secret of success was the restoration of the advantages of d-c excitation without introducing its complexities. In a given frame the rating approaches and may exceed the normal induction motor rating of the frame. It is by far the best fractional hp motor ever built for synchronous applications, and may be competitive with induction motors on some applications. John F. H. Douglas conclude that the current locus and other performance items may be found, using Blondel's two reactance theories [5]. Of course, more exact estimates will be obtained, when improved methods for estimating the motor parameters become available. Another conclusion was that as the magnet materials are improved, more effective magnetization, and better stabilization are found, the power factor and the frame rating will be better. If in addition, cheaper magnets are found, then the range of application will be extended.

PMSM is becoming more popular in adjustable speed drive (ASD) applications [5] due to the development in high energy permanent magnets such as ALNICO, Ferrite, Samarium Cobalt Neodymium Iron-Boron (NdFeB). After developing these new types of special machines, researchers are working on the control of these motors to optimize in design performance and cost. The main feature of the drive system refers to its capability to operate within the given speed and torque limits. Other desirable features of variable speed drives include low space requirement, low maintenance, and capability of the speed or torque to follow the speed or torque command.

The developmental activities are now in a revolutionary stage due to the recent development of semiconductor and microprocessor technologies. Progresses in digital electronics, DSPs and FPGAs, OPAL-RT, dSPACE controller are the motivation to the increasing attention towards the use of PMSMs for high performance variable speed drive and servo drives. PMSM drives attract the interest of researchers and industry for use in various applications such as electric vehicle, rolling mills, textiles industries and marine applications.

1.3 Literature Review

Permanent magnet synchronous motor drives has been a topic of interest for decades and large amount of work has been reported in the literature. The literature review has been classified into broad groups as follows:

1.3.1 Permanent Magnet Motor

Permanent magnets are the vital components of permanent magnet motor as it's provide the excitation replacing the field winding thus avoiding the additional power supply and the corresponding losses. The properties of magnetic materials provide a base of selecting the appropriate materials for the permanent magnet motor [6]. Three basic magnetic parameters are of critical importance for permanent magnet applications in motor. These are residual flux density B_r, coercive force H_c and maximum energy product $BH_{\max}$ [7]. It is the value of B_r which primarily determines which magnetic area perpendicular to the main flux path is required to maintain the air gap operating flux [8]. Coercive force gives a measure of magnet's resistance against demagnetization during short circuit, starting etc and the energy product $BH_{\max}$ is inversely related to total magnet volume required for a given application [3], [9], [10]. The B-H Curve for different magnetic material is shown in Figure 1.1.

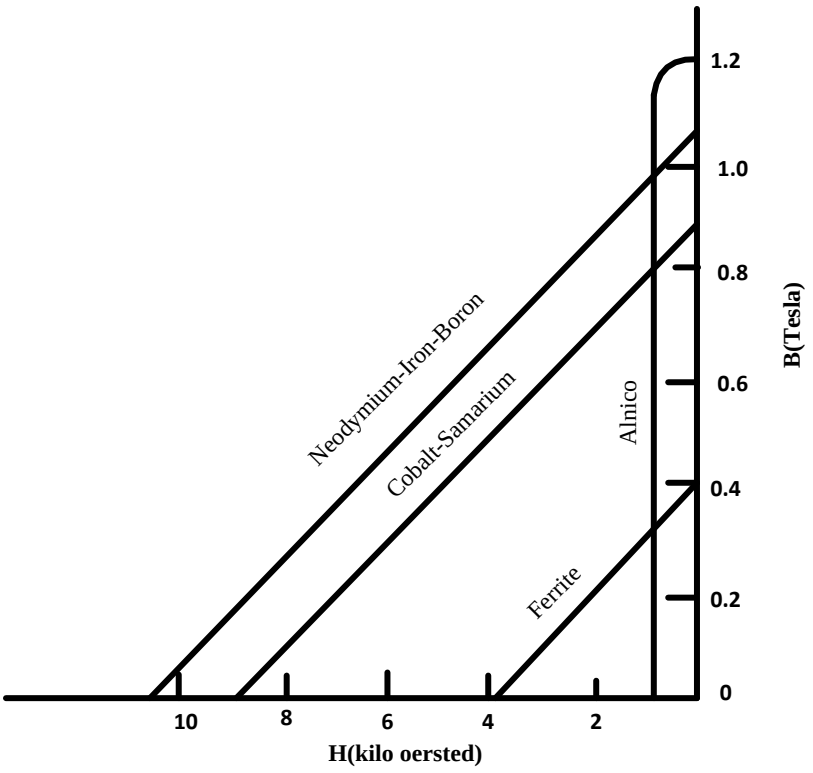

Figure 1.1 B-H Curve for different magnetic material

Nowadays the cost of the magnetic materials like samarium cobalt and neodymium-boron iron is reduced to a great extent and the energy density and coercitivity is also high for this materials. Due to this the PMSM become more attractive and viable to the industrial world [11]. Satisfying the fast dynamic response, high power factor and wide operating speed range operation PMSM has opened up a new prospects in high performance drive application [12], [13]–[16]. The magnetic properties of different magnetic materials are shown in Figure 1.2 and Figure 1.3.

ALNICO: Alnico materials have relatively high residual flux density (B_r) high service temperature tolerance, and good thermal stability, but may be easily demagnetized due to low value of coercive force H_c.

FERRITE: Barium and strontium ferrite materials are low in cost and have excellent demagnetization linearity, hinted by their low maximum energy product ($BH_{\max}$). Permanent magnet machines using these ferrite materials tend to be bulky because of low remanence. Compared to Alnico magnets, ferrite materials are highly resistant to demagnetization and are low in cost.

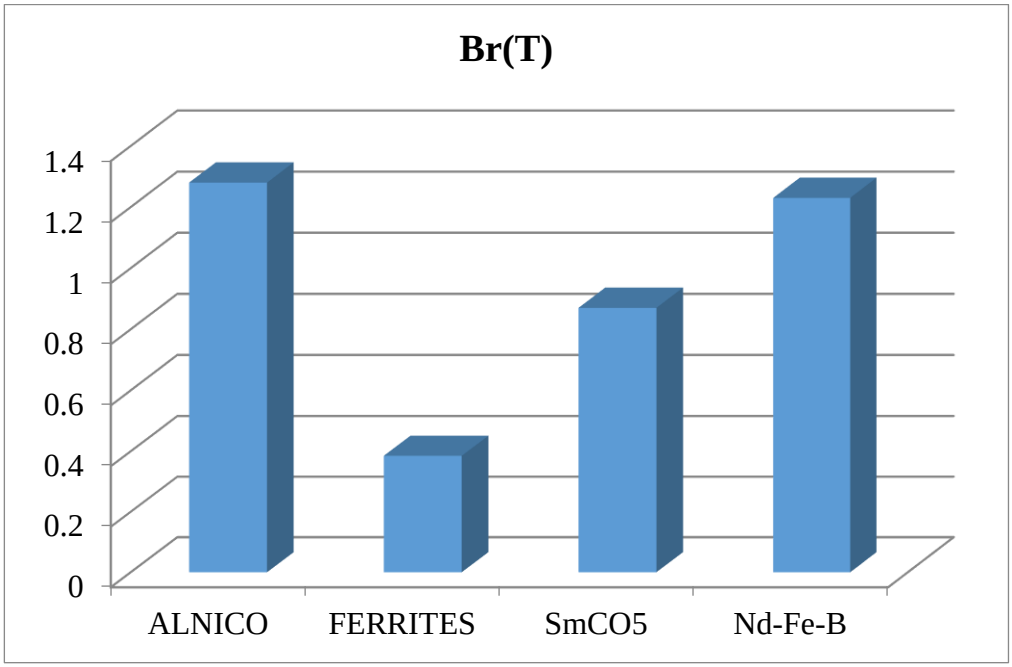

Figure 1.2 Residual flux density of different magnetic materials

COBALT SAMARIUM: Cobalt-Samarium has a higher energy product and excellent temperature insensitivity than the ferrite. However, its high cost restricts its use for application and may require care in handing since the ground powder air mixture is pyrophoric and magnetic force is strong.

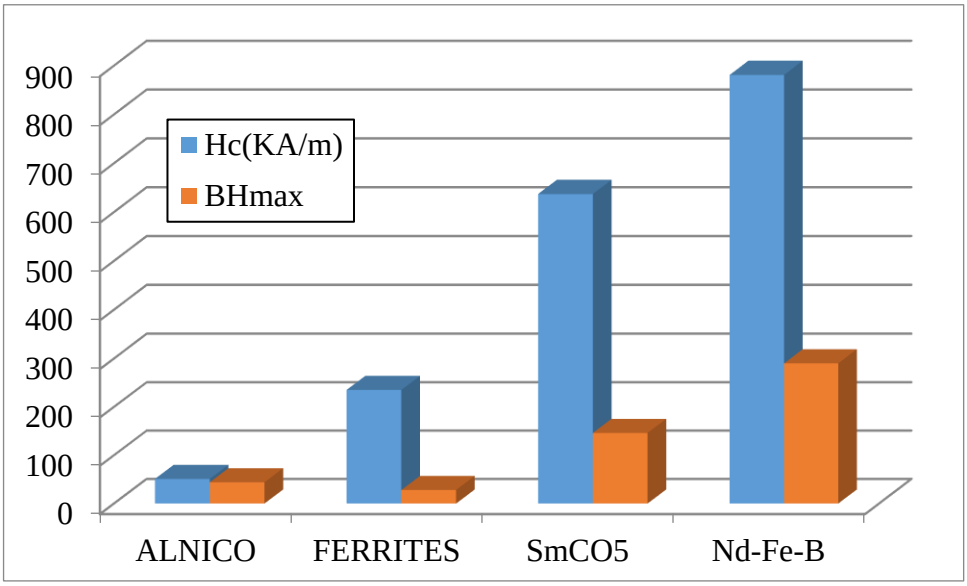

Figure 1.3 Coercive force and maximum energy product of different magnetic materials

NEODYMIUM-BORON-IRON MAGNET: The Neodymium-Boron-Iron magnet (NdBFe) has maximum remanence and coercive force and large energy product BH_{max}. This material, however, has some temperature sensitivity, which must be taken into consideration during machine design. This magnetic material is also cost effective as compared to Cobalt-samarium. Therefore, Neodymium-Boron-Iron magnet is used significantly in permanent magnet motors.

According to the direction of field flux [17], the PMSM are classified as:

a) Axial field motor: In this type of motor the flux direction is parallel to the rotor shaft.

b) Radial field motor: The flux is along the radius of the motor in this type of motor.

Although the axial field motor are coming into prominence in small numbers of application due to their higher power density and acceleration, but radial field motor is most commonly used. In PM motors the excitations are provided by placing the permanent magnet on the rotor [18]–[20]. The elimination of excitation winding reduces the cost and power loss. The placement of permanent magnet classifies PM motor in two different categories as follows:

i) Surface Permanent Magnet Synchronous Motor or SPMSM.

ii) Interior Permanent Magnet Synchronous Motor or IPMSM.

The structures of SPMSM and IPMSM are shown in Figure 1.4(a) and Figure 1.4(b) respectively. The quadrature -axis synchronous inductance of SPMSM equals its direct-axis inductance, i.e., $L_q = L_d$.

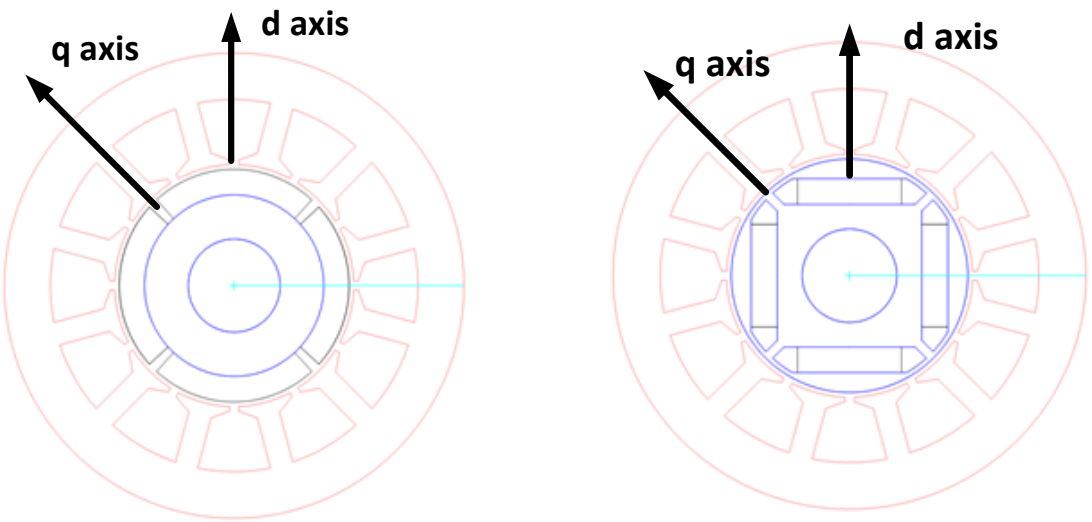

(a) (b)

Figure 1.4 (a) Surface mounted permanent magnet synchronous motor

(b) Interior permanent magnet synchronous motor

The interaction of the magnetic flux and the quadrature-axis current component of stator currents produce magnetic torque in SPM motor [16], [21], whereas IPM structure produces both magnetic and reluctance torque [22]–[24]. Due to the fact that the equivalent air gap is not uniform in IPM Structure. This makes saliency effect [25], [26]. So the quadrature-axis synchronous inductance of IPM is larger than its direct-axis inductance, i.e., $L_q > L_d$. The concept of IPM is to provide robust and solid structure as compared to SPM. The production of reluctance torque makes the IPM most acceptable for traction application [27]–[31]. The comparison of the two type of PMSM structure based on their magnet placement is given in the Table 1.1.

Table 1.1 Comparative analysis of SPMSM and IPMSM

SPMSM	IPMSM
Magnet are placed on the surface of the rotor	Magnet are placed interior portion of the rotor
Construction are easy	Construction are complex
Direct-axis inductance (L_d) is equal to quadrature-axis inductance (L_q)	Quadrature-axis inductance (L_q) is larger than its direct-axis inductance (L_d)
Produced Magnetic torque	Produce both magnetic and reluctance torque
Uniform airgap	Non uniform airgap

1.3.2 Inverter Topologies

The PMSM is generally driven by voltage source inverters [32], [33]. Two-level voltage source inverter (VSI) gained a wide spread acceptance in variable speed drive application [34]. The detail analysis of a voltage source inverter (VSI) fed permanent magnet synchronous motor (PMSM) with a half-controlled bridge converter and an LC filter is presented by Himei, et.al. Author described that the input voltage of the inverter, that is the capacitor voltage, has a ripple of double frequency of the source due to the phase control of the thyristor. The performance of the motor is significantly influenced by the ripple in the capacitor voltage [35].

Gumaste and Slemon describe steady-state analysis of a PMSM drive with a voltage-source inverter. Optimum strategy for controlling the torque in constant torque and constant power regions have been developed assuming position feedback control. The maximum current through the motor is determined with the speed range in the constant power region of the torque speed profile. The minimum current rating of the motors occur when the stator current at base speed is made the same as that at maximum speed [36].

For the voltage source inverter control hysteresis current controllers and PWM current controller is used [37]. The performance difference due to both PWM and hysteresis current controllers is described in [38]–[40]. A two-level fault-tolerant VSI is designed and tested for permanent magnet drives. This inverter can compensate both short-circuit and open-circuit faults in the switching devices. The compensation strategy is fast enough such that there is negligible disturbance in the drive operation. The fault tolerance of the inverter is verified using field-oriented control of a PMSM [41].

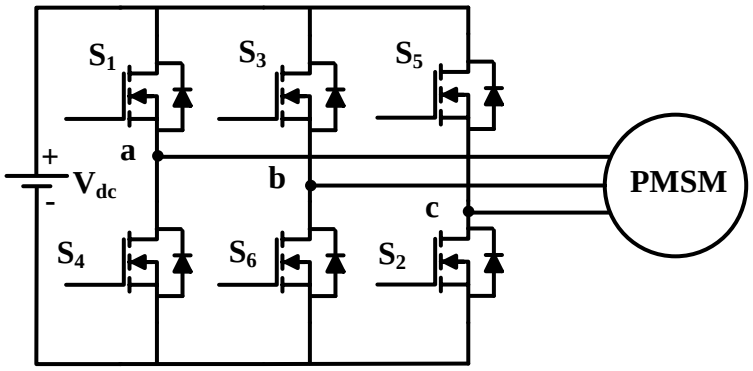

Figure 1.5 Two-level voltage source inverter fed PMSM

Two-level inverter as shown in Figure 1.5 is mostly used to fed the PMSM. However, in case of two-level inverter, the switching frequency is one of the main concerns regarding to the size of passive components, superior control of electric drives and to proliferation power density of inverter. On contradictory, the higher switching frequencies may lead to have higher switching losses, which cause inferior inverter efficiency.

Compare to two-level inverter, three-level inverter produce lower switching losses at higher switching frequencies to get the same dc-link voltage. The other attracting feature is reduction in total harmonic distortion. Lower dv/dt also reduces the voltage stress across the power switches [42]–[56].

If the fundamental output voltage and corresponding power level of the inverter are increased to a high value, the DC link voltage must be increased substantially. However, fast frequency semiconductors have a limitation in the maximum voltage and very high voltage jump will lead to terrible electromagnetic interference and high windings insulation stress. So for the high performance of AC drive systems at increased power level, high quality inverter output with low harmonic loss and generating low torque fluctuation is necessary. The significant reduction in the torque ripple is achieved with use of three-level inverter. Satisfying the application demand, PMSM bring the keen attention of the researchers and technologist. To drive the machine, three-level inverter becomes the most preferred choice replacing the conventional two-level VSI.

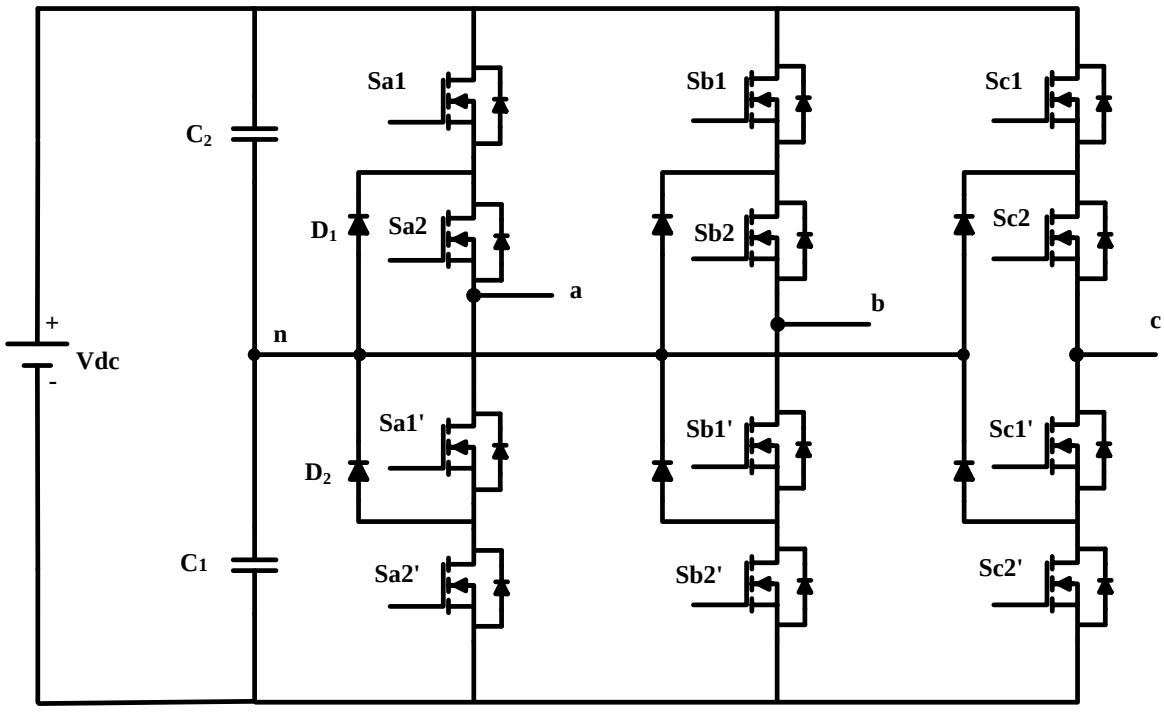

Figure 1.6 Schematic diagram of Multi-level inerter

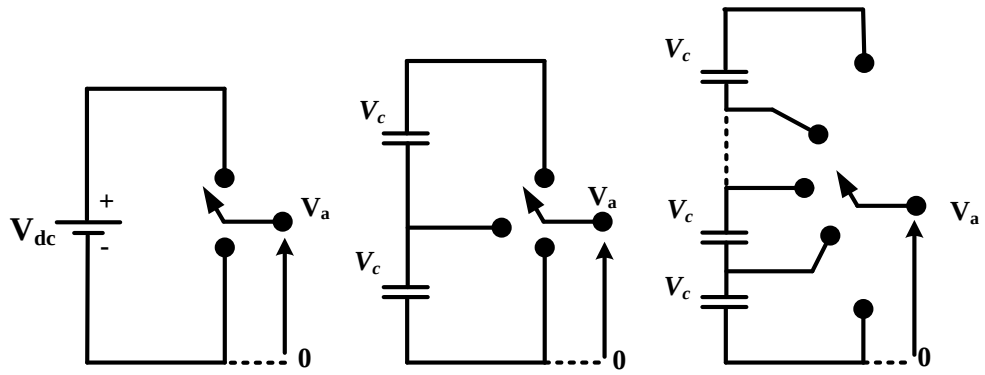

Figure 1.7 One phase leg of an inverter with (a) two-levels; (b) three-levels; (c) n levels [57]

The schematic diagram of multi-level inverter is shown in Figure 1.6. The combination of three-level inverter and PMSM allow to operate at increase dc bus voltage. One phase leg of an inverter with different levels is shown in Figure 1.7. Multilevel inverters are considered today as a very attractive solution for high-power, medium-voltage applications, because of the following reasons [42], [57]–[61]:

- MLI can generate output voltage with extremely low distortion, reduced voltage stress on switching device and lower dv/dt .
- They draw input current with very low distortion.
- They generate smaller common-mode (CM) voltage, thus reducing the stress in the motor bearings. In addition, using sophisticated modulation methods, CM voltages can be eliminated.
- They can operate with a lower switching frequency, so less EMI can be achieved.
- They are fault tolerant, less prone to failure and their cost is relatively low.

There are three benchmark multilevel inverter topologies reported in the literature [62]:

1. Neutral point clamped or diode clamped,
2. Flying capacitor or capacitor clamped and
3. Cascaded H-bridges multilevel inverter.

In the early eighties Akira Nabae et.al. developed a neutral point clamped NPC PWM inverter. In this article , a new neutral point clamped PWM inverter composed of main switching devices which operate as switches for PWM and auxiliary switching device to clamp the output terminal potential to the neutral point potential has been presented [63]. This inverter output contain less harmonic contain as compared with that of a conventional type. It was a milestone in the history of multi-level inverter. The NPC MLI employs clamping diodes and series connected capacitor to produce AC voltage waveform with multiple voltage level.

The inverter can be configured as a three, four, five or any higher level topology, but for higher number of levels the control complexity is increase exponentially. Therefore three-level NPC inverter is vastly used in the PMSM drive application [64]–[67].

Another fundamental multilevel topology, the flying capacitor inverter, involves a series connection of capacitor switching cells. This topology has several unique and attractive features like: Modular in structure and the number of levels can be increased to any arbitrary value, large number of capacitors provide extra ride through capabilities during power outage, and the switching state redundancy provides a great flexibility for the design of the switching pattern and natural balancing of capacitor voltages [57], [58], [60]. But this inverter has some drawback; mainly an excessive number of storage capacitors are required when the number of inverter levels is high. High-level systems are more difficult to package and more expensive with the required bulky capacitors, Capacitors voltages have to be pre-charged at start-up to a value which are close to their nominal values .

The cascaded H bridge multilevel inverter appeared first in 1988, matured during the 1990s and gained more attention after 1997 [68]–[70]. The CMLI family is characterized by cascade connection of modular chopper-cells or H-bridge cells to form each cluster or arm. This brings flexibility to circuit design, and results in low-voltage steps. The CMLI with H-bridge cells are known as Cascade H-bridge (CHB) multilevel inverters and on the other hand, CMLI composed with bidirectional chopper cells are known as Modular Multilevel Inverters (MMI). However, the common concepts hidden in the family members are both “modular” structure and “cascade” connection. The advantageous features of CMLI are as follows: They can achieve high or medium-voltage power levels with mature low-voltage semi-conductor devices and can easily expand to higher number of levels with easy construction, flexibility in converter design. But the requirements of isolated dc sources make the topology bulky and very much costly. On the other hand regeneration is the main concern with this topology, which restricts the application of this inverter in regenerative motor drive application.

Modular multilevel converter (MMC) was proposed in the early 2000s by Prof. R. Marquardt [71] and can be seen as a variation of the cascaded topology. Since it is particularly suitable for the HVDC systems, it immediately made its way into industry. Modularity and scalability, in theory, the output voltage of MMC can be extended to different voltage levels.

In many industrial applications, it is often necessary to control the output voltage of inverter for (1) coping with the variations of the dc input voltage, (2) regulating the voltage of the inverter, and (3) satisfying the constant volts and frequency control requirement in the drives

systems [62], [72], [73]. Many modulation techniques have been developed for controlling the output voltage of a multilevel inverter [73]. Depending upon the operating domain these modulation technique are divided as the state-space vector domain and time-domain [42], [50], [57], [60], [74]–[79].

The state-space vector domain algorithms such as Space Vector Modulation (SVM) based modulation algorithms for multilevel inverters are reported in [62], but, they are not the dominant modulation schemes found in industrial applications [42] as SVM is a computationally intensive method and its complexities increase with increasing number of levels in the inverter [62]. However, these methods have advantages but usually at the expense of more complex implementation. The time-domain approaches such as carrier based pulsewidth modulation (PWM) techniques are the extensions of the classical modulation methods used for two-level VSI [42], [80]. Other time-domain modulation methods that have also been derived from the two-level VSI are multilevel selective harmonic elimination (SHE) [81], selective harmonic mitigation (SHM) [82] and synchronized optimum PWM. These three techniques require offline computations and need to be stored in lookup tables in the digital interface control board. These methods have the advantage in achieving better efficiency. On the negative side, low dynamic performance and calculation burden with higher number of levels limit their applications.

In contrast with the high amount of recently introduced multilevel modulation schemes, no new schemes have made their way to industrial applications, despite the great amount of recent contributions and advances on this topic [42]. The main reason could be that manufacturers favour the proven technology and simplicity of carrier-based PWM schemes over new methods that have advantages but usually at the expense of more complex implementation [42], [80].

To achieve the high performance of PMSM drive systems at increased power levels the multilevel inverter is used [64]. NPC inverter is preferred due its advantages feature [83]. However voltage unbalancing across the capacitor is the main drawback of the NPC inverter [84]–[87]. Researchers give their extensive effort to overcome this problem and developed several voltage balancing technique. Self -balancing property of three-level inverter is presented in [88]. But self-balancing technique is not always adequate as the neutral-point voltage drifts for slight variation in the system parameters.

Carrier pulse width modulation and space vector modulation based voltage balancing technique are studied in [76], [89]–[99]. Various PWM techniques are presented avoiding the

additional cost of front-end circuit. However these techniques have limitation on the range of operation with the changing of the power factor and modulation index [92], [100]. Modified PWM technique increases the computational complexity and digital resource consumption. A balancing circuit is added to the NPC inverter for simple computational control. The detailed study based on the balancing circuit is presented in [85], [101]–[104]. A novel large value ac capacitor using two dc capacitors is presented in [105]. DC-Link capacitance minimization technique is discussed in [106]. The three-level boost converter (TLBC) is most attracting circuit used for voltage balancing in three-level NPC inverter. The advantageous feature is reduced switching losses and lower reverse recovery losses of the diode compared with the conventional boost converters. Based on the previously presented review of the literature, studies on three-level NPC inverted fed PMSM motor drives mainly focus on the investigation on capacitor voltage balancing at the same time boosting of the input voltage. TLBC is used to maintain the DC-link capacitor voltage of the three-level NPC inverter. With the use of TLBC the computational complexity reduces. The main attraction is the boosting feature of the input voltage.

1.3.3 Vector Control Techniques

The vector controlled PMSM drives brought new start in the variable speed drives, replacing the traditional scalar-controlled drives [107]–[109]. The vector control concept reveled in order to achieve high performance [3], [6], [110]–[112]. The simplified block diagram of vector controlled PMSM drive is shown in Figure 1.8. This concept overcomes the inherent coupling effect and the sluggish response of scalar control. To achieve the separate control of torque and speed similar to dc machine the vector control attracts the researchers for implementing in PMSM drives. The control is based on transformation of a three phase time and speed dependent system into a two co-ordinate (d and q) time invariant system.

The basic idea of this control algorithm is to decompose a stator current into a magnetic field-producing component and a torque-producing component [2], [113]. After decomposition both components can be separately controlled like dc machine [114]. The vector controlled PMSM drive has two loops- inner current control loop, and outer speed control loop. The Inner loop is having two- current controllers (d-q), which play an essential role as they directly affects the quality of current fed to the motor and indirectly affects the performance of drive in terms of efficiency and dynamic response [115], [116]. The vector control concept is mathematically presented in [117]. Bouchiker et al. discussed the simplified closed loop operation of the PMSM drive with AC-AC matrix converter using dqo transformation [118].

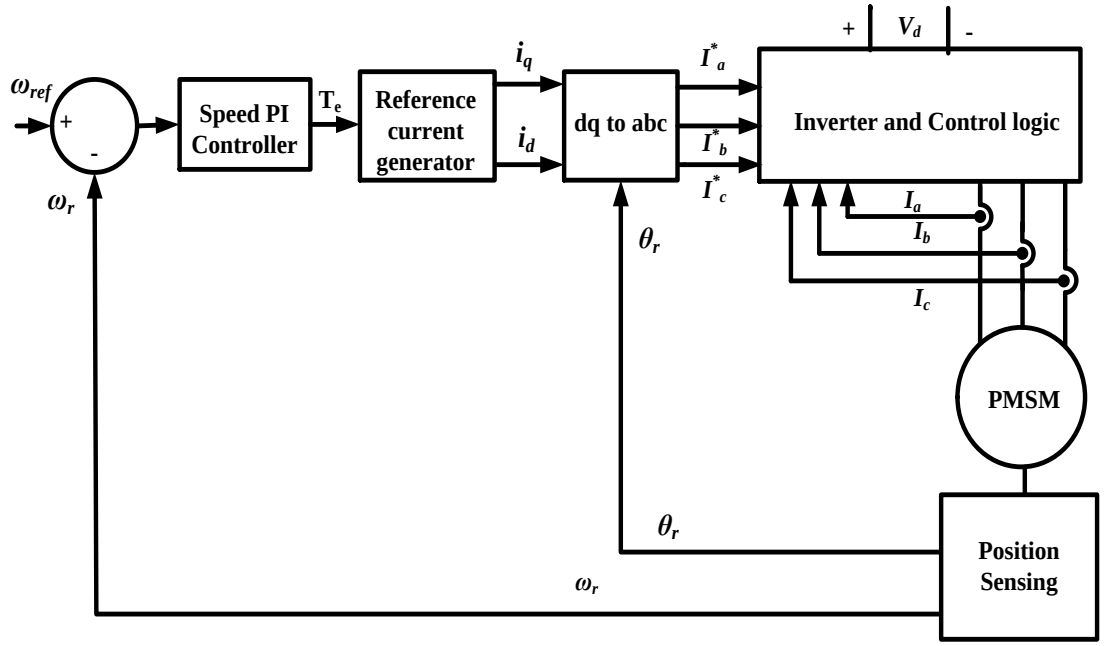

Figure 1.8 Simplified block diagram of vector control of PMSM drive [3]

There are several control technique applied for the PMSM for lower than the base speed and above the base speed operating range [119]–[121]. For below base speed operation zero d-axis current control or constant torque angle control is employed. In this control the torque angle is maintained at 90^0 hence the field or direct axis current is made to be zero. This control is most preferring control in industrial application due its simplicity. To get the optimum machine and inverter utilization the maximum torque per ampere control is introduced. This provides the higher efficiency as compared to the conventional zero d-axis control. For wide speed range application flux weakening technique is used. In PMSM due to permanent magnet structure on the rotor the flux produced in the field is not controlled directly as in case of conventional synchronous motor. So armature reaction takes a vital role in field control. To achieve the flux weakening control negative direct-axis current is injected and armature reaction reduce the airgap flux this interns reduces the flux.

B.K. Bose presented a high performance IPMSM drive system. Smooth operation of the drive is achieved in constant-torque region as well as in the flux-weakening region in both the direction of motion. . In this scheme, control in the constant-torque region is based on the vector stator flux, whereas constant-power region control is implemented by orientation of torque angle of the impressed square wave voltage through the feed forward vector rotator[22]. Metin. Aydin, et.al. introduced the concept of airgap flux control in both weakening and strengthening regions for axial-flux machines [15].

The maximum achievable speed at maximum torque is limited by the inverter capacity. But the application demand forces the researchers to expand the operating limit in the wide speed range operation. In general most off the drives are fed by the current control VSI system. Morimoto et al. examines the vector control method to enlarge the operating limits, which is optimum in the sense of developing maximum output torque within the voltage and current constraints of the inverter. The effect of motors parameters are examined by the simulation studies [122], [123].

Shoudao Huang, et.al. have described the maximum torque per ampere control strategy of permanent magnet synchronous motor. The salient-pole structure is considered in MTPA control strategy. Curve fitting method is used to implement the MTPA control. Flux weakening control is also described for wide speed range of operation [124]. A PMSM with a variable magnetic reluctance field adjustment has been presented by Kou Baoquan, et.al. A new structure of the rotor has introduced and flux-weakening (FW) principle was formulated [125].

A new concept of flux wakening control for PMSM to extend the maximum speed operation is presented by Ki-Chan Kim. In general current vector are used to weaken the magnetic flux. But the magnetic flux linkage is decreased by forming a difference gap between a stator and a rotor in axial direction deprived of moving the current vector [126].

Thomas. M. Jhans et.al. presented special PMSM rotor design with interior permanent magnet suitable for flux weakening operation. The IPM geometry is cylindrical in shape and also mechanically robust and capable of high speed because the magnet are physically contained and protected. In electromagnetic terms, burying the magnet inside the rotor introduce saliency and changes the motor torque production characteristics. In the IPM motor due to magnetic saliency the q axis inductance exceeds the d axis inductance in contrast to the conventional wound rotor salient pole synchronous motor. Due to burying of the permanent magnet material in the rotor of a material or core having high permeability, the magnet operating point shifts such that the margin against the demagnetization is increased [23] .

The calculation of torque in a brushless permanent magnet line start AC motor by means of the flux –MMF diagram in combination with finite element method has been explain by TJE Miller et.al. [127]. Direct torque control concept is mostly used in induction motor drives [128], [129]. Some of the direct torque controlled approach PMSM drives structure is investigated in [130]–[132].

To achieve the wide speed range of operation the drive should operate both the region of operation i.e., constant torque and constant power region. Maximum torque per ampere control is selected for constant torque operation and flux weakening control operates in constant power region by expanding the current and voltage limits of the inverter [133]–[138].

1.3.4 Position Sensing Methods

PM motor with fast dynamic response, good speed regulation and high efficiency demands the information of the rotor position to implement the vector control [139]–[143]. The rotor position can be accurately measured by using four devices available for the position measurement, potentiometer, linear variable differential transformer, optical encoder and resolver. The most commonly used device for motor drives are optical encoders and resolvers. For the low cost applications like fans compressors etc. encoders are used, and for high performance drive applications like servo-drives and electric vehicle resolvers are used where cost of resolver can be justified by the performance of drive. The working principle of the resolver is quite similar to the transformer. Construction wise resolver has three winding. The primary winding of resolver is rotating coil. Two secondary coils are stationary and are placed in the stator by 90˚ apart from each other. This position sensor can measure the initial accurate rotor position at standstill. High-frequency signal in an order of kHz is necessary to excite the primary coil of the resolver. With the rotation of rotor, the induced emf in the secondary coils helps to measure the actual position. Finally, estimation of the rotor position requires the demodulation of the two output signal from the resolver [142]. The dynamic model and the equivalent circuit of resolver have been analyzed in time domain[144]. The diagram of resolver sensor used in PMSM is shown in Figure 1.9.

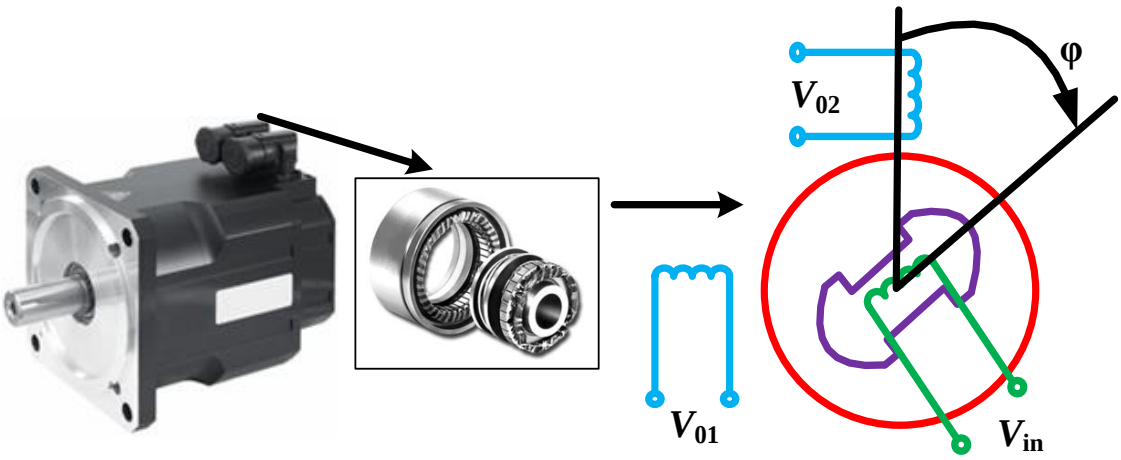

Figure 1.9 Resolver sensor used in PMSM

Since 1991 several researchers gave an idea of the manifolds of the PMSM drive with resolver sensor. But all these articles are mainly focused on the improvement of the measurement accuracy of the RDC But implementation with complete drive system without RDC, is still a fascinating area for the researchers. To reduce the position error produced by the imperfect resolver signal characteristics, different method were presented by calibrating the resolver and RDC [145]. A bang-bang type phase comparator was also implemented for fast tracking. Two pre-filters outside the R/D conversion loop were used as low pass filter [146]. By proper processing of the two resolver output signal (sine and cosine), the reasonably accurate angle measurement was done by dedicated compensation method without a processor and/or a look-up table [147]. A closed-loop linear time-invariant angle tracking observer can also be used to estimate the position and speed of a brake-by-wire actuator. But proper design of open-loop transfer function and selection of a suitable switching threshold is necessary for a stable and accurate angle tracking observer[148]. A cost effective demodulation based position measurement was achieved by Attaianese and Tomasso [149]. But the accuracy depends on the size EPROM. Murakami et al. presented an encoder less servo drive system considering the position control performance[150]. Low cost software based RDC is presented by Di Tommaso [151].

1.3.5 Sensorless Control Techniques

Position sensing is necessary to implement the vector control of PMSM drive. In general the position sensor such as resolver and encoder are used to sense the rotor position. However these sensors increase the cost as well as encumbrance of the drive. This also reduces the control robustness and reliability [152]. Furthermore, due to the difficulties in installation and limited assembly space, various sensorless control technique have been developed for the estimation of rotor position and speed during the last decade [153]. The attractive features of sensorless control are:

- Less maintenance & reduced cost of the drive.
- Compact drive.
- No cabling is required for transducers, easy implementation and reduced noise.
- Suitable for hostile operating environment; temperature and humidity etc.

There are several methods for sensorless control of PMSM. A large number of methods are presented in the literature for sensorless operation of PMSM. These are categories as follows [154]:

- Flux estimation based on the voltage model of PMSM

- Estimators based on inductance variation due to geometrical and saturation effects
- State observers
- Extended Kalman filters
- Back emf based position estimation.
- Sliding mode observers
- Model reference adaptive schemes (MRAS)
- Fuzzy-logic, neural network and artificial intelligence-based estimators
- Low frequency signal injection
- High frequency carrier injection (rotating high frequency carrier injection, pulsating high frequency carrier injection)

The sensorless control in terms of flux estimator based on the voltage model of PMSM is presented in [155]. The performance of the drive with this control is dependent on the accuracy of the estimated stator flux-linkage. This also depends on selected integration algorithm. Although various drift compensation methods have been presented so far, the pure integration in the software or hardware circuits can still be challenging at lower frequencies, where the stator voltage becomes very lesser and are dominated by the ohmic voltage drops.

When the stator winding inductance is a function of rotor position then rotor position can be estimated from the measured winding currents and its rate of change [156]. This estimation method is applicable even when motor is at standstill and back-emf is zero. In case of IPMSM the stator winding phase inductance is function rotor position and varies twice of frequency of rotor speed [154]. In SMPMSM there is no geometrical saliency, the saliency is only due to saturation effect. The rotor position can be estimated by using inductance variations due to magnetic saturation and/or geometrical effects of PMSM [157]. The techniques based on the inductance saliency can estimate the rotor position at standstill and near zero speed, at medium and high speed the inductance saliency measurement is not possible due to back-emf.

One of technique is to construct the state observer based on motor model including electrical and mechanical equations. Then stability of the observer is an important issue in providing accurate position information for motor drive system. In order to stabilize the system gains of the observers has to be optimized. However because of nonlinearity of electrical equations there is difficulty in fixing the optimum gains of observer under any operating condition [154].

The Kalman Filter is a mathematical model that runs in parallel to the actual system and gives estimations of the physical values of a linear system [154]. The Extended Kalman Filter (EKF) has been derived from the classic Kalman Filter to be used with non-linear systems. Once the EKF method converges, the estimation error on the position and the estimation error on the speed are found to be very low, and insensitive to parameter variations [158]–[160]. However, the EKF method presents many drawbacks:

- The EKF estimation is very sensitive to the PM flux linkage error.
- The EKF diverges at start-up and the direction of rotation can be incorrect.
- The gains of the EKF filters are difficult to tune.
- The EKF implies lots of matrix calculation, and thus computing time.
- Zero speed and low speed operation is extremely difficult.

The complexity of the EKF method, and its limitation towards low speeds, make this algorithm not suitable for low cost and high reliability applications.

The rotor position can be estimated based on back electromotive force (EMF) calculated by integration of the total flux linkage on the stator phase circuits. Although this control is simple, it suffers in low speed operation as well as flux-integrator's drift problem. Furthermore, this control is sensitive to the stator resistance variations. The better performances is achieved with the direct determination of back-emf space vector instead of the flux space vector, which also eliminate the flux signal integrator [161]. Back-emf based methods offer adequate performance in the higher speed range [162], [163].

To design a robust control system for a higher-order non-linear system, sliding mode control (SMC) is a proficient technique. Sliding mode observers (SMO) have low parameter sensitivity [164]–[167]. This method is an algorithm that uses the sign of the error on the machine current to update the value of the estimated speed and position stored in the controller. The main advantage of this method is that it does not need extra electronics. Furthermore, the variation of motor parameters has little impact on the results accuracy. However, it has the following drawbacks −

- Does not work at standstill or low speeds.
- The tuning of the gains is quite complicated to ensure convergence.

The MRAS algorithm is well-known for the sensorless control of induction machines. The MRAS based estimation for sensorless control of induction motor has been proved to be effective [168], [169]. The MRAS is one of the best available sensorless algorithms for

PMSM in high performance application similar to induction motor due to its parameter independency [170]–[172]. MRAS based estimation is independent of stator resistance variation. This control is computationally less complex, provides stable operation of the drive and eliminates the integrator problem as back-emf estimation is not necessary. In [171], [173] instantaneous reactive power based speed estimation is presented. The benefit of this method is that it is independent of stator resistance and less sensitive to parameters whereas the most of the observer's performance depends on machine parameters which vary according to temperature. To conquer this an adaptive algorithm with on-line parameter identification is used in [174].

The speed and rotor position of PMSM can be estimated by using fuzzy-logic, neural network and artificial intelligence-based estimators [175]–[179]. These control technique are completely different from the other sensorless control. Among the various available computational intelligence techniques such as ANN, Fuzzy, Genetic Algorithm, the fuzzy logic is found less complicated and easy to implement as compared to others to achieve the same performance. The neural network control is a good choice for control applications. In ANN controller the selection of size of network structure, number of neurons, number of hidden layers, weight coefficients are the major challenges [29]. Moreover the complexity of the ANN controller increases while achieving the robustness in overall system performance, and its real time implementation becomes difficult on given hardware platform where sampling time and processing speed is limited. Similarly in GA the mutation and selecting the new chromosomes are computationally complex and time consuming [154].

The Sensorless control scheme based on high frequency carrier injection use the saliency present in the machine for estimation of rotor position [180], [181]. The goal for this type schemes are to enable high performance control at all speeds including zero speed. Rotating high frequency carrier injection scheme is based on injection a balanced high frequency carrier superimposed on the fundamental excitation. The response to this carrier signal will contain saliency position information if the machine has a saliency. In early stage both current and voltage injection was evaluated. However, the control complexity and cost of the system is increased due to high-precision and high-bandwidth (fast) measurement required for the control scheme. The high frequency signal may produce the torque ripple, which interns produce shaft vibration and audible noises. The switching frequency and the geometry of rotor restrict further to use this control scheme lower speed range operation in some specific motor.

1.4 Scope of Work and Author's Contribution

Permanent Magnet Synchronous Motors (PMSM) are attracting growing attention because of their inherent features like high efficiency, high air gap flux density, high torque-to-inertia ratio, high power density, high acceleration deceleration rates, lower maintenance cost, simplicity and ruggedness. Vector control promises the vast utilization of PMSM in variable speed drives. MLI for medium and high voltage PMSM drive gaining more and more popularity day by day because of their inherent quality of reduced total harmonic distortion (THD), low switching losses, low dv/dt stress, high voltage capability and good electromagnetic compatibility. In this thesis an attempt has been made to investigate the possibility of multi-level inverter implemented for PMSM drive. Neutral point clamped multilevel inverter (NPC MLI) with three-level boost converter (TLBC) has been proposed for the PMSM drive. Problems associated with position sensor, possible solution have been presented. Comparative analyses of different inverter topology implemented for PMSM drive are discussed. The main contributions of the author are summarized as follows:

1. **Mathematical modeling of PMSM drive**
    - The design of an accurate control system requires the mathematical model of actual system being controlled. In this research work, complete mathematical model of the PMSM drive is developed. The drive model mainly consists of four major components, PMSM, inverter, position sensor and a controller.
    - Mathematical modeling of PMSM with saliency and without saliency in different reference frames is presented. Stator reference model of the PMSM is derived and by Park's transformation the stator –referred quantities are transformed on to the rotor thus, rotor reference model of the PMSM is obtained. The PMSM is modeled in synchronously rotating reference frame. The d-q model for permanent magnet synchronous motor is developed in MTALAB. This model consists of dynamic equations of PMSM in terms of the actual parameters and load performance.
    - The equation relating to switching states of the two-level inverter devices with the d-axis and q-axis voltage of the PMSM are derived.
    - To obtain a closed loop operation of PMSM drive, a mathematical model of resolver sensor, speed controller and load is developed.

2. **Investigation on vector control of resolver based RDC less PMSM drive fed by two-level VSI**

- The basic idea of the vector control algorithm is to decompose a stator current into a magnetic field-producing component and a torque-producing component. The vector control scheme is developed for PMSM drive in MATLAB/ Simulink environment.
- In usual practice Resolver to Digital Converter (RDC) are used for position and speed estimation from resolver. But a software based position estimation using the output signal of the resolver has been implemented to eliminate the RDC, which reduce the cost of the drive. In addition, a demodulation based algorithm is implemented to calculate the speed and rotor position.
- Vector control in terms zero d-axis current control and maximum torque per ampere control is implemented in IPMSM.
- Comparative analyses have also been presented for both the control technique.
- Further for wide speed range of operation a MTPA based flux-weakening control algorithm is developed for IPMSM.
- SPMSM drive with zero d-axis current control and its performance is investigated.
- Simulation study is carried out in MATLAB/ Simulink environment. The effects of load variation and speed change on the performance of drive are extensively studied.

3. **Investigation on multi-level inverter fed PMSM drive**

- To achieve the high performance of PMSM drive systems at increased power levels the multi-level inverter fed drive is proposed. Cost effective RDC less software based position estimation is implemented for the proposed PMSM drive. A detailed study on neutral point clamped (NPC) three-level inverter fed PMSM drive with vector control is presented.
- But the disadvantage with this inverter is capacitor voltage balancing. To maintain the voltage across the capacitor, a capacitor voltage balancing technique using three-level boost converter (TLBC) is developed for the proposed drive. The additional advantage of this balancing circuit as compared to the other carrier based PWM technique or SVM technique is the boosting feature, which is most demanding now a day for the electric vehicle application.

- This proposed MLI fed PMSM drive reduces the voltage THD and torque pulsation. Moreover, performance of the proposed balancing scheme is examined by carrying out extensive simulation studies on a surface-mounted permanent magnet synchronous machine with vector control in terms of zero d-axis current control. The detailed simulation study is carried out for the proposed drive system.
- Comparative study between a two-level and a three-level inverter fed PMSM drive is also presented. The performance is enhanced as compared to the conventional two-level VSI fed PMSM drive.

4. Investigation on sensor less multi-level inverter fed PMSM drive

- The information of rotor position is usually obtained by resolvers or encoders attached to rotor shaft. However, the use of these position sensors reduces the noise immunity, and increase the size, cost and weight of the system. Elimination of these position sensors is highly encouraged to increase the reliability, robustness and reduce the cost of drive. Furthermore investigation on sensorless control of (NPC) three-level inverter fed permanent magnet synchronous motor drive has been done to reduce system costs and total hardware complexity, to increase the mechanical robustness and reliability, to reduce the maintenance requirements, to ensure that the inertia of the system is not increased, and to have noise immunity.
- Sensorless controls in terms back-EMF based position estimation and Model Reference Adaptive System (MRAS) based estimation have been implemented.
- Back-EMF based estimation of rotor speed and angular position ensure accurate speed regulation. This method is satisfactory at medium and high-speed.
- Adaptive control seems to be the most promising control strategies. The Model Reference Adaptive System (MRAS) based estimators provide the desired state from two different models, one is reference model and other one is the adjustable model.
- The MRAS is simple and easier to implement as compared to the observer based sensorless schemes with reduced mathematical computation time.
- Exhaustive simulation results are presented to investigate the performance of the sensorless three-level NPC inverter fed PMSM drive during different operating conditions. The simulation results verified the effectiveness and feasibility of the MRAS based estimator in proposed PMSM drive system.

5. Development of laboratory prototype for experimental validation

- In this thesis extensive simulation work is carried out on PMSM drive. In order to validate the simulation of two-level voltage source inverter fed and three-level NPC

inverter fed PMSM drive the following prototypes have been developed in the laboratory and experimentation is carried out.

(i) Two-level voltage source inverter power circuit.

(ii) Three-level neutral point clamped inverter power circuit.

(iii) Capacitor voltage balancing circuit with three-level boost converter.

- The different hardware component as required for the proper operation of experimental set up such as driver circuit, isolation and dead band circuit, dc power supply, voltage and current sensor circuits are designed, developed and interfaced with dSPACE controller.
- A DSP DS1104 of dSPACE has been used for the real-time implementation of control algorithms of two different inverters topology in MATLAB/Simulink environment.
- Extensive experimentation has been carried out to investigate the performance of the drive. In the first part of the experimental work the software based RDC less position estimation is implemented using the resolver based position estimation algorithm to estimate the accurate speed and position. The experimental results show a complete 360^{o} rotation of the drive. The accurate position and speed estimation is achieved.
- In the second part of the experimental work, a two-level inverter fed PMSM drive system is tested in different operating condition. The vector control in terms of zero d-axis current control is implemented. The experimental results validate the simulation results.
- To improve the performance of the drive further experimentation is carried out in three-level NPC inverter fed PMSM drive. To maintain the voltage across the two dc-link capacitors in three-level NPC inverter a TLBC circuit is used. The exhaustive experimentation is carried out on the proposed drive in different operating conditions. The experimental results show the validity and effectiveness of the proposed drive in accordance with the simulation results.
- A comparative analysis is made between two-level inverter and three-level NPC inverter fed PMSM drive.
- Further, the experimentation is also carried out in sensorless control mode with three-level NPC inverter fed drive. The MRAS based estimation is implemented and the results show the validity of the drive with different operating conditions.

1.5 Organization of the Thesis

The thesis is organized in seven chapters and the work incorporated in each chapter is briefly outlined as follows:

Chapter-1 starts with brief overview of the PMSM drive, problems associated with it and their possible solutions. The features of the drive are also discussed here. A comprehensive literature survey on permanent magnet motor, position sensor, vector control, different inverter topology, sensorless control, historical development and application is presented in detail. Finally, scope of work, author's contribution and thesis outline are presented.

Chapter-2 describes the mathematical modelling of the permanent magnet synchronous motor drive system. The drive model consists of PMSM, inverter, position sensor, a speed controller and the load. The modelling of PMSM in both the stationary and rotating reference frame are explained in detail. The inverter model is explained for every possible switching state. The PI controller equation for speed controller is described. The drive model is obtained for vector control scheme. The steady state performance is presented.

Chapter-3 In this chapter a RDC less software based position and speed estimation is proposed for vector control operation of PMSM drive. To investigate the performance of resolver based vector controlled PMSM drive extensive simulation study is carried out using MATLAB/Simulink environment and the simulation results are presented. Two different types of rotor configuration in PMSM have been considered in this study. Vector control in terms of zero d-axis current control and maximum torque per ampere control has been implemented in IPMSM. For wide Range of operation flux weakening control has been implemented. Zero d-axis current control has been studied in SPMSM. Further, the effects of load variation and speed variation on the performance of drive are extensively studied.

Chapter 4 proposes a neutral point clamped (NPC) three-level inverter fed permanent magnet synchronous motor drive. Capacitor voltage balancing topology using three-level boost converter (TLBC) for neutral point clamped (NPC) three-level inverter is presented. The main attracting feature of this control is the boosting of the input voltage and at the same time the balancing of the capacitor voltage. This control also reduces the computational complexity. Exhaustive simulation study is carried out using MATLAB/Simulink environment and the simulation results are presented to investigate the performance of the proposed drive during different operating conditions. Comparative analysis of two-level inverter fed PMSM drive and proposed drive is also presented here.

Chapter-5 presents sensorless control of neutral point clamped (NPC) three-level inverter fed permanent magnet synchronous motor drive. Back-EMF based position estimation and Model Reference Adaptive System (MRAS) based estimation is presented. Exhaustive simulation results are presented to investigate the performance of the sensorless three-level NPC inverter fed PMSM drive at different operating conditions.

Chapter-6 is dedicated to experimental investigation on PMSM drive system. This chapter deals with design of system hardware, dSPACE controller interfacing and experimentation on the laboratory prototype to validate the simulation results presented in previous chapters.

The main conclusion of the presented work and the possible future research work in this area is summarized in **Chapter-7**.

A list of references relevant to this work is given at the end.

CHAPTER 2: MATHEMATICAL MODELLING OF PMSM DRIVE

[This chapter describes the mathematical modelling of the permanent magnet synchronous motor drive system. The drive model consists of PMSM, inverter, position sensor, a speed controller and the load. The modelling of PMSM in both the stationary and rotating reference frame are explained in detail. The inverter model is explained for every possible switching state. The PI controller equation for speed controller is described. The drive model is obtained for vector control scheme.]

2.1 Introduction

The mathematical model of a system is required for accurate design of controller for the system, deciding the controller parameters, simulation analysis and implementation of digital control. The model of the complete drive system is an integrated model of its constituents like inverter, PMSM, resolver, load and controllers. The reference frame plays an important role in the modeling of any machine, as they are like observer platforms in which each of the platforms gives a specific view of system at hand as well as the changes in the system equations. Before proceeding to design and control observation, system review of mathematical model of permanent magnet synchronous motor is presented. The variable transformation is used for the time-varying inductances, coefficients of differential equations to describe the performance behavior of the motor. There are two different reference frames for the modelling depending on which axis reference frame is locked on. The stationary reference frame is fixed with stator and the synchronously rotating reference frame is fixed to the rotor. Although PMSM modeling in both the reference frames are presented in this chapter, but rotor frame of reference is chosen because the position of the rotor magnets determines, independently of the stator voltages and currents the instantaneous induced emf and subsequently the stator currents and torque of the machine [2], [3], [6]. For inverter models, the equivalent circuit models are represented for different possible switching condition. With each switching a particular equivalent circuit model of the inverter is used, which relates input voltage and currents with the output voltage and current. The PI controllers are used as speed controller. These PI controllers are model dependent but sufficient to make the drive sustain small perturbation. Several assumptions are made in developing the model of the drive. These assumptions make the analysis simple without loss of significant accuracy.

2.2 Permanent Magnet Synchronous Motor Drive System

The permanent magnet synchronous motor drive mainly consist of four major components, PMSM, inverter, position sensor and a controller connected as shown in Figure 2.1. A PMSM is a three-phase synchronous motor, which produces the flux by permanent magnets. The PMSM is generally driven by voltage source inverters. The drive system with two different inverters in terms of two-level inverters and multi-level inverter is presented. The operation and control of PMSM requires the knowledge of rotor shaft position. There are four devices available for the position measurement, potentiometer, linear variable differential transformer, optical encoder and resolver. The most commonly used device for motor drives are optical encoders and resolvers. For the low cost applications like fans compressors etc. encoders are used, and for high performance drive applications like servo-drives and electric vehicle resolvers are used where cost of resolver can be justified by the performance of drive. The speed of the drive is controlled implementing the vector control using speed PI controller. The Mechanical load on the motor is generally put through its shaft.

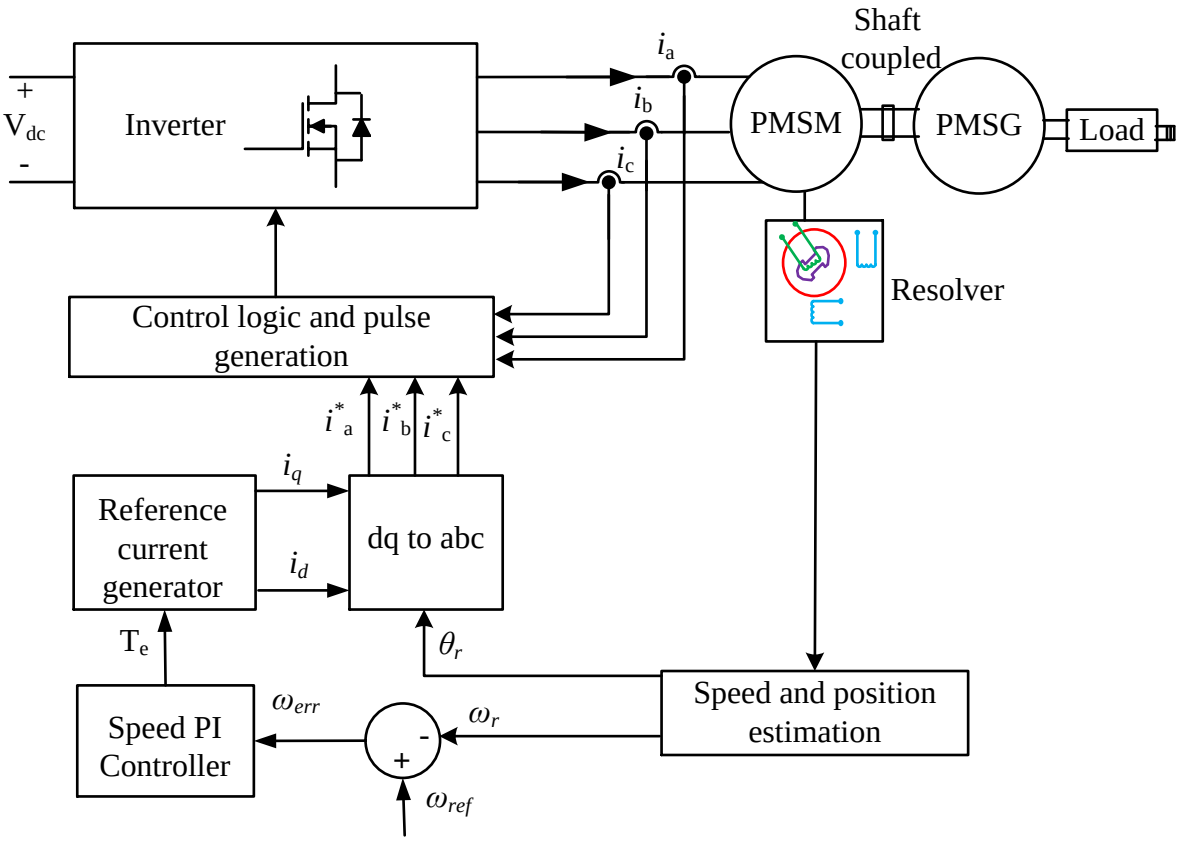

Figure 2.1 Schematic diagram of PMSM drive system

2.3 Mathematical Model of PMSM

The stator of the permanent magnet is same as the stator of a synchronous motor and its rotor consists of multipole permanent magnet. Depending upon the direction of flux the permanent magnet can be classified as radial field motor and axial field motor. In radial field motor direction of flux is along the radius of motor, whereas the direction of flux is perpendicular to radius of motor in case of axial field motors. In general the radial field motors are used in large extent. PMSM has sinusoidal back-emf. In the permanent magnet motors, the magnets can be placed either on the surface of rotor or inside the rotor and so called surface mounted PM motor or interior PM motor. The surface mounted PM motors are easy to build and skewed poles are easily magnetized to reduce the cogging torque [27]–[31]. These types of motors are suitable only for low speed applications because at high speed magnets can be detached from the rotor as they are glued using adhesives on the rotor surface. These motors show very small saliency, practically equal inductances in both the axis Ld=Lq. The permeability of the magnet is equal to air, so for the magnetic flux reluctances in d-axis and q-axis are equal that is why these two inductances are equal. In the interior PM motors, the magnets are buried inside the rotor core [22]–[24]. The manufacturing cost of these motors is high so these motors are not as common as surface mounted PM motors, and are suitable for high speed operation. The interior PM motors show significant saliency because the magnets placed inside rotor creates the air gap which has more permeability than the rotor core [25], [26]. The reluctance in d-axis is higher than q-axis and so the inductance in d-axis is less as compared to q-axis Lq>Ld. The mathematical model of the PMSM is described in detail for both type of motor salient and non-salient. Although PMSM modeling in both the reference frames are presented, but rotor frame of reference is chosen because the position of the rotor magnets determines, independently of the stator voltages and currents the instantaneous induced emf and subsequently the stator currents and torque of the machine.

2.3.1 Mathematical Model of PMSM in Stationary Reference Frame

To investigate the performance of a drive system mathematical modeling of motor plays a key role. The mathematical model of PMSM is required to design control schemes for the drive. For the instantaneous deviation of current and voltage, and the transient and steady state performance of PMSM drive, the mathematical model is usually obtained by using space-phasor theory [3], [6]. Figure 2.2 shows the different reference frames used in mathematical modeling of electrical ac machines. The stator windings are displaced by 120 electrical degrees from each other. The angle between magnetic axis of stator winding ‘a’ and rotor

magnet flux (i.e., d-axis) is called as rotor position angle θ_r. The positive direction is taken in anti-clockwise as shown in where angular velocity of rotor $\omega_r = d\theta_r/dt$ shown in positive direction. The permeability of iron parts in machine is assumed to be infinite, and the radial flux density in the air gap.

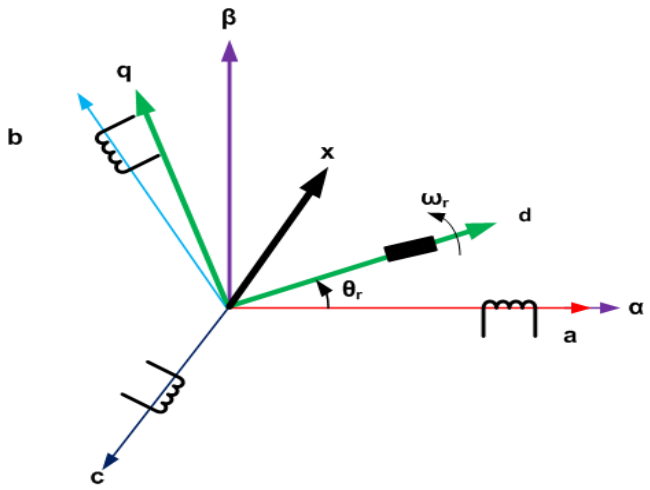

Figure 2.2 Different reference frames

Following assumptions are made for the modeling.

- Stator winding produce sinusoidal mmf distribution.
- Space harmonics in air-gaps are neglected.
- Air-gap reluctance has a constant component as well as sinusoidally varying component.
- Balanced three phase supply voltage is considered.
- Saturation is neglected, although it can be taken into account by parameter changes.
- The back emf is sinusoidal.
- Eddy currents and hysteresis losses are negligible.

The phasor diagram of PMSM is shown in Figure 2.3. To achieve the complete phasor diagram the voltage phase is assumed to be leading to current phasor by phase angle ϕ, and cosine of this angle is known as the power factor of machine.

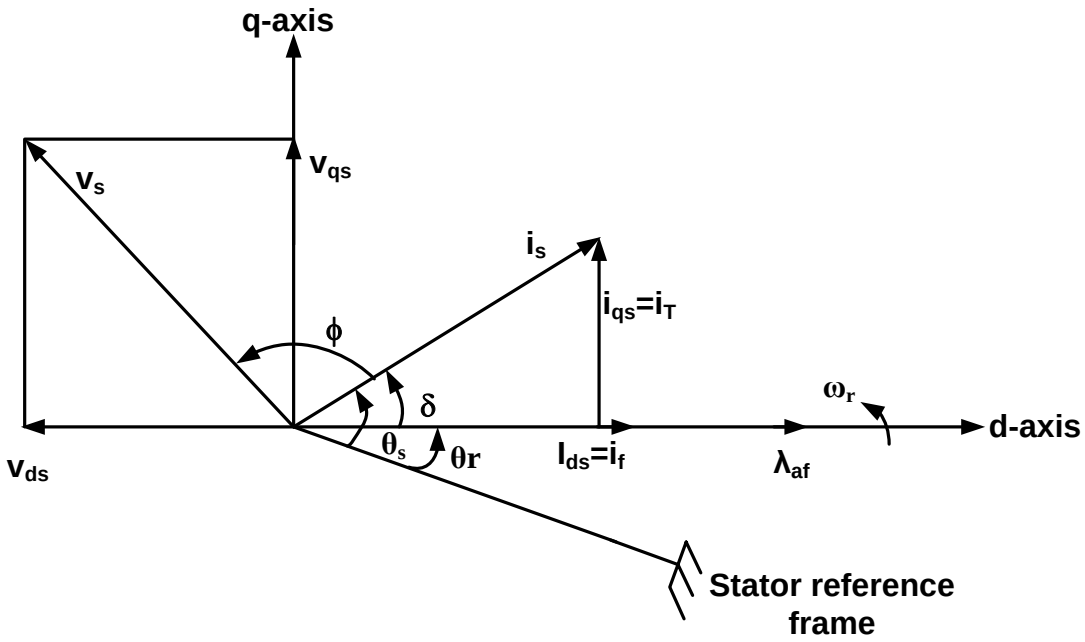

Figure 2.3 Phasor diagram of PMSM [2]

2.3.1.1 PMSM with Saliency

The voltage equations of PMSM can be expressed in terms of instantaneous currents and flux linkages.

$$v_{abcs} = r_{abcs} \cdot i_{abcs} + p\lambda_{abcs} \tag{2.1}$$

$$\lambda_{abcs} = L_{abcs} \cdot i_{abcs} + \lambda_{abcm} \tag{2.2}$$

Where,

$$v_{abcs} = \begin{bmatrix} v_{as} & v_{bs} & v_{cs} \end{bmatrix}^T \tag{2.3}$$

$$i_{abcs} = \begin{bmatrix} i_{as} & i_{bs} & i_{cs} \end{bmatrix}^T \tag{2.4}$$

$$r_{abcs} = diag\begin{bmatrix} R_s & R_s & R_s \end{bmatrix} \tag{2.5}$$

And

$$L_{abcs} = \begin{bmatrix} L_{aa} & L_{ab} & L_{ac} \\ L_{ba} & L_{bb} & L_{bc} \\ L_{ca} & L_{cb} & L_{cc} \end{bmatrix} \tag{2.6}$$

$$\lambda_{abcm} = \begin{bmatrix} \cos\theta_r \\ \cos(\theta_r - 2\pi/3) \\ \cos(\theta_r + 2\pi/3) \end{bmatrix} \tag{2.7}$$

In above equations subscript 's' represents the parameters and variables associated with stator circuit, and subscript 'r' represents the parameters and variables for rotor circuit and 'p' is a differential operator.

In equation (2.6) the winding inductances can be expressed as–

$$L_{aa} = L_{ls} + L_{0s} + L_{2s}\cos 2\theta_r \tag{2.8}$$

$$L_{bb} = L_{ls} + L_{0s} + L_{2s}\cos 2\left(\theta_r - \frac{2\pi}{3}\right) \tag{2.9}$$

$$L_{cc} = L_{ls} + L_{0s} + L_{2s}\cos 2\left(\theta_r + \frac{2\pi}{3}\right) \tag{2.10}$$

$$L_{ab} = L_{ba} = -\frac{1}{2}L_{0s} + L_{2s}\cos 2\left(\theta_r - \frac{\pi}{3}\right) \tag{2.11}$$

$$L_{ac} = L_{ca} = -\frac{1}{2}L_{0s} + L_{2s}\cos 2\left(\theta_r + \frac{\pi}{3}\right) \tag{2.12}$$

$$L_{bc} = L_{cb} = -\frac{1}{2}L_{0s} + L_{2s}\cos 2(\theta_r + \pi) \tag{2.13}$$

In equations (2.8)-(2.13), L_{ls} is the leakage inductance, L_{0s} and L_{2s} are the components of magnetizing inductance of stator winding, λ_m is rotor magnet flux. It is clear from the above equations that the magnetizing inductances are function of rotor position. In case of I interior PM motors L_{0s} while L_{2s} is negative due to the exclusive structure of its rotor, and quadrature-axis magnetizing inductance L_{mq} is larger than L_{md} .

The expression of flux linkage can be written as–

$$\begin{bmatrix} \lambda_{as} \\ \lambda_{bs} \\ \lambda_{cs} \end{bmatrix} = \begin{bmatrix} L_{aa} & L_{ab} & L_{ac} \\ L_{ba} & L_{bb} & L_{bc} \\ L_{ca} & L_{cb} & L_{cc} \end{bmatrix} \begin{bmatrix} i_{as} \\ i_{bs} \\ i_{cs} \end{bmatrix} + \lambda_m \begin{bmatrix} \cos\theta_r \\ \cos(\theta_r - 2\pi/3) \\ \cos(\theta_r + 2\pi/3) \end{bmatrix} \tag{2.14}$$

A three-phase machine can be represented in an equivalent quadrature-phase machine using two-axis theory, where direct and quadrature-axis currents are flowing in the virtual windings similar to actual three-phase currents flowing in the stator winding.

$$i_{\alpha\beta 0s} = T_{abc\to\alpha\beta 0} \cdot i_{abcs} \tag{2.15}$$

Where,

$$T_{abc\to\alpha\beta 0} = \frac{2}{3}\begin{bmatrix} 1 & -1/2 & -1/2 \\ 0 & \sqrt{3}/2 & -\sqrt{3}/2 \\ 1/2 & 1/2 & 1/2 \end{bmatrix} \tag{2.16}$$

The transformation equation (2.16) called Clark transformation, and this new stationary reference frame representing quadrature-phase machine is known as $(\alpha-\beta)$ reference frame. The older stationary reference frame representing three-phase actual machine is called $(a-b-c)$ reference frame. Using equation (2.16) voltage and flux linkage also can be transformed to $(\alpha-\beta)$ reference frame in a similar way, and voltage equation becomes–

$$v_{\alpha\beta 0} = r_{\alpha\beta 0} \cdot i_{\alpha\beta 0} + p\lambda_{\alpha\beta 0} \tag{2.17}$$

Where,

$$\left.\begin{aligned} v_{\alpha\beta 0} &= \begin{bmatrix} v_\alpha & v_\beta & v_0 \end{bmatrix}^T \\ i_{\alpha\beta 0} &= \begin{bmatrix} i_\alpha & i_\beta & i_0 \end{bmatrix}^T \\ \lambda_{\alpha\beta 0} &= \begin{bmatrix} \lambda_\alpha & \lambda_\beta & \lambda_0 \end{bmatrix}^T \end{aligned}\right\} \tag{2.18}$$

and flux linkage equation becomes

$$\lambda_{\alpha\beta 0s} = L_{\alpha\beta 0s} \cdot i_{\alpha\beta 0s} + \lambda_{\alpha\beta 0m} \tag{2.19}$$

Where,

$$L_{\alpha\beta 0} = \begin{bmatrix} L_{ls} + \frac{3}{2}\left(L_{0s} + L_{2s}\cos 2\theta_r\right) & \frac{3}{2}L_{2s}\sin 2\theta_r & 0 \\ \frac{3}{2}L_{2s}\sin 2\theta_r & \frac{3}{2}\left(L_{0s} - L_{2s}\cos 2\theta_r\right) & 0 \\ 0 & 0 & L_{ls} \end{bmatrix} \tag{2.20}$$

$$\lambda_{\alpha\beta m} = \lambda_m \begin{bmatrix} \cos\theta_r \\ \sin\theta_r \end{bmatrix} \tag{2.21}$$

2.3.1.2 PMSM without Saliency

In case of surface mounted (magnetically symmetric) PMSM, the effective air gap is almost uniform which makes the saliency ratio $\left(L_{mq}/L_{md}\right)$ approximately 1.0. So, inductance matrix expressed in (2.6) and (2.20) becomes–

$$L_{abcs} = \begin{bmatrix} L_s & 0 & 0 \\ 0 & L_s & 0 \\ 0 & 0 & L_s \end{bmatrix} \tag{2.22}$$

$$L_{\alpha\beta 0s} = \begin{bmatrix} L_{ls} + L_{ms} & -\frac{1}{2}L_{ms} & -\frac{1}{2}L_{ms} \\ -\frac{1}{2}L_{ms} & L_{ls} + L_{ms} & -\frac{1}{2}L_{ms} \\ -\frac{1}{2}L_{ms} & -\frac{1}{2}L_{ms} & L_{ls} + L_{ms} \end{bmatrix} \tag{2.23}$$

Where, $L_s = L_{ls} + \frac{3}{2}L_{ms}$, L_s is stator magnetizing inductance.

It is important to note here that transformed inductance matrix by Park or Clark Transformation (discussed latter) reduces to a diagonal matrix, which, by effect magnetically decouples the variables in every reference frame other than (a-b-c) reference frame.

For star-connected PMSM without saliency the voltage equations in (α–β) reference frame.

$$v_{\alpha\beta s} = r_{\alpha\beta s} \cdot i_{\alpha\beta s} + L_{\alpha\beta s} \cdot i_{\alpha\beta s} + e_{\alpha\beta s} \tag{2.24}$$

Where

$$\begin{aligned} r_{\alpha\beta s} &= \begin{bmatrix} R_s & 0 \\ 0 & R_s \end{bmatrix} \\ L_{\alpha\beta s} &= \begin{bmatrix} L_s & 0 \\ 0 & L_s \end{bmatrix} \\ e_{\alpha\beta s} &= \begin{bmatrix} e_{\alpha s} \\ e_{\beta s} \end{bmatrix} = \omega_r \lambda_m \begin{bmatrix} -\sin\theta_r \\ \cos\theta_r \end{bmatrix} \end{aligned} \tag{2.25}$$

In (2.24) the term $e_{\alpha\beta s}$ represents the induced back-emf in the winding of fictitious phase-quadrature machine. This voltage equation can be written in state-space form by taking stator current as independent variable as–

$$\dot{i}_{\alpha\beta s} = -L_{\alpha\beta s}{}^{-1} r_{\alpha\beta s} \cdot i_{\alpha\beta s} + L_{\alpha\beta s}{}^{-1} \left(v_{\alpha\beta s} - e_{\alpha\beta s} \right) \tag{2.26}$$

In matrix form it can be written as–

$$\begin{bmatrix} \dot{i}_{\alpha s} \\ \dot{i}_{\beta s} \end{bmatrix} = \begin{bmatrix} -R_s/L_s & 0 \\ 0 & -R_s/L_s \end{bmatrix} \begin{bmatrix} i_{\alpha s} \\ i_{\beta s} \end{bmatrix} + \begin{bmatrix} 1/L_s & 0 \\ 0 & 1/L_s \end{bmatrix} \left(\begin{bmatrix} v_{\alpha s} \\ v_{\beta s} \end{bmatrix} - \begin{bmatrix} e_{\alpha s} \\ e_{\beta s} \end{bmatrix} \right) \tag{2.27}$$

This equation (2.27) is the dynamic model of PMSM mostly used in designing the different sensorless algorithms.

Although PMSM modeling in both the reference frames are presented, but rotor frame of reference is chosen because the position of the rotor magnets determines, independently of the stator voltages and currents the instantaneous induced emf and subsequently the stator currents and torque of the machine [3], [6]. In case of induction machine the rotor fluxes are not independent variables, they are influenced by the stator voltages and currents, and due to that reason any frame of reference is suitable for the dynamic modelling of induction machine. When rotor reference frame is considered, it means the equivalent q and d axis windings are transformed to the reference frame that are revolving at rotor speed. The consequence is that there is zero speed differential between the rotor and stator magnetic fields and the stator q and d axis windings have a fixed phase relationship with the rotor magnet axis, which is the d axis in the modeling.

2.3.2 Mathematical Modeling of PMSM in Rotating Reference Frame

The control process is implemented here in d-q reference frame, because in d-q reference frame quantities are independent and can be controlled separately, which is the basic purpose of the vector control. R.H. Park established a new approach to implement the transformation of the variables which replace the time-variant variables (with respect to rotor side) associated with stator winding to time-invariant variables associated with fictitious winding rotating with the rotor. The Park's transformation is expressed as–

$$f_{dq0s} = T_{abc \to dq0} \cdot f_{abcs} \tag{2.28}$$

$$T_{abc\to dq0} = T_{abc\to\alpha\beta0}T_{\alpha\beta0\to dq0} = \frac{2}{3}\begin{bmatrix} \cos\theta_r & \cos(\theta_r - 2\pi/3) & \cos(\theta_r - 4\pi/3) \\ -\sin\theta_r & -\sin(\theta_r - 2\pi/3) & -\sin(\theta_r - 4\pi/3) \\ 1/2 & 1/2 & 1/2 \end{bmatrix} \quad (2.29)$$

$$T_{\alpha\beta0\to dq0} = \begin{bmatrix} \cos\theta_r & \sin\theta_r & 0 \\ -\sin\theta_r & \cos\theta_r & 0 \\ 0 & 0 & 1 \end{bmatrix} \quad (2.30)$$

and inverse Park's transformation is expressed as–

$$f_{abc} = T_{dq0\to abc} \cdot f_{dq0} \quad (2.31)$$

Where,

$$T_{dq0\to abc} = \left(T_{abc\to dq0}\right)^{-1} = \begin{bmatrix} \cos\theta_r & -\sin\theta_r & 1 \\ \cos(\theta_r - 2\pi/3) & -\sin(\theta_r - 2\pi/3) & 1 \\ \cos(\theta_r - 4\pi/3) & -\sin(\theta_r - 4\pi/3) & 1 \end{bmatrix} \quad (2.32)$$

In above transformation equations 'f' denote a variable that may voltage, current or flux linkage. For a three-phase balanced system the transformation matrix of equation (2.28) reduces to–

$$Tabc \to dq = \frac{2}{3}\begin{bmatrix} \cos\theta_r & \cos(\theta_r - 2\pi/3) & \cos(\theta_r - 4\pi/3) \\ \sin\theta_r & \sin(\theta_r - 2\pi/3) & \sin(\theta_r - 4\pi/3) \end{bmatrix} \quad (2.33)$$

2.3.2.1 PMSM with Saliency

In rotor reference frame the voltage equation of (2.17) becomes–

$$v_{dq0s} = r_s \cdot i_{dq0s} + T_{abc\to dq0} \cdot p\left[\left(T_{abc\to dq0}\right)^{-1}\right]\lambda_{dq0s} + p\lambda_{dq0s} \quad (2.34)$$

$$\lambda_{dq0s} = L_{dq0s} \cdot i_{dq0s} + \lambda_{dq0m} \quad (2.35)$$

Where,

$$\lambda_{dq0m} = \begin{bmatrix} \lambda_m & 0 & 0 \end{bmatrix}^T$$

$$L_{dq0} = \begin{bmatrix} L_d & 0 & 0 \\ 0 & L_q & 0 \\ 0 & 0 & L_0 \end{bmatrix}$$

$$L_d = L_{ls} + L_{md} = L_{ls} + \frac{3}{2}\left(L_{0s} + L_{2s}\right)$$
$$L_q = L_{ls} + L_{mq} = L_{ls} + \frac{3}{2}\left(L_{0s} - L_{2s}\right)$$
$$L_0 = L_{ls}$$

The L_{md} and L_{mq} can be obtained in terms of L_{0s} and L_{2s} as–

$$\begin{aligned} L_{md} &= \frac{3}{2}\left(L_{0s} + L_{2s}\right) \\ L_{mq} &= \frac{3}{2}\left(L_{0s} - L_{2s}\right) \end{aligned} \tag{2.36}$$

And the L_{0s} and L_{2s} can be obtained from L_{md} and L_{mq} as–

$$\begin{aligned} L_{0s} &= \frac{2}{3}\left[\frac{L_{md} + L_{mq}}{2}\right] = \frac{1}{3}\left(L_{md} + L_{mq}\right) \\ L_{0s} &= \frac{2}{3}\left[\frac{L_{md} - L_{mq}}{2}\right] = \frac{1}{3}\left(L_{md} - L_{mq}\right) \end{aligned} \tag{2.37}$$

In above L_d and L_q are direct-axis inductance and quadrature-axis inductance respectively. The second term of voltage equation of (2.34) can found as–

$$T_{abc\to dq0} \cdot p\left[\left(T_{abc\to dq0}\right)^{-1}\right] = \omega_r \begin{bmatrix} 0 & -1 & 0 \\ 1 & 0 & 0 \\ 0 & 0 & 0 \end{bmatrix} \tag{2.38}$$

Where

$$p\left[\left(T_{abc\to dq0}\right)^{-1}\right] = \omega_r \begin{bmatrix} -\sin\theta_r & -\cos\theta_r & 0 \\ -\sin\left(\theta_r - 2\pi/3\right) & -\sin\left(\theta_r - 2\pi/3\right) & 0 \\ -\sin\left(\theta_r - 4\pi/3\right) & -\sin\left(\theta_r - 42\pi/3\right) & 0 \end{bmatrix}$$

The voltage equation (2.34) is usually written in form of–

$$v_{ds} = R_s \cdot i_{ds} + L_d \frac{di_{ds}}{dt} - \omega_r L_q i_{qs} \tag{2.39}$$

$$v_{qs} = R_s \cdot i_{qs} + L_q \frac{di_{qs}}{dt} + \omega_r \left(L_d i_{ds} + \lambda_m\right) \tag{2.40}$$

$$v_{0s} = R_s i_{0s} + L_{0s} \frac{di_{0s}}{dt} \tag{2.41}$$

Under steady-state condition the speed of synchronously rotating reference frame is considered to be equal to speed of the rotor, in that case rate of change of flux is neglected and voltage equations ((2.39)-(2.41)) turns into form of–

$$V_{ds} = R_s \cdot I_{ds} - \omega_r L_q I_{qs} \tag{2.42}$$

$$V_{qs} = R_s \cdot I_{qs} + \omega_r \left(L_d I_{ds} + \lambda_m \right) \tag{2.43}$$

$$V_{0s} = R_s i_{0s} = 0 \tag{2.44}$$

The capital letters are used for quantities in steady-state.

In rotor reference frame the generated electromagnetic torque in terms of stator quantities is as–

$$T_e = \left(\frac{3}{2}\right)\left(\frac{P}{2}\right)\left(\lambda_{ds} i_{qs} - \lambda_{qs} i_{ds}\right) \tag{2.45}$$

By putting the values of λ_{ds} and λ_{qs} in above equation, it becomes in the form of–

$$T_e = \left(\frac{3}{2}\right)\left(\frac{P}{2}\right)\left[\lambda_m i_{qs} - \left(L_q - L_d\right) i_{qs} i_{ds}\right] \tag{2.46}$$

Where, '*P*' is the number of pole of the machine.

2.3.2.2 PMSM without Saliency

For the PMSM without saliency $L_d = L_q = L_s$, so the inductance matrix in rotor reference frame becomes–

$$L_{dq0} = \begin{bmatrix} L_s & 0 & 0 \\ 0 & L_s & 0 \\ 0 & 0 & L_0 \end{bmatrix} \tag{2.47}$$

Similar to $(\alpha - \beta)$ reference frame, here in $(d - q)$ reference frame the voltage equations are obtained as–

$$v_{ds} = R_s \cdot i_{ds} + L_s \frac{di_{ds}}{dt} - \omega_r L_s i_{qs} \tag{2.48}$$

$$v_{qs} = R_s \cdot i_{qs} + L_s \frac{di_{qs}}{dt} + \omega_r \left(L_s i_{ds} + \lambda_m \right) \tag{2.49}$$

In the steady-state above equations becomes–

$$V_{ds} = R_s \cdot I_{ds} - \omega_r L_s I_{qs} \tag{2.50}$$

$$V_{qs} = R_s \cdot I_{qs} + \omega_r \left(L_s I_{ds} + \lambda_m \right) \tag{2.51}$$

And the generated electromagnetic torque is given by–

$$T_e = \left(\frac{3}{2} \right) \left(\frac{P}{2} \right) \lambda_m i_{qs} \tag{2.52}$$

It is clear from equations (2.46) and (2.52) that in case of PMSM with saliency both direct and quadrature-axis components of stator current are used, and in case of PMSM without saliency only quadrature-axis component of stator current is used for production of torque.

2.4 Inverter for Permanent Magnet Synchronous Motor

The inverter converts the dc link voltage into variable frequency and variable magnitude voltage for the PMSM. To operate the inverter only two stator currents are sensed and third currents are negative sum of the two currents. Three phase reference currents are generated, which produce desired torque to accelerate and deaccelerate the motor for the desired speed regulation. The three phase actual stator currents are compared with respective three-phase reference currents and currents errors are produced. The three phase current errors are processed through PI controller to generate the modulating signal for the PWM generator [38]–[40]. Carrier based PWM technique is used to generate the pulses to the inverter.

The permanent magnet synchronous motor is generally driven by two-level voltage source inverter (VSI) [32], [33]. Figure 2.4 shows a circuit diagram of the PWM inverter along with equivalent circuit of the motor. DC link voltage is represented by a dc voltage source V_{dc} and three voltages represent back-emfs of the PMSM windings. Three are six MOSFET switches in the inverter with inbuilt anti parallel diode in parallel to each MOSFET switch to provide for freewheeling path. A device is ‘ON’ state if a high gate pulse is applied or the anti-parallel diode across it is conducting. Similarly the device is defined as off state if a low gate pulse is present and its antiparallel diode is not freewheeling. In the inverter legs at any instant; if upper MOSFET switch or its parallel diode is ‘ON’ then lower switch and its

parallel diode of the corresponding leg is 'OFF' and vice versa. Hence at any instant of inverter operation there are eight possible states of the inverter switches as shown in the Figure 2.5(a) to Figure 2.5 (h).

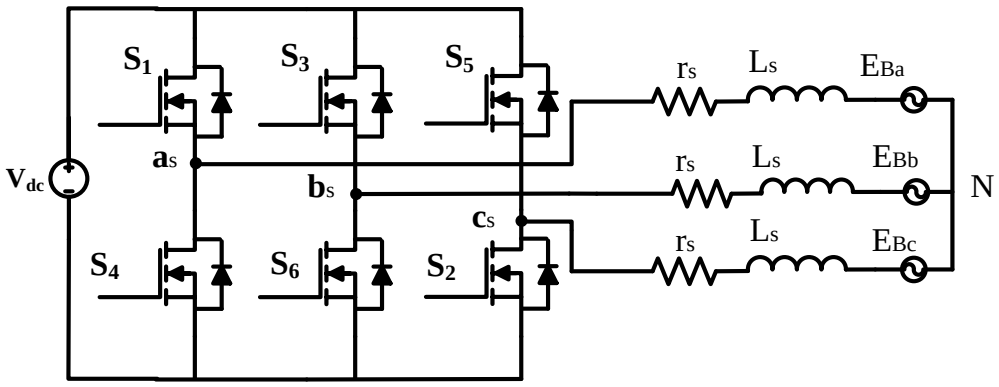

Figure 2.4 Circuit diagram of the PWM inverter along with equivalent circuit of the motor

For different switching states, the voltages across the PMSM phase winding are given in the Table 2.1. If all the upper switches of the three legs are simultaneous 'ON' the magnitude of voltages applied across the phase winding is zero as shown in the Figure 2.5 (g). Similarly, when the three switches of the lower legs are simultaneously 'ON' the voltage applied across the three phase windings is zero, i.e, the terminals of the PMSM are short circuited as shown in the Figure 2.5 (h). Table 2.1 shows the phase voltages for each possible switching position and figure shows the respective equivalent circuit of the inverter and the PMSM. The transformed values of the stator phase voltage V_{as}, V_{bs} and V_{cs} on the rotor d-q axis for each switch position is also given in the Table 2.1. For a particular switching state serial number 'n' and freewheeling state 'FW'; the d-q voltage equation are formulated as

$$v_q = \frac{2}{3}\left[(-1)^n v_c \cos(\theta + \frac{2\pi n}{3})\right].FW \tag{2.53}$$

$$v_d = \frac{2}{3}\left[(-1)^n v_c \sin(\theta + \frac{2\pi n}{3})\right].FW \tag{2.54}$$

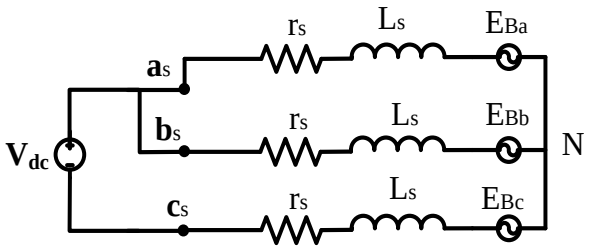

(a) $(S_1, S_2, S_3, S_4, S_5, S_6)$ = (1,1,1,0,0,0)

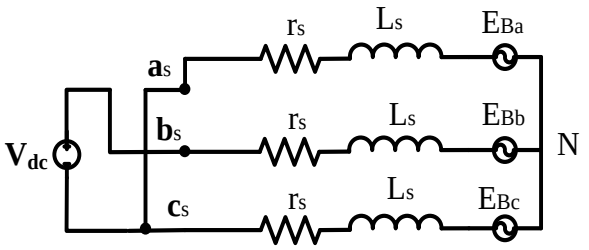

(b) $(S_1, S_2, S_3, S_4, S_5, S_6)$ = (0,1,1,1,0,0)

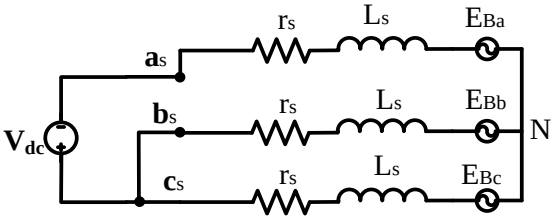

(c) $(S_1, S_2, S_3, S_4, S_5, S_6)$ =(0,0,1,1,1,0)

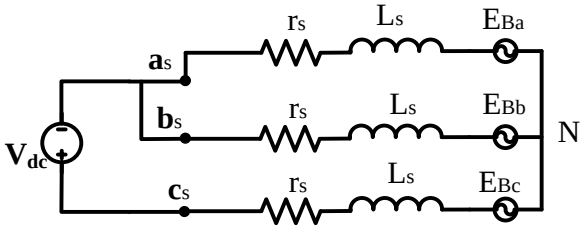

(d) $(S_1, S_2, S_3, S_4, S_5, S_6)$ = (0,0,0,1,1,1)

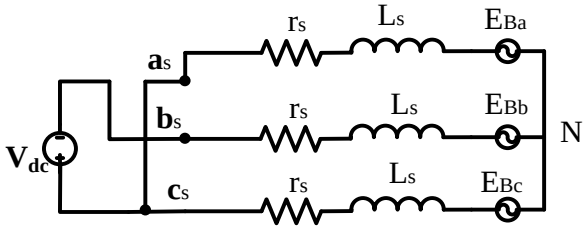

(e) $(S_1, S_2, S_3, S_4, S_5, S_6)$ = (1,0,0,0,1,1)

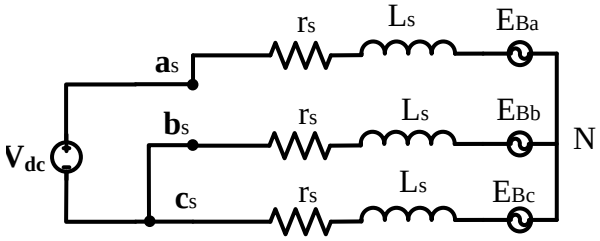

(f) $(S_1, S_2, S_3, S_4, S_5, S_6)$ = (1,1,0,0,0,1)

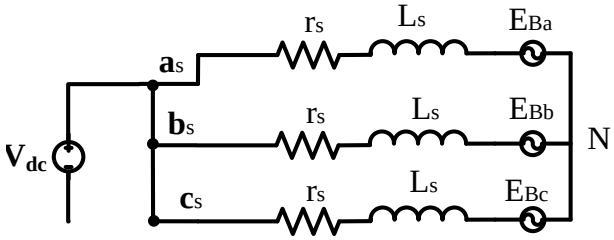

(g) $(S_1, S_2, S_3, S_4, S_5, S_6)$ =(1,0,1,0,1,0)

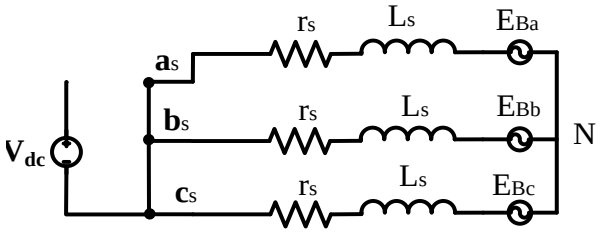

(h) $(S_1, S_2, S_3, S_4, S_5, S_6)$ = (0,1,0,1,0,1)

Figure 2.5 Different switching states

Table 2.1 Switching parameter of PWM inverter and PMSM

Sl. No 'n'	Switching states Switch 'ON'=1; Switch 'OFF'=0; $(S_1, S_2, S_3, S_4, S_5, S_6)$	V_{as}	V_{bs}	V_{cs}	FW	$v_q = \frac{2}{3}\left[v_{as}\cos\theta + v_{bs}\cos(\theta - 2\pi/3) + v_{cs}\cos(\theta + 2\pi/3)\right]$ $v_d = \frac{2}{3}\left[v_{as}\sin\theta + v_{bs}\sin(\theta - 2\pi/3) + v_{cs}\sin(\theta + 2\pi/3)\right]$
1	(1,1,1,0,0,0)	$\frac{V_{dc}}{3}$	$\frac{V_{dc}}{3}$	$-\frac{2V_{dc}}{3}$	1	$v_q = \frac{2}{3}\left[-v_{dc}\cos(\theta + 2\pi/3)\right]$ $v_d = \frac{2}{3}\left[-v_{dc}\sin(\theta + 2\pi/3)\right]$
2	(0,1,1,1,0,0)	$-\frac{V_{dc}}{3}$	$\frac{2V_{dc}}{3}$	$-\frac{V_{dc}}{3}$	1	$v_q = \frac{2}{3}\left[v_{dc}\cos(\theta - 2\pi/3)\right]$ $v_d = \frac{2}{3}\left[v_{dc}\sin(\theta - 2\pi/3)\right]$
3	(0,0,1,1,1,0)	$-\frac{2V_{dc}}{3}$	$\frac{V_{dc}}{3}$	$\frac{V_{dc}}{3}$	1	$v_q = \frac{2}{3}\left[-v_{dc}\cos\theta\right]$ $v_d = \frac{2}{3}\left[-v_{dc}\sin\theta\right]$
4	(0,0,0,1,1,1)	$-\frac{V_{dc}}{3}$	$-\frac{V_{dc}}{3}$	$\frac{2V_{dc}}{3}$	1	$v_q = \frac{2}{3}\left[v_{dc}\cos(\theta + 2\pi/3)\right]$ $v_d = \frac{2}{3}\left[v_{dc}\sin(\theta + 2\pi/3)\right]$
5	(1,0,0,0,1,1)	$\frac{V_{dc}}{3}$	$-\frac{2V_{dc}}{3}$	$\frac{V_{dc}}{3}$	1	$v_q = \frac{2}{3}\left[-v_{dc}\cos(\theta - 2\pi/3)\right]$ $v_d = \frac{2}{3}\left[-v_{dc}\sin(\theta - 2\pi/3)\right]$
6	(1,1,0,0,0,1)	$\frac{2V_{dc}}{3}$	$-\frac{V_{dc}}{3}$	$-\frac{V_{dc}}{3}$	1	$v_q = \frac{2}{3}\left[v_{dc}\cos\theta\right]$ $v_d = \frac{2}{3}\left[v_{dc}\sin\theta\right]$
7	(1,0,1,0,1,0)	0	0	0	0	$v_q = 0\,;\ v_d = 0$
8	(0,1,0,1,0,1)	0	0	0	0	$v_q = 0\,;\ v_d = 0$

2.5 Resolver Sensor

The accurate position estimation is the key of closed loop control in PMSM drives system. For high performance drive applications, the most commonly used device for sensing the position in PMSM is resolver [142], [149]. The operating principle of resolver is like a rotary transformer. Among the three winding, the rotating reference winding is fixed on the rotor and two secondary stationary coils are placed in quadrature (shifted by 90°) with one another as shown in Figure 2.6.

$$V_{in}(t) = \hat{V}_{in}.\sin \omega_{ref} t \tag{2.55}$$

$$V_{01}(\phi, t) = \hat{V}_{in}.k.\sin \phi.\sin \omega_{ref} t \tag{2.56}$$

$$V_{02}(\phi, t) = \hat{V}_{in}.k.\cos \phi.\sin \omega_{ref} t \tag{2.57}$$

High-frequency signal in the frequency of kHz is applied to excite the primary coil. In consequence of the excitement applied on the primary winding V_{in}, and along with the angular movement of the motor shaft, the respective voltages are generated by resolver secondary winding V_{01} and V_{02}.

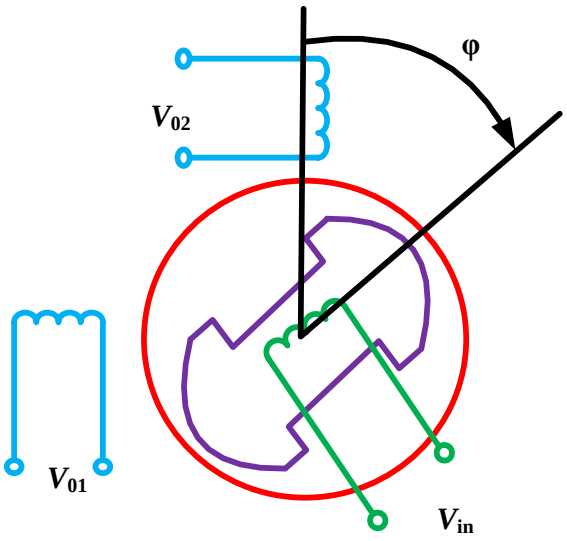

Figure 2.6 Internal construction of resolver

The frequency of the two output sine and cosine signal is same as frequency of the excitation signal but the amplitudes variation depends on the shaft angle [144]. Generally a resolver to digital converter is used to get the accurate position from the resolver. But instead of using

RDC the position is estimated from the resolver using software based resolver algorithm which is described in detail in the next chapter.

The Equivalent Circuit of Resolver

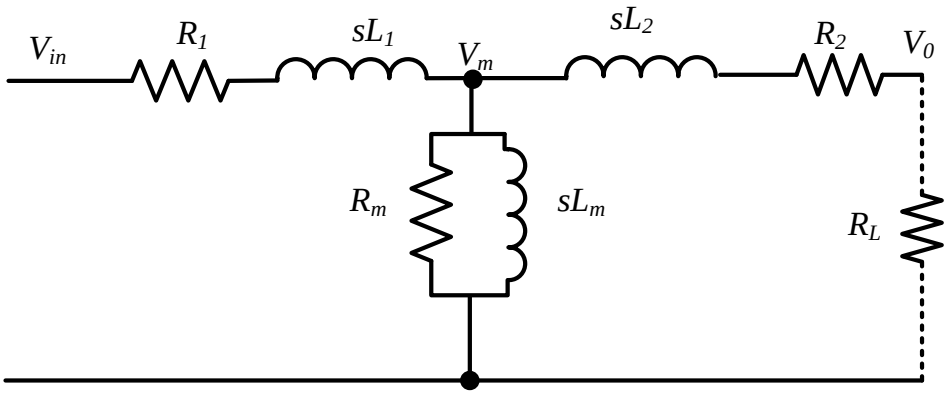

Figure 2.7 Equivalent circuit of resolver

The Figure 2.7 shows the equivalent circuit model of the resolver neglecting the back-emf produced by rotation. R_1 represents the primary resistance and L_1 shows the inductance. The output resistance and inductance are R_2 and L_2. The excitation resistance and inductance are R_m and L_m. The equivalent output resistance of load is R_L. The input reference signal is V_{in} and output signal is V_{01} and V_{02} assuming excitation resistance $R_m >> sL_m$, the transfer function of the resolver is simplified as:

$$\frac{V_0(s)}{V_{in}(s)} = \frac{s(R_L L_m / R_1 (R_2 + R_L))}{(s(L_2/R_2 + R_L)+1)(s((L_m + L_1 + L_m L_1/L_2)/R_1)+1)} \tag{2.58}$$

There are one zero and two poles in the transfer function. The poles of the resolver transfer function are given as:

$$S_1 = \frac{R_1}{L_m + L_1 + L_m L_1/L_2}, \quad S_2 = \frac{R_2 + R_L}{L_2} \tag{2.59}$$

2.6 Speed Controller

In a vector controlled PMSM drive two control loops are required. Outer one is the speed control loop consists of one speed controller, which processes the speed error. PI controller as a speed controller nullifies the steady state speed error $\left(\omega_r^* - \omega_r\right)$. The output of speed controller is basically torque reference, which multiplies by inverse of torque constant K_t. The speed error can be minimized only by changing the electromagnetic torque generated by

motor, depending on whether speed error is negative or positive. Vector control for PMSM drives provides decoupling control between flux and torque components, and is able to achieve the good performance similar to dc motor in adjustable speed drive application. In such high performance drive speed controller plays a vital role as it directly affects the current reference input to current controllers and indirectly affects the performance of motor in terms of efficiency, dynamic response etc.

At k^{th} sampling instant motor speed error of the controller is given by

$$\omega_{error}(k) = \omega_m^*(k) - \omega_m(k) \tag{2.60}$$

And the change in speed error is given by

$$\Delta\omega_{error}(k) = \omega_{error}(k) - \omega_{error}(k-1) \tag{2.61}$$

The torque command for the $(k+1)^{th}$ sampling period is

$$T_e^*(k+1) = T_e^*(k) + K_P\Delta\omega_{error}(k) + K_I\omega_{error}(k) \tag{2.62}$$

A limit of the torque command is imposed as

$$T_e^*(k+1) = \begin{cases} T_{e\max}^* \ for \quad T_e^*(k+1) \geq T_{e\max}^* \\ -T_{e\max}^* \ for \quad T_e^*(k+1) \leq -T_{e\max}^* \end{cases} \tag{2.63}$$

The q-axis current command in terms of the torque command is

$$I_q^*(k+1) = \frac{T_e^*(k+1)}{K_t} \tag{2.64}$$

A limiter is applied to saturate the controller output at maximum inverter or motor (which is small) current rating. The output of the limiter is written as

$$I_q^*(k+1) = \begin{cases} I_{q\max}^* \ for \quad I_q^*(k+1) \geq I_{q\max}^* \\ -I_{q\max}^* \ for \quad I_q^*(k+1) \leq -I_{q\max}^* \end{cases} \tag{2.65}$$

The d axis reference current is kept zero. The Park's transformation is applied to obtain abc axis referred three-phase currents from the dq0 axis currents for the hysteresis current controller of the PWM inverter.

2.7 Load

The Mechanical load on the motor is generally put through its shaft. The mechanical equation of the drive system is as-

$$T_e = T_l + B\omega_m + J\frac{d\omega_m}{dt} \tag{2.66}$$

This mechanical equation is used to obtain the rotor speed as-

$$\omega_m = \int\left(\frac{T_e - T_l - B\omega_m}{J}\right)dt \tag{2.67}$$

Here ω_m is the mechanical rotor speed; the electrical rotor speed ω_r can be obtained from this-

$$\omega_r = \frac{P}{2}\omega_m \tag{2.68}$$

2.8 Steady State Performance of PMSM Drive

The PMSM rotor position and speed feed back are obtained through a resolver. Under steady state operating condition, the drive variable like speed, frequency and current are constant. For steady-state analysis of the PMSM drive following assumptions are made:

- The dc link voltage is ripple free.
- There are no losses in the inverter i.e., switching devices are ideal.
- The harmonics in the developed torque resulting from the current harmonics are neglected.
- Current delivered by the current controller/inverter are sinusoidal i.e., only fundamental components of the stator winding currents are considered.
- All motor parameters are constant and independent of frequency.
- Speed and current controller are ideal.
- Delays imposed by various current and voltage sensors are neglected.
- Saturations are neglected.

In steady-state operating conditions of the PMSM, the differential terms in the dqo-axis equation (the terms with d/dt) are kept zero.

In the steady-state the equations becomes–

$$V_{ds} = R_s \cdot I_{ds} - \omega_r L_q I_{qs} \tag{2.69}$$

$$V_{ds} = R_s \cdot I_{ds} - \omega_r L_q I_{qs} \tag{2.70}$$

$$V_{qs} = R_s \cdot I_{qs} + \omega_r \left(L_d I_{ds} + \lambda_m \right) \tag{2.71}$$

And the generated electromagnetic torque is given by–

$$T_e = K_t I_{qs} \tag{2.72}$$

Where V_q, V_d, I_q and I_d denote steady-state (constant) quantities. The motor speed is constant at steady-state condition, hence, the load torque equation is written as

$$T_e = T_l + B\omega_m \tag{2.73}$$

The vector control of the PMSM drive provides independent control of q-axis and d-axis components of the current.

Performance Characteristics

The rotor position of the PMSM is fed back to synchronize the stator mmf with the permanent magnet rotor mmf. The PWM inverter controls amplitude and phase of the motor current using the speed controlled command. Fast speed response is achieved by controlling the maximum torque to armature current ratio. The following steady-state performance characteristics of the vector controlled SPMSM are plotted using the above equation and the corresponding simulation. (i) Armature current versus torque (ii) Speed versus torque.

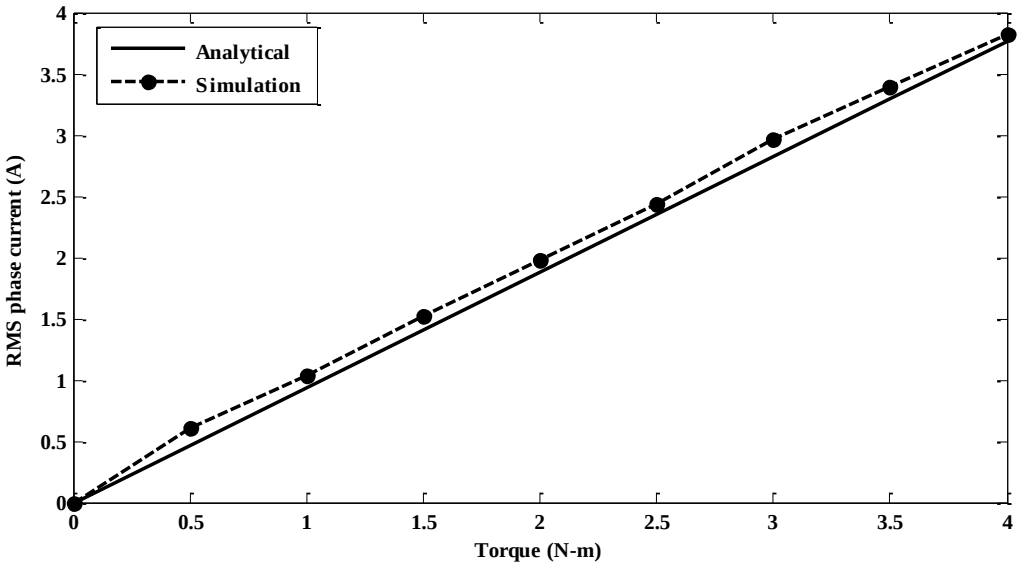

Figure 2.8 Motor torque v/s current characteristics

The toque-current relationship is given by equation(2.72). For a constant speed (ω_r) operation the motor load torque is varied and corresponding stator phase currents are calculated with

known value of torque constant (K_t). The motor torque versus armature phase current (r.m.s. value) is plotted for an operating speed 900 rpm. The Figure 2.8 shows the analytical and simulated torque versus armature phase current characteristics. The torque versus characteristics is found linear; hence, torque to current ratio is constant.

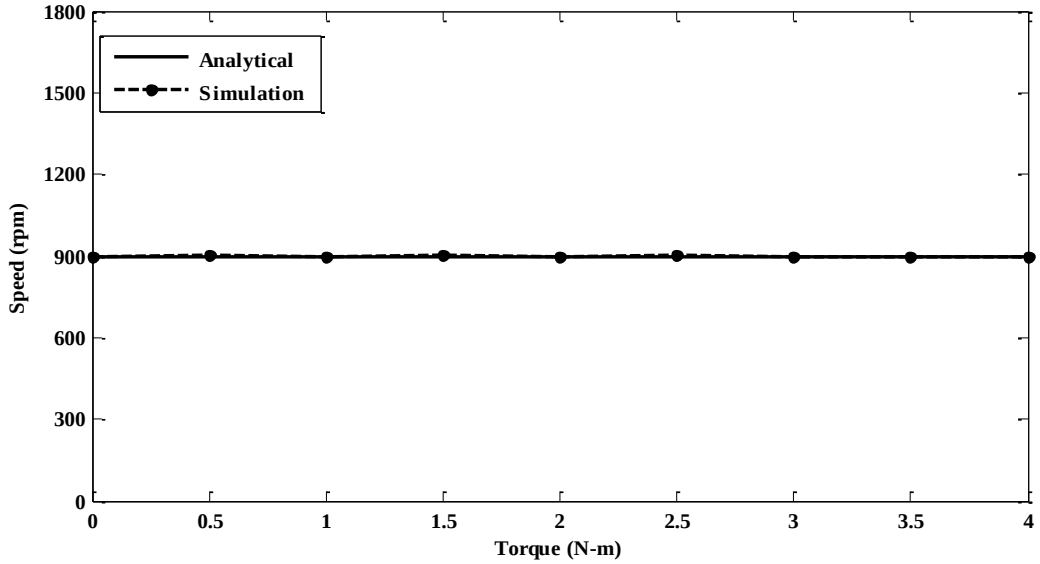

Figure 2.9 Torque v/s constant reference speed characteristics

There are two types of torque v/s speed characteristics, obtained by (i) controlling the speed at a fixed value and varying the load torque and by (ii) keeping a constant load torque and varying motor speed. Figure 2.9 shows analytical and simulated torque versus speed characteristics at reference speed 900 rpm. The speed is controlled at a constant value and the load torque is varied. Figure 2.10 shows torque v/s speed characteristics curve for a constant reference torque. The motor load torque is kept constant and speed is varied.

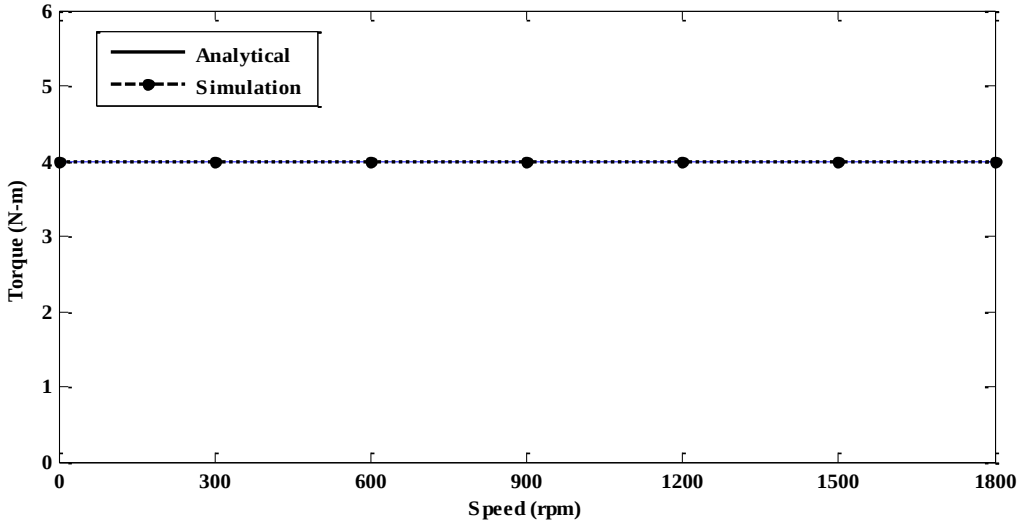

Figure 2.10 Constant reference torque v/s speed characteristics

2.9 Conclusion

In this chapter the mathematical model of PMSM in stationary and rotating reference frame is presented. The selection of reference frame depends on the control requirement. The mathematical model is presented for both type of PMSM, with saliency (IPMSM) and without saliency (SPMSM). Analytical models for two-level voltage source inverter topologies are developed. These mathematical models are based on the use of switching functions and the determination of state equations for the phase currents and the DC capacitor voltages. Resolver position sensor circuitry, mathematical equations is also presented. The mathematical model of speed control loop and the load equation is also described. The steady state model is presented and the performance characteristics are plotted.

CHAPTER 3: VECTOR CONTROL OF RESOLVER BASED PMSM DRIVE

[RDC less software based position and speed estimation has been discussed. The performance of resolver based vector controlled PMSM drive has been studied. Two different type of rotor configuration has been considered in this study. Vector control in terms of Zero d-axis current control and Maximum torque per ampere control has been implemented. For wide speed range of operation, flux weakening control has been implemented.]

3.1 Introduction

The application demand of electric motors is increasing rapidly with increasing technological advancement. With the technological progress Permanent Magnet Synchronous Motors (PMSM) are widely used with current-controlled voltage source inverters for industrial and traction applications, because of their high power density, relatively small rotor inertia and high efficiency. In PM motors, the magnets can be placed in two different ways on the rotor [18]–[20]. Depending on the placement they are classified as follows i) Interior permanent magnet motor. ii) Surface permanent magnet motor. Simulation study has been done in MATLAB/SIMULINK environment for both type of PMSM. The vector controlled PMSM drives brought renaissance in the variable speed drives, replacing the traditional scalar-controlled drives [3], [107]–[109]. PM motor with fast dynamic response, good speed regulation and high efficiency demands the information of the rotor position to implement the vector control. The rotor position can be accurately measured by using the resolver sensor. Robust structure and noise insensitivity are the attracting features of the resolver sensor. In traditional practice resolver to digital converter (RDC) are used for position and speed estimation. A Resolver-to-Digital or a Synchro-to-Digital converter is a device, which is used to convert the output signals of resolver to a digital output corresponding to the shaft angle and velocity [142]. But a detailed study of a software based position estimation using the output signal of the resolver without using RDC is discussed in this chapter. In industrial applications, especially servo drives a constant torque operation is desired, where as in case of traction applications, both constant torque and constant power operations are necessary. Performance investigation in resolver based RDC less PMSM drive with vector control in terms of Zero d-axis current control and Maximum torque per ampere control has been done in this section. Back EMF is proportional to permanent magnet field and motor speed. Since

maximum inverter voltage is limited, PMSM motor cannot operate in speed regions where the back electromotive force is higher than maximum output voltage of the inverter. An obvious consequence of reaching voltage limit is disturbed current dynamics, saturation of current regulators and degraded torque production which may cause system instability. Wide speed range can be achieved with flux weakening[3], [124]. However in case of PMSM, instead of direct control of permanent magnet flux, air-gap flux is weakened with demagnetizing current in direct axis, which in turn gives indirect Flux-Weakening (FW) of permanent magnets.

3.2 Resolver Based Position Sensing

The working principle of the resolver is identical to a rotary transformer. Construction wise resolver has three winding. The primary winding of resolver is rotating coil. Two secondary coils are stationary and are placed in the stator by 90˚ apart from each other.

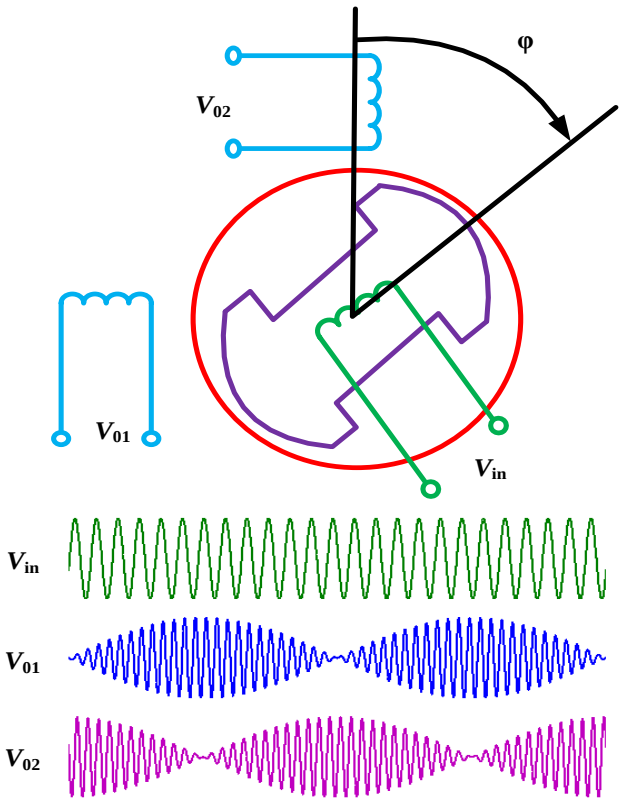

Figure 3.1 Internal structure of resolver

In general a resolver to digital converter (RDC) is required to estimate the rotor position. But software based position estimation is achieved for the proposed drive system without using RDC. High-frequency signal is applied to excite the primary coil of the resolver. With the rotation of rotor, the induced emf in the secondary coils helps to measure the actual position. Finally, the rotor position estimation is done by demodulating the output signal of the resolver. In consequence of the excitement applied on the primary winding Vin, and along

with the angular movement of the motor shaft, the respective voltages are generated by resolver secondary winding V_{01}, V_{02}. The internal structure and the input out signal of the resolver are shown in Figure 3.1.

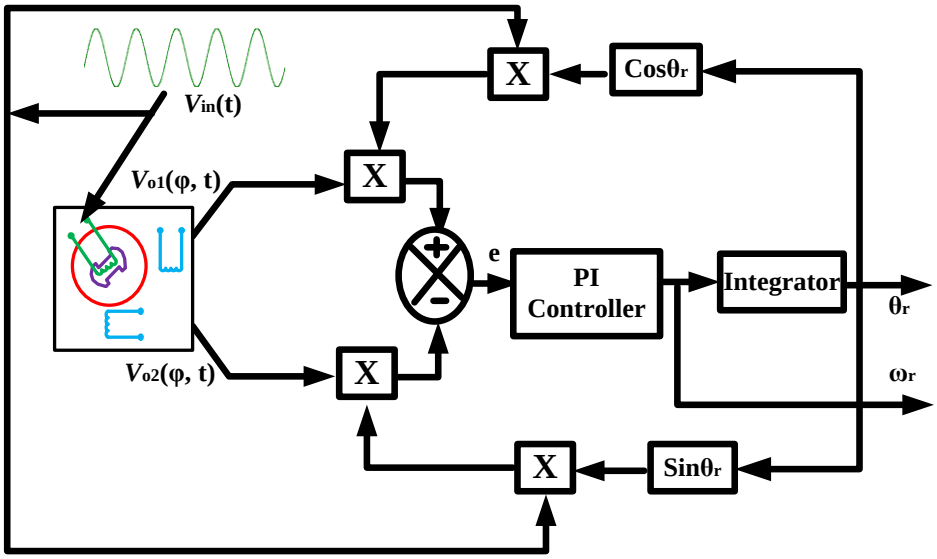

Figure 3.2 Schematic diagram of position estimation algorithm from resolver

The frequency of the two output sine and cosine signal is same as frequency of the excitation signal but the amplitudes variation depends on the shaft angle. Instead of using RDC the resolver algorithm proposed here is software based. The Schematic diagram of position estimation algorithm is shown in Figure 3.2. The equations related to the primary and secondary winding are defined as–

$$V_{in}(t) = \hat{V}_{in}.\sin\omega_{ref}t \tag{3.1}$$

$$V_{01}(\phi,t) = \hat{V}_{in}.k.\sin\phi.\sin\omega_{ref}t \tag{3.2}$$

$$V_{02}(\phi,t) = \hat{V}_{in}.k.\cos\phi.\sin\omega_{ref}t \tag{3.3}$$

Where, k is the resolver's turn ratio, $\hat{V}_{in}$ implies the peak value, ϕ is the rotor position in rad, and ω_{ref} is the frequency of the excitation signal in (rad /sec).

The error signal nearer to zero is the difference between actual angle (ϕ) and the computed angle (θ). The feedback loop and PI controller provides the speed. The rotor position is obtained by integration of the motor speed.

The error calculation is based on following trigonometric relation given by-

$$e = (\hat{V}_{in}.\sin\omega_{ref}t.\cos\theta)(\hat{V}_{in}.k.\sin\phi.\sin\omega_{ref}t) - (\hat{V}_{in}.\sin\omega_{ref}t.\sin\theta)(\hat{V}_{in}.k.\cos\phi.\sin\omega_{ref}t) \quad (3.4)$$

$$e = \hat{V}_{in}(t).(\hat{V}_{in}k.\sin\omega_{ref}t)(\sin\phi\cos\theta - cos\phi\sin\theta) \quad (3.5)$$

The above expression can be written in form of

$$e = A.\sin(\phi - \theta) \quad (3.6)$$

Where,

$$A = \hat{V}_{in}(t).(\hat{V}_{in}k.\sin\omega_{ref}t) \quad (3.7)$$

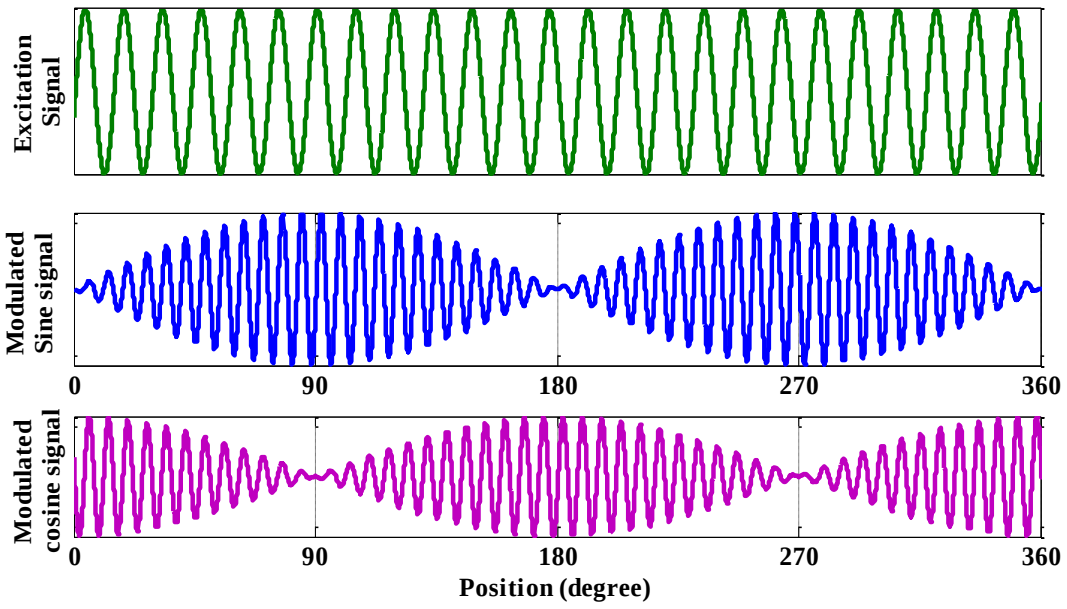

.

Figure 3.3 Simulation result of the resolver input and modulated output signal with complete 360º rotation

The output signal of resolver with the input signal at complete 360˚ rotation of the rotor shaft is shown in the Figure 3.3. The output signal of the resolver for its four quadrants has been shown in the Figure 3.4.

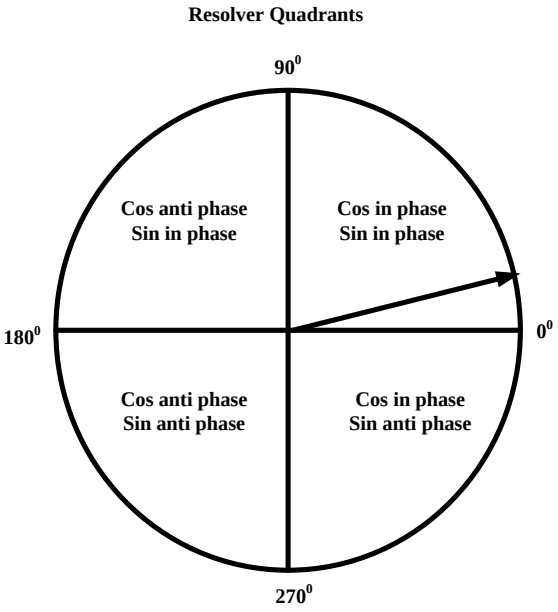

Figure 3.4 Resolver output signal at complete 360° rotation

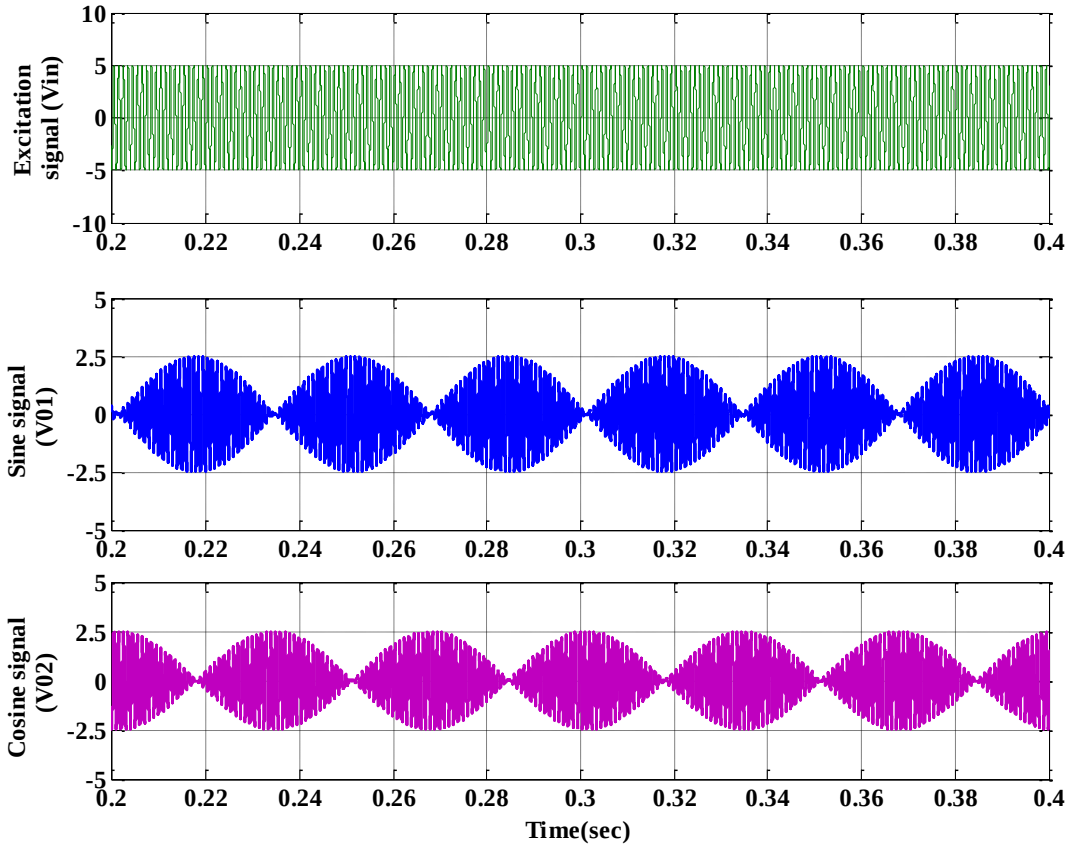

Figure 3.5 Simulation results of the resolver input and modulated output signal

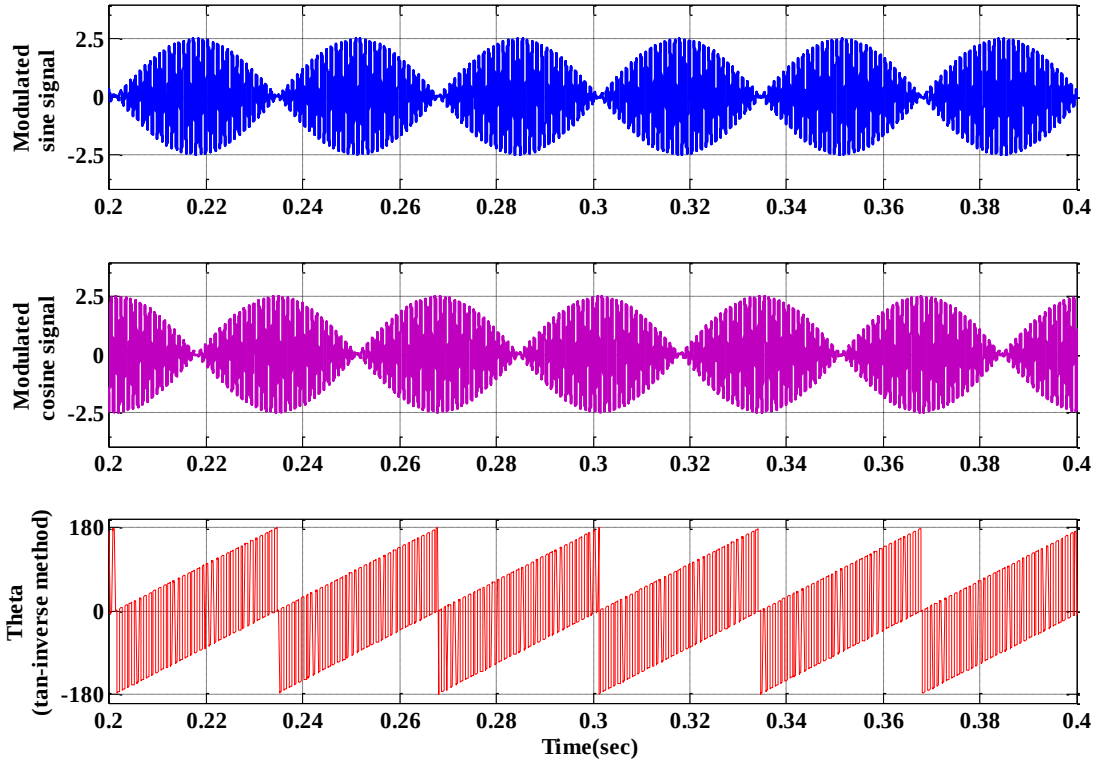

Figure 3.6 Simulation results of the resolver modulated output signal with theta by tan inverse method

The high frequency (1 kHz) excitation signal is applied to the resolver. When the rotor is rotated, the resolver induces the two modulated signals shown in the Figure 3.5. If we apply the tan inverse rule based on the modulated sine and cosine output signal to calculate the position θ then there will be error on the calculated position as shown in the Figure 3.6. Trace 1 and 2 represents the modulated sine and cosine output signal from the resolver. Trace 3 in this figure represents the calculated rotor position with simple tan inverse method. The equation $\theta = \arctan\left[\frac{V_{01}(\phi,t)}{V_{02}(\phi,t)}\right]$ has been used to calculate the rotor position by tan inverse method. It is observed that there is an oscillation in calculated rotor position.

The high frequency (1 kHz) excitation signal is applied to the resolver. When the rotor is rotated, the resolver induces the two modulated signals. To obtain the rotor position from the resolver, these modulated signals are demodulated by the proposed algorithm. Trace 1 in the Figure 3.7 denotes the modulated output sine signal & the trace 2 denotes the demodulated sine signal. And Trace 1 in the Figure 3.8 denotes the modulated output cosine signal & the trace 2 denotes the demodulated cosine signal. Figure 3.9 shows the demodulated sine and cosine signal. Estimated position from the resolver algorithm is shown in the Figure 3.10.

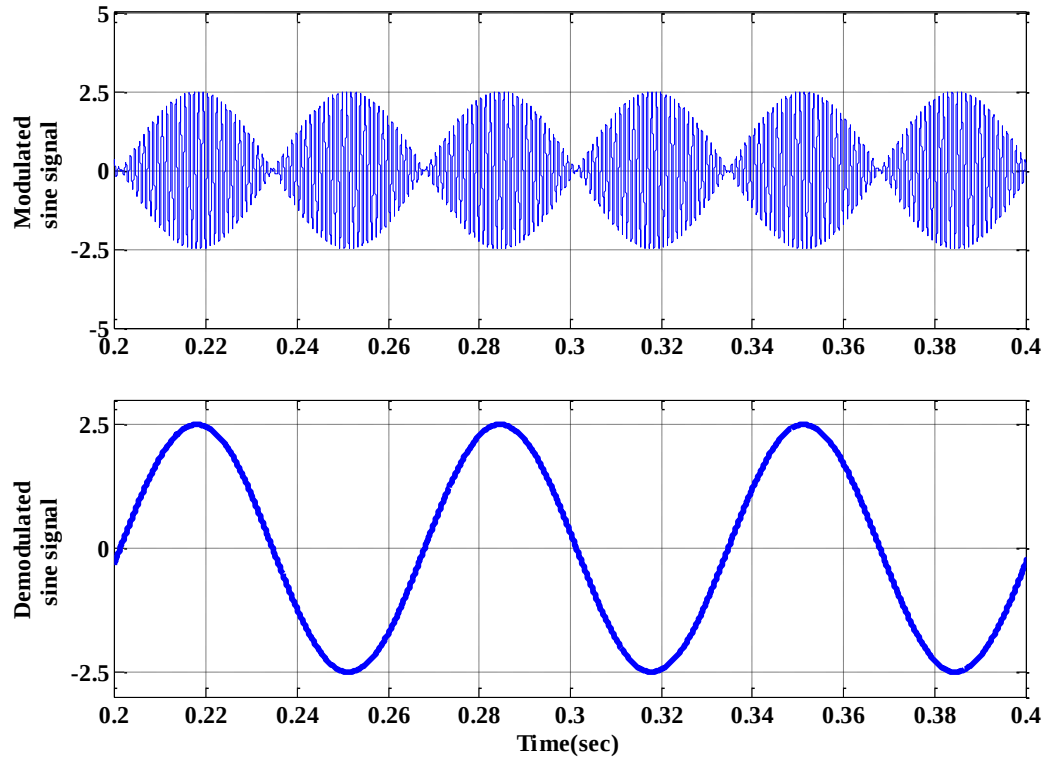

Figure 3.7 Simulation results of the modulated & demodulated sine signal

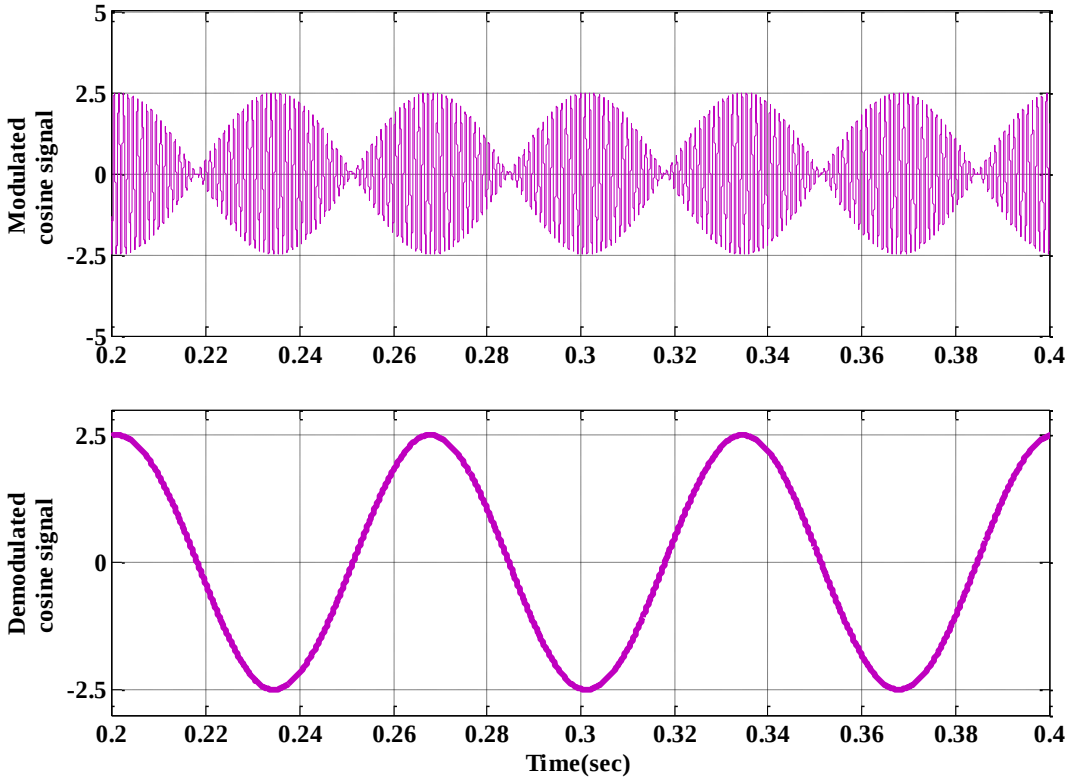

Figure 3.8 Simulation results of the modulated & demodulated cosine signal

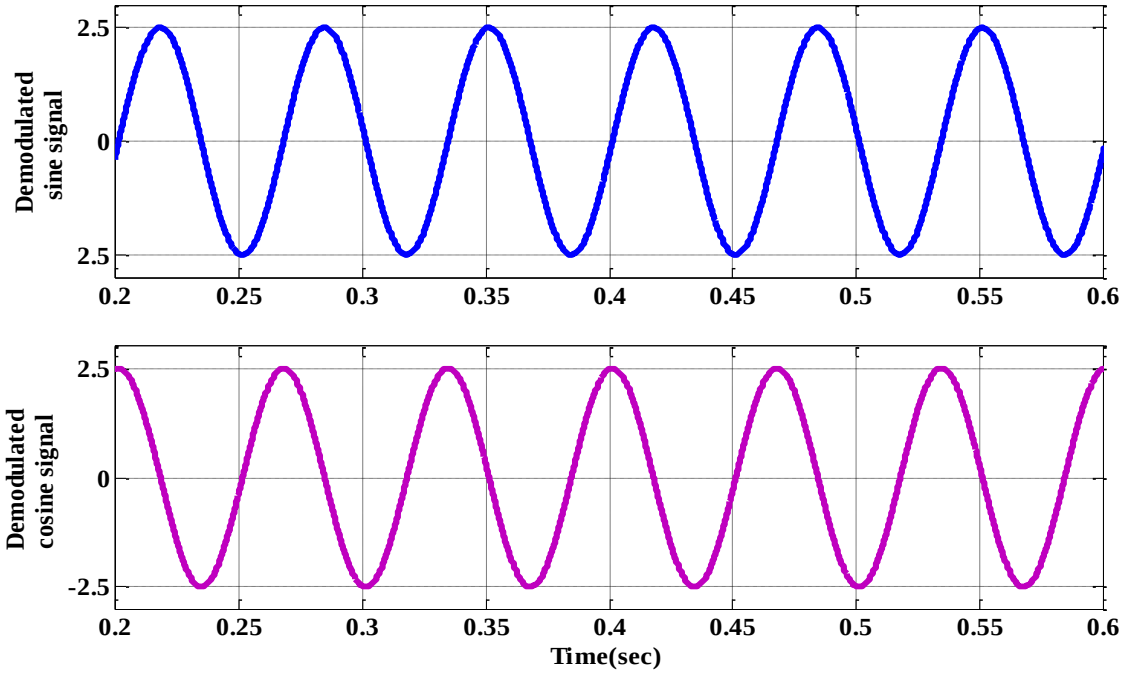

Figure 3.9 Simulation results of the demodulated sine & cosine signal

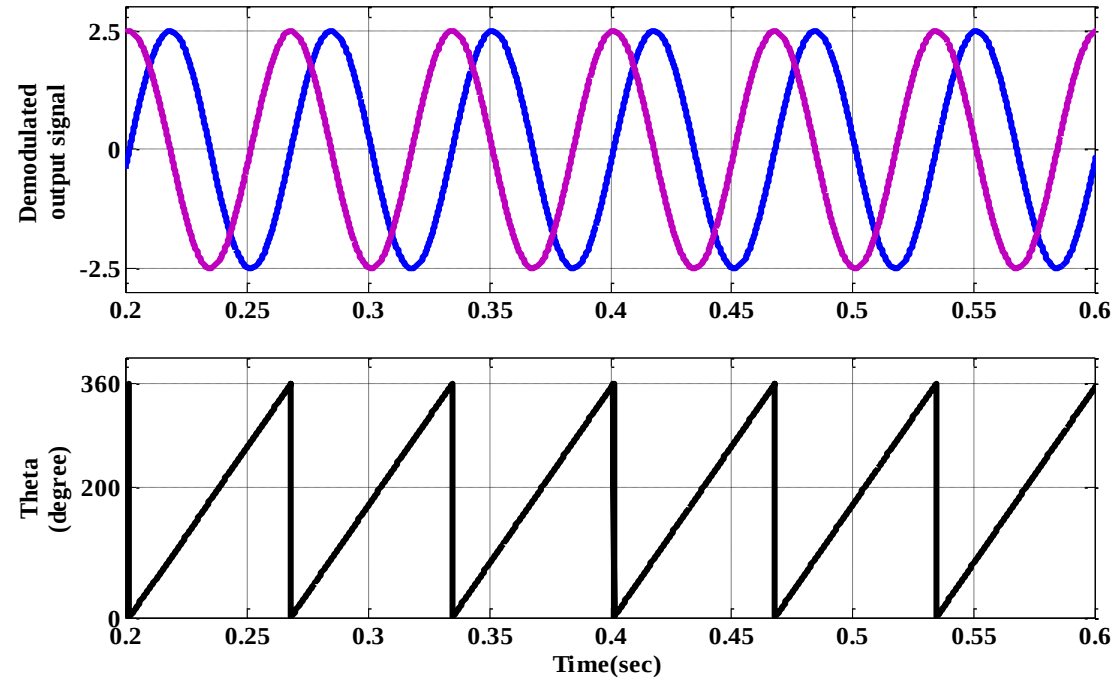

Figure 3.10 Simulation results of the demodulated sine & cosine signal with theta

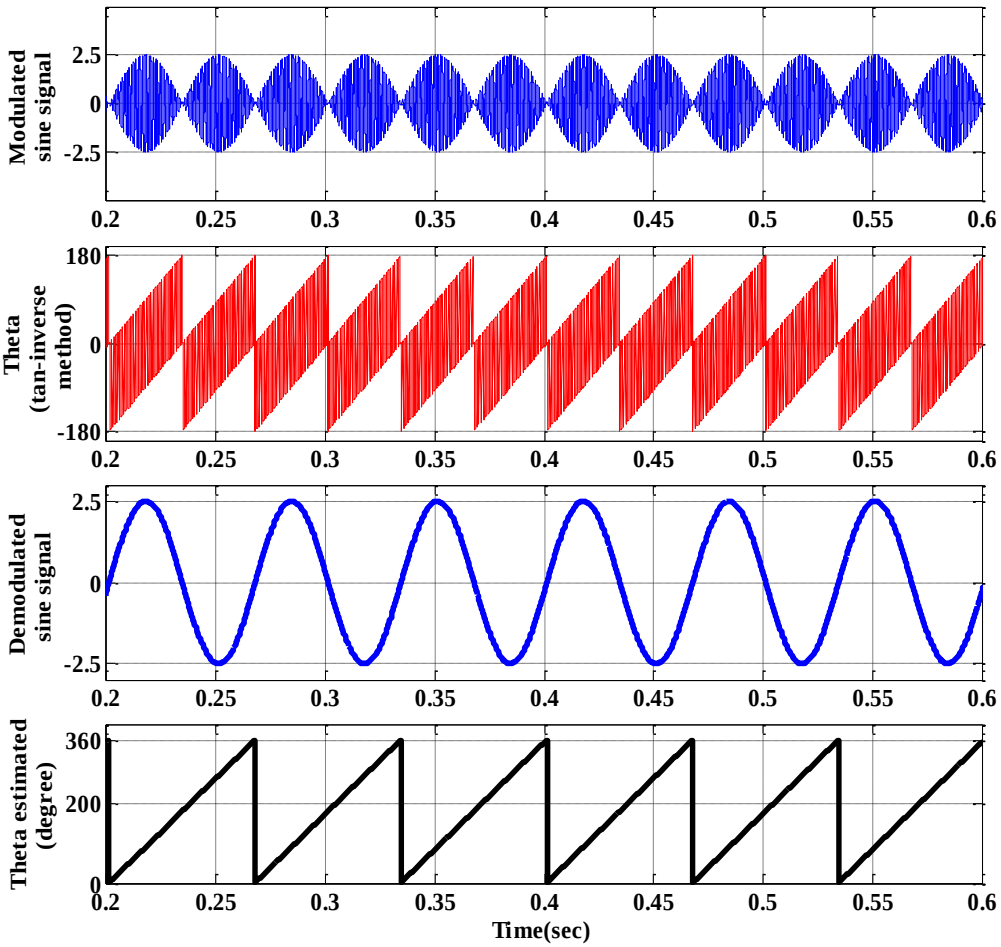

Figure 3.11 Simulation results of the modulated & demodulated sine signal with theta comparison

It is observed that conventional tan-inverse method based estimation produces oscillation in estimated position. This problem can be overcome using the position estimation algorithm from resolver. It is also noticed from the Figure 3.11 that the software based position estimation algorithm provides the accurate position for PMSM drive. Software based position estimation eliminates the use of resolver to digital converter, which in terns reduces the cost of the drive.

Table 3.1 Comparative analysis of position estimation by conventional tan-inverse method and position estimation algorithm from resolver

Conventional tan-inverse method	Position estimation algorithm from resolver
Oscillation are more	Oscillation free
-180^{o} to $+ 180^{o}$ rotation is estimated	Complete 360^{o} shaft rotation is estimated
Accurate position sensing is difficult	Estimate accurate position
Modulated signal based estimation	Demodulated signal based estimation

3.3 Vector control of PMSM Drive

The vector controlled PMSM drives draw the key attention in the variable speed drives, replacing the traditional scalar-controlled drives. Accurate position sensing plays the vital role to implement the vector control in PMSM drive with fast dynamic response, good speed regulation and high efficiency [117]. The vector control is based on transformation of a three phase time and speed dependent system into a two co-ordinate (d and q) time invariant system, which makes the PMSM structure similar to that of a DC machine [2], [6]. Vector controlled machines need two components as input references: first is the torque component (aligned with the q co-ordinate) and second is the flux components (aligned with d co-ordinate).

The input excitation to machine from stator side is done to separate torque and flux channels by vector control. The vector control of PMSM is derived from the dynamic model of PMSM considering the currents as inputs. Three-phase currents are−

$$i_{as} = i_s \sin\left(\omega_r t + \delta\right) \tag{3.8}$$

$$i_{bs} = i_s \sin\left(\omega_r t + \delta - \frac{2\pi}{3}\right) \tag{3.9}$$

$$i_{cs} = i_s \sin\left(\omega_r t + \delta + \frac{2\pi}{3}\right) \tag{3.10}$$

Where ω_r , is the electrical rotor speed, δ, is the angle between stator current phasor and rotor field and known as torque angle. The rotor field travels at speed same as rotor speed which is ω_r electrical rad/sec. In PMSM direct control of torque becomes complicated due to inherent coupling effects. Decoupling between torque and flux producing components can be provided by vector control algorithm and it also makes the control easier. Vector or decoupling control makes the dynamics of ac drives similar to that of dc drives, and with current control, problems of the conventional stability limit of ac machine does not arise.

The stator currents in rotor reference frame are obtained as given in Equation (3.11)

$$\begin{bmatrix} i_{ds} \\ i_{qs} \end{bmatrix} = \frac{2}{3}\begin{bmatrix} \sin\theta_r & \sin\left(\theta_r - 120\right) & \sin\left(\theta_r + 120\right) \\ \cos\theta_r & \cos\left(\theta_r - 120\right) & \cos\left(\theta_r + 120\right) \end{bmatrix}\begin{bmatrix} i_a \\ i_b \\ i_c \end{bmatrix} \tag{3.11}$$

The stator currents can be expressed as−

$$\begin{bmatrix} i_{ds} \\ i_{qs} \end{bmatrix} = i_s \begin{bmatrix} \cos\delta \\ \sin\delta \end{bmatrix} \tag{3.12}$$

It is to be observed that d-axis and q-axis currents are constant in rotor reference frame, as the torque angle δ is constant for a given load torque. The rotor flux is on the d-axis of machine, and which is on the rotor and rotating with the angular velocity ω_r electrical rad/sec from a stationary reference point termed as stator reference frame. The components of stator current phasor on rotating d-axis and q-axis (rotor reference frame) are constant for a given stator current phasor and given torque angle. The stator current component only along d-axis produces flux, and hence named as flux-producing component of stator current and can be denoted as i_f. This current partially contributes the d-axis flux and remaining part of rotor flux is contributed by permanent magnets (PMs). The generated PM flux can be assumed to be generated by an equivalent current source i_f.

The component of stator current which is in quadrature to rotor flux produces the torque in interaction with rotor flux, so called torque-producing component i_T, which is similar to armature current in case of DC machine. So the d-axis and q-axis components of stator current can be represented as−

$$i_{ds} = i_f \tag{3.13}$$

$$i_{qs} = i_T \tag{3.14}$$

The permanent magnets can be placed in two different ways on the rotor. As discussed in the chapter 1. Depending on the placement they are classified as follows:

iii) Interior permanent magnet motor.

iv) Surface permanent magnet motor

3.3.1 Interior Permanent Magnet Synchronous Motor Drive

In interior PMSM, the equivalent air gap is not uniform. This provides saliency effect. As a result, the quadrature-axis synchronous inductance of IPM is larger than its direct-axis inductance, i.e., $L_q > L_d$. Due to saliency effect in addition to the magnetic torque, reluctance torque is produced by IPM motor [22]. Vector control has been implemented in terms of zero d-axis current control (ZDAC) and Maximum torque per ampere control (MTPA) in IPMSM. The vector control strategy has been discussed below.

3.3.1.1 Zero Direct Axis Current Control

The torque angle is defined as the angle between the q-axis current and the d-axis in the rotor reference frame. This angle is maintained at 90^0 in the case of the ZDAC control strategy. The ZDAC control strategy is the extensively utilized control strategy by the industry. The d-axis current is effectively maintained at zero in this control strategy [2]. The main advantage of this control strategy is that it simplifies the torque control mechanism by linearizing the relationship between torque and current. This means that a linear current controller results in linear control over torque as well. In dc motors the current and magnet fields are always maintained at an angle of 90^o. Therefore, the ZDAC control strategy makes a PMSM operate in a similar way to the dc motor. This makes the ZDAC control strategy very attractive for industrial designers who are used to operating dc motor drives.

The stator voltage equations are:

$$V_{qs}^r = r_q i_{qs}^r + p\lambda_{qs}^r + \omega_r \lambda_{ds}^r \tag{3.15}$$

$$V_{ds}^r = r_d i_{ds}^r + p\lambda_{ds}^r - \omega_r \lambda_{qs}^r \tag{3.16}$$

$$V_{0s}^r = r_s i_{0s}^r + p\lambda_{0s}^r \tag{3.17}$$

Where r_q and r_d are the q-axis and d-axis winding resistance. V_{qs}^r and V_{ds}^r are the q and d-axis voltage in the rotor reference frame. i_{qs}^r and i_{ds}^r are the q and d-axis current. The flux linkages are

$$\lambda_{qs}^r = L_q i_{qs}^r \tag{3.18}$$

$$\lambda_{ds}^r = L_d i_{ds}^r + \lambda_m^r \tag{3.19}$$

By considering constant magnet flux linkage $p\lambda_m^r = 0$

$$V_{qs}^r = (r_s + pL_q) i_{qs}^r + \omega_r L_d i_{ds}^r + \omega_r \lambda_m^r \tag{3.20}$$

$$V_{ds}^r = (r_s + pL_d) i_{ds}^r - \omega_r L_q i_{qs}^r \tag{3.21}$$

In rotor reference frame the generated electromagnetic torque in terms of stator quantities is as–

$$T_e = \frac{3}{2} \cdot \frac{P}{2} (\lambda_{ds}^r i_{qs}^r - \lambda_{qs}^r i_{ds}^r) \tag{3.22}$$

Which upon substitution of the flux linkages in terms of the inductance and current

$$T_e = \frac{3}{2}.\frac{P}{2}\{(\lambda_m^r i_{qs}^r + (L_d - L_q) i_{ds}^r i_{qs}^r\} \tag{3.23}$$

The equivalent circuit of permanent magnet synchronous motor in rotor reference frame is shown in Figure 3.12.

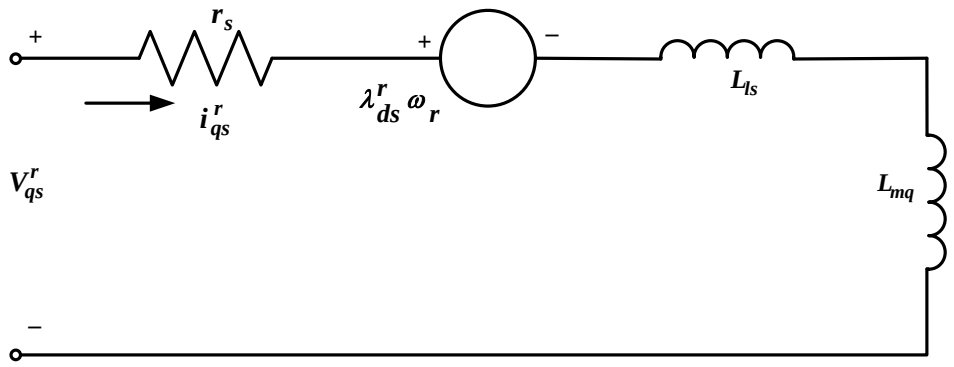

(a)

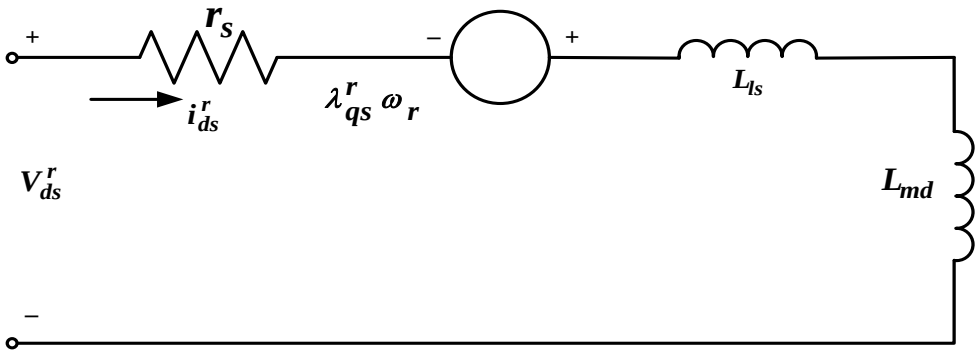

(b)

Figure 3.12 (a) & (b) Equivalent circuit of PMSM in rotor reference frame

If the d-axis current made equal to zero

$$i_{ds}^r = 0 \tag{3.24}$$

By putting this value in equation for electromagnetic torque we can get

$$T_e = \frac{3}{2}.\frac{P}{2}\lambda_m^r i_{qs}^r \tag{3.25}$$

Rewriting this equation it can be seen that q axis current become a function of torque.

$$i_{qs}^{r} = \frac{T_e}{\left(\frac{3}{2}\right).\left(\frac{P}{2}\right)\lambda_m^r} \tag{3.26}$$

The constant torque angle phasor diagram is shown in Figure 3.13.

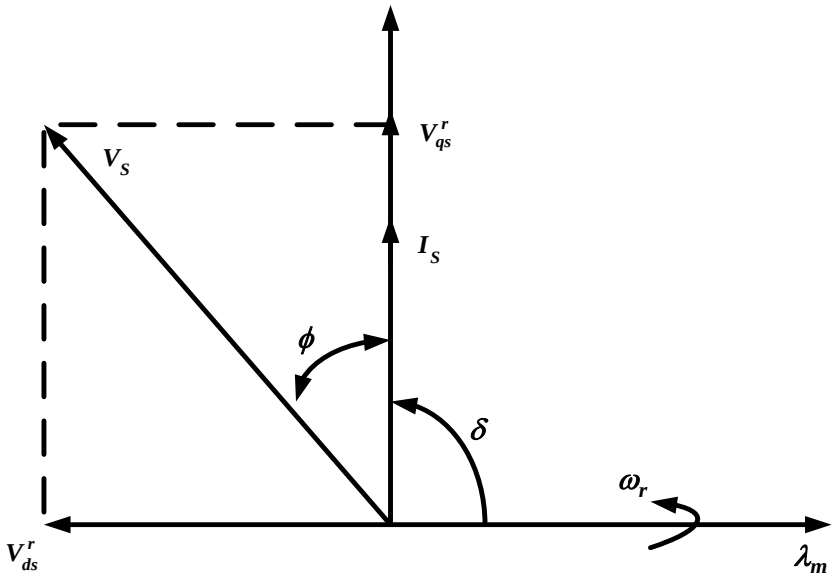

Figure 3.13 Constant torque-angle or Zero d-axis control phasor

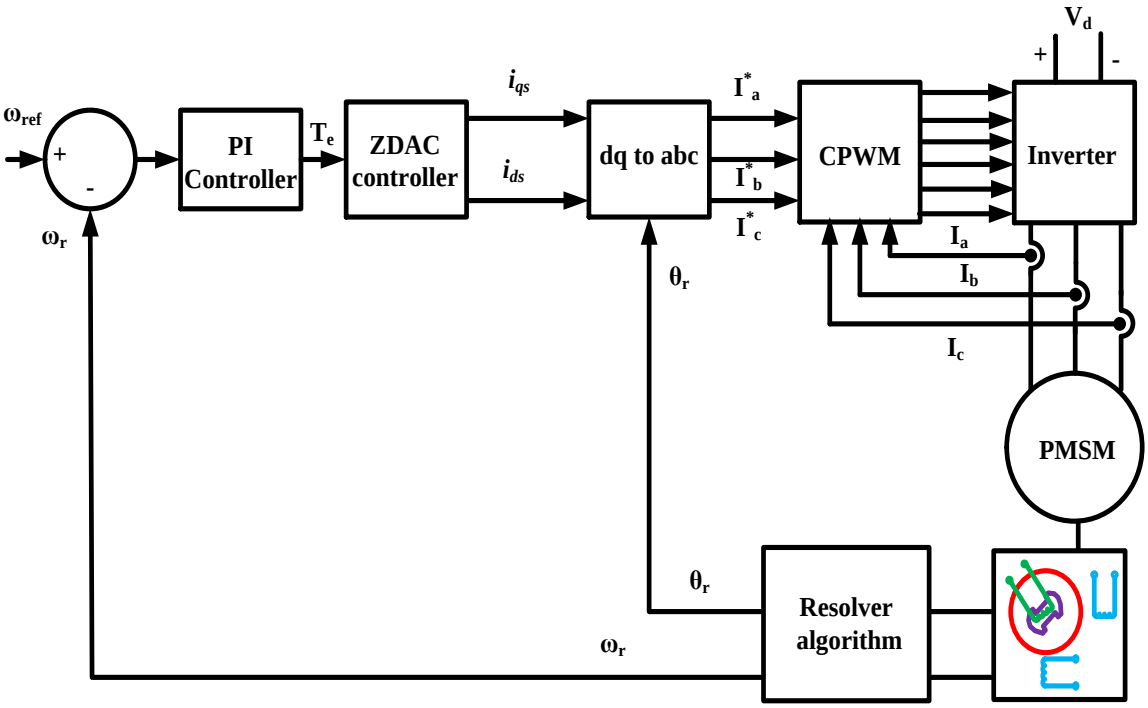

Figure 3.14 Block diagram of ZDAC controlled PMSM drive

The block diagram of the ZDAC controlled PMSM drive is shown in Figure 3.14. The speed error is fed to PI controller. PI controller generates the torque command T_e. From this torque

command the current command i_{qs} are generated with the help of equation (3.24) and i_{ds} make equal to zero. The absolute position signal θ_r convert the rotor rotating frame signal into stationary reference frame signal I^*_a , I^*_b and I^*_c . The gate signal of the inverter is generated using the error between the two current I^*_a , I^*_b and I^*_c and actual current I_a , I_b and I_c with the carrier based PWM controller.

3.3.1.2 Simulation Results of IPMSM with ZDAC Control.

The performance of the drive at different operating condition has been investigated in MATLAB/Simulink environment. The specification of the simulated interior permanent magnet motor has been shown in the Table 3.2.

Table 3.2 Specification of simulated Motor

stator phase resistance	0.9585Ω
Torque Constant	1.092
d-axis inductance (L_d)	0.004987 H
q-axis inductance (L_q)	0.005513 H
Moment of inertia (J)	0.0006329kg-m2
No of poles	8
DC link voltage	300 V

The transient response of the speed control loop obtained for step variation in reference speed from 900 rpm to 1200 rpm is shown in Figure 3.15. The response is plotted for different sets of K_P and K_I. The ripples/over shoot and settling time corresponding for these chosen values of K_P and K_I are summarized in Table 3.3. The comparison of various transient response curves show that for K_P = 0.0046 and K_I= 0.08, the system is giving best results. The drives has been simulated with speed PI controller gain K_P= 0.0046 and K_I= 0.08.

Table 3.3 Performance for different controller parameters

Case	K_P	K_I	Settling Time	Ripples/Overshoot
1	K_P =0.0004	K_I =0.0.03	1.5s	more/ large deep
2	**K_P =0.0046**	**K_I =0.08**	**0.25s**	**less**
3	K_P =0.00042	K_I =0.00079	1.6s	very less
4	K_P =0.00045	K_I =0.0076	1.4s	more

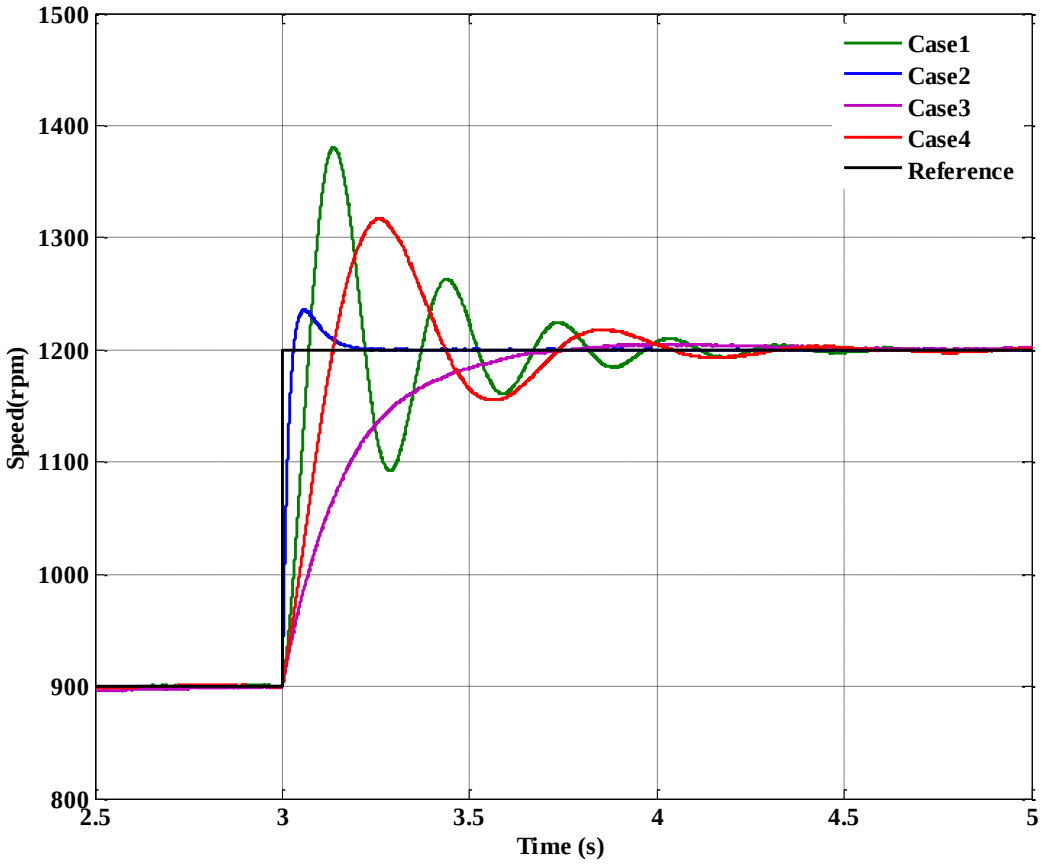

Figure 3.15 Transient response of speed controller for IPMSM drive

The starting response of the drive has been shown in the Figure 3.16. Trace 1 in the Figure 3.16 represents the threes phase stator current. Trace 2 represents the speed of the motor in rpm and trace 3 denotes the torque developed by the machine. The reference value of speed is kept 900 rpm and the motor is started with no load. It is observed that the motor reaches its reference speed value. Initial starting torque is high. The stator current is also high at the time of starting.

The performance of the drive with ZDAC control at speed changing operation also has been investigated. A change in speed reference of 300 rpm has been applied. The speed reference increased from 900rpm to 1200 rpm. The response of the drive at speed changing operation has been shown in the Figure 3.17. At 2 sec the speed reference has been increased from 900 rpm to 1200 rpm. At this time the torque is increased by the motor to reach the reference speed. Due to that the stator current is also slightly increased at that time. The torque reduced once the reference speed value reached. The performance of the drive at speed decreasing condition has been shown in the Figure 3.18. At time 2 sec the speed reference value is changed from 900 rpm to 600 rpm. To reach the reference speed value the torque of motor decreased to negative value. The torque regains its original value once the reference speed value reached.

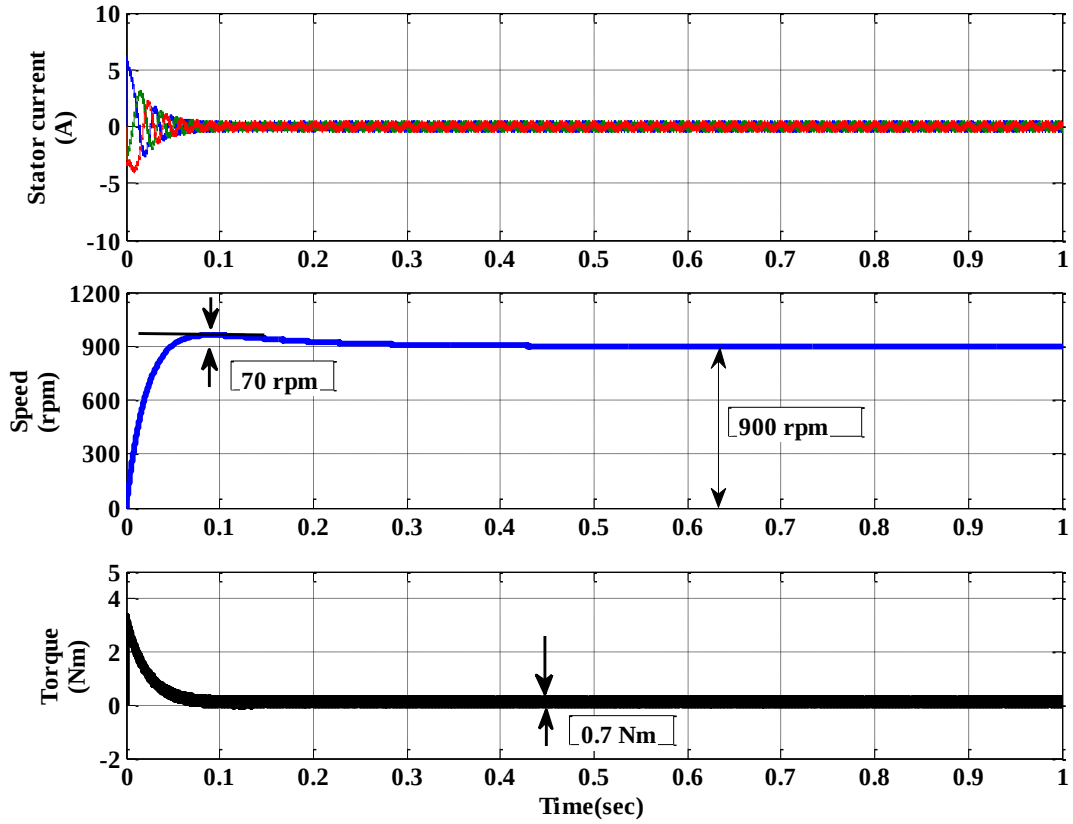

Figure 3.16 Response of the drive at starting

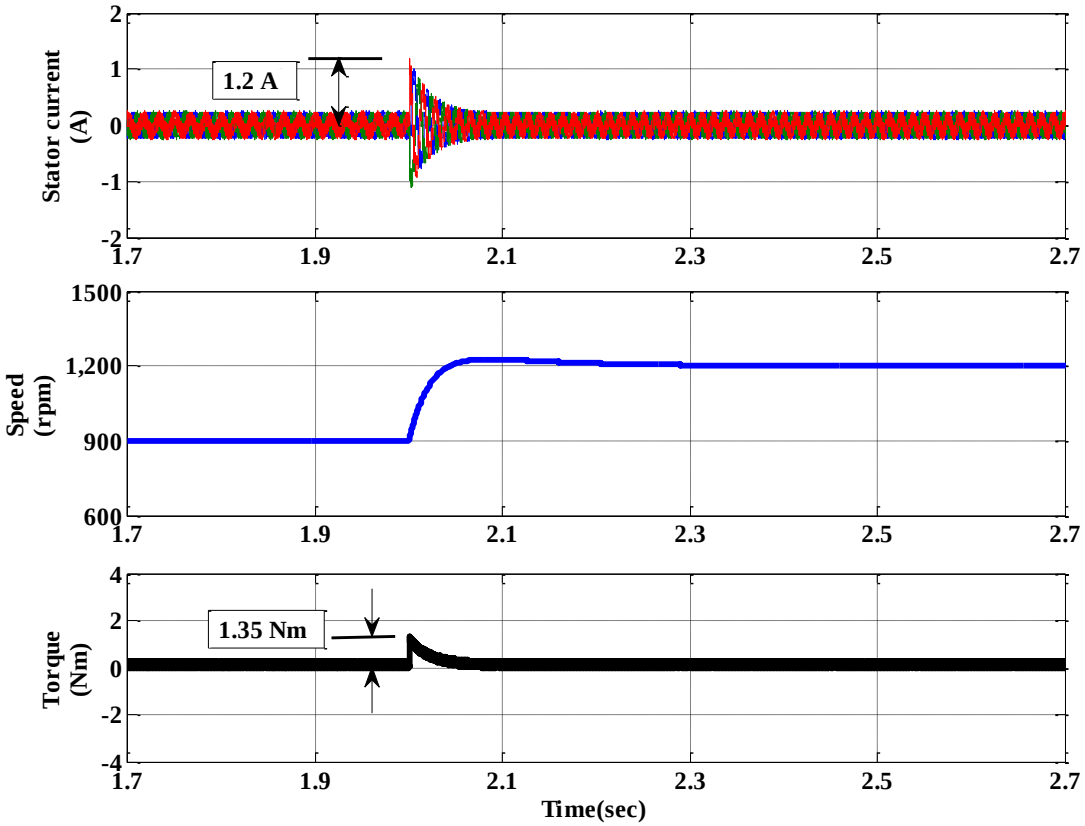

Figure 3.17 Response of the drive at speed increasing

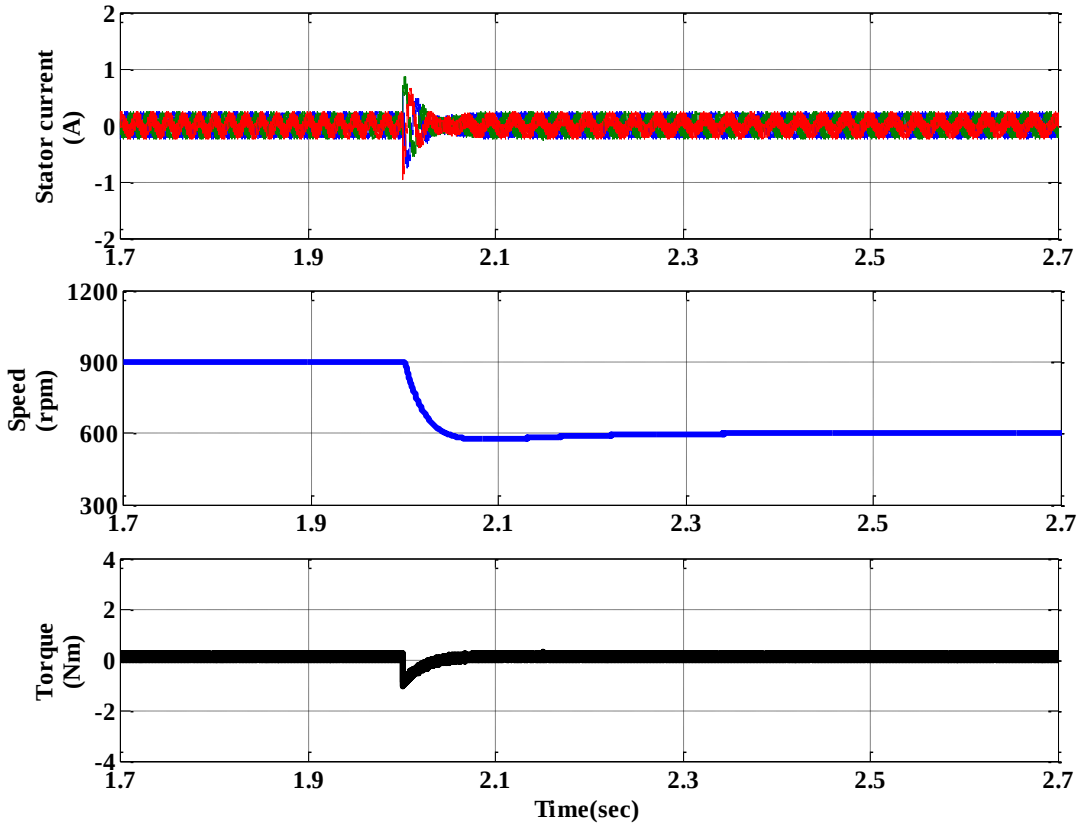

Figure 3.18 Response of the drive at speed decreasing

To investigate the performance under loading condition a load of 4Nm is applied to the motor and simulation results are obtained. The response of the drive at increasing load has been shown in the Figure 3.19. A step load of 4 Nm is applied at 2 sec. It is observed that the stator current is increased at the time of loading. It is also observed that there is dip in the speed response. This dip is due to the loading. This speed response reaches the reference due to the closed loop operation of the drive. The magnified view of the torque response and stator current has been shown in the Figure 3.20. Trace 1 indicates the stator current and trace 2 represents the torque. The performance of the drive at decreasing load has been shown in the Figure 3.21. At 2 sec the 4Nm load has been removed. Trace 1 indicates the stator current at loading condition and the load removal condition. Due to the step change in load the speed is slightly increased and reaches again the reference speed value. So it is observed that the ZDAC controlled IPMSM drive gives the desired performance at different operating condition.

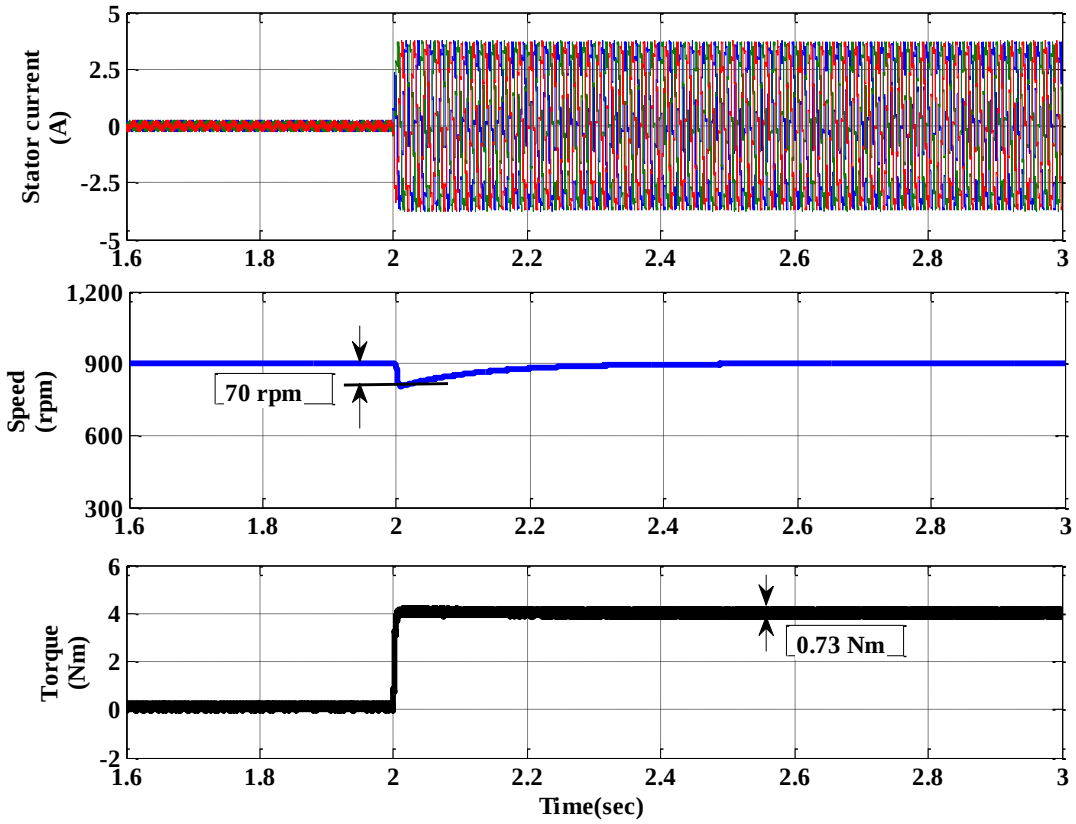

Figure 3.19 Response of the drive at load increasing

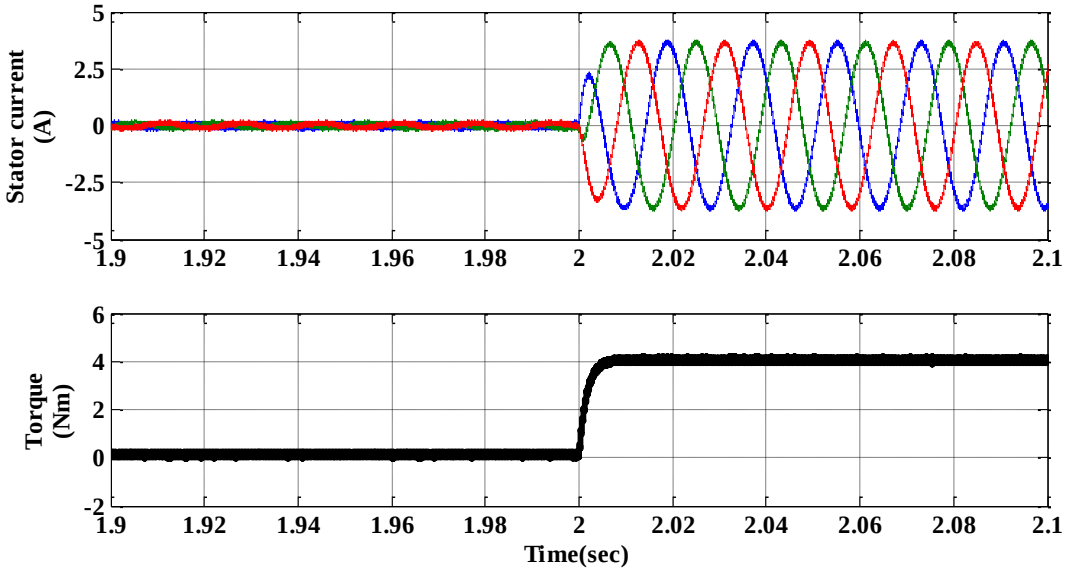

Figure 3.20 Magnified view of load current and torque

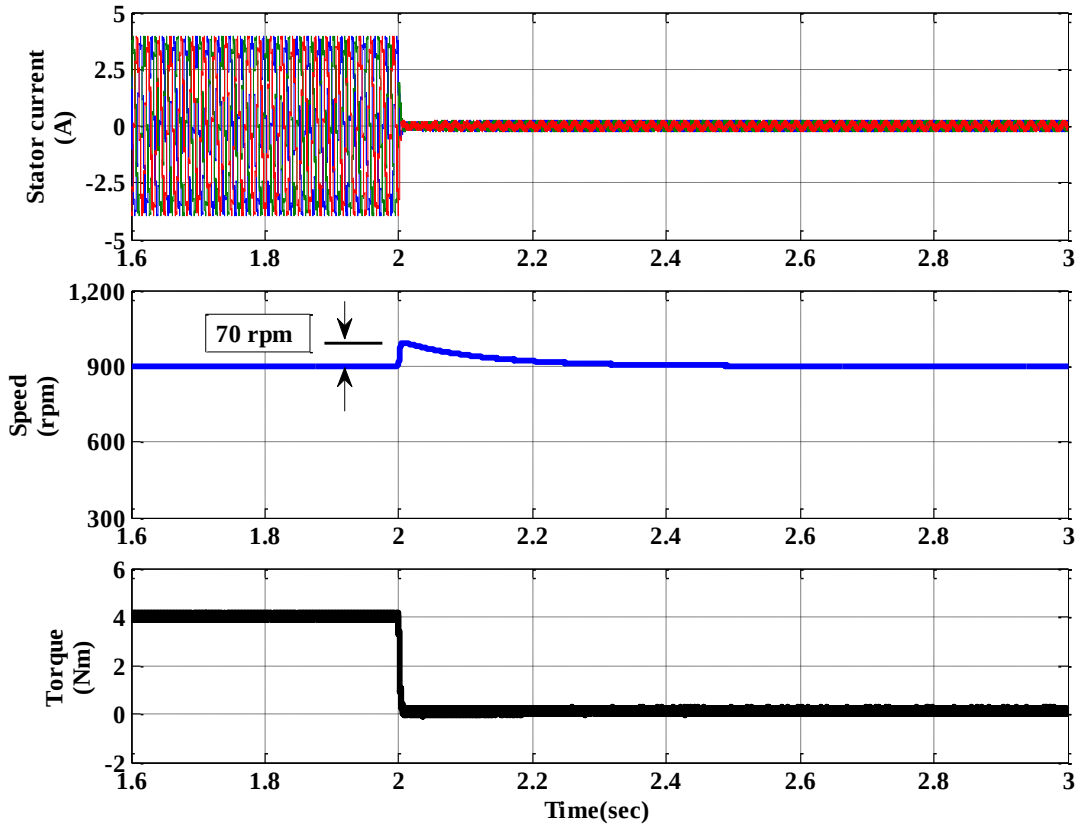

Figure 3.21 Response of the drive at load decreasing

3.3.2 Maximum Torque Per Ampere Control

The MTPA control strategy provides maximum torque for a given current. So the copper loss for a given torque is minimized. This implies a minimum converter rating as well as its maximum efficiency. The torque developed in IPM machine has two component i) The torque due to the interaction of the magnetic flux and q-axis stator current and ii) The reluctance torque.

The constant torque loci of the interior permanent magnet synchronous motor (IPMSM) in terms of the two-axis stator current i_{qs} and i_{ds} is plotted from the torque equation. The MTPA trajectory on constant torque loci is shown in the Figure 3.22 with blue lines; where on every locus the point which is nearest to the origin corresponds to the minimum stator current. So the maximum torque per ampere curve is obtained by connecting the point's dcbaoa′b′c′d′. For positive torque the polarity of i_{qs} is positive whereas the polarity of i_{ds} is negative. Negative i_{ds} contributes an additive reluctance torque component. The polarity of torque can be reversed by reversing the current i_{qs}. On each value of constant torque loci there is a

MTPA point. Corresponding to that point, i_{qs} and i_{ds} is calculated. So from MTPA lookup table i_{qs} and i_{ds} are generated for different torque value. The block diagram of MTPA controlled PMSM drive is shown in Figure 3.23.

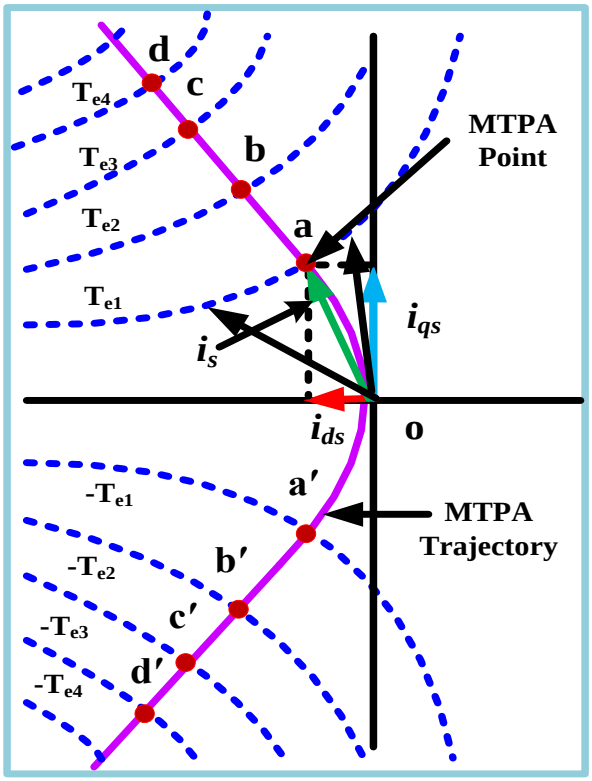

Figure 3.22 MTPA Trajectory on constant torque loci

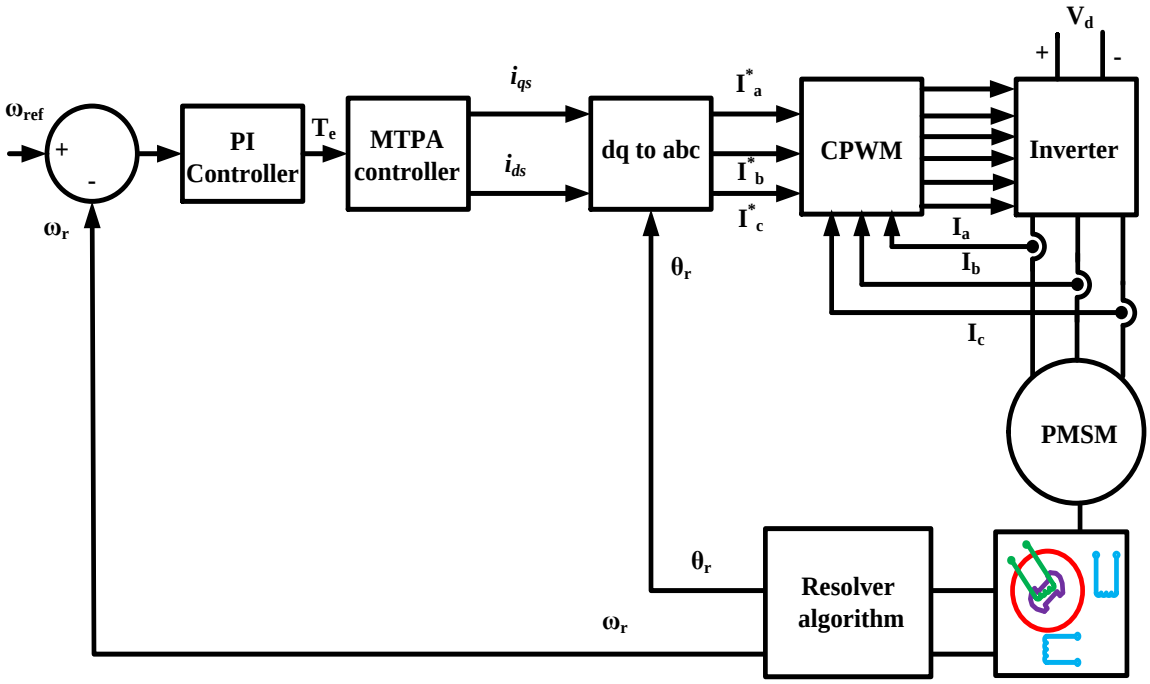

Figure 3.23 Block diagram of MTPA controlled PMSM drive

The IPMSM drives with maximum torque per ampere control has been simulated with speed PI controller gain K_P= 0.0046 and K_I= 0.08 and the specification of the simulated motor is given in the Table 3.2. The starting response of the drive at no load condition has been shown in the Figure 3.24. Trace 1 in the Figure 3.24 represents the stator current. Trace 2 represents the speed of the motor in rpm and trace 3 denotes the torque developed by the machine. 900 rpm is kept as the reference speed value. It is observed that the starting torque is high. The stator current is also high at the time of starting. A change in speed reference of 300 rpm has been applied to the drive and the performance of the drive with MTPA control has been investigated. The response of the drive at speed changing operation has been shown in the Figure 3.25. At 2 sec the speed reference has been increased from 900 rpm to 1200 rpm. At this time the torque is increased by the motor to reach the reference speed. The torque reduced once the reference speed value reached. The performance of the drive at speed decreasing condition has been shown in the Figure 3.26. At time 2 sec the speed reference value is changed from 900 rpm to 600 rpm. To reach the reference speed value the torque of motor decreased to negative value. The torque regains its original value once the reference speed value reached.

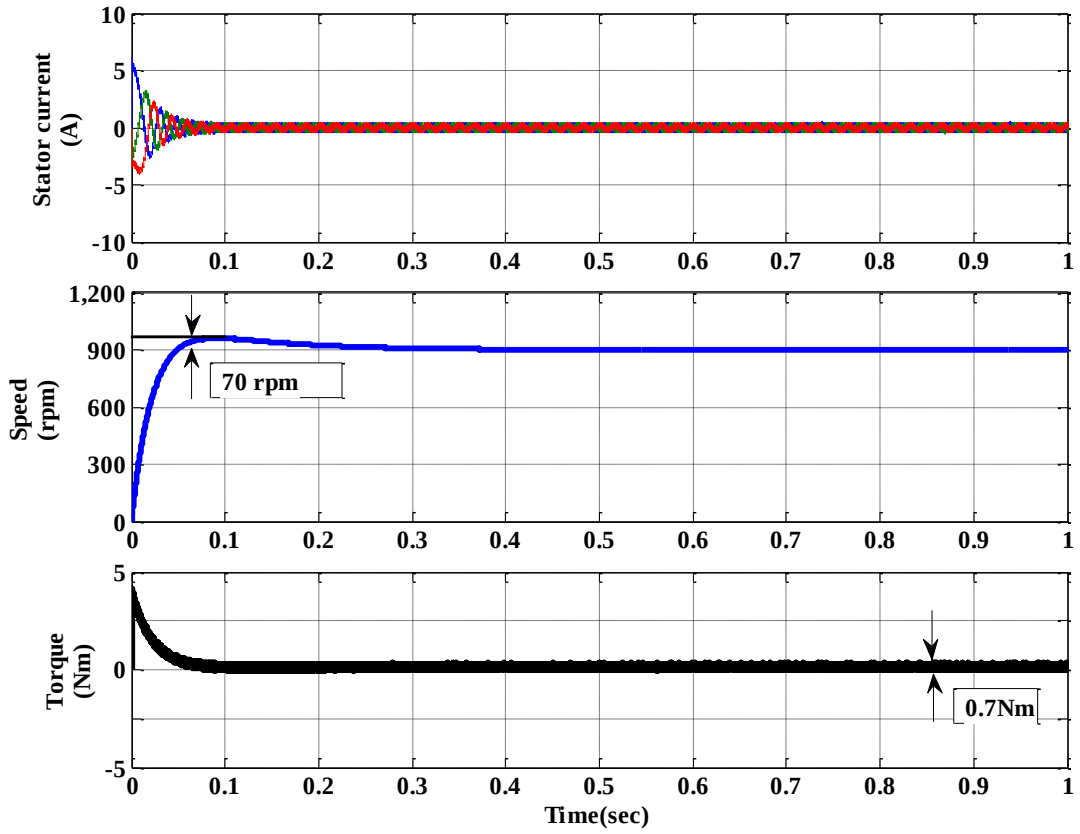

Figure 3.24 Response of the drive at starting

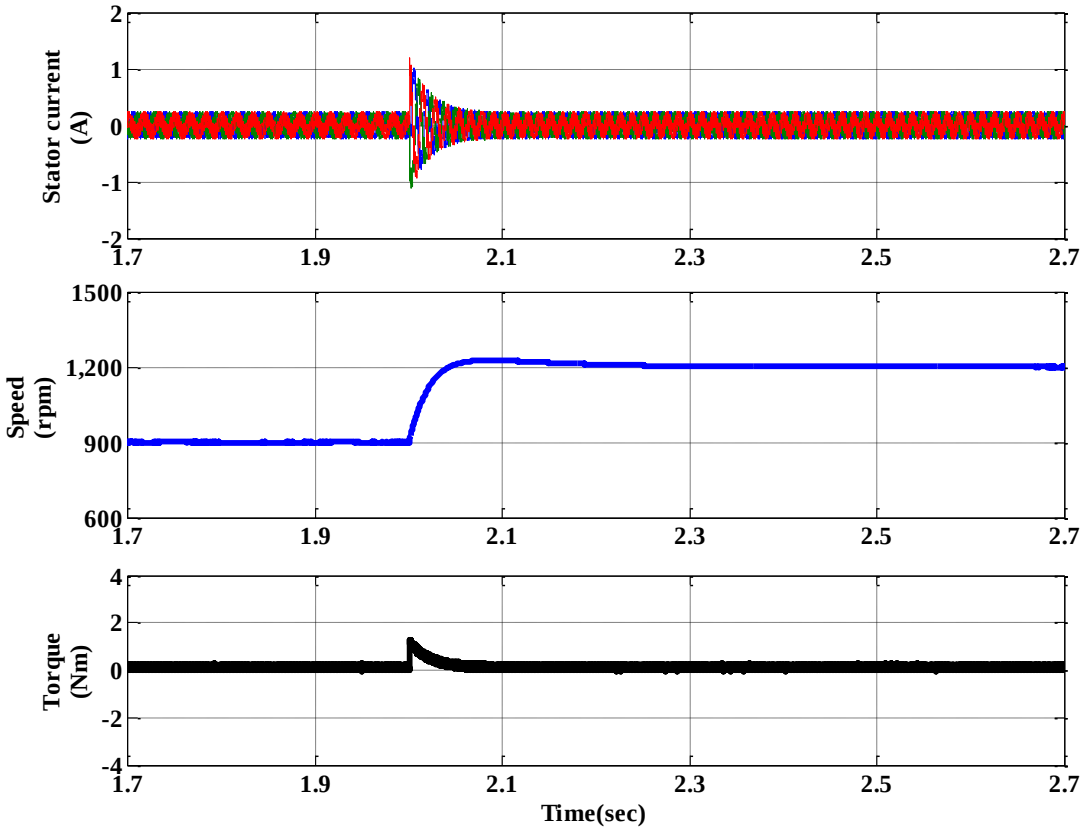

Figure 3.25 Response of the drive at step change (increasing) in speed reference

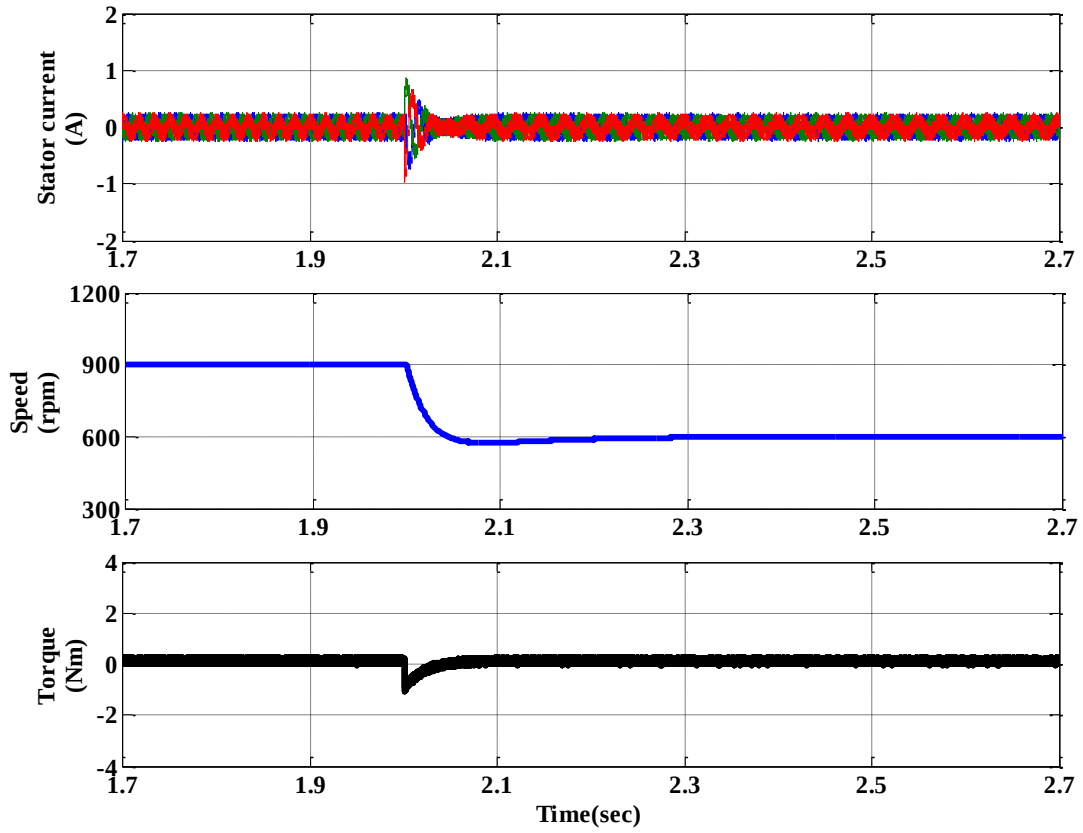

Figure 3.26 Response of the drive at step change (decreasing) in speed reference

Further investigation has been done at loading condition. A load of 4Nm is applied to the motor and simulation results are obtained. The response of the drive at increasing load has been shown in the Figure 3.27. A step load of 4 Nm is applied at 2 sec. It is observed that the stator current is increased at the time of loading. This speed response reaches the reference due to the closed loop operation of the drive. In MTPA control of PMSM it is noticed from the simulation result that d axis current value is not zero as in case of conventional ZDAC control. It is also analyze that q- axis current in MTPA mainly produces the required torque. The d-axis and q-axis current at loading condition has been shown in the Figure 3.28. The performance of the drive at decreasing load has been shown in the Figure 3.29. At 2 sec the 4Nm load has been removed. Trace 1 indicates the stator current at loading condition and the load removal condition. Due to the step change in load the speed is slightly increased and reaches again the reference speed value. So it is observed that the MTPA controlled IPMSM drive gives the desired performance at different operating condition.

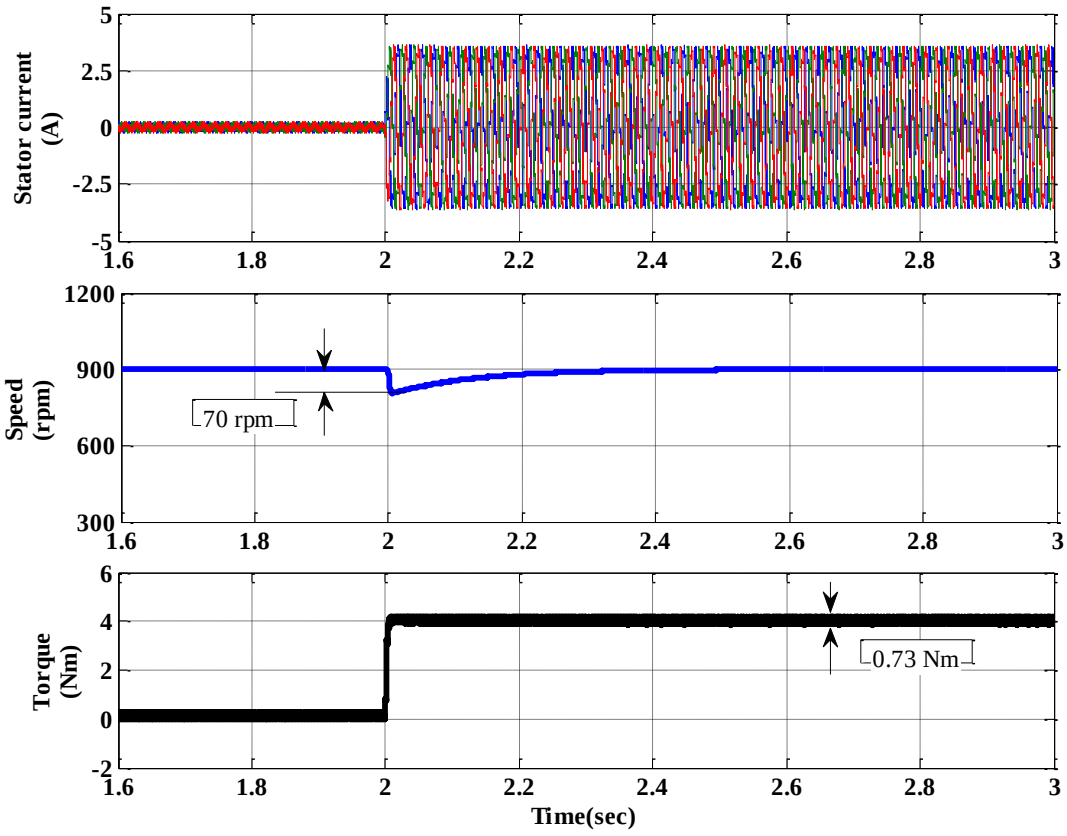

Figure 3.27 Response of the drive at load increasing

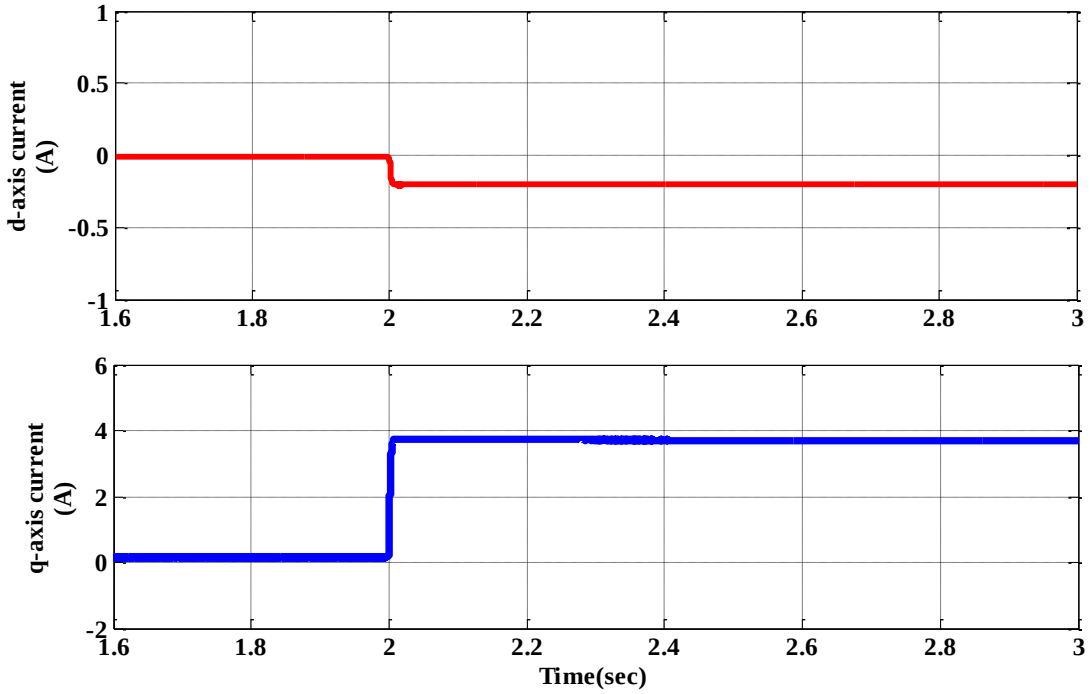

Figure 3.28 d- axis and q-axis current at load increasing

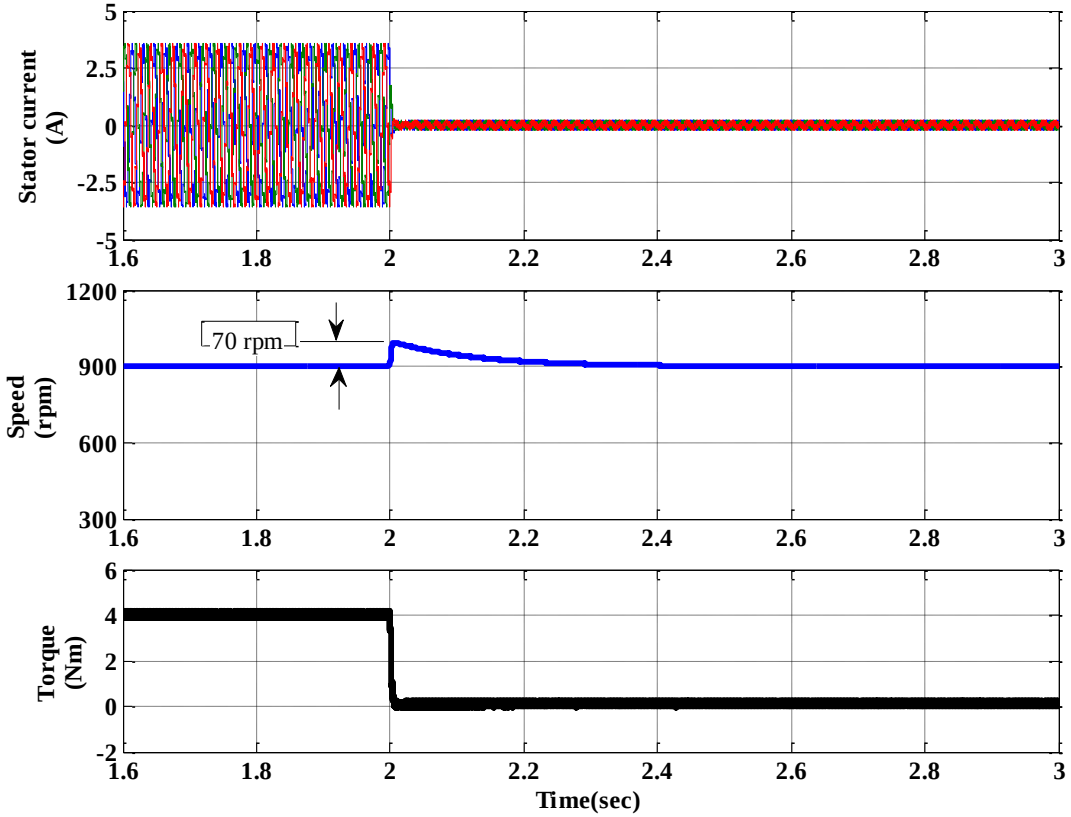

Figure 3.29 Response of the drive at load decreasing

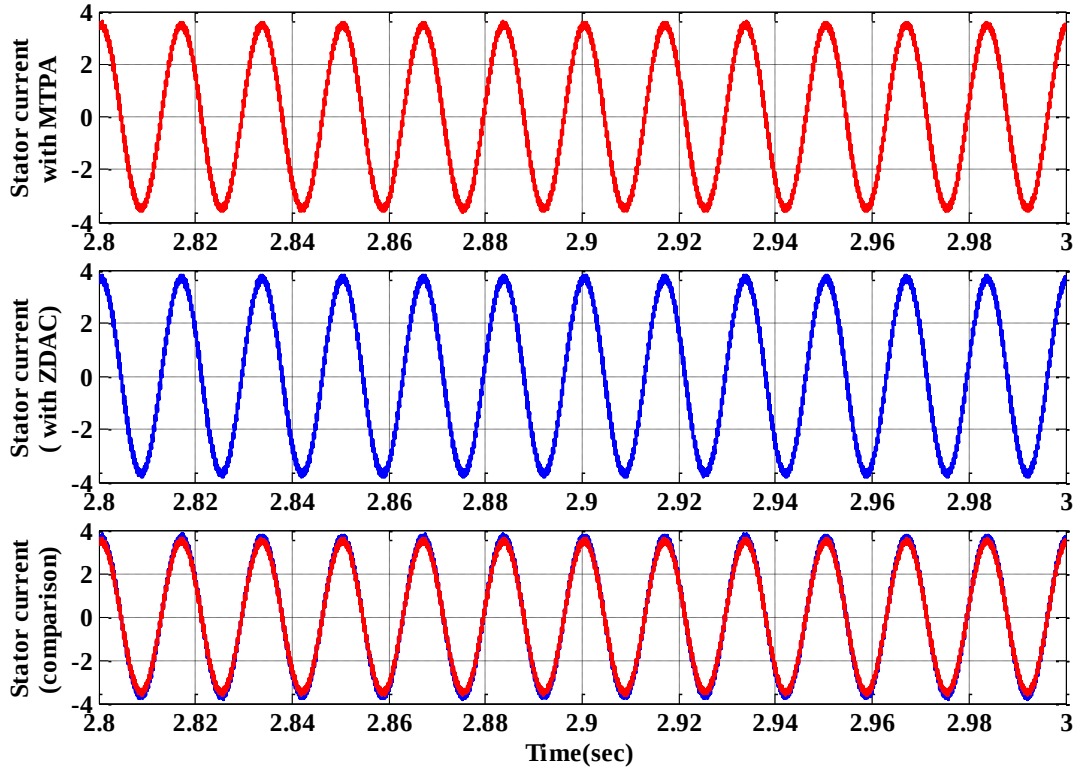

Figure 3.30 Stator current with MTPA & ZDAC control at loading condition

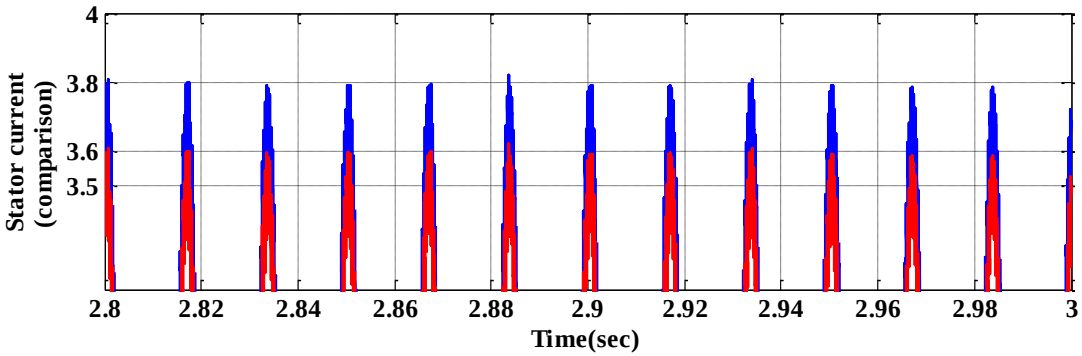

Figure 3.31 Magnified view of stator current with MTPA & ZDAC control

The stator current with two different control has been shown in the Figure 3.30. The magnified view of stator current with ZDAC and MTPA control has been shown in the Figure 3.31. It is observed that MTPA control provides the less stator current as compared to the ZDAC control. The comparative analysis of ZDAC and MTPA is presented in Table 3.4. The comparative study shows that Maximum torque per ampere control strategy in interior PMSM is efficient control as compared to zero d-axis current control. MTPA controlled PMSM gives equal torque and speed as compared to ZDAC, but at the same time MTPA reduce the stator current. Electrical power loss is minimized due to reduced stator current in MTPA. So MTPA optimizes the drive efficiency. MTPA is most suitable for high saliency motor drive. Maximum torque can be achieved without exceeding the current limit of the inverter.

Table 3.4 Comparative analysis of ZDAC Control and MTPA control

ZDAC control	MTPA Control
Stator current is high (3.8 A)	Stator current is low (3.6 A)
Efficiency less as compared to MTPA	Efficiency improves
Simple control	Complex as compared to ZDAC
Can be implemented in both IPMSM and SPMSM	Implemented in IPMSM
Stator losses are more	Stator losses are less

3.3.3 Flux-Weakening Control

The motor drive is operated with rated flux linkages up to a speed where the ratio between the induced emf and stator frequency (V/f) is maintained constant. After the base frequency, the V/f ratio is reduced due to the limit of the inverter dc voltage source which is fixed. Above rated speed the induced emf will exceed the maximum input voltage, making the flow of current into machine phases impractical. To overcome this situation, the induced emf is constrained to be less than the applied voltage by weakening the air gap flux linkages. The flux-weakening is made to be inversely proportional to the stator frequency, so that the induced emf is a constant and will not increase with the increasing speed. In permanent magnet motors, as the magnets resemble a “fixed excitation flux” source, the magnetic field cannot be varied as in a separately excited DC motor and Induction motor by controlling the field current. The principle of flux-weakening control of PMSM is to increase opposite direct axis current and use armature reaction to reduce air gap flux, which equivalently reduces flux and achieves the purpose of flux-weakening control.

3.3.3.1 Field Weakening Control with MTPA

The MTPA control strategy is utilized in high performance applications where efficiency is important. This control strategy provides maximum torque for a given current thus minimizes copper losses for a given torque. So the converter rating is minimum as well as its efficiency is maximum. If we considered the operation of a IPMSM, it can run in two mode of operation as follows:

1. Constant torque region.
2. Constant power region or flux weakening region.

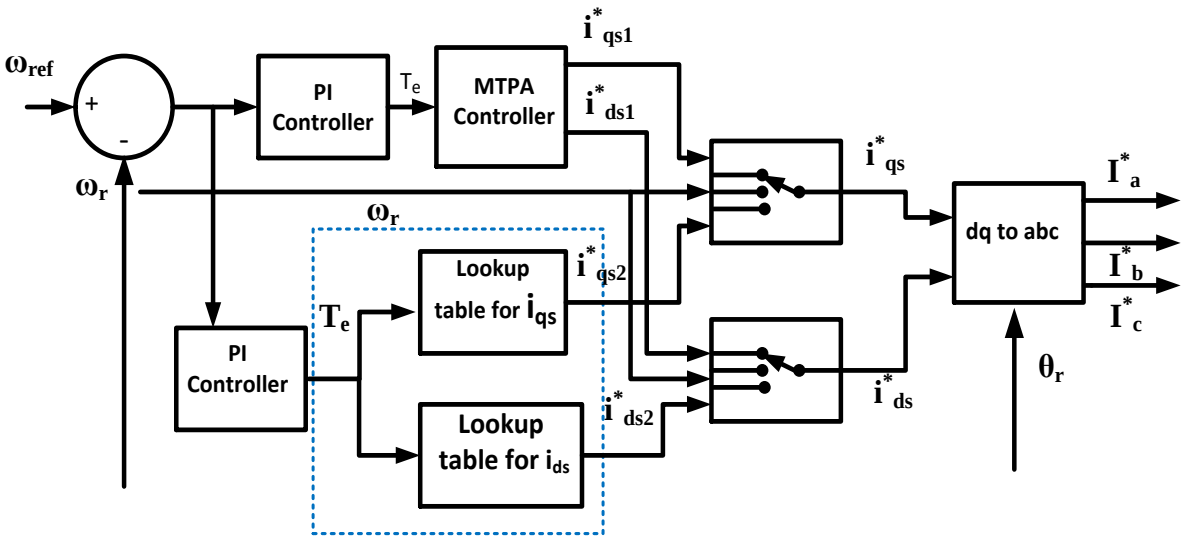

Figure 3.32 Operation of flux weakening controller with MTPA controller

MTPA control can be implemented in constant torque region whereas flux weakening control is implemented in constant power region. The operation of flux weakening controller with MTPA control is presented in Figure 3.32. So for getting wide speed operation it is needed to run the motor in constant torque region as well as constant power region.

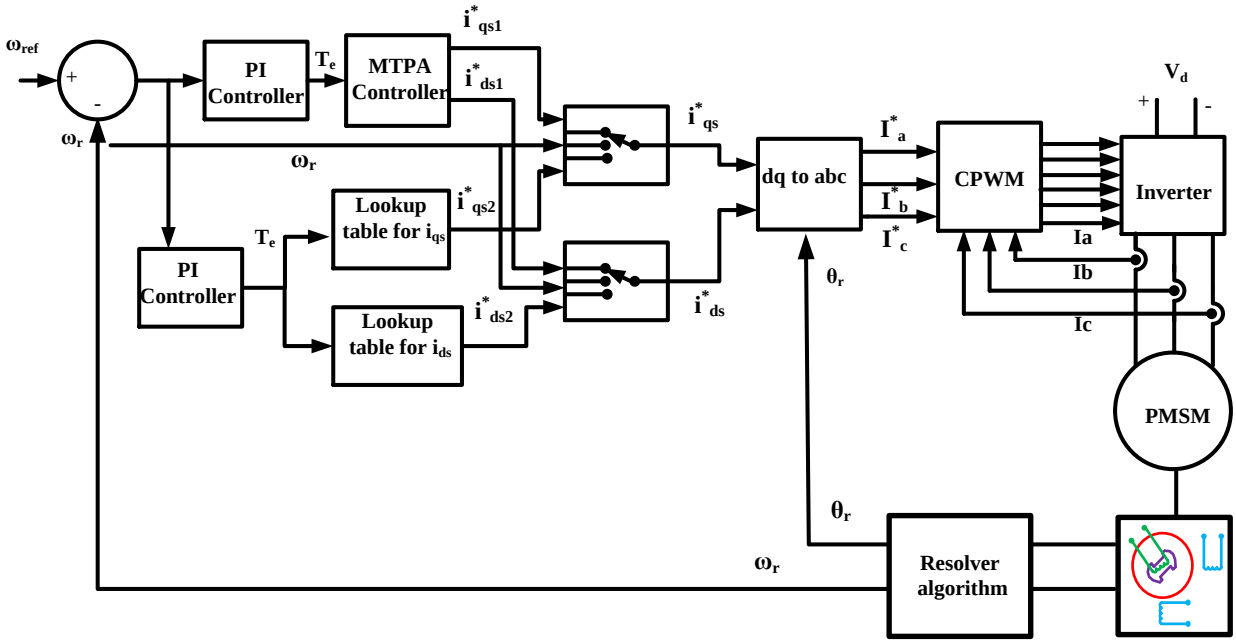

Figure 3.33 Block diagram of PMSM drive for wide speed range operation.

Up to base speed motor will run in constant torque region above base speed motor will run in flux weakening region. The block diagram of complete drive system for wide speed range of operation is shown in Figure 3.33. For constant torque region operation we will consider MTPA control and above base speed operation the control will transferred to flux weakening

controller. For constant torque region operation PI controller will generate the torque reference on the basis of speed error. Based on the torque reference q-axis and d-axis current can be generated from the MTPA lookup table. The current value say i^*_{qs1} and i^*_{ds1}. So up to base speed these current value i^*_{qs1} and i^*_{ds1} will generate I^*_a , I^*_b and I^*_c current command.

Above base speed operation the torque command can be generated according to the flux weakening algorithm. Based on this torque command q-axis and d-axis current can be generated from the lookup table, which is generated by flux weakening algorithm. The current value say i^*_{qs2} and i^*_{ds2} . So above base speed these current value i^*_{qs2} and i^*_{ds2} will generate I^*_a , I^*_b and I^*_c current command. Based on the speed value the switching status is selected for generating the i^*_{qs} and i^*_{ds}. Based on I^*_a , I^*_b and I^*_c current command and actual current I_a , I_b and I_c the gate signal of the inverter can be generated with the help carrier based PWM controller.

3.3.3.2 Development of Flux Weakening Control Algorithm

The flux wakening control of IMPSM drive provides the wide speed range of operation. The control algorithm has been developed in MATLAB to achieve wide speed range of operation of the drive. The development of the control algorithm has been discussed below.

The fundamental stator voltage can be relate with dc link voltage as

$$V_s = \frac{2V_d}{\pi} \tag{3.27}$$

$$V^r_{qs} = (r_s + pL_q)i^r_{qs} + \omega_r L_d i^r_{ds} + \omega_r \lambda^r_m \tag{3.28}$$

$$V^r_{ds} = (r_s + pL_d)i^r_{ds} - \omega_r L_q i^r_{qs} \tag{3.29}$$

Where V_d the dc is link voltage of the inverter and V_s is the stator voltage. This is related with steady state V^r_{qs} and V^r_{ds} component of stator phase voltage as:

$$V_s = \sqrt{(V^r_{qs})^2 + (V^r_{ds})^2} \tag{3.30}$$

Where,

$$V^r_{qs} = \omega_r L_d i^r_{ds} + \omega_r \lambda^r_m \tag{3.31}$$

$$V^r_{ds} = -\omega_r L_q i^r_{qs} \tag{3.32}$$

Equation (3.31) and (3.32) can be derived from Equation (3.28) and (3.29) respectively at steady state condition. In this case the stator resistance drop is neglected.

And stator current can be related as:

$$(I_s)^2 = (i_{qs}^r)^2 + (i_{ds}^r)^2 \tag{3.33}$$

This equation can be considered as an equation of a circle. Rewriting the equation we can get the following equation.

$$I_s = \sqrt{(i_{qs}^r)^2 + (i_{ds}^r)^2} \tag{3.34}$$

Rewriting the equation 3.30 with substituting the values V_s ,V_{qs}^r and V_{ds}^r.

$$\frac{4V_d^2}{\pi^2} = (\omega_r L_d i_{ds}^r + \omega_r \lambda_m^r)^2 + (-\omega_r L_q i_{qs}^r)^2 \tag{3.35}$$

This can be modified to form

$$\frac{(i_{ds}^r + \frac{\lambda_m^r}{L_d})^2}{(\frac{2V_d}{\pi\omega_r L_d})^2} + \frac{(i_{qs}^r)^2}{(\frac{2V_d}{\pi\omega_r L_q})^2} = 1 \tag{3.36}$$

This is an equation of an ellipse in the form

$$\frac{(i_{ds}^r - C)^2}{(A)^2} + \frac{(i_{qs}^r)^2}{(B)^2} = 1 \tag{3.37}$$

Where,

$$A = \frac{2V_d}{\pi\omega_r L_d} \ , \ B = \frac{2V_d}{\pi\omega_r L_q} \text{ , and } C = -\frac{\lambda_m^r}{L_d}$$

For any value of rotor speed, the stator current phasor is directed away from the origin of the q-d plane to a point on the ellipse, but there is a maximum voltage it must be always located inside the ellipse. Such an ellipse is called as voltage-limit ellipse. The voltage-limit ellipse has been shown in the Figure 3.34 with magenta lines. The ellipse is constructed from the equation (3.36) using the machine parameter. For each value of rotor speed there will be a voltage-limit ellipse. The axis of the ellipse is inversely proportional to the rotor speed. The

equation (3.33) represents the equation of a circle. This circle can be considered as a current limit circle. To achieve maximum torque in flux weakening region, the machine must be operated in both voltage limited and current limited mode simultaneously, which can be described as the intersection of the voltage and current limit.

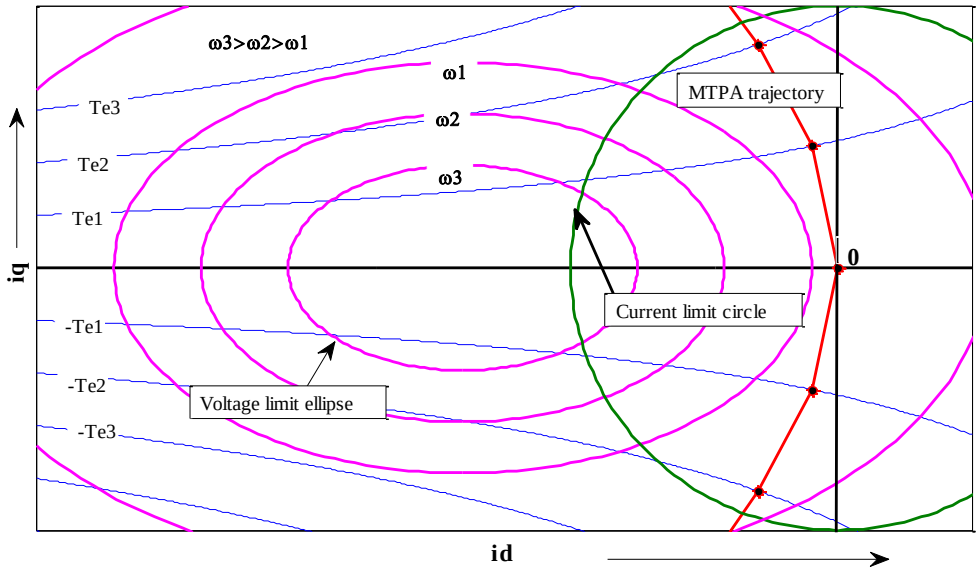

Figure 3.34 Current limit, voltage limit and the operating region of motor

The algorithm has been developed in MATLAB. The programming code has been written in MATLAB. The control algorithm can be described with the help of flowchart as shown in Figure 3.35.

The generation of voltage limit ellipse

The voltage limit ellipse can be generated from equation (3.37) for different value of speed.

The generation of current limit circle

The current limit circle can be generated from equation (3.33). In this study the maximum current limit has considered as 10 A.

Torque command generation on speed changing

In flux weakening mode of operation the IPMSM has less maximum torque capability than constant mode and this maximum torque capability inversely proportional to the speed. From equation (3.37), for a specific voltage and speed, a set of q-d axis current value is obtained, which forms an ellipse. Now out of these set of q-d axis current value those value is considered which satisfy the equation (3.34). It means the q-d axis current is limited by maximum stator current (10A). Using this value of q-d axis current the torque command is generated for different speed. From above discussion it is noticed that based on the current,

speed and available dc link voltage, how much maximum torque is produced by the motor is obtained.

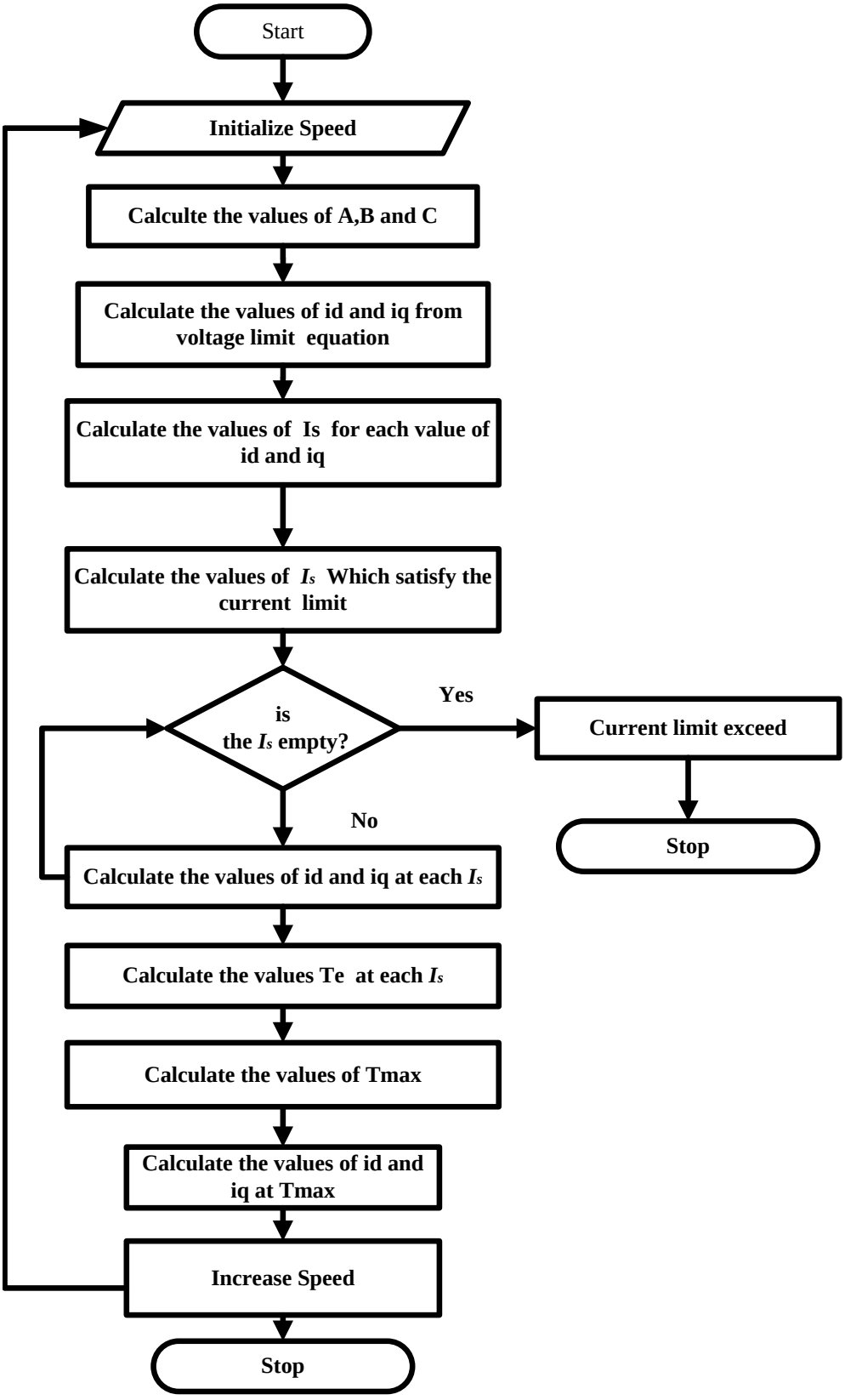

Figure 3.35 Flowchart of the Flux weakening control algorithm

Current command generation

In flux weakening mode q-d axis current is calculated based on the speed, torque and dc link voltage. This implies that the crossover point of constant torque loci and voltage limited ellipse for a speed gives a set q-d axis current. This q-d axis current is used to produce I^*_a , I^*_b and I^*_c current command.

3.3.3.3 Simulation Results of Field Weakening Control

The performance of the interior permanent magnet synchronous motor in wide speed rang of operation has been investigated using flux weakening control. The specification of the simulated motor has been given in Table 3.2. The maximum current limit has been considered as 10A. High speed operation has been achieved in terms of MTPA control with Flux weakening algorithm without exceeding the voltage and current limit. The performance of the IPMSM drive for high speed operation with varying load condition also has been studied. Flux weakening controller for IPMSM is very useful for the drive where both the mode of operation such as constant torque and constant power is required. Flux weakening algorithm has been implemented for high speed operation. In this control scheme q-axis and d-axis current is generated from lookup table. Flowchart has been given for generating the lookup table. The simulation result shows the different speed range operation of IPMSM Drive. The performance of the drive for wide speed range of operation at no load has been shown in the Figure 3.36.

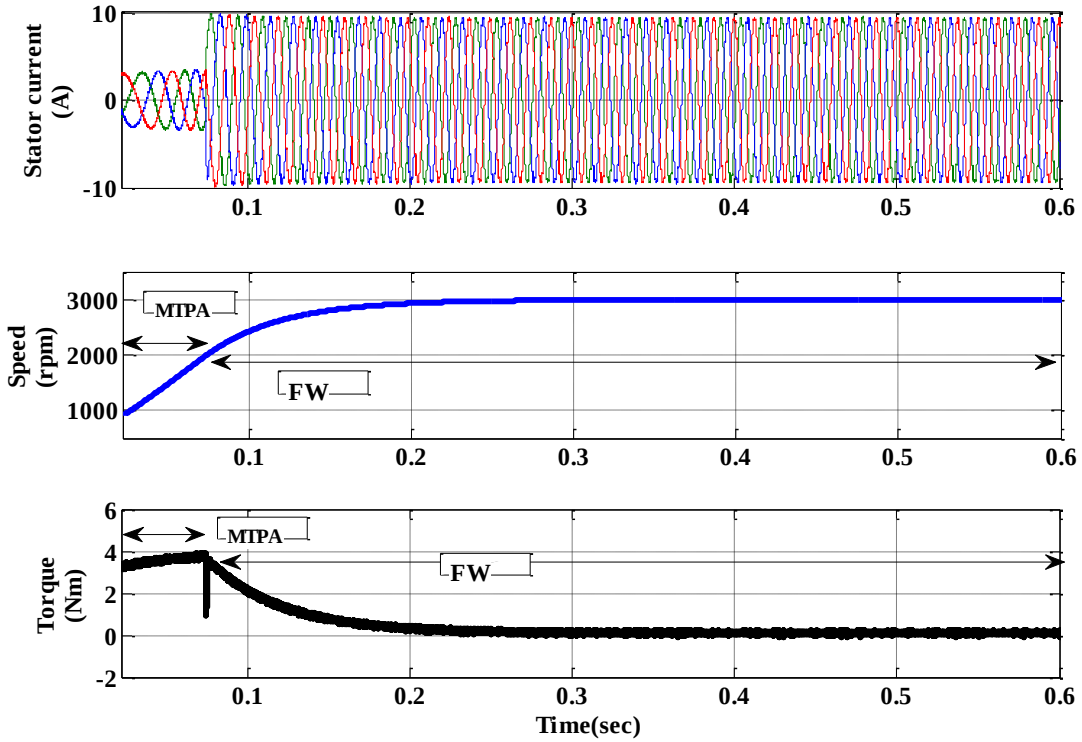

Figure 3.36 Simulation result of PMSM drive in wide speed range of operation

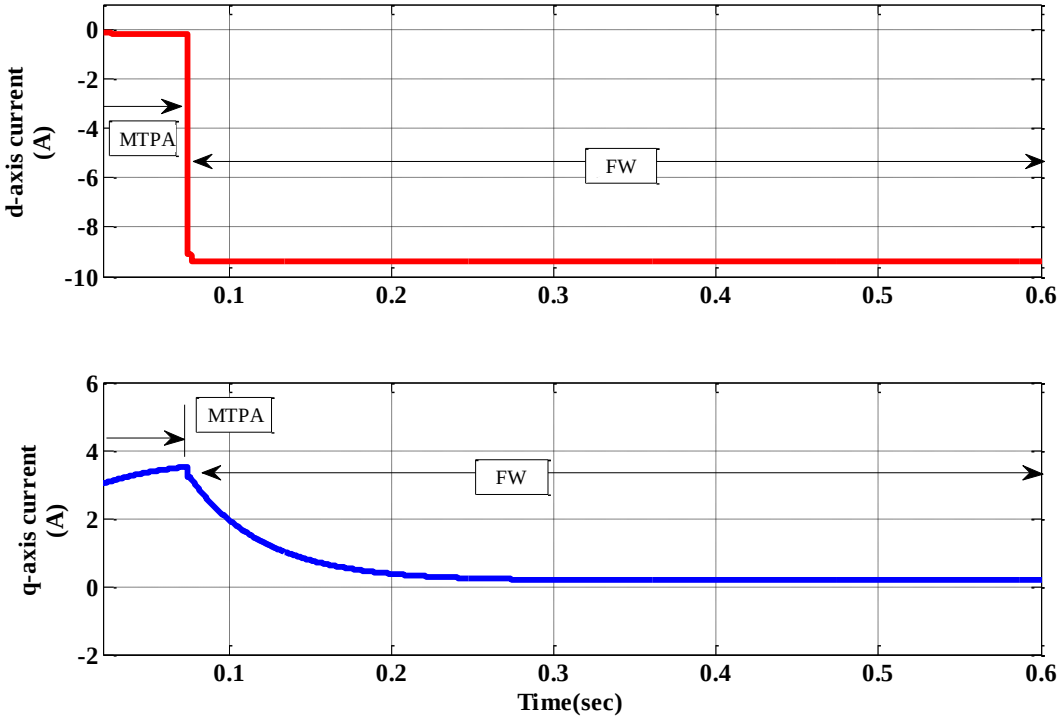

Figure 3.37 Simulation result of d-axis and q-axis current in wide speed range of operation

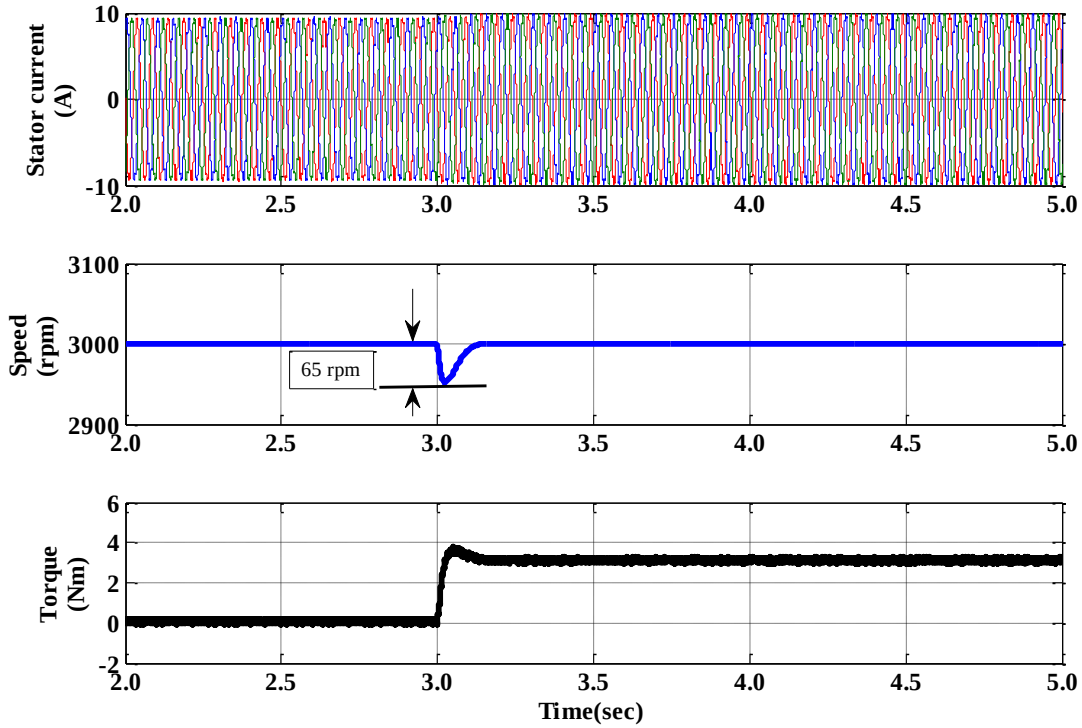

Figure 3.38 Simulation result of the drive at loading condition in wide speed range of operation

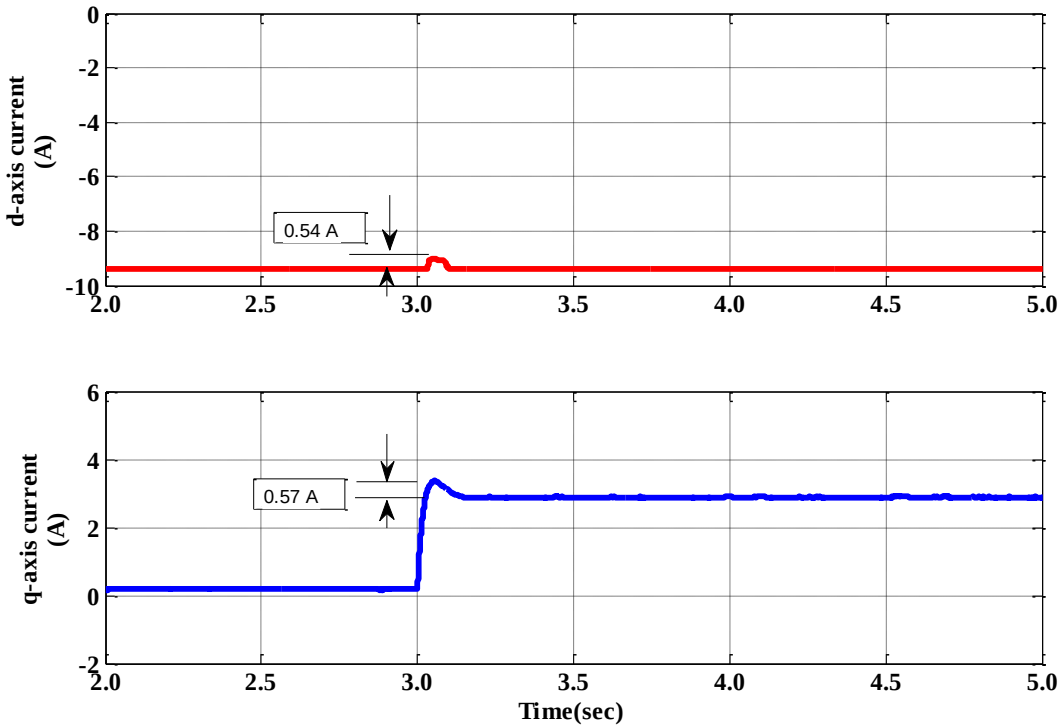

Figure 3.39 Simulation result of d-axis and q-axis current at loading in wide speed range of operation

It is observed that the motor is running for wide speed range i.e from 1000 rpm to 3000rpm. The base speed of the motor is 2000rpm. The MTPA controller is operated upto 2000rpm speed. When motor reaches the speed above 2000rpm the flux weakening controller is operated. Shifting of the controller is done automatically using speed feedback. Based on the motor speed the appropiate controller will take place. It is also observed that upto the base speed the motor runs in constant torque mode and above base speed the motor opeates in flux weakening mode. The d-axis current and q-axis current for wide speed range of operation is shown in the Figure 3.37. Trace 1 represents the d-axis current and trace 2 represents the q-axis current. It is noticed that in flux weakening mode the d-axis current is negetive. In flux wekening mode it is also noticed that wide speed of operation is achived without exceeding the current limit. The performance of the drive in flux wekening mode with loading condition has been shown in the Figure 3.38. At time 3 sec 3Nm load has been applied to the motor. It is observed that the speed is also maintained at 3000rpm with application of load without excedding the current limit. The corresponding d-axis and q-axis current at loading condition is shown in the Figure 3.39. It is noticed that the d-axis current is negetive .

3.3.4 Surface Permanent Magnet Motor

In surface permanent magnet synchronous motor (SPMSM) the quadrature -axis synchronous inductance of SPM equals its direct-axis inductance, i.e., $L_q=L_d$. As a result, only electromagnetic torque can be produced by SPM motor, which arises from the interaction of the magnetic flux and the quadrature-axis current component of stator currents. Due to the non-saliency the MTPA control is not applicable in surface permanent magnet motor. So the vector control in terms of zero d-axis current control (ZDAC) is implemented in SPMSM.

3.3.4.1 Zero Direct Axis Current Control

The control technique is same as discussed in the section 3.3.1.1. But the permanent magnet structure has been considered as surface mounted. The ZDAC control strategy is the most widely utilized control strategy by the industry. The d-axis current is effectively maintained at zero in this control strategy. The main advantage of this control strategy is that it simplifies the torque control mechanism by linearizing the relationship between torque and current. This means that a linear current controller results in linear control over torque as well. In dc motors the current and magnet fields are always maintained at an angle of 90^o. Therefore, the ZDAC control strategy makes a PMSM operate in a similar way to the dc motor. This makes the ZDAC control strategy very attractive for industrial designers who are used to operating dc motor drives.

3.3.4.2 Performance Evaluation of SPMSM with ZDAC Control

The performance of the drive at different operating condition has been investigated. The Specification of the simulated surface permanent magnet motor has been shown in the Table 3.5.

Table 3.5 Specification of simulated surface permanent magnet motor

d-axis inductance (Ld)	5.15mH
q-axis inductance (Lq)	5.15mH
Torque Constant	0.75 Nm/A
No of poles (p)	8
DC link voltage	300 V
Moment of inertia (J)	0.000062kg-m^2
Total load inertia	0.001914 kg-m^2
Damping friction	0.0041N-m/rad

The speed PI controller is tuned for the SPMSM drive system with different gain parameters. A step variation in reference speed from 900 rpm to 1200 rpm is applied and the transient response of the speed control loop is obtained for different value of K_P and K_I. The transient response plotted for different sets of K_P and K_I is shown in Figure 3.40. The ripples/over shoot and settling time corresponding for these K_P and K_I are summarized in Table 3.6. The comparison of various transient response curves show that for K_P = 0.0036 and K_I= 0.0032, the system is giving best results.

Table 3.6 Overshoots and settling times for different controller parameter at step change in reference speed in SPMSM drive

Case	K_P	K_I	Settling Time	Ripples/Overshoot
1	K_P =0.0005	K_I =0.02	1.45s	large
2	K_P =0.0003	K_I =0.0018	2.2s	Medium
3	**K_P =0.0036**	**K_I =0.0032**	**0.15s**	**very less**
4	K_P =0.00038	K_I =0.00035	3.5	less

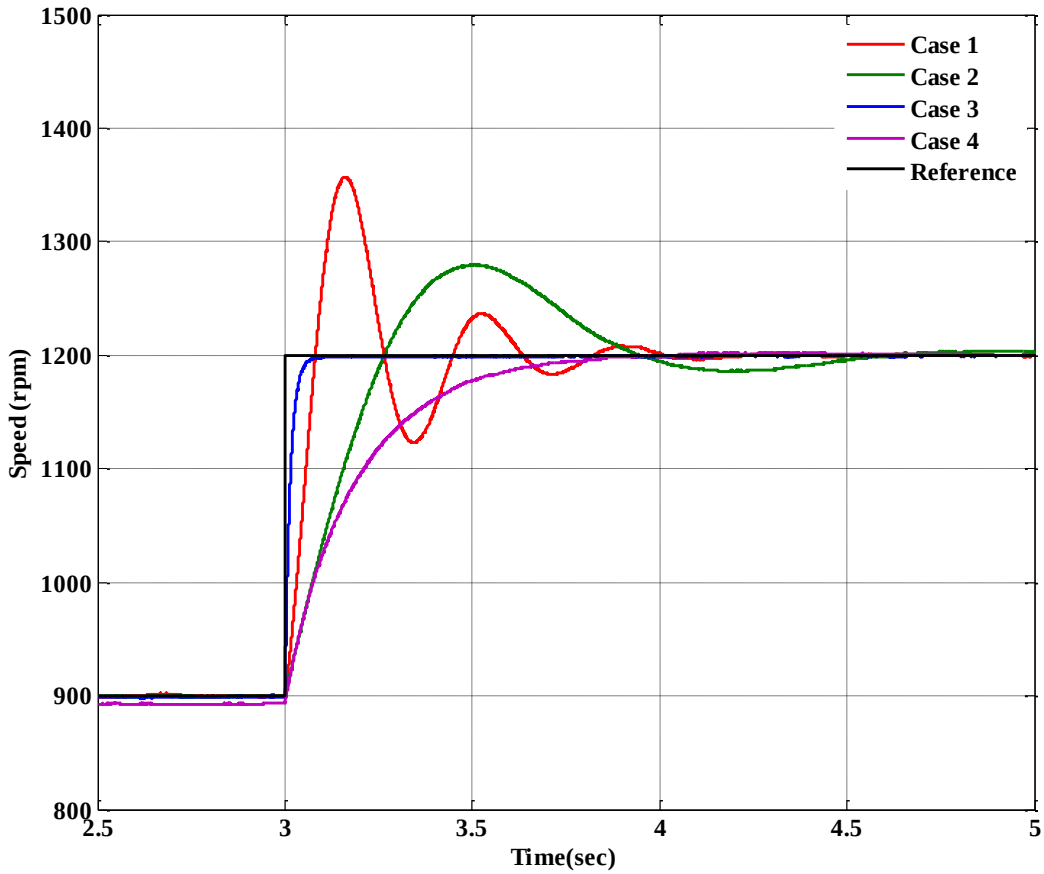

Figure 3.40 Transient response of speed controller for SPMSM drive

The drives has been simulated with K_P=0.0036 and K_I= 0.0032 Values. The starting response of the drive has been shown in the Figure 3.41. The reference value of speed is kept 900rpm and the motor is started with no load. It is observed that the motor reaches its reference speed value. Initial starting torque is high. The stator current is also high at the time of starting.

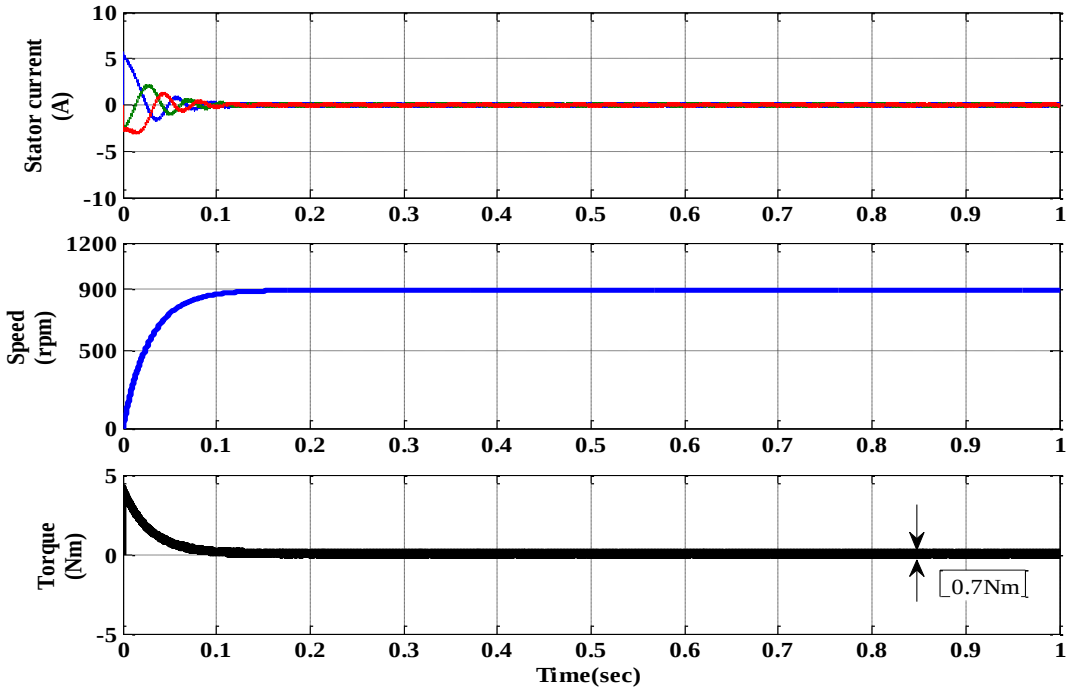

Figure 3.41 Response of the drive at starting

To investigate the performance under loading condition a load of 4Nm is applied to the motor and simulation results are obtained. The response of the drive at increasing load has been shown in the Figure 3.42. A step load of 4 Nm is applied at 1 sec. It is observed that the stator current is increased at the time of loading. It is also observed that there is dip in the speed response. This dip is due to the loading. This speed response reaches the reference due to the closed loop operation of the drive. The magnified view of the torque response and stator current has been shown in the Figure 3.43. The performance of the drive at 50% load removal has been shown in the Figure 3.44. At 2 sec the load has been decreased from 4Nm to 2Nm. The drive performance at complete load removal has been shown in the Figure 3.45. Trace 1 indicates the stator current at loading condition and the load removal condition. Due to the step change in load the speed is slightly increased and reaches again the reference speed value. So it is observed that the ZDAC controlled SPMSM drive gives the desired performance at loading condition.

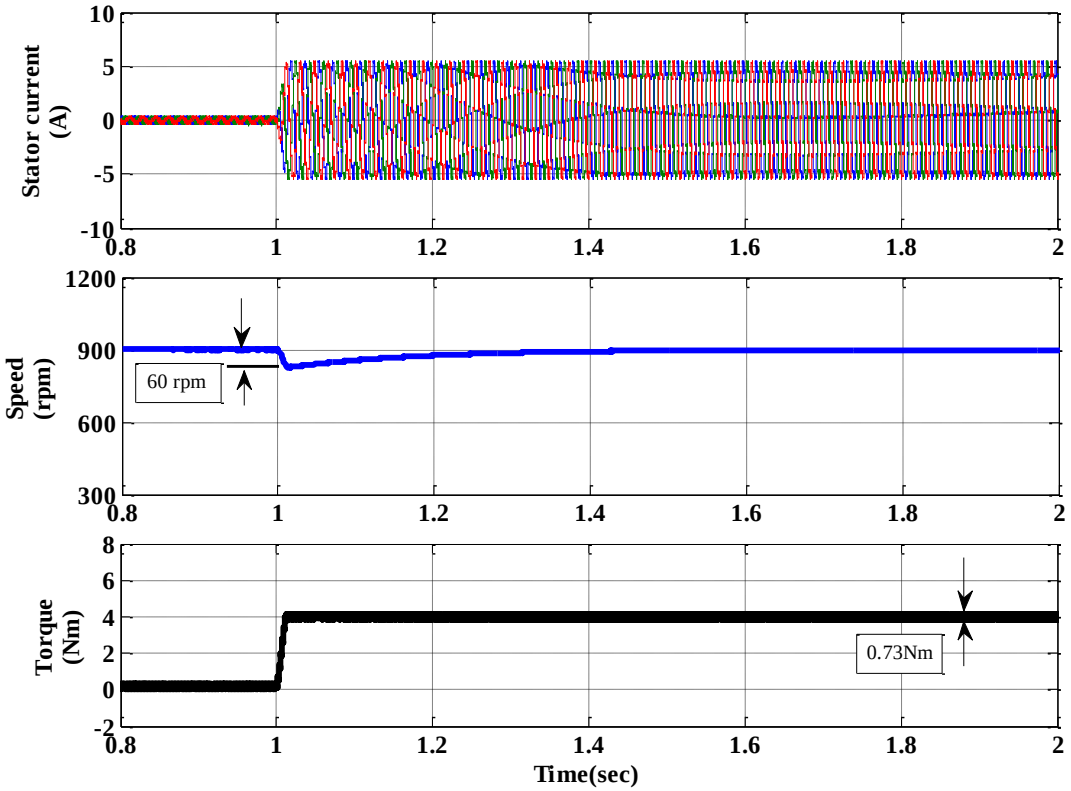

Figure 3.42 Response of the drive at loading condition

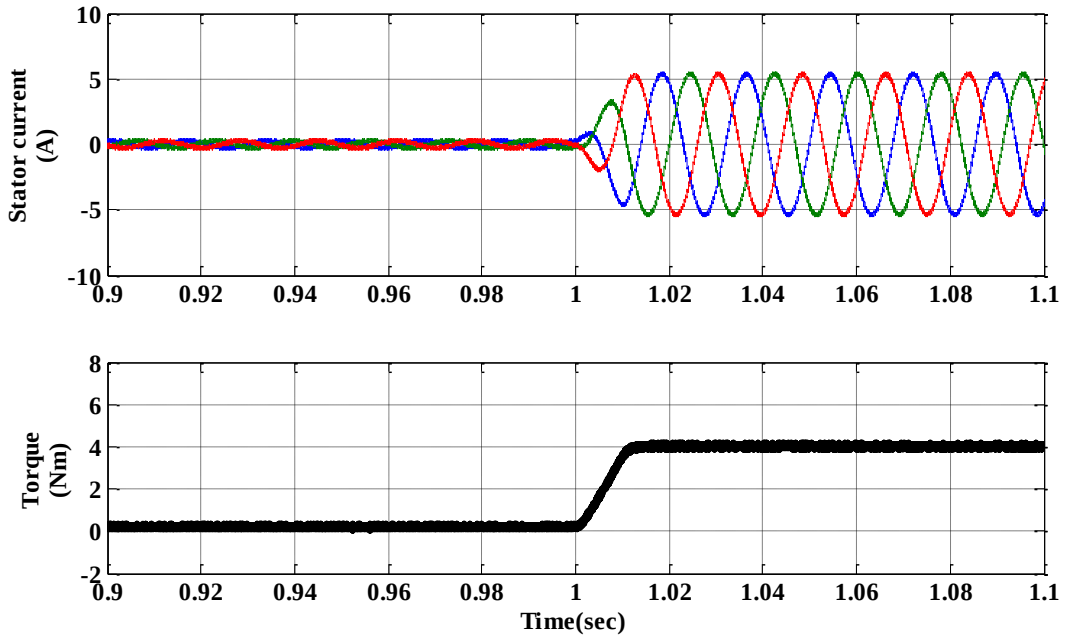

Figure 3.43 Magnified view of the drive response at loading

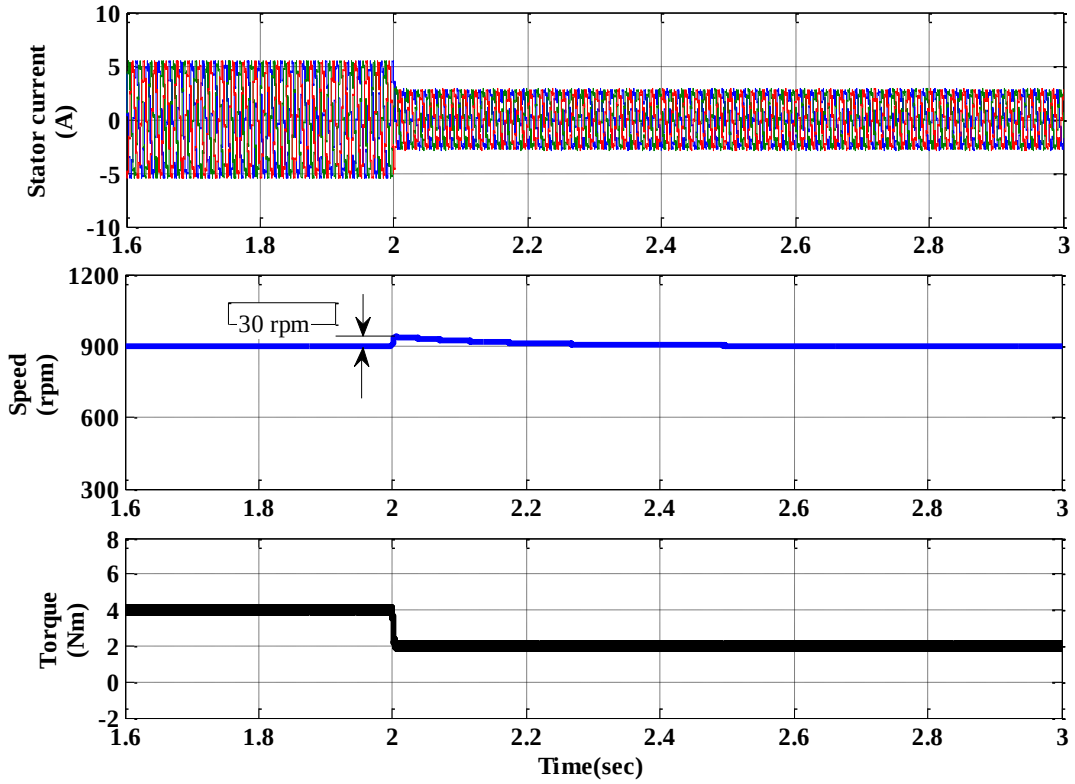

Figure 3.44 Response of the drive at 50% load removal

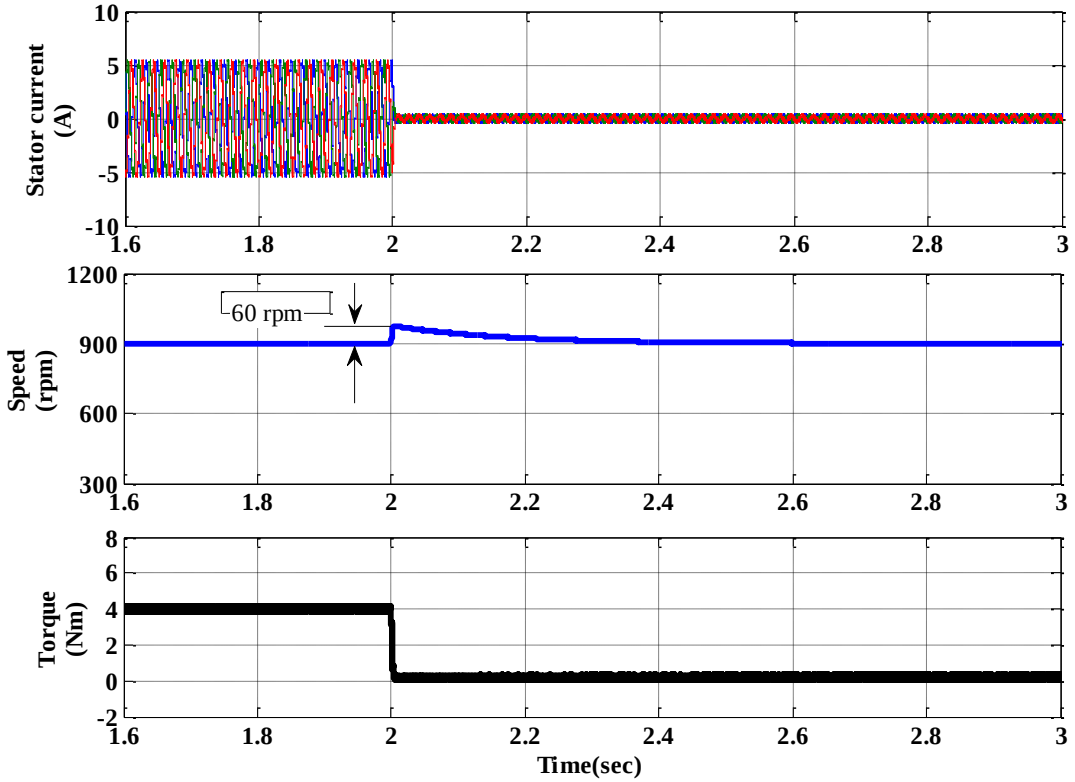

Figure 3.45 Response of the drive at load removal

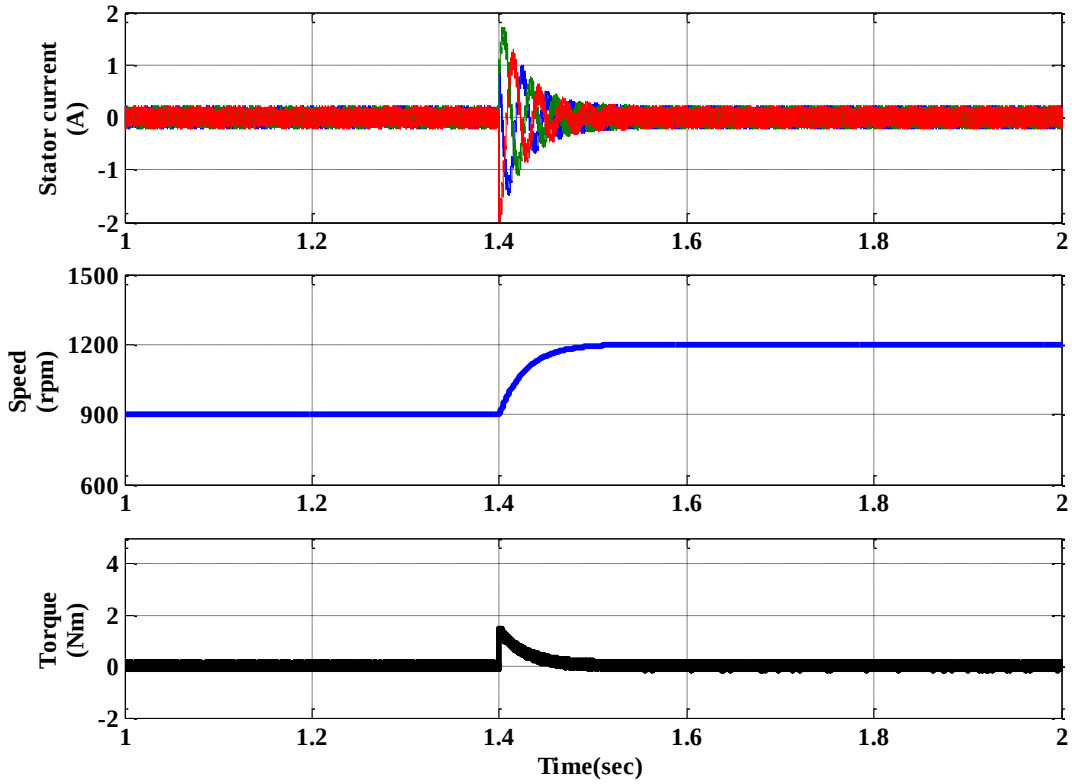

Figure 3.46 Response of the drive at speed increasing

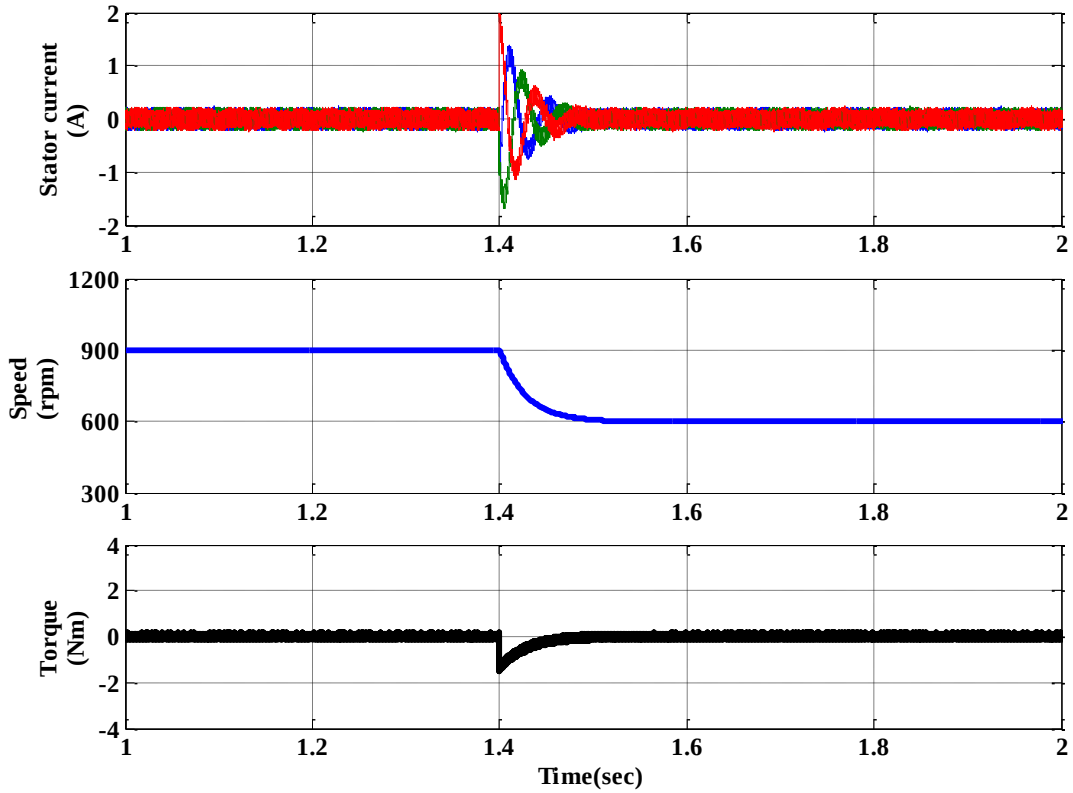

Figure 3.47 Response of the drive at speed decreasing

The performance of the drive with ZDAC control at speed changing operation also has been investigated. A change in speed reference of 300 rpm has been applied. The speed reference

increased from 900rpm to 1200 rpm. The response of the drive at speed changing operation has been shown in the Figure 3.46. At 1.4 sec the speed reference has been increased from 900 rpm to 1200 rpm. At this time the torque is increased by the motor to reach the reference speed. Due to that the stator current is also slightly increased at that time. The torque reduced once the reference speed value reached. The performance of the drive at speed decreasing condition has been shown in the Figure 3.47. At time 1.4 sec the speed reference value is changed from 900 rpm to 600 rpm. To reach the reference speed value the torque of motor decreased to negative value. The torque regains its original value once the reference speed value reached.

3.4 Conclusion

Resolver to Digital Converter (RDC) is used for position and speed estimation from resolver in usual practice. However, a software based position estimation using the output signal of the resolver has been done to eliminate the RDC, which reduce the cost of the drive. High frequency signals are applied to excite the resolver's primary winding. In addition, a demodulation based algorithm is implemented to calculate the speed and rotor position. Furthermore, the dynamic performance of the drive is simulated in MATLAB/ Simulink environment. Vector control in terms of zero d-axis current control and Maximum torque per ampere control is implemented in IPMSM. Comparative analysis also has been done for both the control technique. Further for wide speed of operation a MTPA based flux-weakening control algorithm is implemented for IPMSM. SPMSM drive with zero d-axis current control and its performance is investigated. Further, the effects of load variation and speed change on the performance of drive are extensively studied.

CHAPTER 4: MULTI-LEVEL INVERTER FED PMSM DRIVE

[A neutral point clamped (NPC) three-level inverter fed permanent magnet synchronous motor drive is presented in this chapter. Capacitor voltage balancing topology using three-level boost converter (TLBC) for neutral point clamped (NPC) three-level inverter is presented. The main attracting feature of this control is the boosting of the input voltage and at the same time the balancing of the capacitor voltage. This control also reduces the computational complexity. Exhaustive simulation results are presented to investigate the performance of the three-level NPC inverter fed PMSM drive under different operating condition. Comparative analysis of two-level inverter fed PMSM drive and three-level NPC inverter fed PMSM drive is also presented.]

4.1 Introduction

The vector controlled PMSM drives brought renaissance in the variable speed drives, replacing the traditional scalar-controlled drives. In industrial drives two-level inverter are generally used to fed the PMSM. However, in case of two-level inverter, the switching frequency is one of the main concerns regarding to the size of passive components, superior control of electric drives and to proliferation power density of inverter. On contradictory, the higher switching frequencies may lead to have higher switching losses, which cause inferior inverter efficiency. Compare to two-level inverter, three-level inverter produce lower switching losses at higher switching frequencies to get the same dc-link voltage. The other attracting feature is reduction in total harmonic distortion. Lower dv/dt also reduces the voltage stress across the power switches [42]–[56]. The significant reduction in the torque ripple is achieved with the use of three-level inverter. Satisfying the application demand, PMSM bring the keen attention of the researchers and technologist. To drive the machine, three-level inverter becomes the most preferred choice replacing the conventional two-level VSI. The combination of three-level inverter and PMSM allow to operate at increase dc bus voltage. Three different topologies of multilevel inverters are used in industrial applications: neutral point clamped or diode clamped, flying capacitor or capacitor clamped and a cascaded H-bridges multilevel inverter. The neutral point clamed (NPC) or diode clamped multilevel inverter is one of the most preferred choices of multilevel topologies. But voltage unbalancing across the capacitor is the main drawback of the NPC inverter. A capacitor voltage balancing topology using three-level boost converter (TLBC) for neutral point clamped (NPC) three-

level inverter has been proposed for surface permanent magnet synchronous motor drive (SPMSM). The main attracting feature of the proposed control is the boosting of the input voltage and at the same time the balancing of the capacitor voltage. This control also reduces the computational complexity. Extensive simulation study has been done to investigate the performance of the proposed drive at different operating condition. A detailed comparative study between a two-level and a three-level inverter fed PMSM drive also has been presented in this chapter.

4.2 Multi-Level Inverter Topologies

Traditionally, in two-level voltage source inverter, the load can be connected either to the upper or lower line of the DC link. The DC link voltage needs to be increased substantially to increase the fundamental output voltage and corresponding power level of the inverter. However, fast frequency semiconductors have a limitation in the maximum voltage and very high voltage jump will lead to terrible electromagnetic interference and high windings insulation stress. So for the high performance of AC drive systems at increased power level, high quality inverter output with low harmonic loss and generating low torque fluctuation is necessary. Multilevel inverters are an emerging technology that can achieve the desired performance of the drive. Harmonic reduction and high DC link voltage level in multilevel approach promising the best alternative of the conventional two-level inverter. The basic three different configurations in multilevel inverter circuit topologies are used [62]. They are:

- Neutral point clamped or diode-clamped MLI
- Flying-capacitors or capacitor clamped MLI
- Cascaded MLI

The neutral point clamed (NPC) or diode clamped multilevel inverter is one of the most preferred choices of multilevel topologies

4.2.1 Neutral Point Clamped or Diode-Clamped MLI

The NPCMLI, a new pioneering converter topology was introduced in the early 1980s. This inverter generates a multilevel voltage waveform at its output by connecting in series a number of semiconductor switches within the inverter. NPC inverter can be extended to generate more output-voltage levels. Multilevel inverters consist of an array of power semiconductors and capacitor voltage sources, the output of which produce voltages with stepped waveforms [57]. NPC diodes link the midpoint of the “indirect series connection” of the main switches to the neutral point of the inverter.

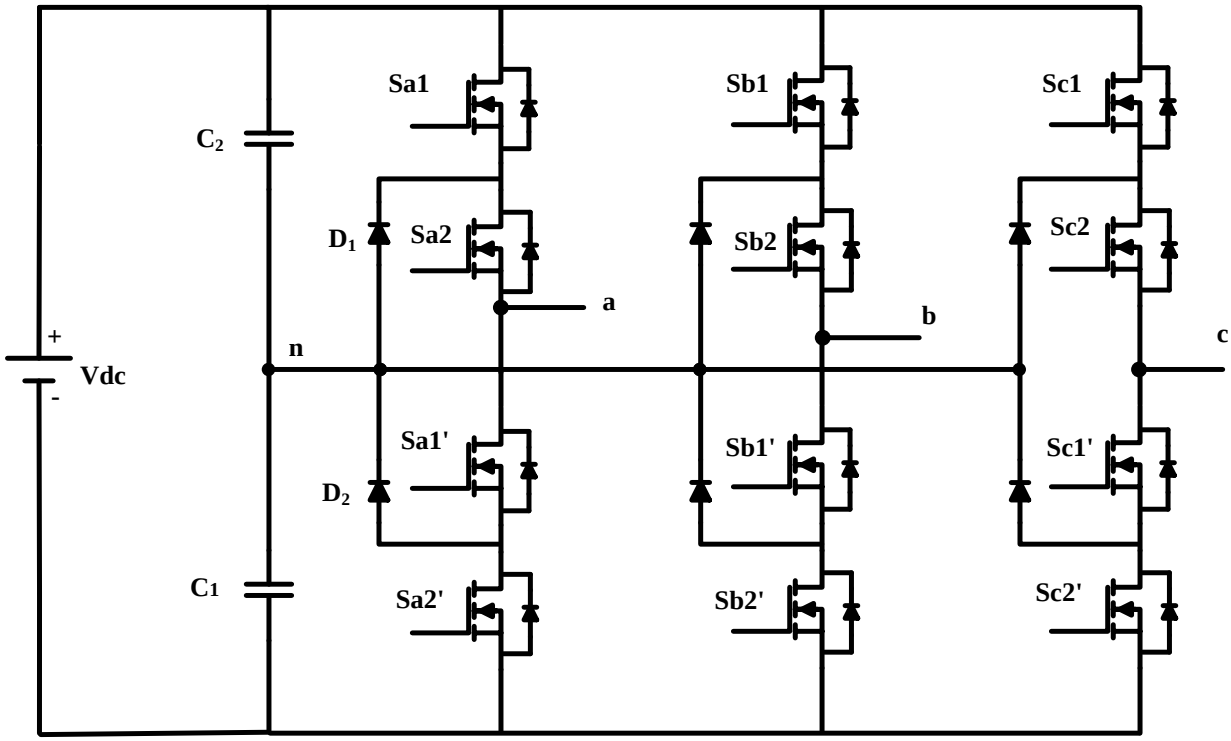

Figure 4.1 Schematic diagram of three-level NPC inverter

A three-level NPC inverter is shown in the Figure 4.1. Two series-connected capacitors, C_1 and C_2 split the DC-link voltage into three levels. The neutral point *n* is the junction point of two capacitors. The output voltage v_{an} has three states: $+V_{dc}/2$, *0* and $-V_{dc}/2$. For voltage level $+V_{dc}/2$, switches S_{a1} and S_{a2} need to be turned on; for $-V_{dc}/2$, switches S'_{a1} and S'_{a2} need to be turned on; and for the 0 level, S_{a2} and S'_{a1} need to be turned on.

Table 4.1 Switching states of one phase

Switching States	Switching Status (Phase A)				Inverter pole Voltage v_{an}
	S_{a1}	S_{a2}	S'_{a1}	S'_{a2}	
P	1	1	0	0	$+V_{dc}/2$
O	0	1	1	0	0
N	0	0	1	1	$-V_{dc}/2$

The key components that distinguish this circuit from a conventional two-level inverter are D_1 and D_2. These two diodes clamp the switch voltage to half the level of the DC-bus voltage. A complementary switch pair is defined as turning one switch on will remain the other turned off. For three-level NPC inverter, the complementary pairs are (S_{a1}, S'_{a1}) and (S_{a2}, S'_{a2}).

To summarize, though the NPC inverter has some drawbacks such as additional clamping diodes and possible deviation of neutral point voltage, but the three-level NPC inverter offers the following attractive features [62] :

- **No dynamic voltage sharing problem**. Each of the switches in the NPC inverter withstands only half of the total dc voltage during commutation.
- **Static voltage equalization without using additional components**. The static voltage equalization can be achieved when the leakage current of the top and bottom switches in an inverter leg is selected to be lower than that of the inner switches.
- **Low THD and dv/dt**. The waveform of the line-to-line voltages is composed of five voltage levels, which leads to lower THD and dv/dt in comparison to the two-level inverter operating at the same voltage rating and device switching frequency.

4.2.2 Flying Capacitor MLI

In an m level structure, the flying capacitor multilevel inverter (FC-MLI) requires (m−1) DC link capacitors and $(m-1).(m-2)/2$ auxiliary capacitors per phase. To clamp the voltage bulky capacitors are necessary instead of diodes as in case of NPC. There should be equal voltage rating of each capacitor and the main power switch. The schematic diagram of there-level flying capacitor inverter is shown in the Figure 4.2. For three -level inverter the number of devices required are four per leg, same as that of diode clamped inverter. For three- level inverter one capacitor is required per phase. It has some advantages such as no clamping diodes like NPC inverter and no separate dc supplies like H-bridge inverter topology is required [57], [62]. This inverter topology is free from of voltage balancing problem as there are number of paths available to produce required voltage. Thus it has inherent voltage balancing property, i.e it eliminates most significant problem in multilevel inverter. There is no need of close loop control of capacitor voltages as this voltages settle down to constant DC voltage but close loop can be used to control the swings in capacitor voltage.

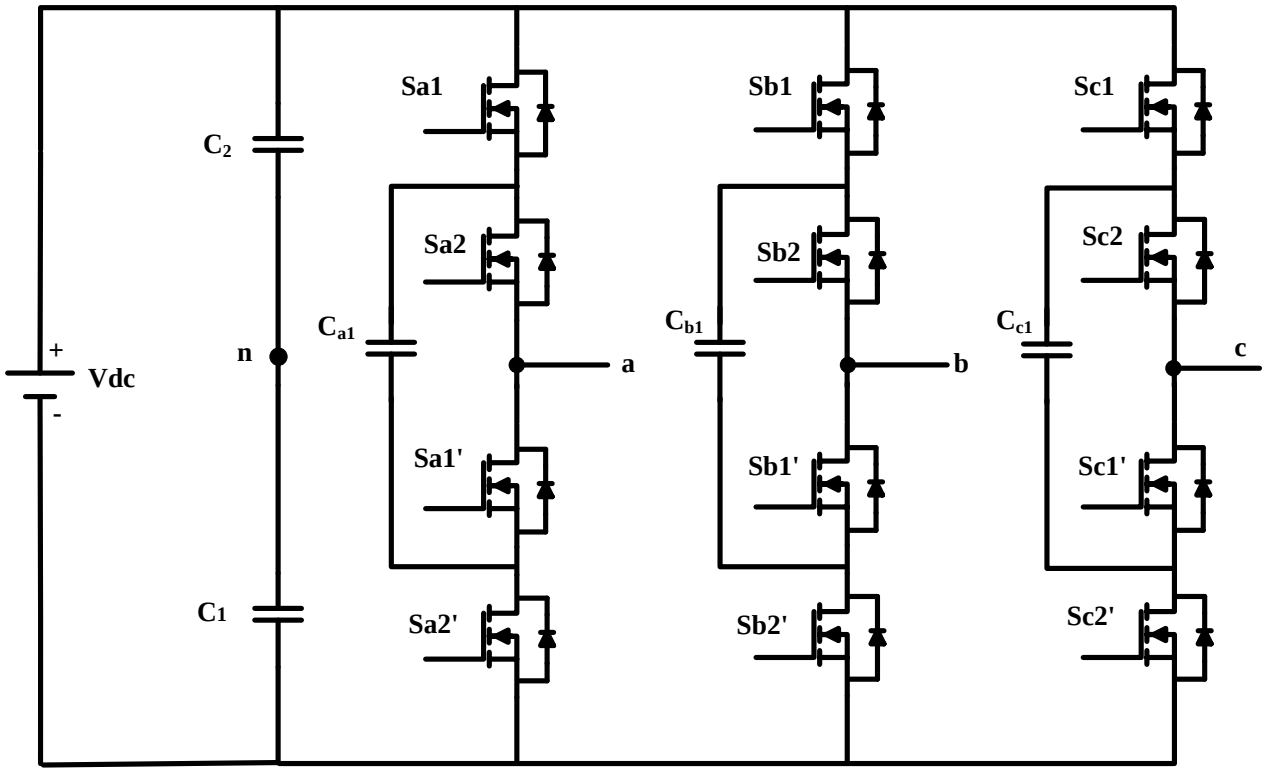

Figure 4.2 Schematic diagram of three-level Flying capacitor inverter

The FCMLI provides a three-level output across a and *n, i.e* v_{an} .The output voltage v_{an} has three states: $+V_{dc}/2$, *0* and $-V_{dc}/2$. For voltage level $+V_{dc}/2$, switches S_{a1} and S_{a2} need to be turned on; for $-V_{dc}/2$, switches S'_{a1} and S'_{a2} need to be turned on; and for the 0 level, (S_{a1} and S'_{a1}) or (S_{a2} and S'_{a2}) need to be turned on. Clamping capacitors C_{a1} is charged when S_{a1} and S'_{a1} are turned on, and is discharged when S_{a2} and S'_{a2} are turned on. The charge of C_{a1} can be balanced by a proper selection of the 0-level switch combinations. Drawback of this topology is with low switching frequency and low capacitor voltage, Voltage swings may occur in middle voltage levels. Thus it increases voltage stress across switching devices.

4.2.3 Cascaded MLI

The basic structure of cascaded inverter is based on the connection of H-bridges (HBs). The power circuit for three-level cascaded inverter with three HBs (HB_1, HB_2 and HB_3) in each phase is shown in the Figure 4.3. Each HB is supplied by a separate dc source. The resulting phase voltage is synthesized by the addition of the voltages generated by the different HBs. If the DC link voltages of HBs are identical, the multi-level inverter is called the cascaded multi-level inverter or CMLI. For an m-level inverter, (m-1)/2 full bridge inverters are required in each phase. Number of output phase voltage levels in a cascade multilevel inverter

is 2k+1, where k is the number of dc sources. The CHB multilevel inverter requires a number of isolated dc supplies. In cascaded multilevel inverter, the DC link voltages of HBs are identical.

$$V_{dc1} = V_{dc2} = V_{dc3} = V_{dc} \tag{4.1}$$

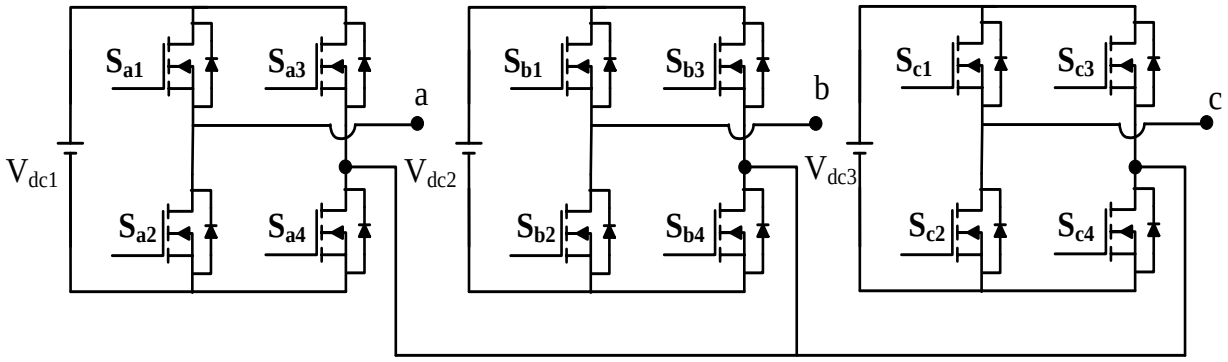

Figure 4.3 Schematic diagram of three-level cascaded inverter

4.2.4 Comparative Evaluation of Multilevel Inverter for PMSM Drive

The selection of individual inverter topologies for PMSM applications depends on their performance, cost, size, and implementation factors.

Table 4.2 Comparison of power component requirements among multi-level inverter topologies

Power component	Inverter topology		
	NPCMLI	FCMLI	CMLI
Main switching devices (Per phase-leg)	$2(m-1)$	$2(m-1)$	$2(m-1)$
Anti-parallel diodes (Per phase-leg)	$2(m-1)$	$2(m-1)$	$2(m-1)$
Clamping diodes (Per phase-leg)	$(m-1)(m-2)$	0	0
DC bus capacitors	$(m-1)$	$(m-1)$	$\frac{(m-1)}{2}$
Flying capacitors	0	$\frac{(m-1)(m-2)}{2}$	0

Table 4.2 gives the comparison of power component required for the above discussed multi-level inverter topologies. The comparison of multi-level inverter topologies based on their

implementation factors is given in Table 4.3. Although FCMLI have a natural voltage balancing operation and modular structure, but its application in PMSM drive is limited due to the requirement of large number of capacitors and their initialization process (pre-charge). On the other hand NPCMLI topologies seem to be the most suited for PMSM drive applications. Although the main problem associated with the NPCMLI is voltage unbalancing at higher levels.

Table 4.3 Comparison of multi-level inverter topologies based on implementation factors

Implementation factor	Inverter topology		
	NPCMLI	FCMLI	CMLI
Specific requirements	Clamping diodes	Additional capacitors and their initialization	Isolated dc sources
Modularity	Medium	High	Very high
Design and implementation complexity	Low	Medium	Least (with transformer-less applications)
Control concerns	Voltage balancing	Voltage setup	Power sharing

4.2.5 Mathematical Model of Multi-level Inverter

The initial step to implement the different control strategies is to simulate the system and to find out the response of the system. The analytical models of the multilevel inverters are presented. Mathematical models are based on the determination of state equations for dynamical variables [61]. These models are conspicuous by their extreme simplicity in front of other previous analytical models presented in the literature. In this thesis Neutral point clamped multilevel structure is considered. The circuit diagram of three-level NPC inverter is shown in the Figure 4.1. The details mathematical models are described below.

Neutral point clamped or diode clamped inverter model

Figure 4.4 shows the commutation model of a three-phase three-level neutral point clamped inverter. In a three-level inverter, it can be seen that each phase can be connected to level 0, 1 or 2. The mathematical model uses the switching functions Sij for i $\in$ {a,b,c} and j $\in$ {0,1,2}.

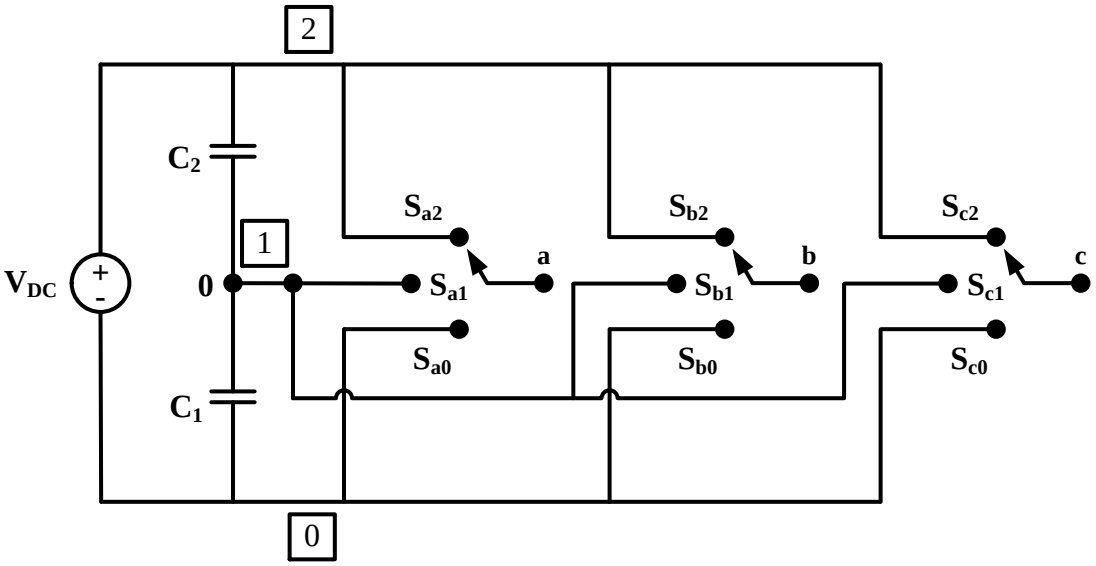

Figure 4.4 Commutation model of three-level neutral point clamped inverter

Three-level neutral point clamped inverter can be easily extended increasing the number of levels. The commutation model of the N-level NPC inverter is shown in Figure 4.5. In the N-level case, the mathematical model uses switching functions Sij where i Є {a,b,c} and j Є {0,1,…, N-1}.

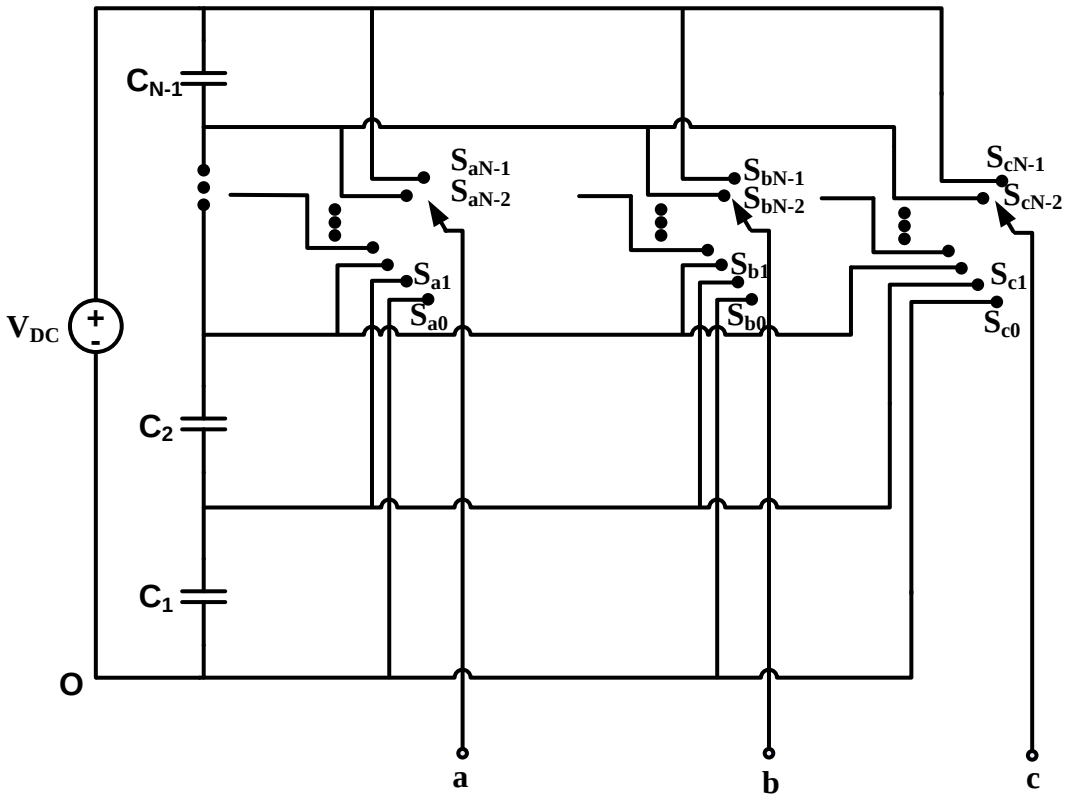

Figure 4.5 Commutation model of N-level neutral point clamped inverter

All developed mathematical models are calculated assuming that multilevel inverters are connected to three-phase RL loads. The N-level NPC inverter connected to this load is represented in Figure 4.6.

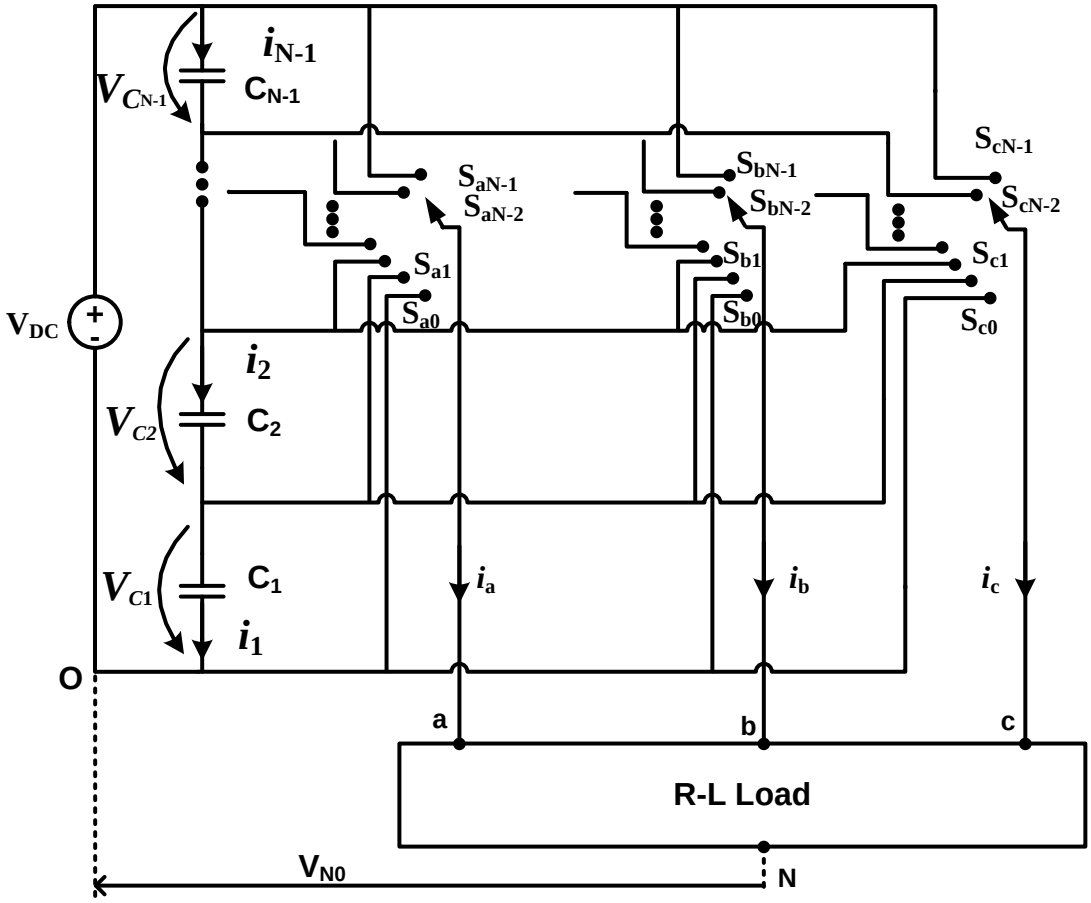

Figure 4.6 Commutation model of N-level neutral point clamped inverter connected to RL load

$$i_1 = C_1 \frac{dV_{c1}}{dt} = \frac{N-2}{N-1}F_1 - \frac{N-3}{N-1}F_2 - \frac{N-4}{N-1}F_3 - ..... - \frac{1}{2}F_{\frac{N-1}{2}} - ... - \frac{3}{N-1}F_{N-4} - \frac{2}{N-1}F_{N-3} - \frac{1}{N-1}F_{N-2} \quad (4.2)$$

$$i_2 = C_2 \frac{dV_{c2}}{dt} = \frac{1}{N-1}F_1 - \frac{N-3}{N-1}F_2 - \frac{N-4}{N-1}F_3 - ... - \frac{1}{2}F_{\frac{N-1}{2}} - ... - \frac{3}{N-1}F_{N-4} - \frac{2}{N-1}F_{N-3} - \frac{1}{N-1}F_{N-2} \quad (4.3)$$

$$i_3 = C_3 \frac{dV_{c3}}{dt} = \frac{1}{N-1}F_1 + \frac{2}{N-1}F_2 - \frac{N-4}{N-1}F_3 - ... - \frac{1}{2}F_{\frac{N-1}{2}} - ... - \frac{3}{N-1}F_{N-4} - \frac{2}{N-1}F_{N-3} - \frac{1}{N-1}F_{N-2} \quad (4.4)$$

$$i_4 = C_4 \frac{dV_{c4}}{dt} = \frac{1}{N-1}F_1 + \frac{2}{N-1}F_2 + \frac{3}{N-1}F_3 - ... - \frac{1}{2}F_{\frac{N-1}{2}} - ... - \frac{3}{N-1}F_{N-4} - \frac{2}{N-1}F_{N-3} - \frac{1}{N-1}F_{N-2} \tag{4.5}$$

$$\begin{aligned} i_{N-1} = C_{N-1}\frac{dV_{c(N-1)}}{dt} &= \frac{1}{N-1}F_1 + \frac{2}{N-1}F_2 + \frac{3}{N-1}F_3 + ... \\ &+ \frac{1}{2}F_{\frac{N-1}{2}} + ... - + \frac{N-4}{N-1}F_{N-4} + \frac{N-3}{N-1}F_{N-3} - \frac{N-2}{N-1}F_{N-2} \end{aligned} \tag{4.6}$$

Where,

$$F_i = (S_{ai}i_a + S_{bi}i_b + S_{ci}i_c) \tag{4.7}$$

And finally, the state equations of the DC-Link capacitors voltages are presented.

$$\frac{dV_{C1}}{dt} = \frac{1}{C_1}\left(-f_1F_1 - f_2F_2 - f_3F_3 - ... - \frac{1}{2}F_{\frac{N-1}{2}} - ... - g_3F_{N-4} - g_2F_{N-3} - g_1F_{N-2}\right) \tag{4.8}$$

$$\frac{dV_{C2}}{dt} = \frac{1}{C_2}\left(g_1F_1 - f_2F_2 - f_3F_3 - ... - \frac{1}{2}F_{\frac{N-1}{2}} - ... - g_3F_{N-4} - g_2F_{N-3} - g_1F_{N-2}\right) \tag{4.9}$$

$$\frac{dV_{C3}}{dt} = \frac{1}{C_3}\left(g_1F_1 + g_2F_2 - f_3F_3 - ... - \frac{1}{2}F_{\frac{N-1}{2}} - ... - g_3F_{N-4} - g_2F_{N-3} - g_1F_{N-2}\right) \tag{4.10}$$

$$\frac{dV_{C4}}{dt} = \frac{1}{C_4}\left(g_1F_1 + g_2F_2 + g_3F_3 - ... - \frac{1}{2}F_{\frac{N-1}{2}} - ... - g_3F_{N-4} - g_2F_{N-3} - g_1F_{N-2}\right) \tag{4.11}$$

$$\frac{dV_{C(N-1)}}{dt} = \frac{1}{C_{N-1}}\left(g_1F_1 + g_2F_2 + g_3F_3 + ... + \frac{1}{2}F_{\frac{N-1}{2}} + ... + f_3F_{N-4} + f_2F_{N-3} - f_1F_{N-2}\right) \tag{4.12}$$

Where,

$$\begin{aligned} f_i &= \frac{N-1-i}{N-1} \\ g_i &= \frac{i}{N-1} \end{aligned} \tag{4.13}$$

In order to determine the state equations for the phase currents, the output phase voltages with respect to 0 (lowest point of the DC-Link) are calculated as follows.

$$V_{a0} = S_{a1}V_{C1} + S_{a2}(V_{C1} + V_{C2}) + S_{a3}(V_{C1} + V_{C2} + V_{C3}) + \ldots + S_{a(N-2)}(V_{C1} + V_{C2} + \ldots + V_{C(N-2)}) + S_{a(N-2)}V_{DC} - L\frac{di_a}{dt} \quad (4.14)$$

$$V_{b0} = S_{b1}V_{C1} + S_{b2}(V_{C1} + V_{C2}) + S_{b3}(V_{C1} + V_{C2} + V_{C3}) + \ldots + S_{b(N-2)}(V_{C1} + V_{C2} + \ldots + V_{C(N-2)}) + S_{b(N-2)}V_{DC} - L\frac{di_b}{dt} \quad (4.15)$$

$$V_{c0} = S_{c1}V_{C1} + S_{c2}(V_{C1} + V_{C2}) + S_{c3}(V_{C1} + V_{C2} + V_{C3}) + \ldots + S_{c(N-2)}(V_{C1} + V_{C2} + \ldots + V_{C(N-2)}) + S_{c(N-2)}V_{DC} - L\frac{di_c}{dt} \quad (4.16)$$

The voltage of the neutral point of the load with respect to 0 is determined as follows.

$$V_{N0} = \frac{V_{a0} + V_{b0} + V_{c0}}{3} \quad (4.17)$$

The phase voltages with respect to the neutral point of the load are determined.

$$\left.\begin{aligned} V_{aN} &= V_{a0} - V_{N0} = R_a i_a \\ V_{bN} &= V_{b0} - V_{N0} = R_b i_b \\ V_{cN} &= V_{c0} - V_{N0} = R_c i_c \end{aligned}\right\} \quad (4.18)$$

And finally, the phase currents state equations are presented.

$$\begin{aligned} \frac{di_a}{dt} = &-\frac{R_a}{L}i_a + \frac{V_{C1}}{3L}\left[2\left(S_{a1} + \ldots + S_{a(N-2)}\right) - \left(S_{b1} + \ldots + S_{b(N-2)}\right) - \left(S_{c1} + \ldots + S_{c(N-2)}\right)\right] + \\ &+ \frac{V_{C2}}{3L}\left[2\left(S_{a2} + \ldots + S_{a(N-2)}\right) - \left(S_{b2} + \ldots + S_{b(N-2)}\right) - \left(S_{c2} + \ldots + S_{c(N-2)}\right)\right] + \\ &+ \frac{V_{C3}}{3L}\left[2\left(S_{a3} + \ldots + S_{a(N-2)}\right) - \left(S_{b3} + \ldots + S_{b(N-2)}\right) - \left(S_{c3} + \ldots + S_{c(N-2)}\right)\right] + \\ &+ \ldots\ldots\ldots + \\ &+ \frac{V_{C(N-2)}}{3L}\left(2S_{a(N-2)} - S_{b(N-2)} - S_{c(N-2)}\right) + \\ &+ \frac{V_{DC}}{3L}\left(2S_{a(N-1)} - S_{b(N-1)} - S_{c(N-1)}\right) \end{aligned} \quad (4.19)$$

$$\frac{di_b}{dt} = -\frac{R_b}{L} i_b + \frac{V_{C1}}{3L}\left[-\left(S_{a1}+...+S_{a(N-2)}\right)+2\left(S_{b1}+...+S_{b(N-2)}\right)-\left(S_{c1}+...+S_{c(N-2)}\right)\right]+$$
$$+\frac{V_{C2}}{3L}\left[-\left(S_{a2}+...+S_{a(N-2)}\right)+2\left(S_{b2}+...+S_{b(N-2)}\right)-\left(S_{c2}+...+S_{c(N-2)}\right)\right]+$$
$$+\frac{V_{C3}}{3L}\left[-\left(S_{a3}+...+S_{a(N-2)}\right)+2\left(S_{b3}+...+S_{b(N-2)}\right)-\left(S_{c3}+...+S_{c(N-2)}\right)\right]+$$
$$+.....+$$
$$+\frac{V_{C(N-2)}}{3L}\left(-S_{a(N-2)}+2S_{b(N-2)}-S_{c(N-2)}\right)+$$
$$+\frac{V_{DC}}{3L}\left(-S_{a(N-1)}+2S_{b(N-1)}-S_{c(N-1)}\right)$$

(4.20)

$$\frac{di_c}{dt} = -\frac{R_c}{L} i_c + \frac{V_{C1}}{3L}\left[-\left(S_{a1}+...+S_{a(N-2)}\right)-\left(S_{b1}+...+S_{b(N-2)}\right)+2\left(S_{c1}+...+S_{c(N-2)}\right)\right]+$$
$$+\frac{V_{C2}}{3L}\left[-\left(S_{a2}+...+S_{a(N-2)}\right)-\left(S_{b2}+...+S_{b(N-2)}\right)+2\left(S_{c2}+...+S_{c(N-2)}\right)\right]+$$
$$+\frac{V_{C3}}{3L}\left[-\left(S_{a3}+...+S_{a(N-2)}\right)-\left(S_{b3}+...+S_{b(N-2)}\right)+2\left(S_{c3}+...+S_{c(N-2)}\right)\right]+$$
$$+.....+$$
$$+\frac{V_{C(N-2)}}{3L}\left(-S_{a(N-2)}-S_{b(N-2)}+2S_{c(N-2)}\right)+$$
$$+\frac{V_{DC}}{3L}\left(-S_{a(N-1)}-S_{b(N-1)}+2S_{c(N-1)}\right)$$

(4.21)

4.2.6 Causes of Neutral-Point Voltage Deviation in NPC MLI

The neutral-point voltage may be affected by a several factors, which includes unbalanced dc capacitors due to manufacturing tolerances, inconsistency in switching device characteristics and unbalanced three-phase operation. When the NPC inverter is used in the drives, the operating mode of the drive may also influence the neutral-point voltage [62]. Figure 4.7 shows the effect of motoring and regenerative operations of the drive on neutral-point voltage shift. When the drive is in the motoring mode as shown in Figure 4.7 (a) where the dc current i_d flows from the dc source to the inverter, the P-type state [POO] causes the neutral-point voltage v_n to rise while the N-type state [ONN] makes v_n to decline. An opposite action takes place in the regenerative mode in which the dc current reverses its direction as shown in Figure 4.7 (b).

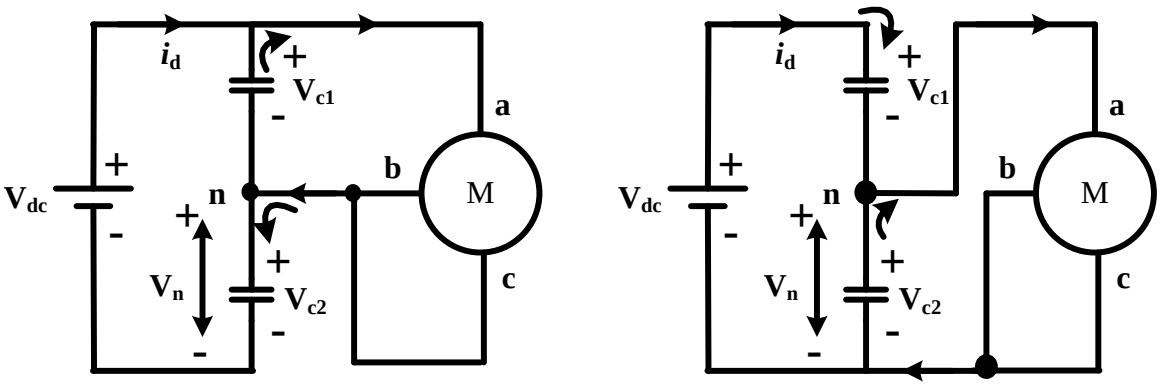

(a) Motoring operation

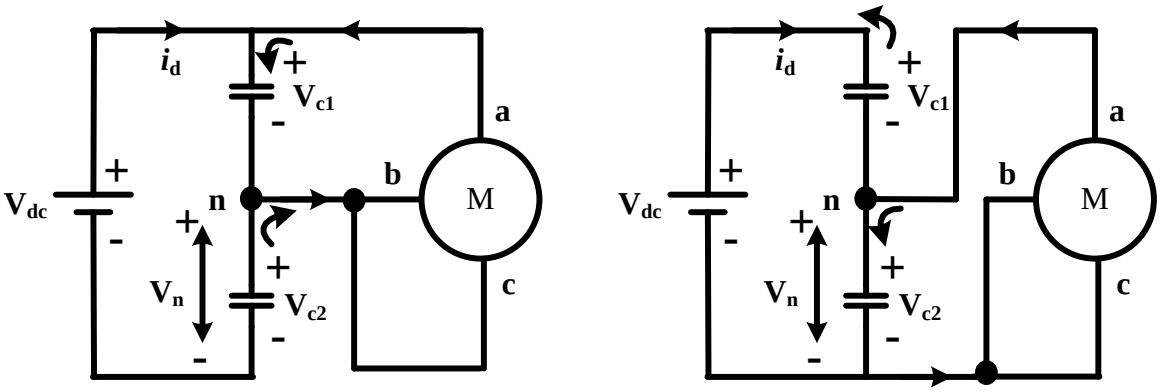

(b) Regenerative operation

Figure 4.7 Effect of drive operating modes on neutral-point voltage deviation [62]

To minimize the neutral-point voltage shift, a voltage balancing control schemes is needed to be implemented.

4.3 Control and Modulation Strategies

The modulation methods used in MLI can be classified according to switching frequency, as shown in the Figure 4.8. Methods that work with high switching frequencies have many commutations for the switching devices in one period of the fundamental output voltage. Carrier based sinusoidal PWM (SPWM) is popular method that uses the level shifted technique to reduce the harmonics in the load voltage [57]. Space vector PWM (SVPWM) is other alternative used by MLI. But it increases the computational complexity. Low switching frequencies methods have one or two commutations per switching device during one cycle of the output voltage, generating a staircase waveform. Multilevel selective harmonic elimination and the space vector control (SVC) are used in low frequency methods.

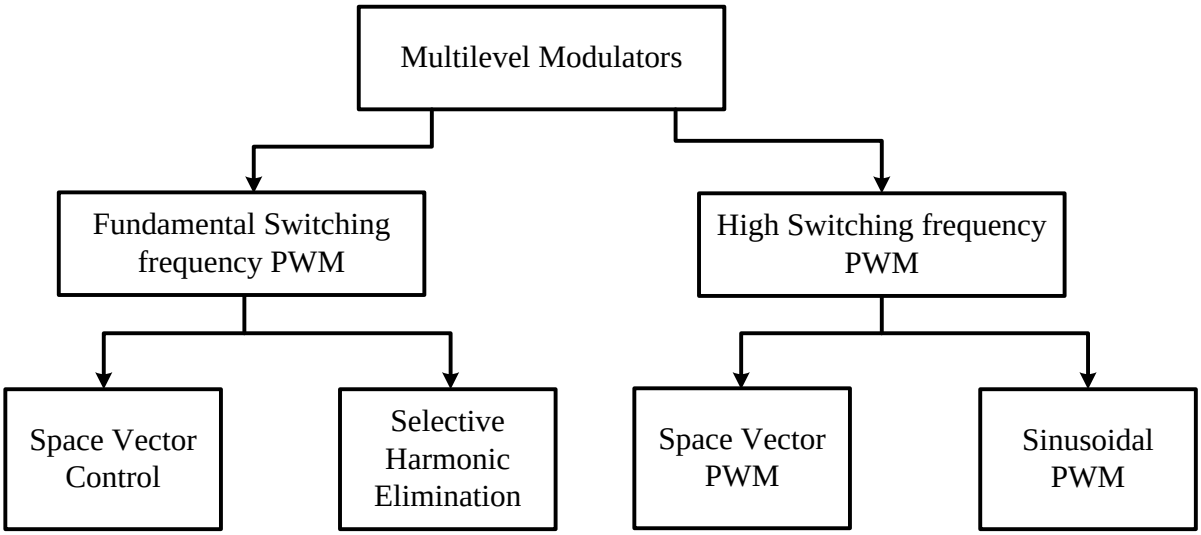

Figure 4.8 Classification of multi-level inverter control schemes [57]

A level-shifted carrier-based modulation scheme is used for NPC three-level inverters. For m-level NPC inverter using level-shifted multicarrier modulation scheme requires (m–1) triangular carriers, all having the same frequency and amplitude. The (m–1) triangular carriers are vertically disposed such that the bands they occupy are contiguous.

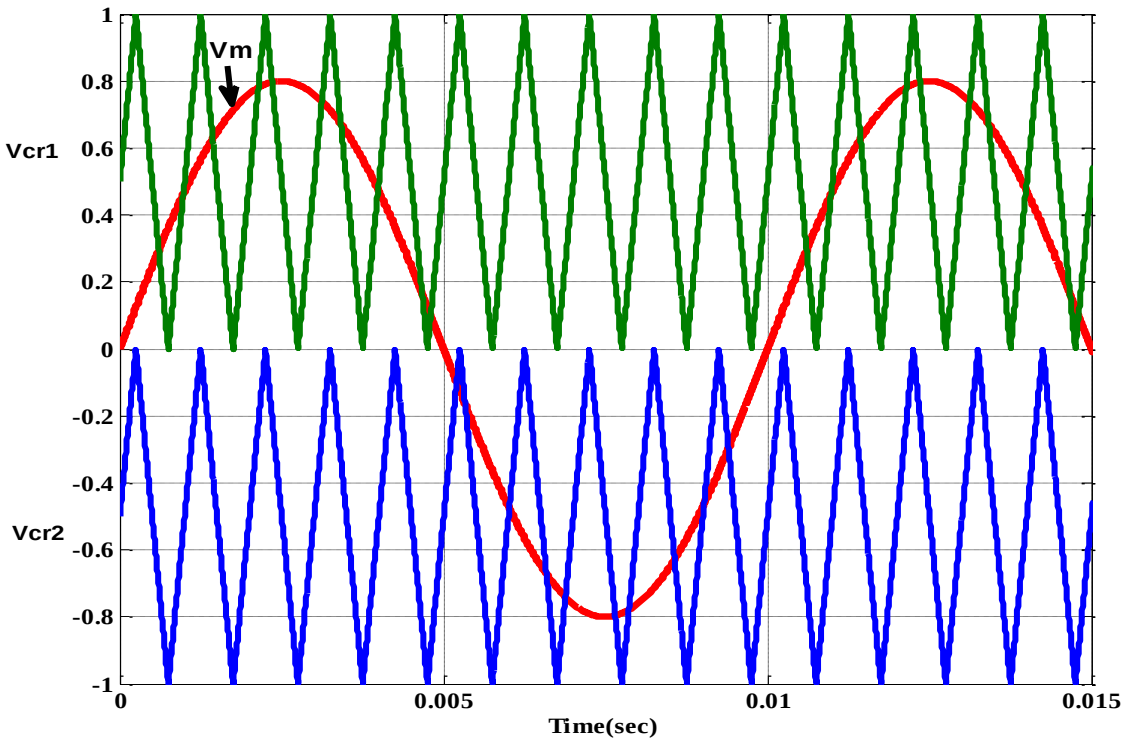

Figure 4.9 Level shifted in phase disposition

The in-phase disposition (IPD) modulation produces superior harmonic profile than the alternative phase opposite disposition (APOD) modulation scheme. The frequency modulation index is given by $m_f = f_{cr} / f_m$, which remains the same as that for the phase-shifted modulation scheme whereas the amplitude modulation index is defined as

$$m_a = \frac{\hat{V}_m}{\hat{V}_{cr}(m-1)} \qquad for \quad 0 \le m_a \le 1 \tag{4.22}$$

Where $\hat{V}_m$ is the peak amplitude of the modulating wave v_m and $\hat{V}_{cr}$ is the peak amplitude of each carrier wave. Figure 4.9 shows the level-shifted in-phase disposition (IPD) modulation scheme for three-level NPC inverter. The upper and lower carrier, V_{cr1} and V_{cr2}, are used to generate the gating pulse for the switches. The modulating signal is generated by processing the current error in PI controller. The switch S_{a1} is turned on when the phase A modulating signal v_{ma} is higher than the corresponding carriers V_{cr1}. The switches S_{a2} are turned on when the phase a modulating signal v_{ma} is higher than the corresponding carriers V_{cr2}. The gate signals for the lower switches in each leg are complementary to their corresponding upper switches.

4.4 Proposed NPC Three-level Inverter Fed PMSM Drive

The schematic block diagram of the proposed drive has been shown in the Figure 4.10.

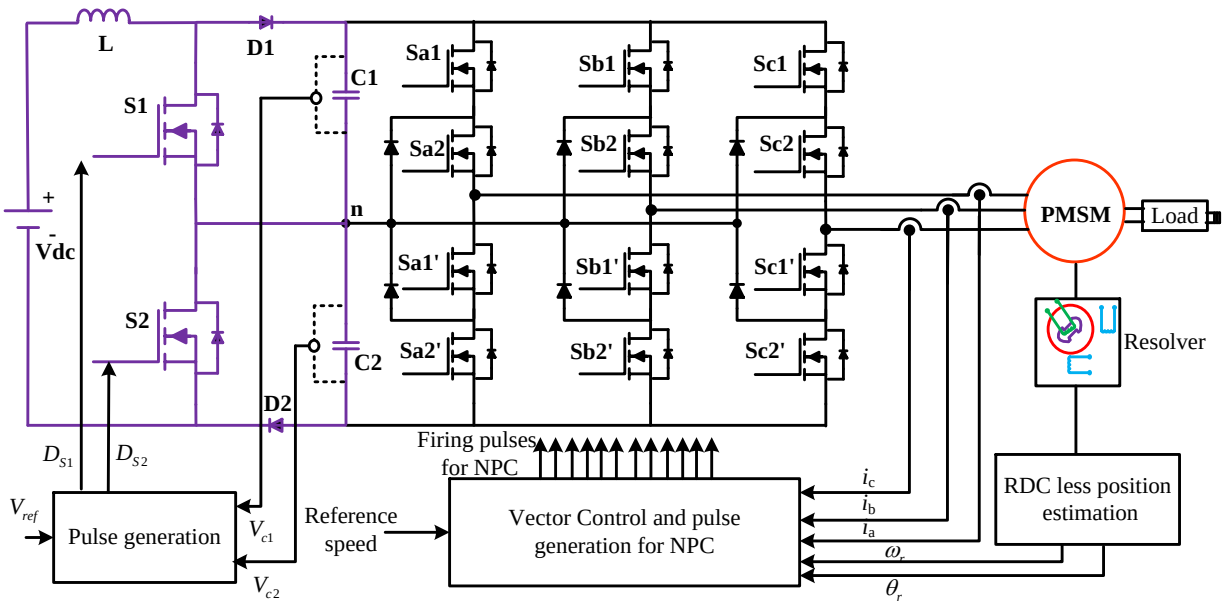

Figure 4.10 Schematic diagram of the proposed PMSM drive system

The application demand of electric motor is increasing rapidly with technological advancement. According to the technological progress three-level inverter becomes the most preferred choice replacing the conventional two-level VSI to fed the PMSM. A NPC inverter has been used in the proposed drive purpose.

4.4.1 Capacitor Voltage Balancing

Voltage unbalancing across the capacitor is the main drawback of the NPC inverter [84]. Researchers give their extensive effort to overcome this problem and developed several voltage balancing technique. Self -balancing property of three-level inverter is presented in [88]. But self-balancing technique is not always adequate as the neutral-point voltage drifts for slight variation in the system parameters. Carrier pulse width modulation and space vector modulation based voltage balancing technique are studied in [76], [89]–[99]. Modified PWM technique increases the computational complexity and digital resource consumption. A balancing circuit is added to the NPC inverter for simple computational control. The detailed study based on the balancing circuit is presented in [85], [101]–[104]. DC-Link capacitance minimization technique is discussed in [106]. The Three-Level Boost Converter (TLBC) is most attracting circuit used for voltage balancing in three-level NPC inverter. The advantageous feature is reduced switching losses and lower reverse recovery losses of the diode compared with the conventional boost converters. Based on the previously presented review of the literature, studies on three-level NPC inverted fed PMSM motor drives mainly focus on the investigation on capacitor voltage balancing at the same time boosting of the input voltage. TLBC is used to maintain the DC-link capacitor voltage of the three-level NPC inverter. With the use of TLBC the computational complexity reduces. The main attraction is the boosting feature of the input voltage.

4.4.2 Capacitor Voltage Balancing with Three-Level Boost Converter

DC-link capacitor (C_1 and C_2) voltage balancing is achieved using three-level boost converter (TLBC). Due to some attractive feature like less switching losses and less recovery voltage of the diode TLBC draw the keen attention to the researchers and technologist for high power application.

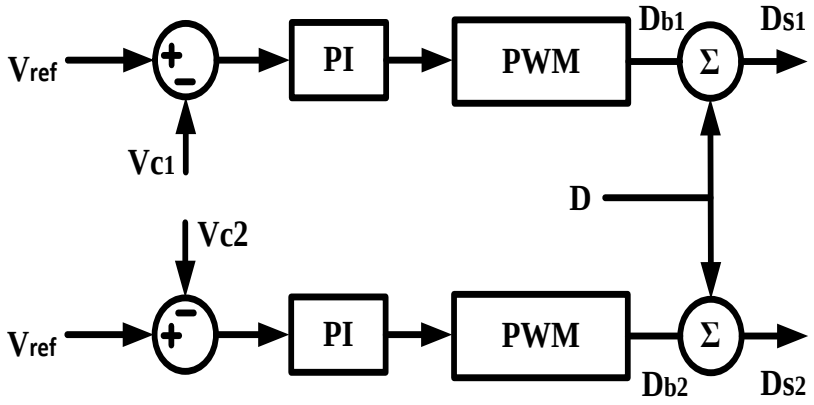

Figure 4.11 Schematic diagram of capacitor voltage balancing circuit using TLBC circuit

The inductor current ripple is also less. This requires a smaller size inductor as compared to the conventional boost converter. The voltage balancing circuit is shown in Figure 4.11. The schematic diagram of dc capacitor voltage balancing along with boosting is shown in Figure 4.11. The proper value of D must be selected to maintain the boosting of the input dc at desired voltage level by using (4.23). This can charges the capacitors C1 and C2 alternatively and make them theoretically balanced. In practical, the parameters of the components are not exactly balanced because of the various modes of operation and transient conditions of NPC fed PMSM drive.

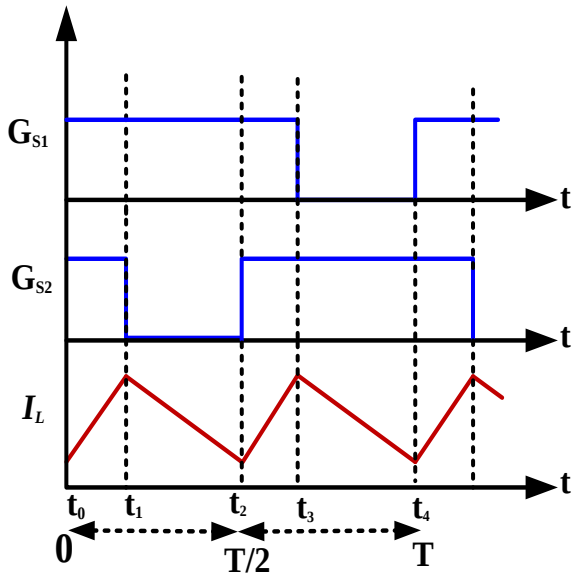

Figure 4.12 Gate signal of the two switches of TLBC

To ensure equal voltages on C1 and C2, a voltage balancing circuit is used as shown in Figure 4.11. The individual balancing control has been implemented for both the capacitors. The voltages Vc1 and Vc2 are compared with the magnitude of reference voltage Vref separately and the error is processed through the proportional integral (PI) controller. The output of the PI controller is processed through PWM to evaluate the duty ratios for balancing the capacitor voltages. The duty ratios Db1 and Db2 have been added with D which is selected for the desired output voltage of the dc link, to determine the duty ratios for the switches S1 and S2 respectively.

Both the switches of TLBC are turned on and off alternately. The difference of the desired capacitor voltage V_{ref} and actual capacitor Voltages V_{c1} and V_{c2} is processed through the PI controller. The ref signal of the PI controller and the carrier signal is compared using comparator which in terns generate the switching signal to the two switches S_1 & S_2.

The duty ratio is controlled by the PI controller. The output voltage equation of the TLBC is given as

$$V_0 = V_{c2} + V_{c1} = \frac{2Vdc}{(2-D)} \tag{4.23}$$

D is the duty ratio. It is varied from 0 to 1.

The current ripple for the conventional boost inverter is

$$\Delta I = \frac{VdcDT_{SW}}{L} \tag{4.24}$$

T_{SW} Represent the switching period of the conventional BC.

The current ripple for three-level boost converter is

$$\Delta I = \frac{V_0(1-V_{dc}/V_0)(2V_{dc}/V_0-1)}{2Lf_{SW}} \tag{4.25}$$

If we compare the above equation it is observed that the current ripple in TLBC is 50% reduced as compared to the conventional one.

The typical firing signal of the two switches is shown in the Figure 4.12. The circuit diagram of TLBC at different operating modes is shown in the Figure 4.13. It is observed that S1 and S2 both the switches are ON at the period $t_0 < t < t_1$ and $t_2 < t < t_3$.The inductor current flows as marked by the blue line as shown in Figure 4.13 (a). At this time period the energy is stored in the inductor. The switch S1 is ON and S2 is OFF during the period $t_1 < t < t_2$. In this time

period the capacitor C2 is charged, so the voltage across the capacitor VC2 increases. The inductor stored energy is transferred to C2 and the inductor current gradually reduces. At the time period $t_3 < t < t_4$ the switch S1 is OFF and S2 is ON. In this period of time the capacitor C1 gets charged and VC1 is increases. The inductor current gradually reduces at this period of time.

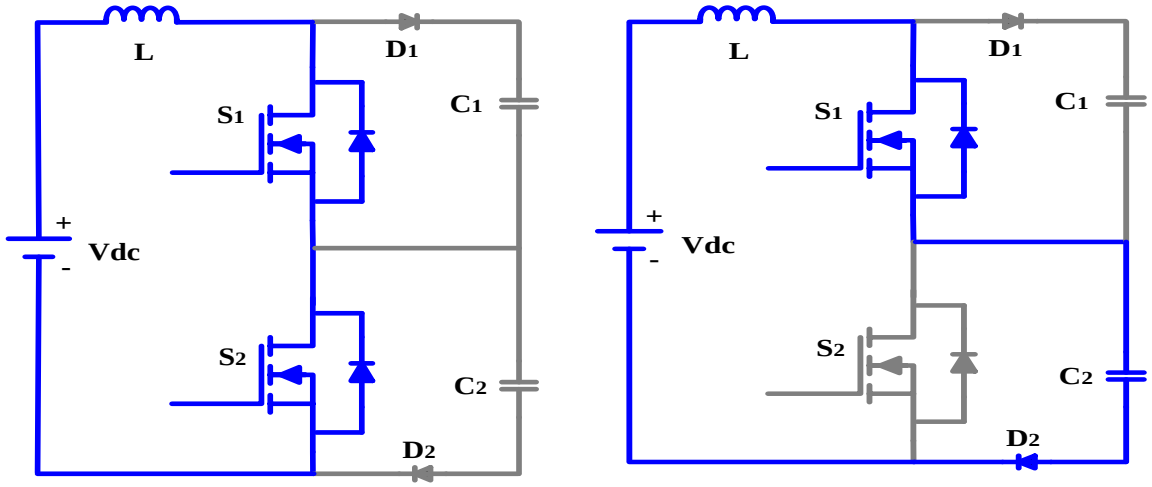

(a) $t_0 < t < t_1$ and $t_2 < t < t_3$

(b) $t_1 < t < t_2$

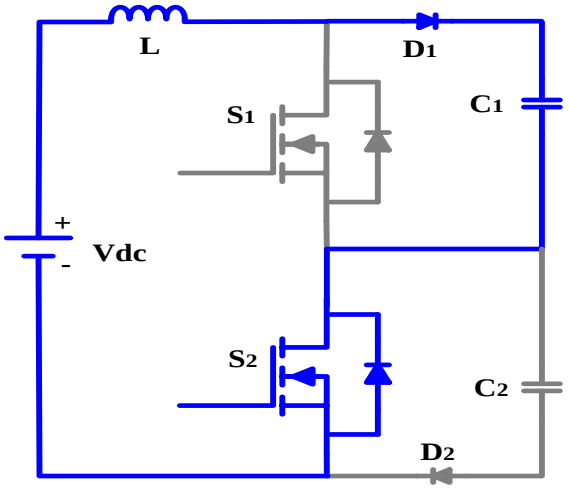

(c) $t_3 < t < t_4$.

Figure 4.13 Capacitor voltage balancing using TLBC for complete time period T

4.5 Performance Evaluation of the Proposed Drive

The specifications of the PMSM drive used in this study are listed in Table 4.4. The NPC inverter suffers from the voltage balancing problem. As a first step towards the investigation of the three-level NPC inverter fed PMSM drive, the drive is operated without any voltage balancing circuit. The input voltage V_{dc} is given as 300V. The capacitor voltage across the two capacitors and their potential difference at the time of load applied is shown in the Figure 4.14.

Table 4.4 Specification of the proposed drive

Input dc voltage (V_{dc})	200 V
Inductance of TLBC (L)	7 mH
Capacitance of C_1 and C_2	2200 μF
Voltage across capacitor C_1 and C_2	150 V
Torque Constant	0.75Nm/A
Phase inductance (L_d, L_q)	5.15mH
Moment of inertia (J)	0.000062kg-m^2
Total load inertia	0.001914 kg-m^2
No of poles (p)	8
Damping friction	0.0041N-m/rad

It is noticed that when the drive is operated without voltage balancing circuit, the capacitor voltage across the two capacitors are unequal. At no load condition the potential difference between the two capacitors C_1 & C_2 is small. This difference increases at transient operation of the drive. It is observed that when (at time 1 sec) the 4 Nm load is applied to the motor the potential difference between the two capacitors C_1 & C_2 increase. Trace 1 in the Figure 4.14 shows the torque, whereas trace 2 and trace 3 represents the capacitor voltages V_{c1} and V_{c2} across the two capacitor C_1 and C_2. The deviation of the two capacitor voltage is shown in trace 4. The potential difference between the two capacitors is shown in trace 5. It is observed that the potential difference gradually increase after the loading instant.

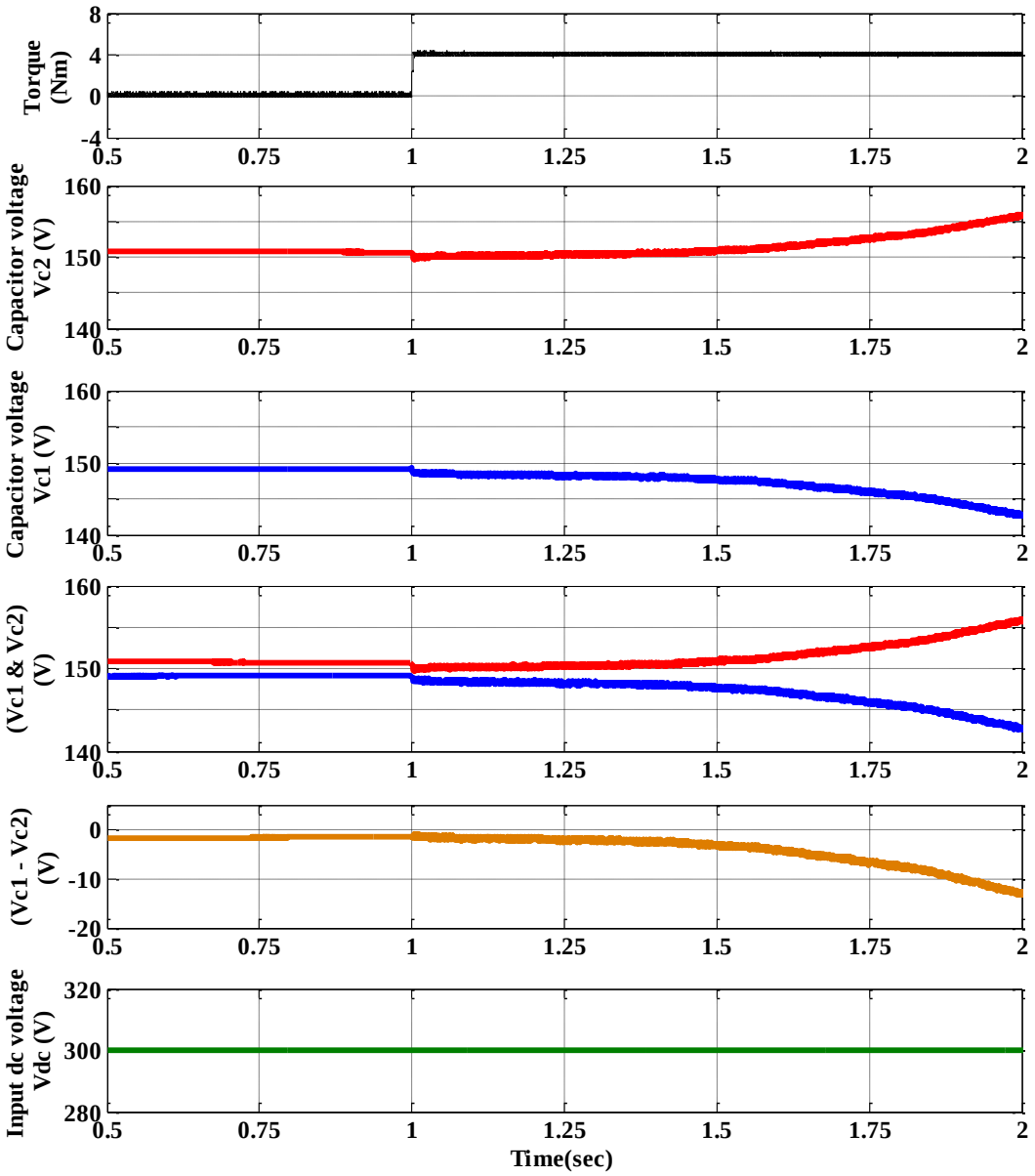

Figure 4.14 Capacitor voltage at loading condition without any voltage balancing

To overcome the capacitor voltage balancing problem a three-level boost converter (TLBC) circuit has been implemented. The proposed PMSM drive with resolver sensor is simulated using three-level boost converter (TLBC) with neutral point clamped (NPC) three-level inverter. The capacitor voltages with load changing operation are shown in the Figure 4.15. It is observed that during the no-load operation both the capacitor voltages are maintained to the reference value 150 V.

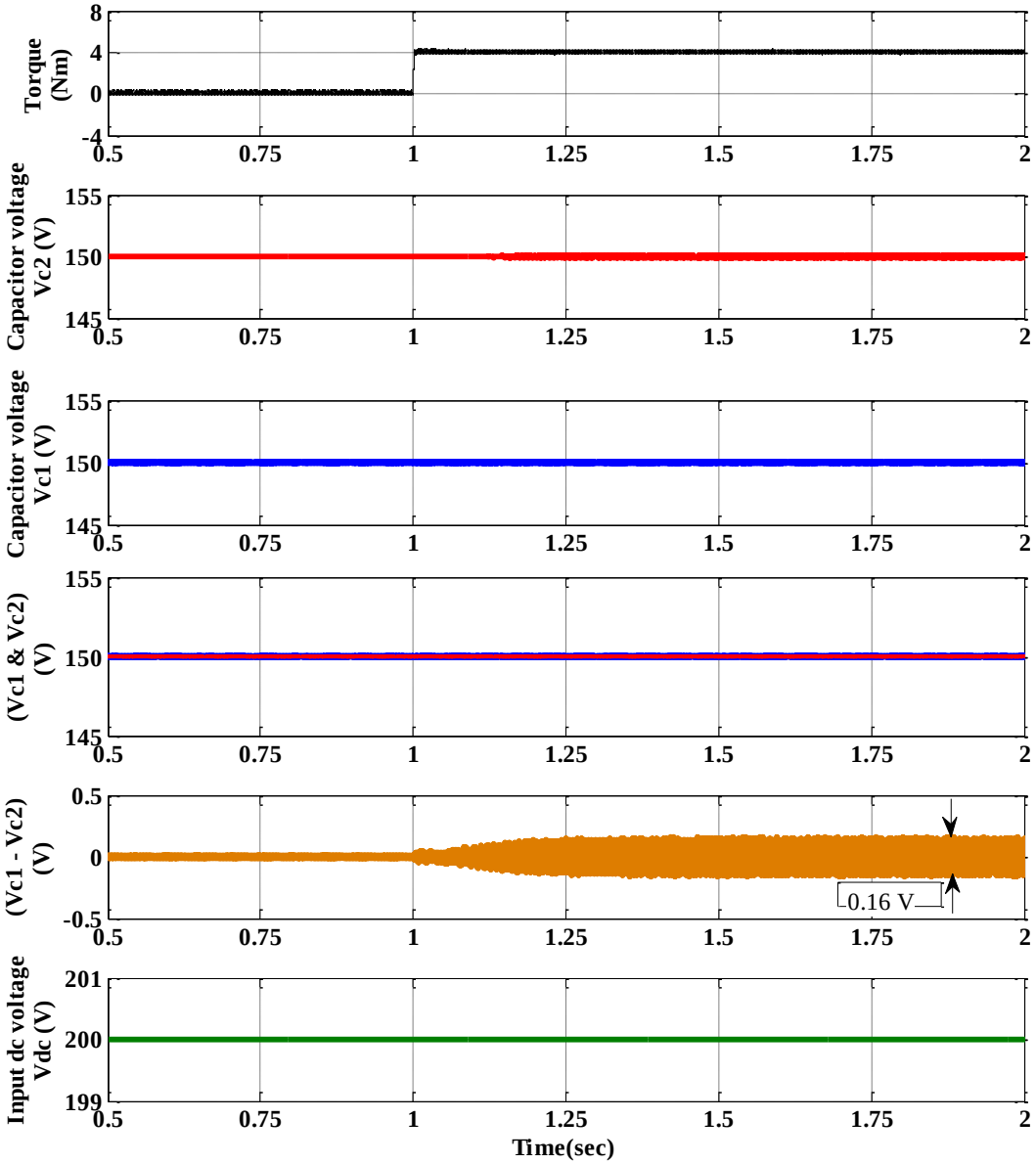

Figure 4.15 Capacitor voltage at loading condition with TLBC circuit

It is also noticed that during loading operation both the capacitor voltage are equally maintained to 150V. The input voltage to the NPC inverter is maintained at 300 V with the help of TLBC by selecting the duty ratio (D) of 0.667, whereas the input dc voltage (V_{dc}) is 200 V. The voltages V_{c1} and V_{c2} across the two capacitors C_1 and C_2 are depicted by trace 2 and trace 3 in the Figure 4.15. This is noticed that the equal voltage sharing is done by both the capacitor. Both the voltages V_{c1} and V_{c2} are presented in trace 4 to show the difference in two capacitor voltage. But the potential difference between the two capacitors is very less which is shown in trace 5. It is observed that the voltages difference between the capacitors at the time of loading in NPC three-level inverter with using TLBC circuit is maintained at less than 0.5V, which is quite satisfactory. The dc input voltage to the inverter is 200 V. But with

using of TLBC circuit the voltages across each capacitor is achieved 150V. So the effective voltage across the NPC three-level inverter is the sum of two capacitor voltages i.e. 300 V. So the proposed three-level NPC inverter fed PMSM drive with TLBC circuit provides the added advantageous boosting feature along with the capacitor voltage balancing. The capacitor voltages at starting of the motor with no load operation are shown in Figure 4.16.

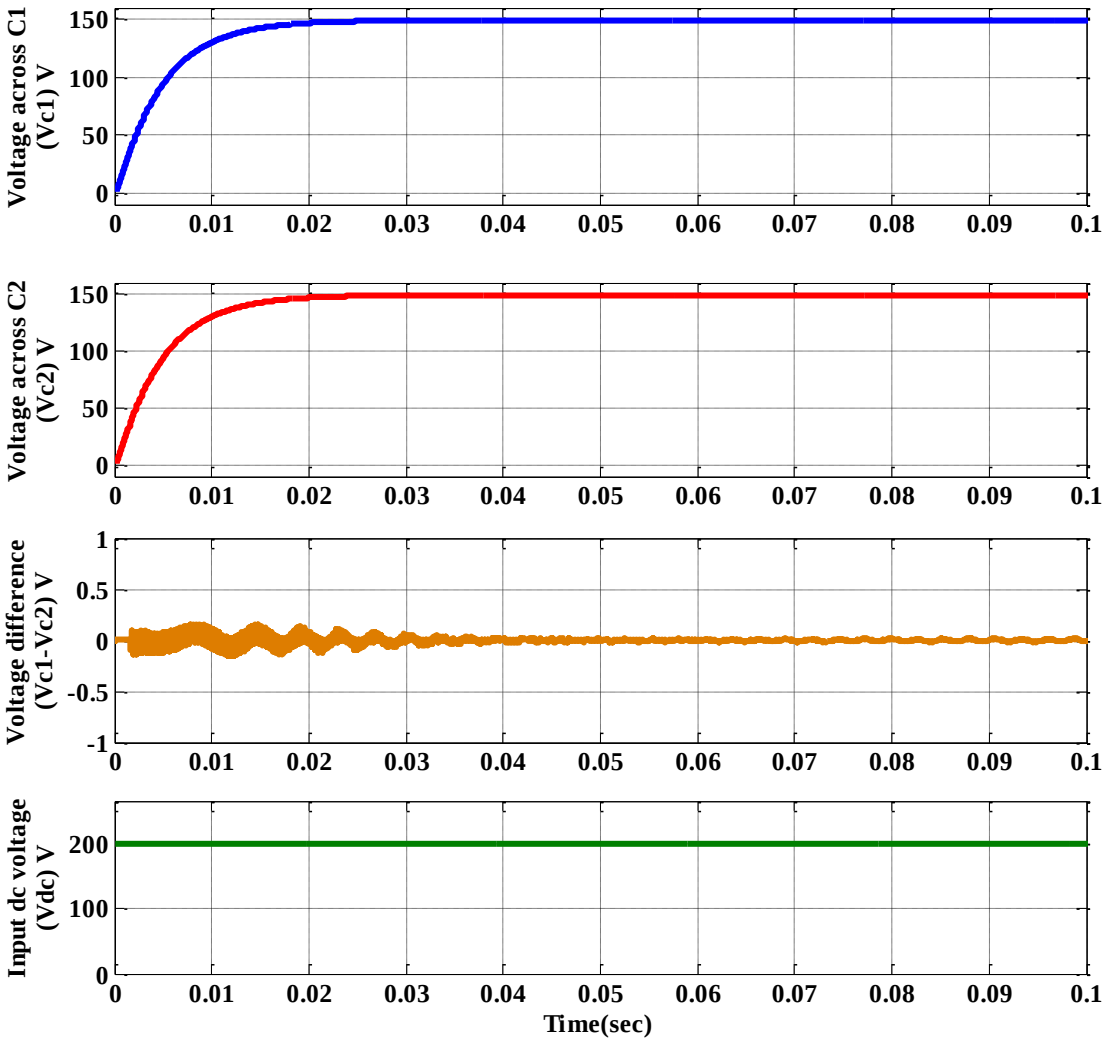

Figure 4.16 Simulation results of input voltage and capacitor voltage with TLBC balancing circuit

Trace 1 represents the voltage across the capacitor C_1 and the trace 2 represents the voltage across capacitor C_2. It is observed that with the use of TLBC in three-level NPC inverter the voltage across the capacitors are maintained at desired value 150 V. The voltage difference is shown in trace 3 is quite less. So the dc link voltage is perfectly balanced with the use of TLBC in three-level NPC. The simulated three-phase line to line voltage waveform of three-level NPC inverter is shown in the Figure 4.17. This is observed that the three-level NPC

inverter introduce the more steps in the line to line voltages which improves the voltages quality i.e. more close to sinusoidal. Trace 1, 2 and 3 simultaneously shows the line to line voltages of the three-level NPC inverter V_{ab} , V_{bc} and V_{ca}. The fundamental frequency is kept 100 Hz.

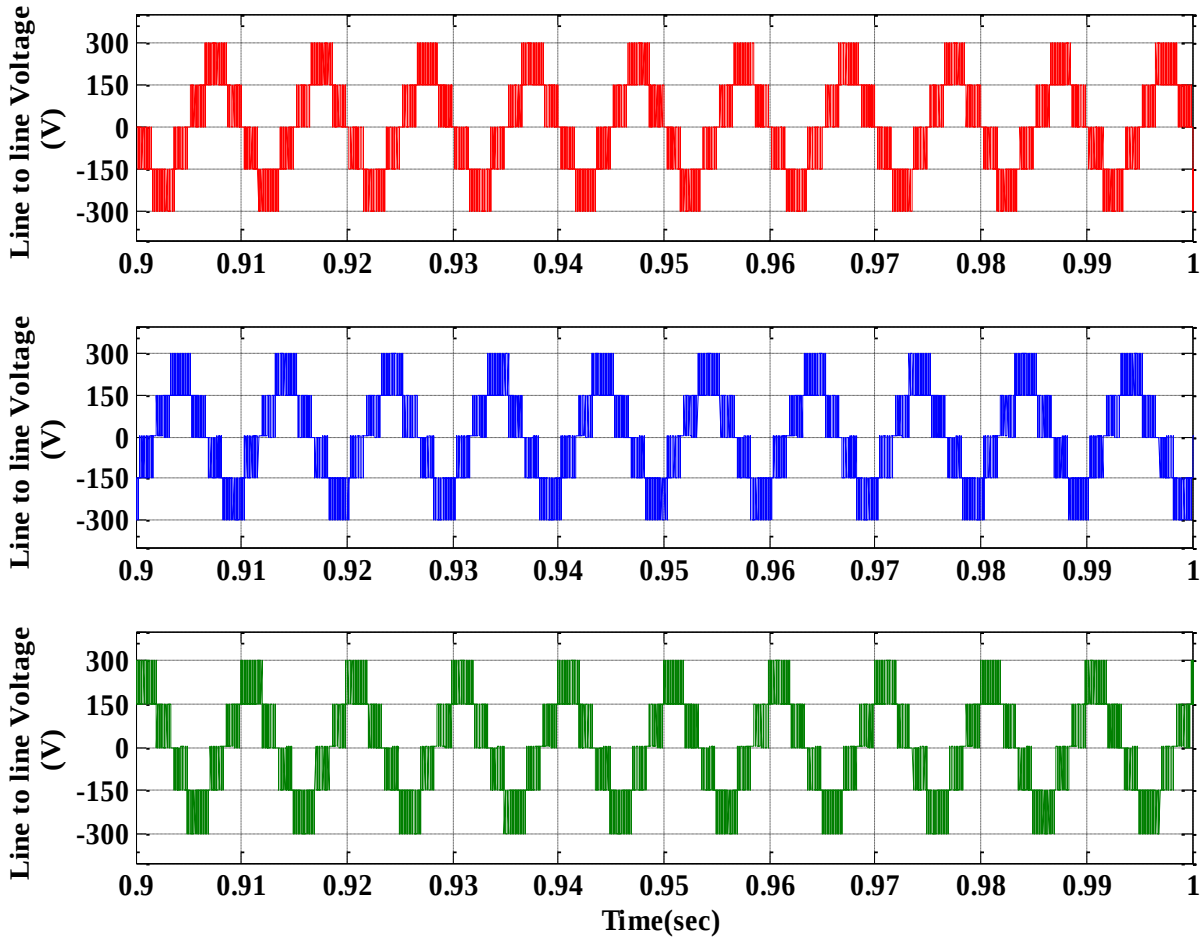

Figure 4.17 Line to line voltage of three-level NPC inverter

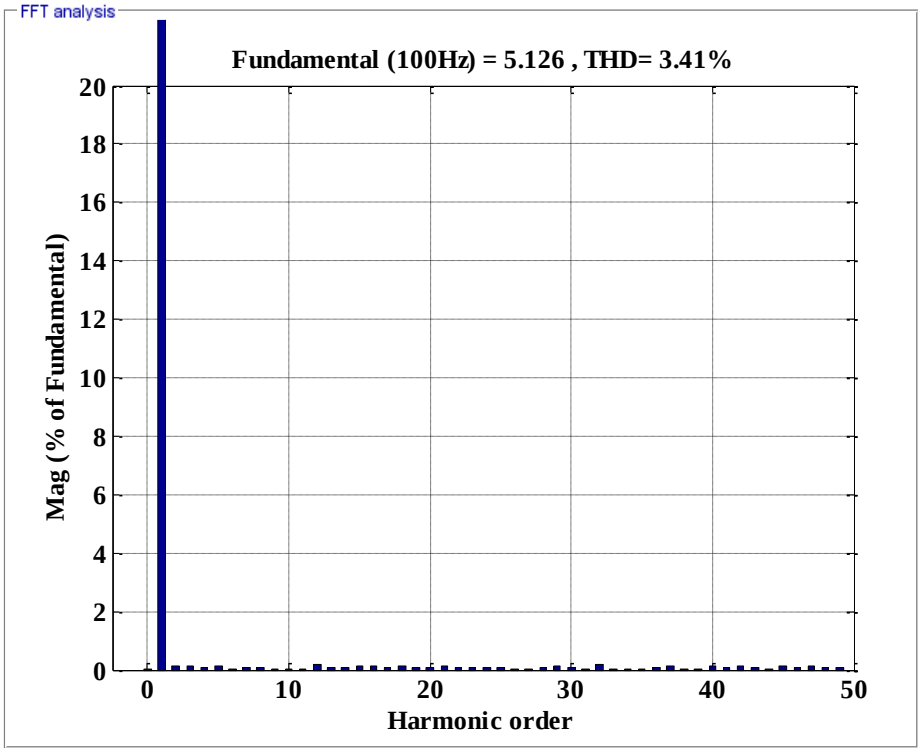

Figure 4.18 Current THD of the three-level inverter fed drive

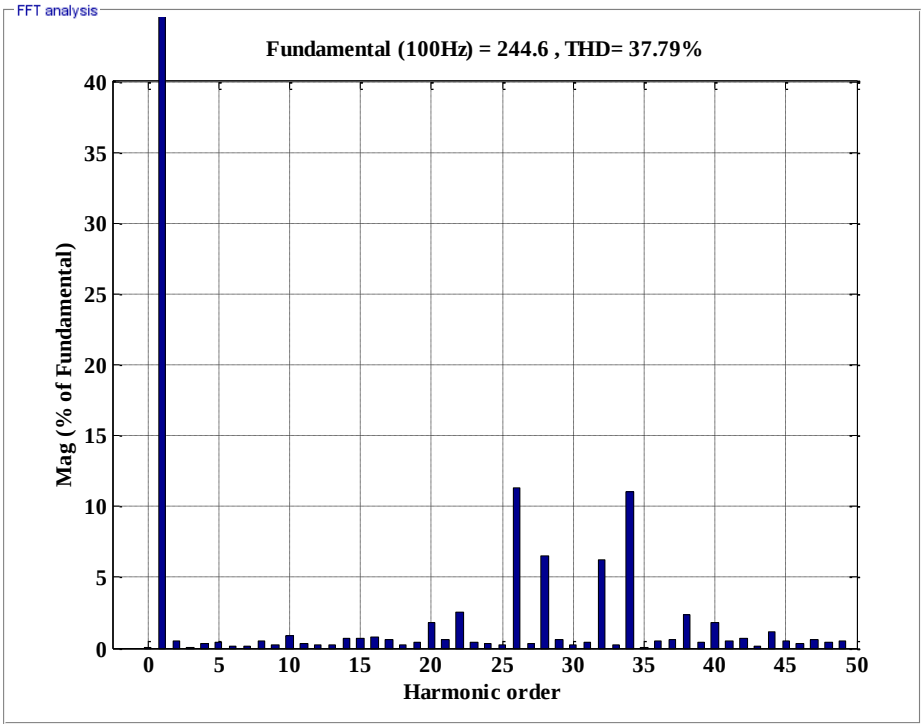

Figure 4.19 Voltage THD of the three-level inverter fed drive

Compare to two-level inverter, three-level inverter produce lower switching losses at higher switching frequencies to get the same dc-link voltage. Lower dv/dt also reduces the voltage stress across the power switches. The other attracting feature is reduction in total harmonic distortion (THD). The three-level NPC inverter improves the voltages quality hence the THD is reduced. The current THD and voltages THD is shown in the Figure 4.18 and Figure 4.19. It is observed that the current THD in three-level NPC inverter is 3.41%, whereas the voltage THD is 37.79%. The performance of the proposed three-level NPC inverter fed PMSM drive with zero d-axis current control has been investigated in different operating condition. RDC less software based position estimation from the resolver sensor has been used to estimate the accurate position to implement the vector control. Based on the availability of the motor prototype in the laboratory the proposed drive is simulated with surface permanent magnet synchronous motor. The specification of the proposed drive is shown in the Table 4.4.

The starting response of the proposed three-level NPC inverter fed PMSM drive has been shown in the Figure 4.20. The drives has been simulated with K_P=0.0036 and K_I=0.0032 Values. The reference value of speed is kept 900 rpm and the motor is started with no load. It is observed that the motor reaches its reference speed value as depicted by trace 2. Initial starting torque is high. The stator current is also high at the time. It reduces when the motor reaches its reference speed value.

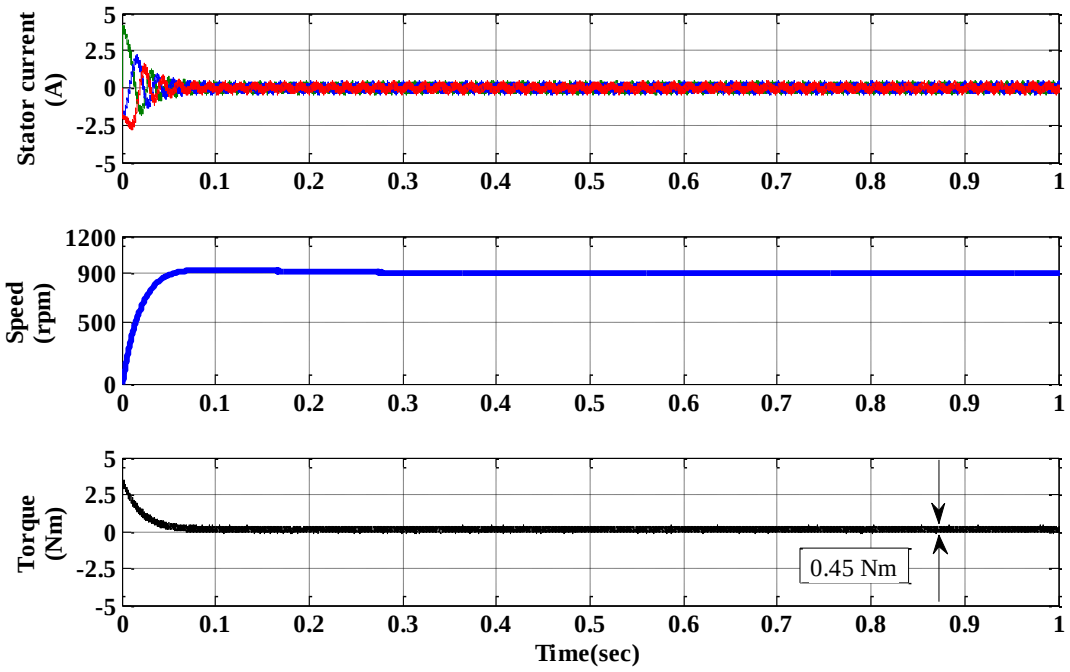

Figure 4.20 Starting response of the PMSM drive fed from three-level inverter

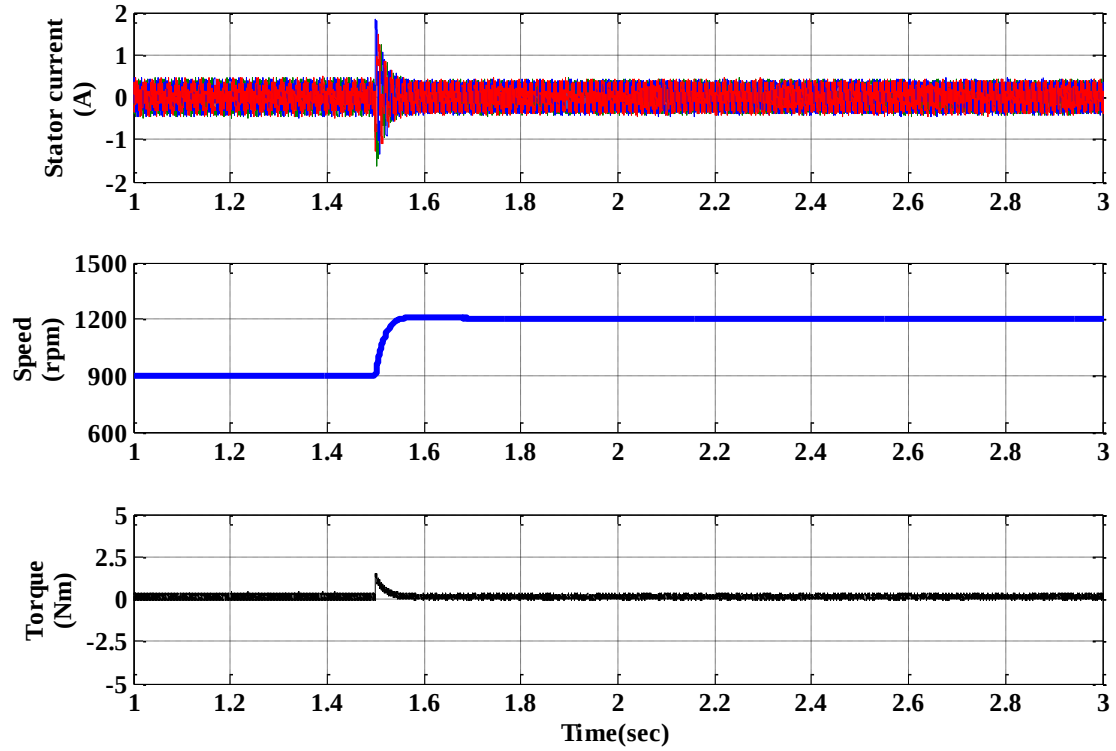

Figure 4.21 Response of the drive at speed increasing condition

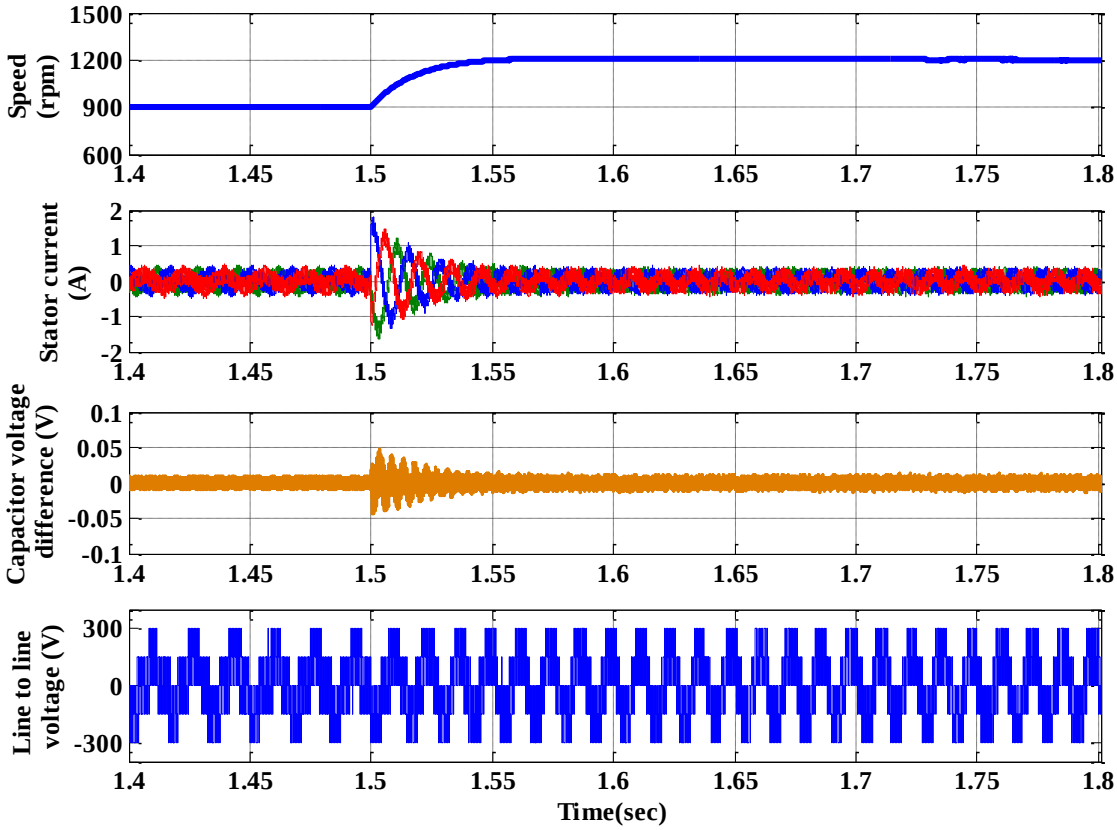

Figure 4.22 Stator current, capacitor voltage difference and line to line voltage at speed changing operation

The performance of the proposed drive with ZDAC control at speed changing operation also has been investigated. The speed reference increased from 900rpm to 1200 rpm. A change in

speed reference of 300 rpm has been applied. The response of the drive at speed changing operation has been shown in the Figure 4.21. At 1.5 seconds the speed reference has been increased from 900 rpm to 1200 rpm. At this time the torque is increased by the motor to reach the reference speed. Due to that the stator current is also slightly increased at that time. The torque reduced once the reference speed value reached. The capacitor voltage difference at the time of speed increasing operation is shown in the Figure 4.22. The simulated results clearly shows that the potential difference between the two dc-link capacitors are very less i.e. below 0.1 V. The line to line voltage at the time of speed changing is also presented in trace 4.

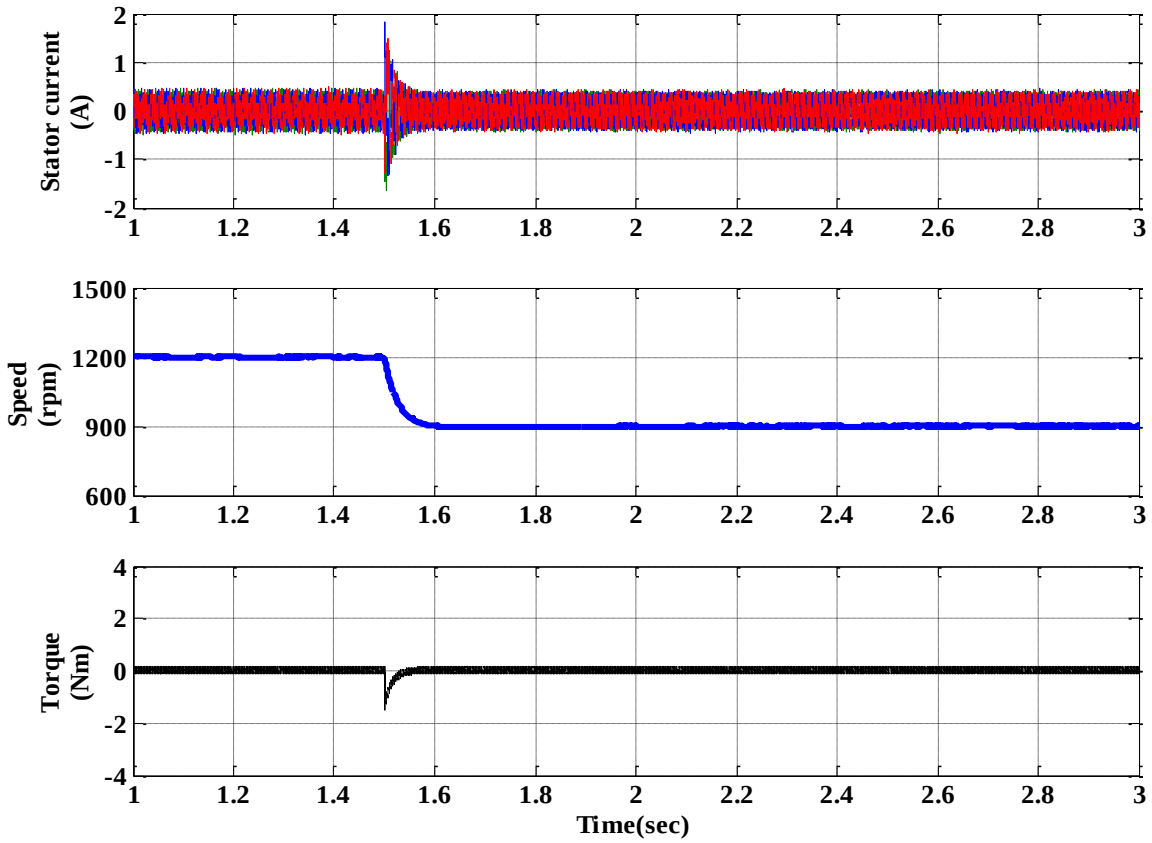

Figure 4.23 Response of the drive at speed decreasing condition

The performance of the drive at speed decreasing condition has been shown in the Figure 4.23. At time 1.5 sec the speed reference value is changed from 1200 rpm to 900 rpm. To reach the reference speed value the torque of motor decreased to negative value. The torque regains its original value once the reference speed value reached. The capacitor voltage balancing in proposed drive at speed decreasing operation also investigated. The simulation results shown in the Figure 4.24 validate the satisfactory performance of the proposed drive. It is observed that the voltage difference is also maintained at vey lower value. This means that the voltages sharing between the two dc-link capacitor are equal. The levels in the line to line voltages are also maintained at the time of speed changing.

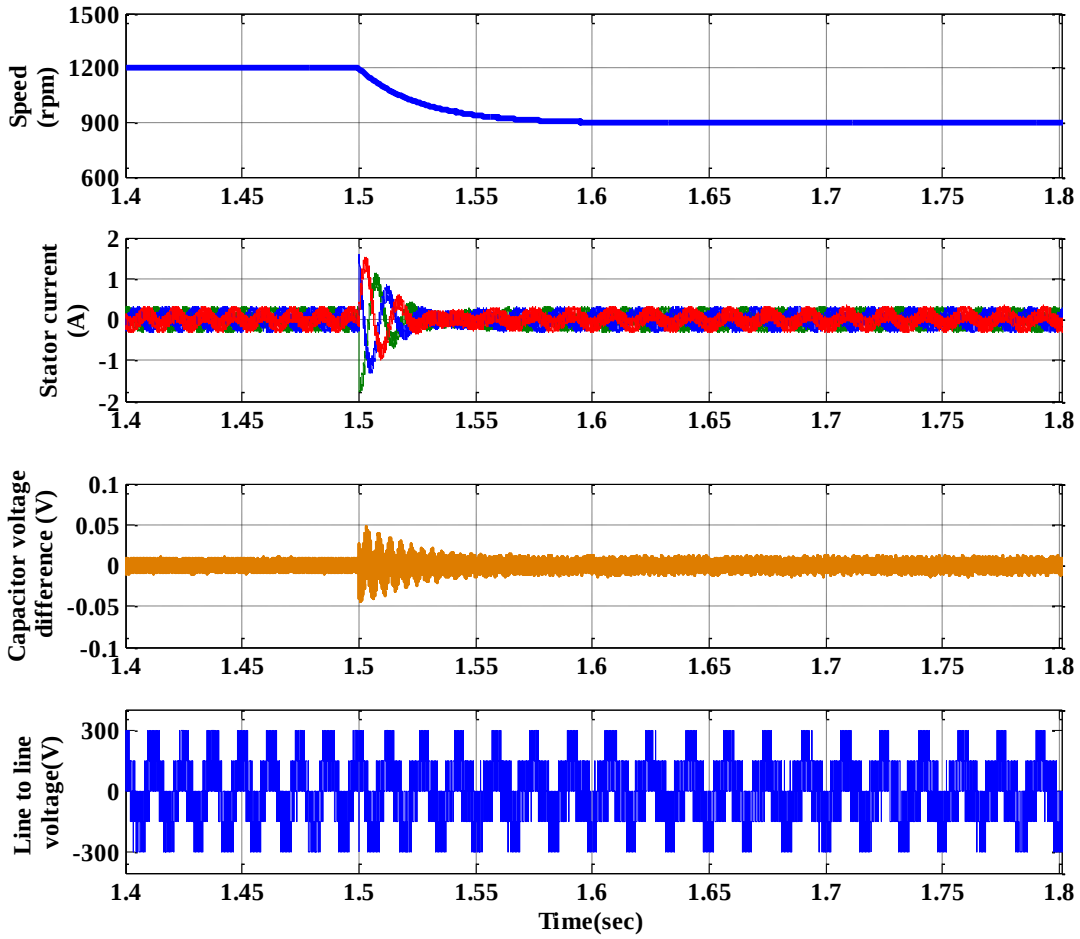

Figure 4.24 Stator current, capacitor voltage difference and line to line voltage at speed decreasing operation

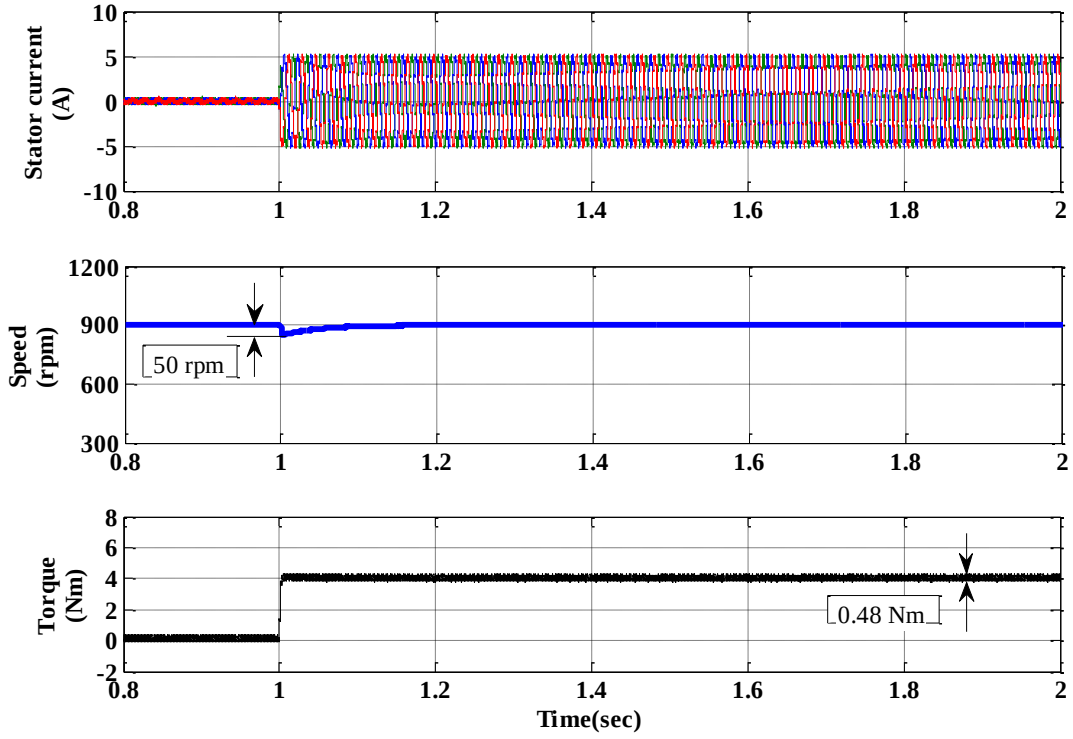

Figure 4.25 Performance of the drive at loading condition

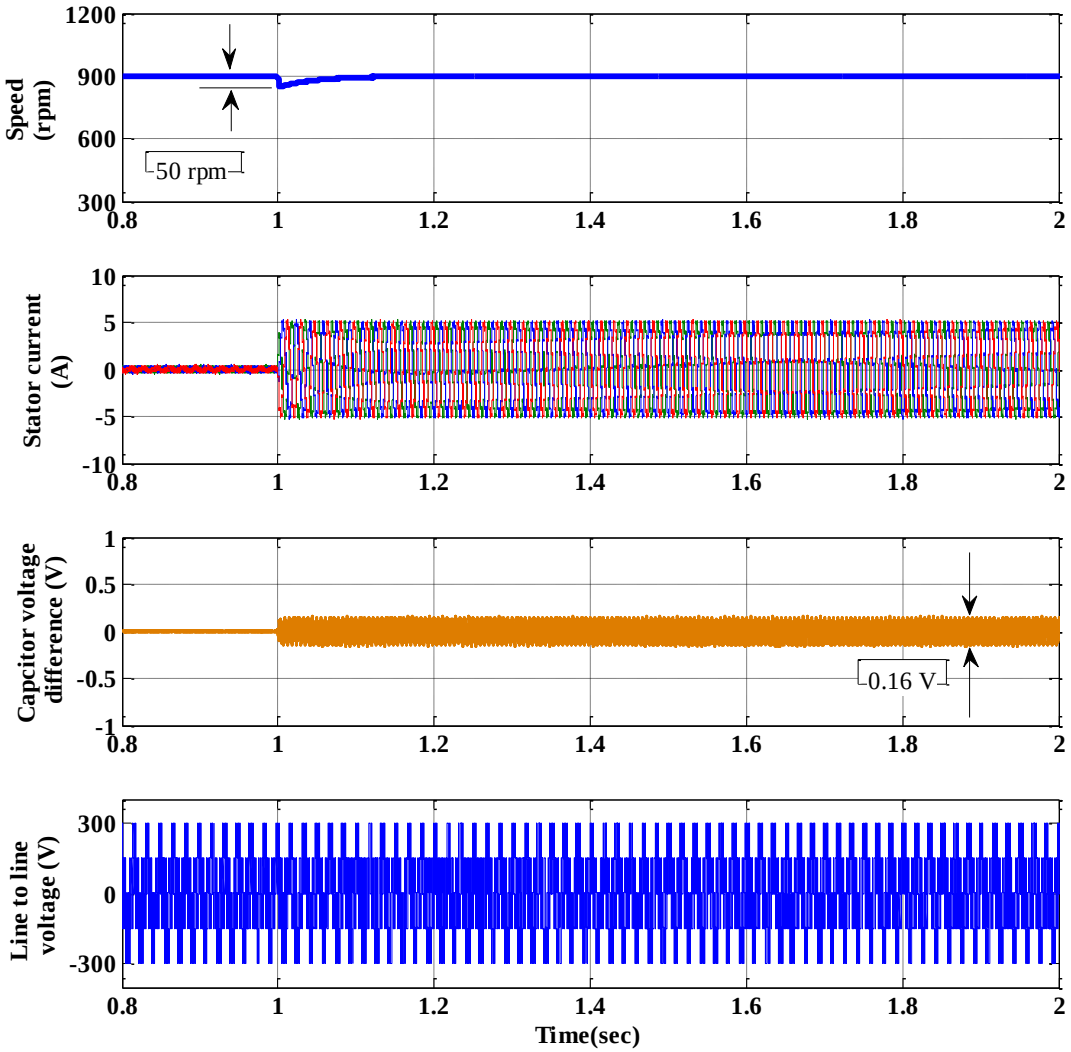

Figure 4.26 Speed response & capacitor voltage balancing at loading condition

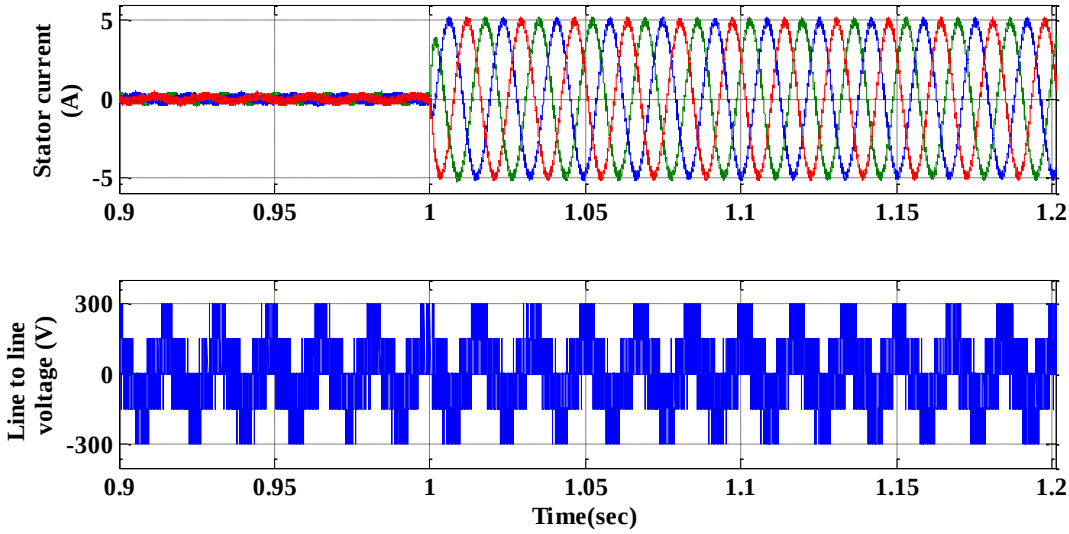

Figure 4.27 Magnified view of stator current and line to line voltage at loading condition

To investigate the performance under loading condition a load of 4Nm is applied to the motor and simulation results are obtained. The response of the drive at increasing load has been shown in the Figure 4.25. A step load of 4 Nm is applied at 1 sec. It is observed that the stator current is increased at the time of loading. It is also observed that there is dip in the speed response. This dip is due to the loading. This speed response reaches the reference due to the closed loop operation of the drive. The Figure 4.26 depicts the performance of the drive maintaining the capacitor voltage difference within the desired value. The magnified view of the stator current and line to line voltage has been shown in the Figure 4.27. So it is observed that the proposed three-level NPC inverter fed PMSM drive provides the desired performance at different operating condition.

4.6 Comparative Analysis of Two-level and Three-level Inverter Fed PMSM Drive

Conventionally, in two-level voltage source inverter is used in PMSM drive. If the fundamental output voltage and corresponding power level of the inverter are increased to a high value, the DC link voltage must be increased substantially. However, fast frequency semiconductors have a limitation in the maximum voltage and very high voltage jump will lead to terrible electromagnetic interference and high windings insulation stress. So for the high performance of PMSM drive systems at increased power level, high quality inverter output with low harmonic loss and generating low torque fluctuation is necessary. Three-level NPC inverter is an emerging technology that can overcome these disadvantages. Three-level NPC inverter fed PMSM drive promising the better performance in terms of harmonic reduction, high DC link voltage level and lower torque repulsion. The comparative performance investigation has been done between the two-level inverter and three-level NPC inverter fed PMSM drive at different operating condition. Both the cases vector control in terms of zero d-axis current control has been implemented. RDC less software based position estimation from the resolver sensor has been used to estimate the accurate position and speed to implement the vector control. The starting response of the drive for two different inverters has been shown in the Figure 4.28 and Figure 4.29 simultaneously. It is observed that when the PMSM motor is fed with three-level inverter the performance is improved as compared to the two-level inverter. Torque ripple is minimized with three-level inverter.

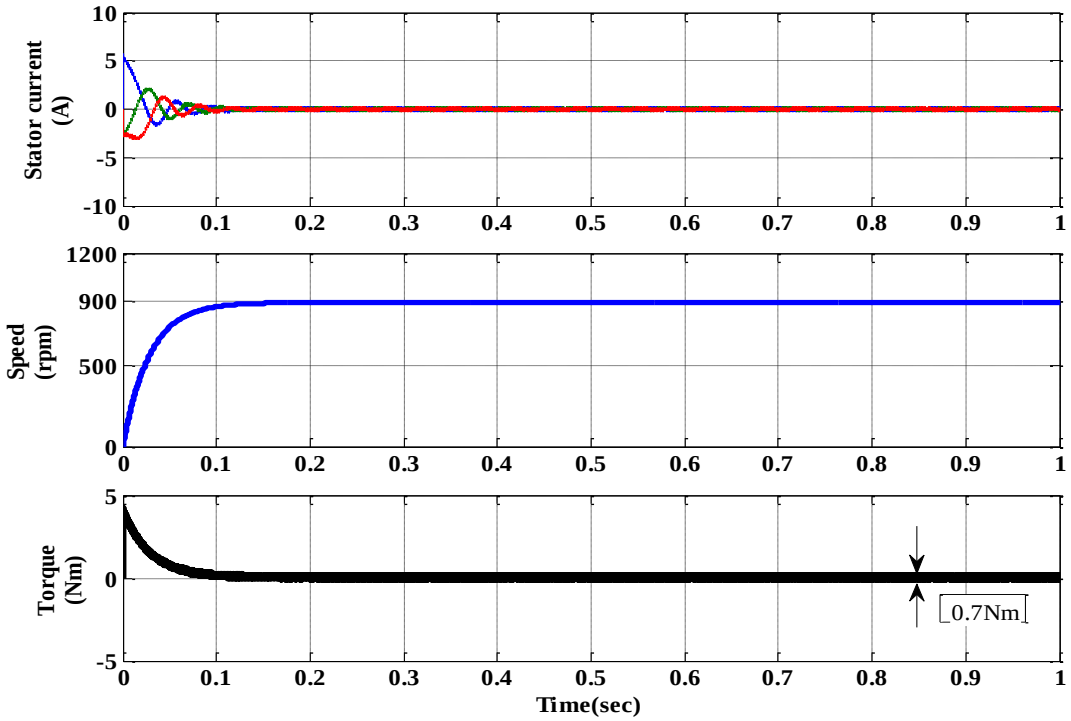

Figure 4.28 Starting response of the PMSM drive fed from two-level inverter.

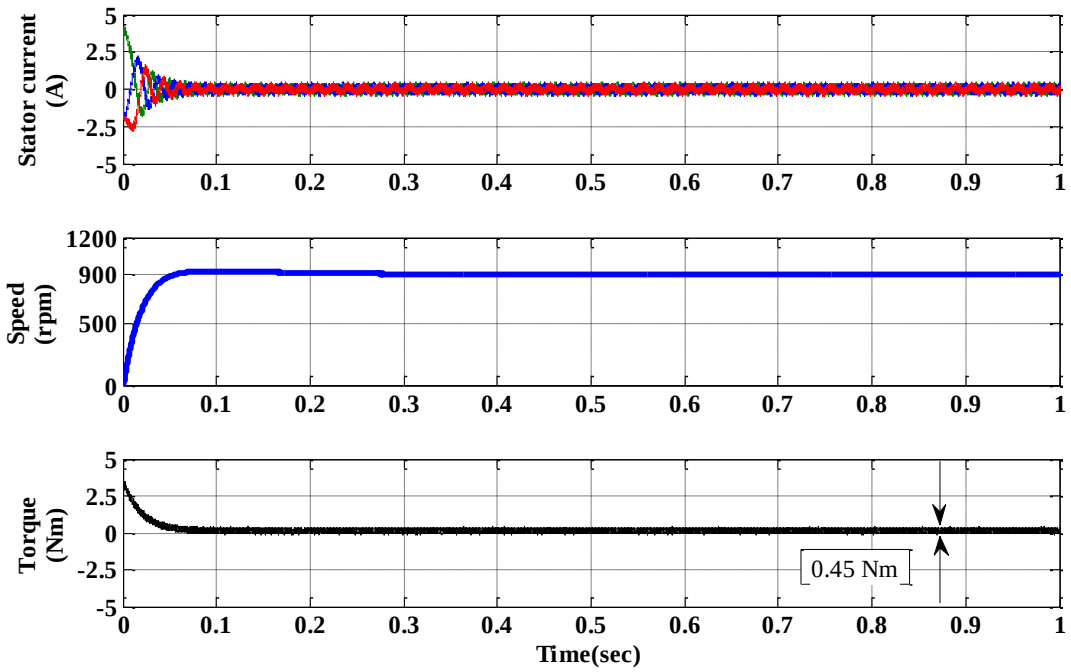

Figure 4.29 Starting response of the PMSM drive fed from three-level inverter.

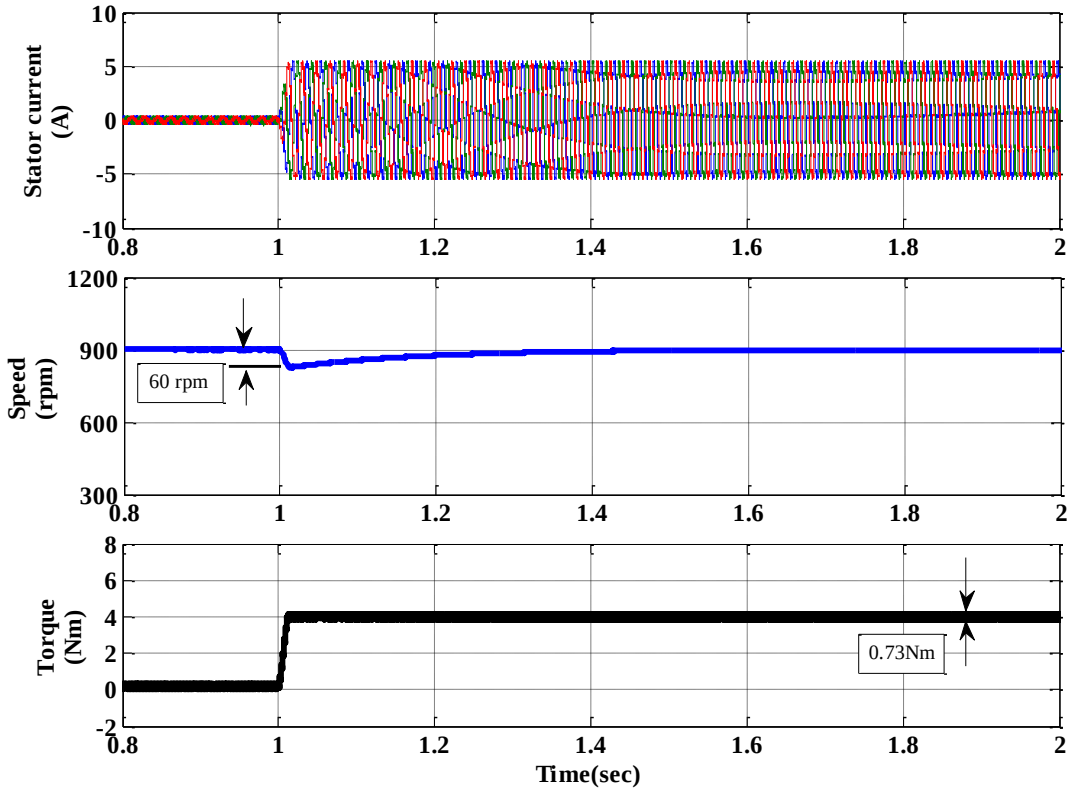

Figure 4.30 Response of the PMSM drive fed from two- level inverter at loading condition

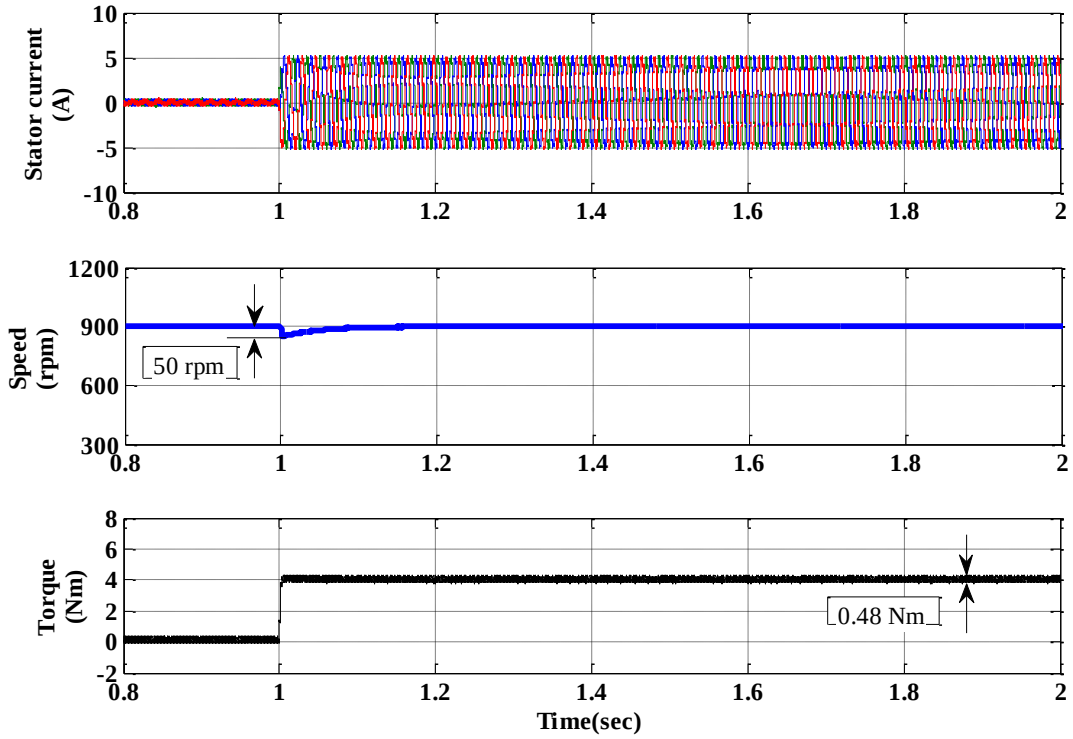

Figure 4.31 Response of the PMSM drive fed from three-level inverter at loading condition

Further to investigate the performance of the drive with two different inverters at loading condition, the simulation has been done. Figure 4.30 shows the drive response with two-level inverter and Figure 4.31 shows the drive response with three-level NPC inverter. At 1 second

4 Nm load has been applied to both the cases. This is noticed that the torque ripple is reduced in three-level NPC inverter fed drive.

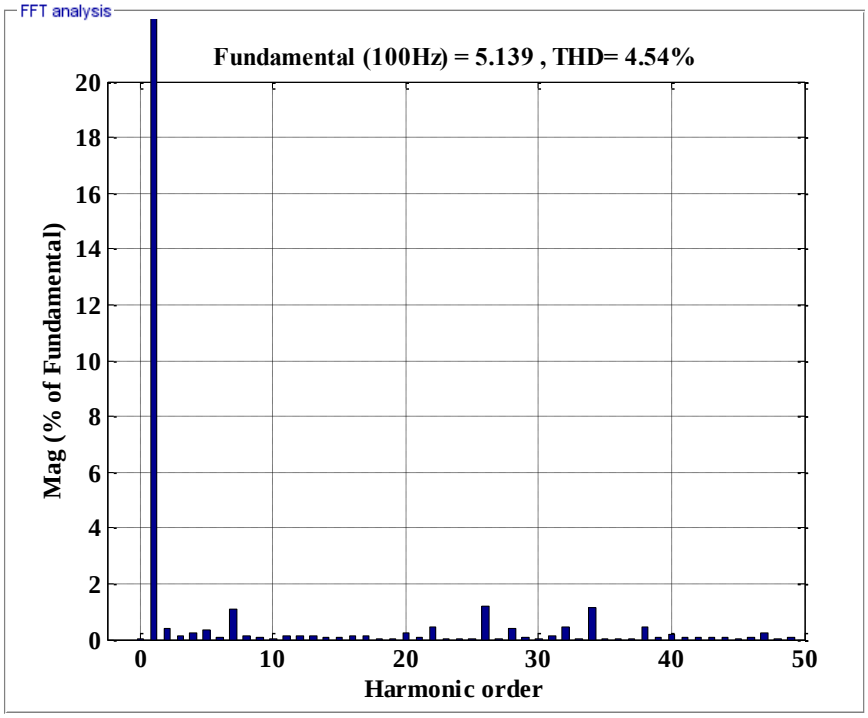

Figure 4.32 Current THD of PMSM drive fed from two- level inverter

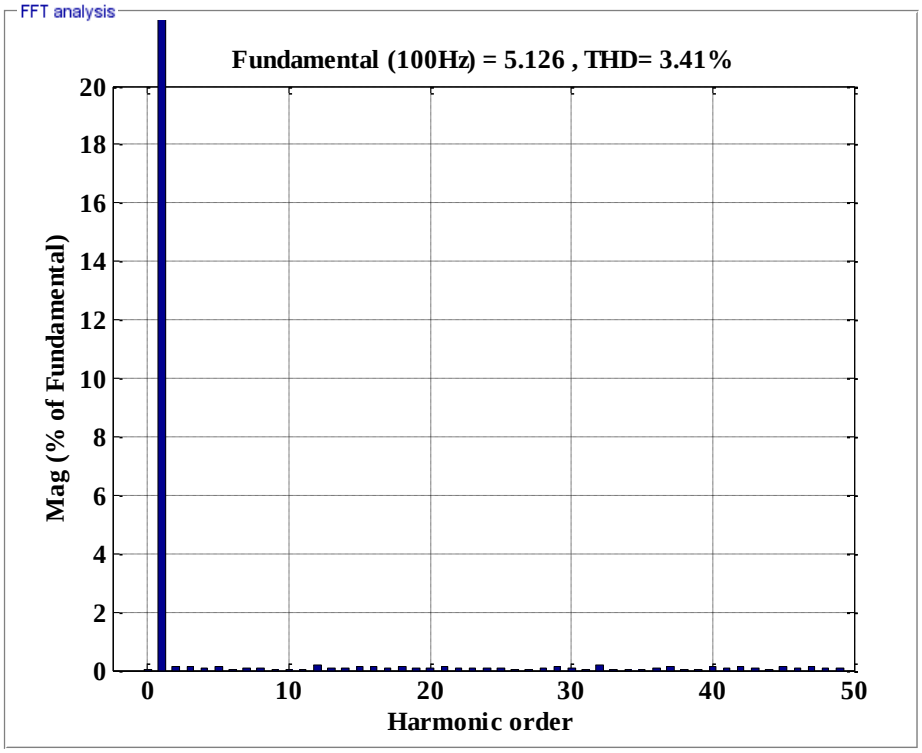

Figure 4.33 Current THD of PMSM drive fed from three -level inverter

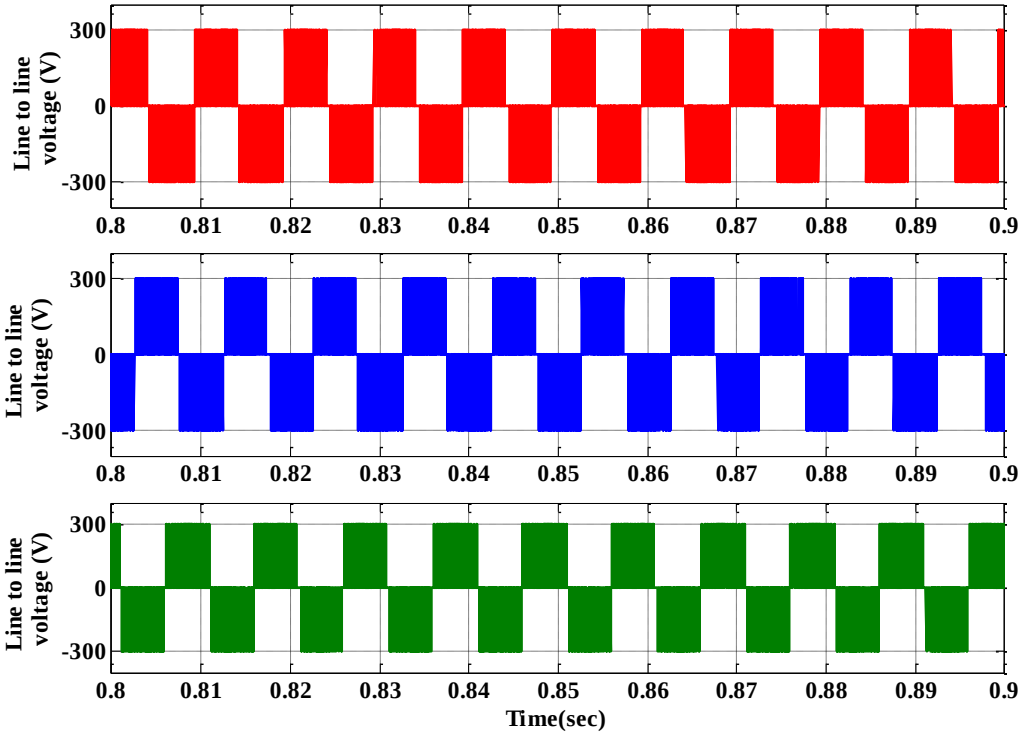

Figure 4.34 Line to line voltage of PMSM fed from two- level inverter

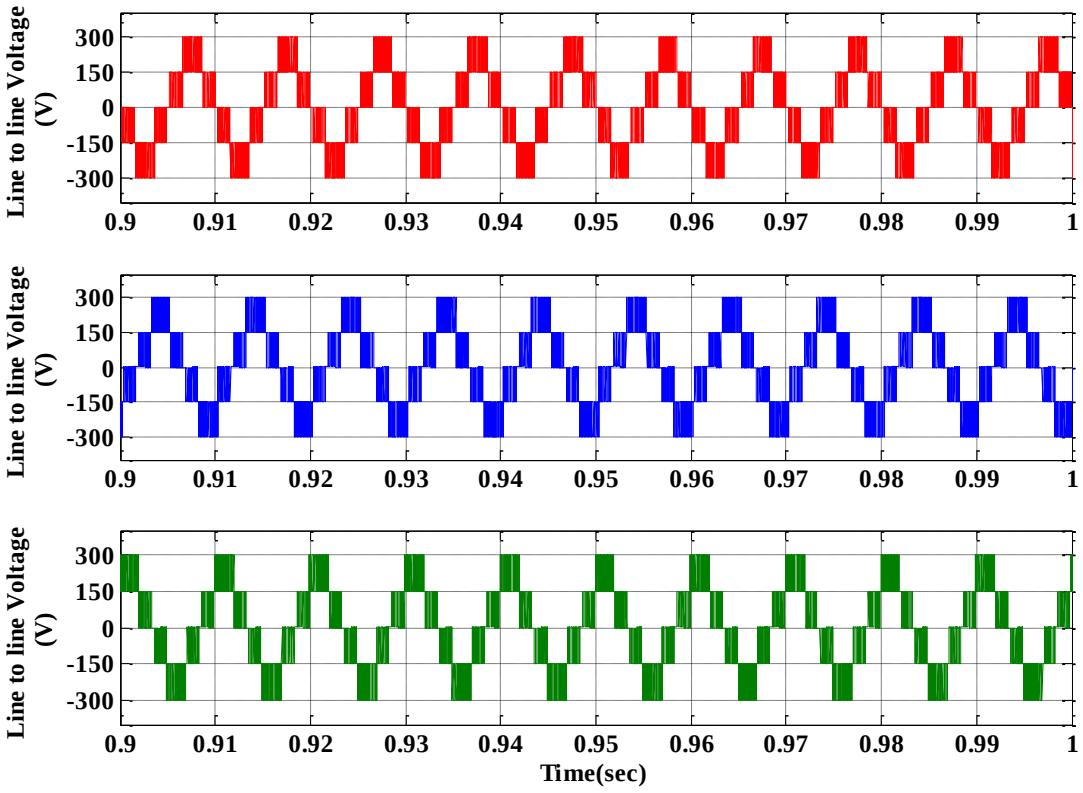

Figure 4.35 Line to line voltage of PMSM fed from three- level inverter

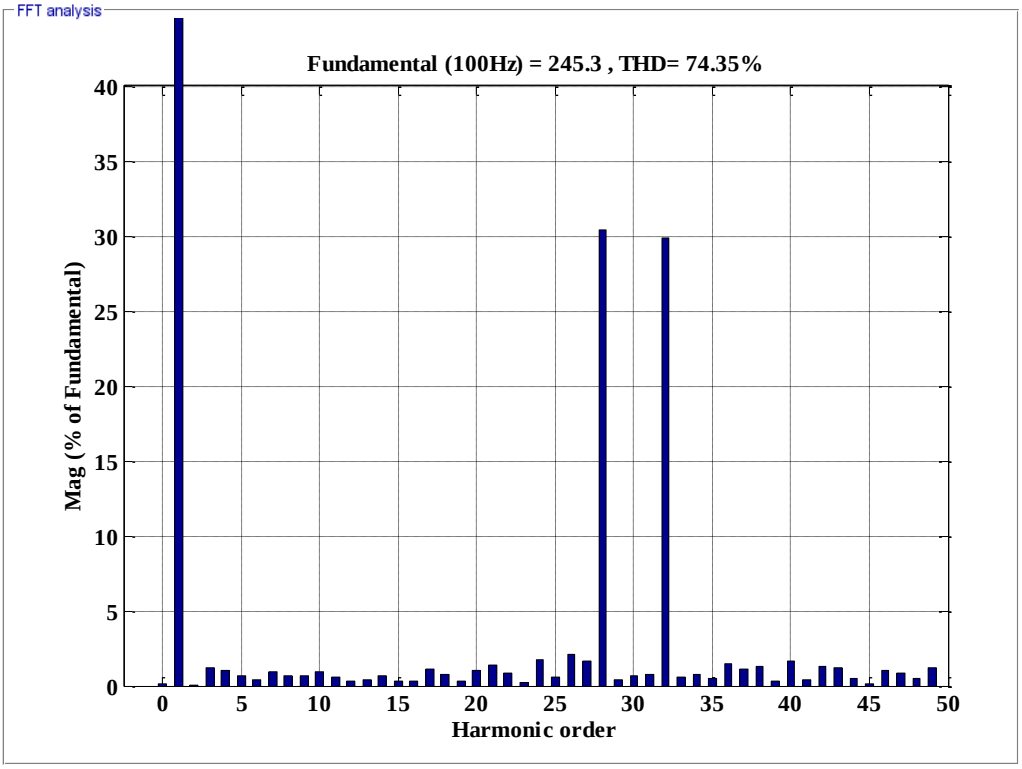

Figure 4.36 Voltage THD of PMSM drive fed from two- level inverter

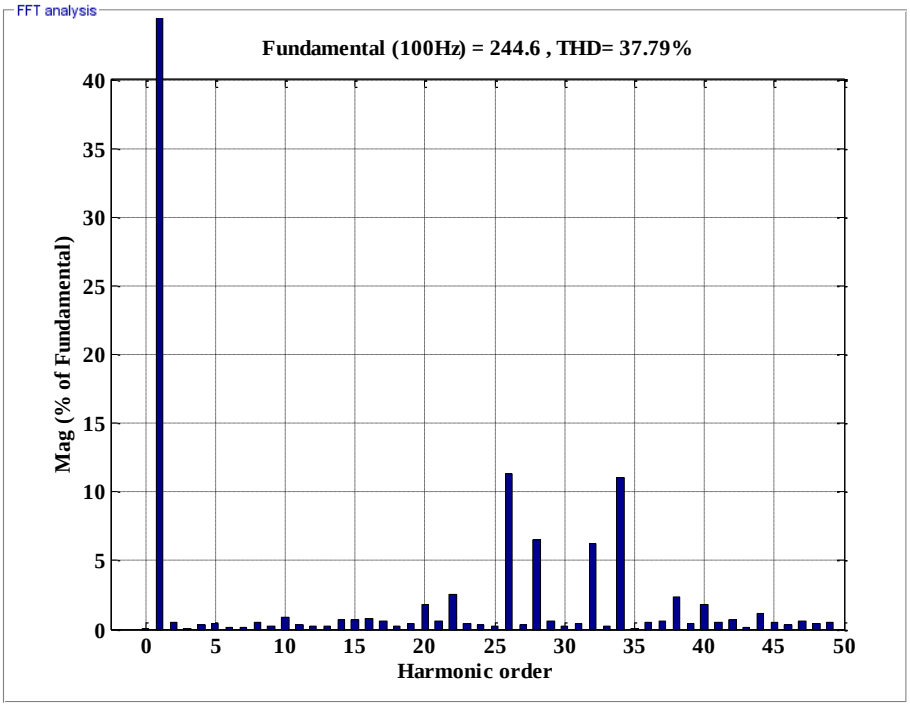

Figure 4.37 Voltage THD of PMSM drive fed from three- level inverter

NPC three-level inverter fed PMSM drive draw the key attention to the researchers and technologist due to reduction in total harmonic distortion (THD). The comparative analysis is made in terms of current THD and voltage THD for both the inverter. The fundamental

frequency is kept 100Hz for the simulation analysis. The three-level NPC inverter improves the voltages quality. The current THD when the motor is fed from two-level inverter is shown in the Figure 4.32. It is observed that the current THD is 4.54%. The current THD, when the PMSM is fed from three-level NPC inverter is shown in the Figure 4.33. This is noticed that the current THD in three-level NPC inverter is 3.41% which is less as compared to two-level inverter. The line to line voltage of both the inverter is shown in Figure 4.34 and Figure 4.35 respectively. From Figure 4.36 it is observed that the voltage THD is 74.35% when fed from two-level inverter. But with three-level inverter the voltage THD is 37.79% as shown in Figure 4.37. It can be observed that, in case of the three-level inverter, the harmonic distortion is almost 50% lower than that of the two-level inverter.

Table 4.5 Comparative analysis of two-level inverter and three-level NPC inverter

Different indices	Inverter	
	Two-level inverter	Three-level NPC inverter
Torque ripple	18.4%	12.2%
Current THD	4.54%	3.41%
Voltage THD	74.35.%	37.79%

4.7 Conclusion

A detailed study on NPC three-level inverter fed PMSM drive with vector control is presented. Cost effective RDC less software based position estimation is used for proposed PMSM drive. A voltage balancing technique using TLBC is developed for three-level NPC inverter fed permanent magnet synchronous motor drive. The additional advantage of this balancing circuit as compared to the other carrier based PWM technique or SVM technique is the boosting feature, which is most demanding now a day for the electric vehicle application. The proposed MLI fed PMSM drive reduces the voltage THD and torque pulsation. Moreover, performance of the proposed balancing scheme is examined by carrying out extensive simulations studies on a surface-mounted permanent magnet synchronous machine with ZDAC control. The detailed simulation study is carried out for the proposed drive system. Comparative study between a two-level and a three-level inverter fed PMSM drive is also presented. The better performance is achieved in three-level inverter fed PMSM drive as compared to the conventional two-level VSI fed PMSM drive.

CHAPTER 5: SENSORLESS OPERATION OF PMSM DRIVE

[Sensorless control of neutral point clamped (NPC) three-level inverter fed permanent magnet synchronous motor drive is presented in this chapter. Back-emf based position estimation and Model Reference Adaptive System (MRAS) based estimation is presented. Exhaustive simulation results are presented to investigate the performance of the sensorless three-level NPC inverter fed PMSM drive under various operating condition.]

5.1 Introduction

The information of rotor position is usually obtained by resolvers or encoders attached to rotor shaft. However, the use of these position sensors reduces the noise immunity, and increase the size, cost and weight of the system. Elimination of these position sensors is highly encouraged to increase the reliability and robustness and reduce the cost of drive. So Furthermore investigation on sensorless control of (NPC) three-level inverter fed PMSM drive is carried out, to achieve cost effective system and to reduced total hardware complexity, to increase the mechanical robustness and reliability, to reduce the maintenance necessities, [152]–[154]. Sensorless controls in terms back-emf based position estimation and Model Reference Adaptive System (MRAS) based estimation are implemented. Although back-emf based position estimation provides adequate performance in higher speed of operation range, but it suffers in lower speed of operation. Furthermore this control technique is also motor parameter sensitive. Among the existing sensorless approaches adaptive control seems to be the most promising control strategies. This method is simple and computationally less complex [168]–[174]. Extensive simulations study is carried out for the proposed drive system in MATLAB/ Simulink.

5.2 Sensorless Control of PMSM

There are a lot of sensorless control strategies in the literature, each of them having its own advantages, disadvantages and limitations. In general to implement the vector control in PMSM drive the position is sensed using encoder and resolver sensor. The control without this kind of sensor is known as sensorless control. The term “sensorless control” does not mean that PMSM is being controlled without any sensor. It actually describes the position sensorless control which means that no position sensor will be used only voltage and current sensors are used in the entire control algorithm. These measured voltages and currents are

used in different calculations and used to estimate the rotor position and speed of PMSM. Some of the advantageous features of sensorless control are:

- Compact drive with reduced maintenance,
- No cabling is required for transducers, easy implementation and reduced noise,
- Decreased cost of drive,
- Suitable for hostile operating environment; temperature and humidity etc.

There are several methods for sensorless control of PMSM. A large number of methods are presented in the literature for sensorless operation of PMSM. Performance wise comparison with their advantage and limitations are given in Table 5.1.

Table 5.1 Comparison of different sensorless control technique

Method	Implementation	negative aspect	Parameter dependency	Earnings
Back -emf	Easy	Poor dynamic performance	High	Low cost
MRAS	Less complex	Tuning of PI	Yes (except R_s)	Free from integration
Observer	Medium	Computation time	Yes	Good dynamic performance
EKF	Complex	Computation time	Low	Robust
Artificial intelligence	Medium	Need fast processor	Medium	Robust Good noise rejection
SMC	Medium	Chattering	Medium	No extra electronics

5.3 Back-EMF Based Sensorless Control of Three-Level Inverter Fed PMSM Drive

Researchers and technologist have been persistent in their efforts to develop various sensorless-control techniques for PMSM drive eliminating the conventional position sensor. All the solutions that have been proposed during the last few years have advantages and

drawbacks and cannot be considered resolute for the widest range of applications. The rotor position can be estimated based on back electromotive force (EMF) calculated by integration of the total flux linkage on the stator phase circuits. Although this control is simple, it suffers in low speed operation as well as flux-integrator's drift problem. Furthermore, this control is sensitive to the stator resistance variations. The better performances is achieved with the direct determination of back-emf space vector e_s instead of the flux space vector, which also eliminate the flux signal integrator [161]. Back-emf based methods offer adequate performance in the higher speed range [162], [163].

5.3.1 Position and Speed Estimation Using Back-EMF Method

The control scheme is based on estimation of back-emf space vector which makes the system less susceptible against the EMI problem. This is also reliable and cost effective. The sensorless control scheme using back-emf based estimation technique in three-level NPC inverter fed PMSM drive system, is implemented with vector control mode considering $i_d = 0$. Sensor-less control based on back-emf based estimation also provides high dynamic performance.

The expression of the back-EMF space vector components for a balanced three-phase system is,

$$\vec{e_s} = \vec{v_s} - R\vec{i_s} = e_{s\alpha} + je_{s\beta} \tag{5.1}$$

$$\vec{e_s} = [v_a - \frac{j}{\sqrt{3}}(v_a + 2v_b)] - R[i_a - \frac{j}{\sqrt{3}}(i_a + 2i_b)] \tag{5.2}$$

$$\vec{e_s} = v_a - Ri_a + \frac{j}{\sqrt{3}}[(v_a + 2v_b) - R(i_a + 2i_b)] \tag{5.3}$$

Where v_a, v_b is the A phase and B phase voltage i_a and i_b is the phase current, $\vec{i_s}$ Stator currents space vector, $e_{s\alpha}$ and $e_{s\beta}$ real and imaginary axes component of the back-emf e_s. The argument of the back-emf clearly is not the real rotor position. The real rotor position is given by the difference between the argument of e_s in the stator reference frame and the argument of the same one in the rotating *dqo* frame. The block diagram of the back-emf based sensorless control of three-level NPC inverter fed PMSM drive is shown in Figure 5.1.

A simple analysis on the machine model at steady state with $i_d = 0$ gives the following expression for rotor position:

$$\theta = \arctan\left[\frac{e_{s\beta}}{e_{s\alpha}}\right] - \arctan\left[\frac{\lambda_m}{L_d i_q}\right] \tag{5.4}$$

$$\theta = \arctan\left[\frac{v_\beta - Ri_\beta}{v_\alpha - Ri_\alpha}\right] - \arctan\left[\frac{\lambda_m}{L_d i_q}\right] \tag{5.5}$$

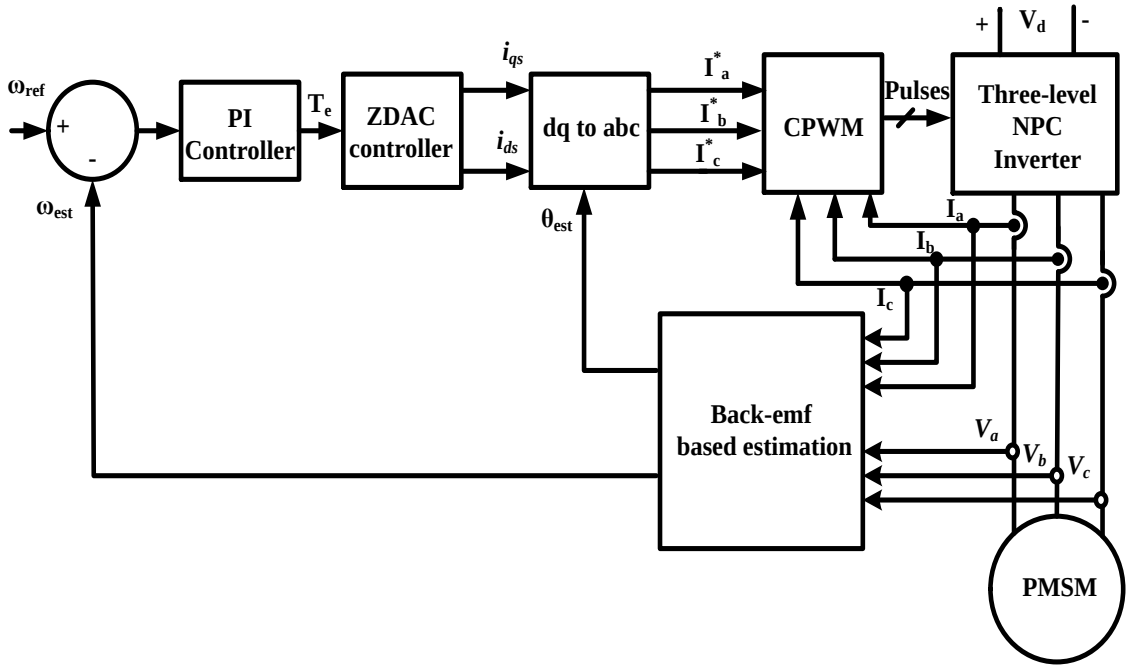

Figure 5.1 Block diagram of back-emf based sensorless control of three-level NPC inverter fed PMSM drive

The reference speed command is given as ω_{ref}. The estimated speed from the back-emf based estimation is ω_{est}. The speed error is processed through PI speed controller which generates the reference torque value as shown in the Figure 5.1. Using the vector control technique in terms of zero-d axis current control i_q currents are generated based on this torque reference. In this control the d-axis current is zero ($i_d = 0$). The i_d and i_q current are transformed in I^*_a, I^*_b and I^*_c using the estimated position θ_{est}. The gate signal of the inverter is generated using the reference current I^*_a, I^*_b and I^*_c and actual current I_a, I_b and I_c with the carrier based PWM technique.

5.3.2 Performance Evaluation of Back-emf Based Sensorless Control of PMSM Drive

The simulation is performed for back-emf based sensorless control of three-level NPC inverter fed PMSM drive and the results are presented. The actual rotor position and the estimated rotor position using back-emf based estimation method are presented in the Figure 5.2. It is observed that the estimated rotor position is following the actual rotor position of the motor with very less error.

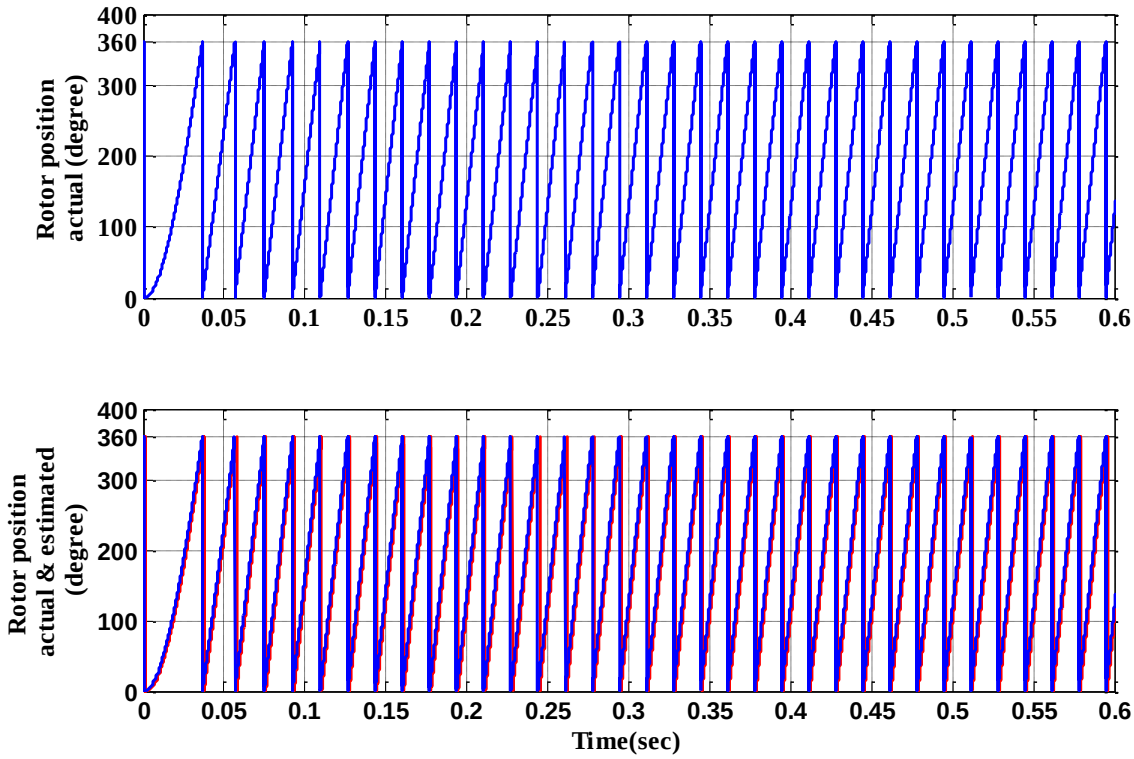

Figure 5.2 Rotor position, actual and estimated with back-emf based sensorless control

The motor reference speed 900 rpm is applied. The response of the drive is presented in the Figure 5.3. It is noticed that estimated rotor speed follows reference one with good accuracy. The discrepancy can be overcome by proper adjustment of PI speed controller gains. At starting motor produce the high torque. So the stator current is also high in that region. After reaching the reference speed the stator current reduces to some lower value. Estimated rotor position has been used for implementing the vector control in terms of zero d-axis current control of PMSM drive. Estimated speed has been used in the speed control loop.

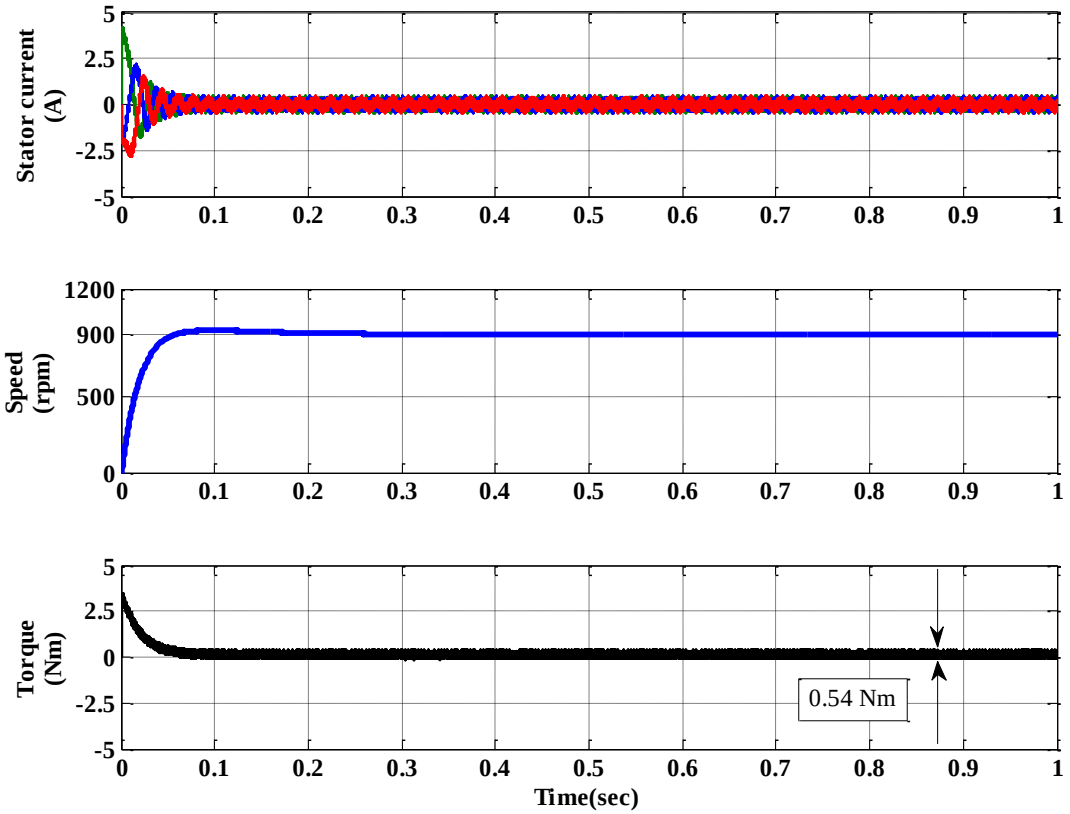

Figure 5.3 Starting response of the drive with back-EMF based sensorless control

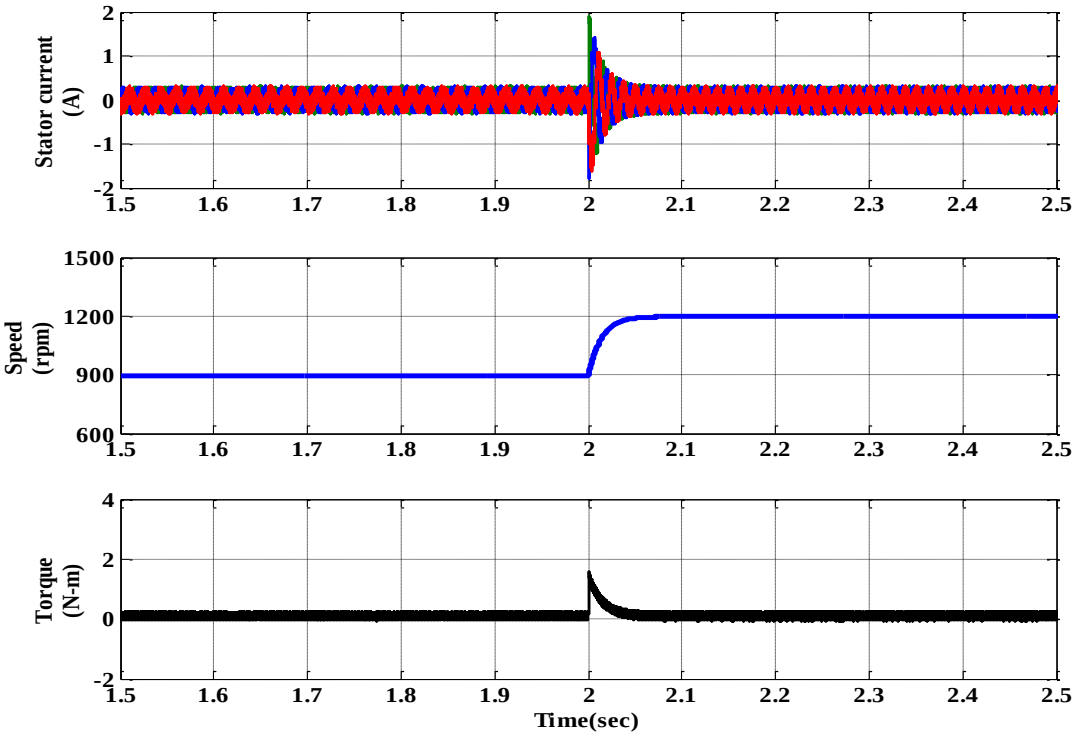

Figure 5.4 Performance of the drive at speed changing operation with back-EMF based sensorless control

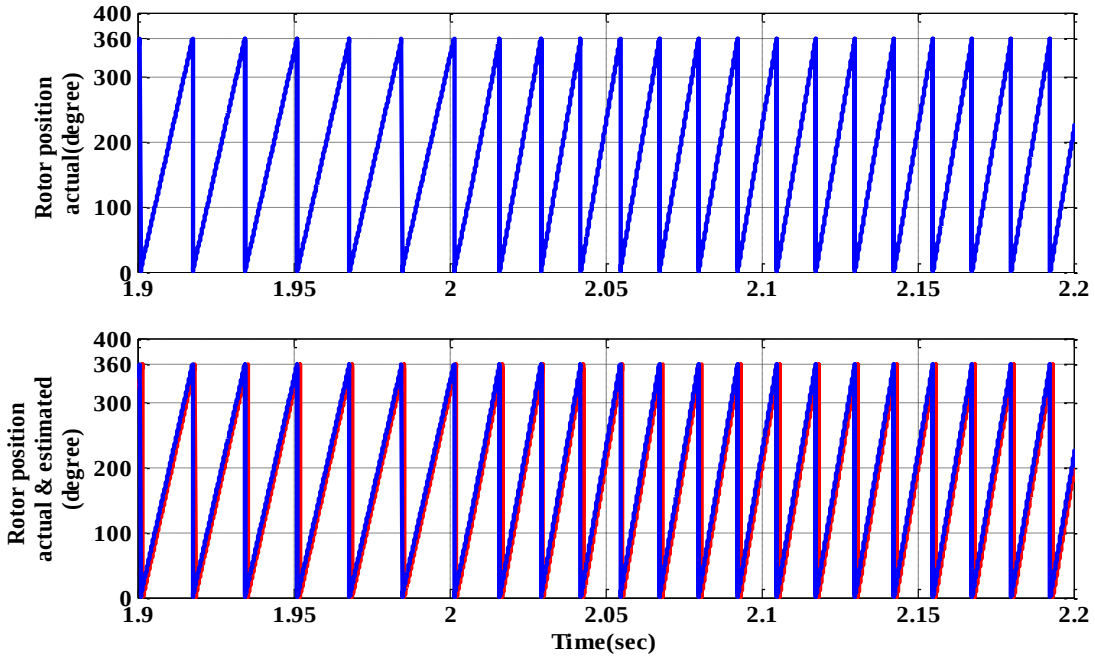

Figure 5.5 Rotor position at speed changing operation with back-EMF based sensorless control

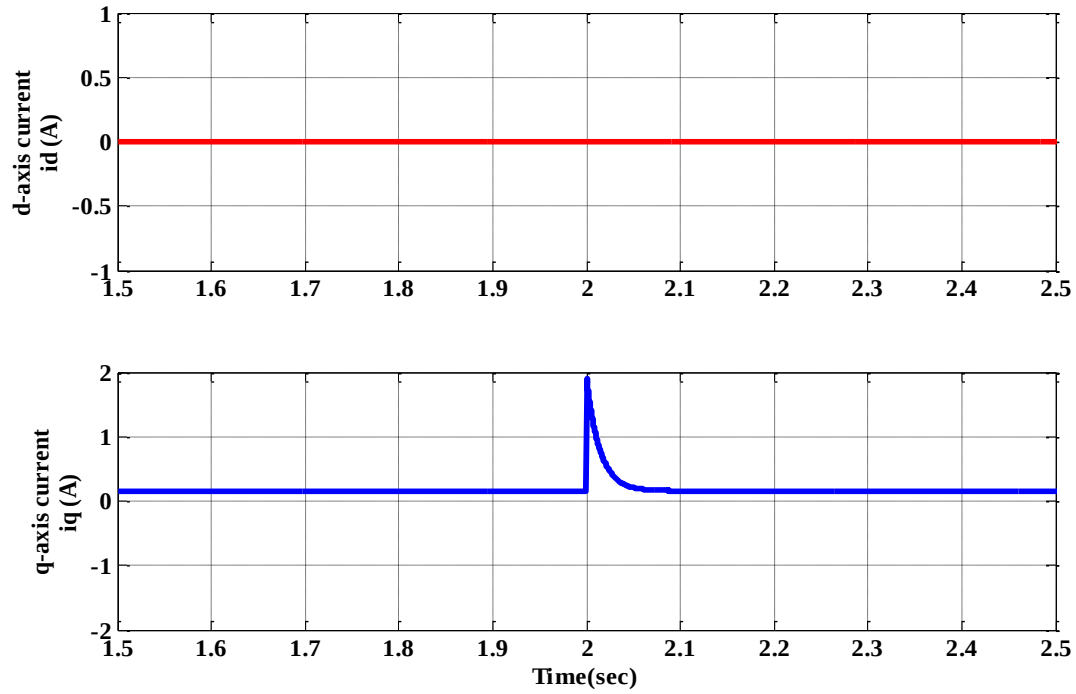

Figure 5.6 d-axis and q-axis current at speed changing operation with back-emf based position estimation method

The performance of the proposed drive at speed changing operation also has been investigated. The speed reference increased from 900rpm to 1200 rpm. A change in speed reference of 300 rpm has been applied. The response of the drive at speed changing operation has been shown in the Figure 5.4. At 2 second the speed reference command has been increased from 900 rpm to 1200 rpm. At this time the torque is increased by the motor to

reach the reference speed. Due to that the stator current is also slightly increased at that time. The torque reduced once the reference speed value reached. The rotor position estimated using back-emf based estimation algorithm at speed changing operation has been shown in Figure 5.5. The torque producing component of stator current is depicted in Figure 5.6. The d-axis current is fixed at zero.

To investigate the performance under loading condition a load of 4Nm is applied to the motor and simulation results are obtained. The response of the drive at increasing load has been shown in the Figure 5.7. A step change in load of 4 Nm is applied at 2 sec. It is observed that the stator current is increased at the time of loading. It is also observed that the torque producing component of the stator current is also increased due to the loading, which is shown in Figure 5.8. This speed response reaches the reference speed command. The estimated rotor position using back-emf estimation method at loading condition is presented in Figure 5.9. This method is satisfactory at medium and high-speed where back-emf is very low. There are two major deficiencies in the back-emf integration method at low speed are: pure integration problem and sensitivity to the stator resistance. The integrator has some advantage of reducing the switching losses. Since the back-emf varies with speed, the conduction period of inverter switches routinely adjusts inversely proportional to speed and the switching also adjusts automatically with change in speed.

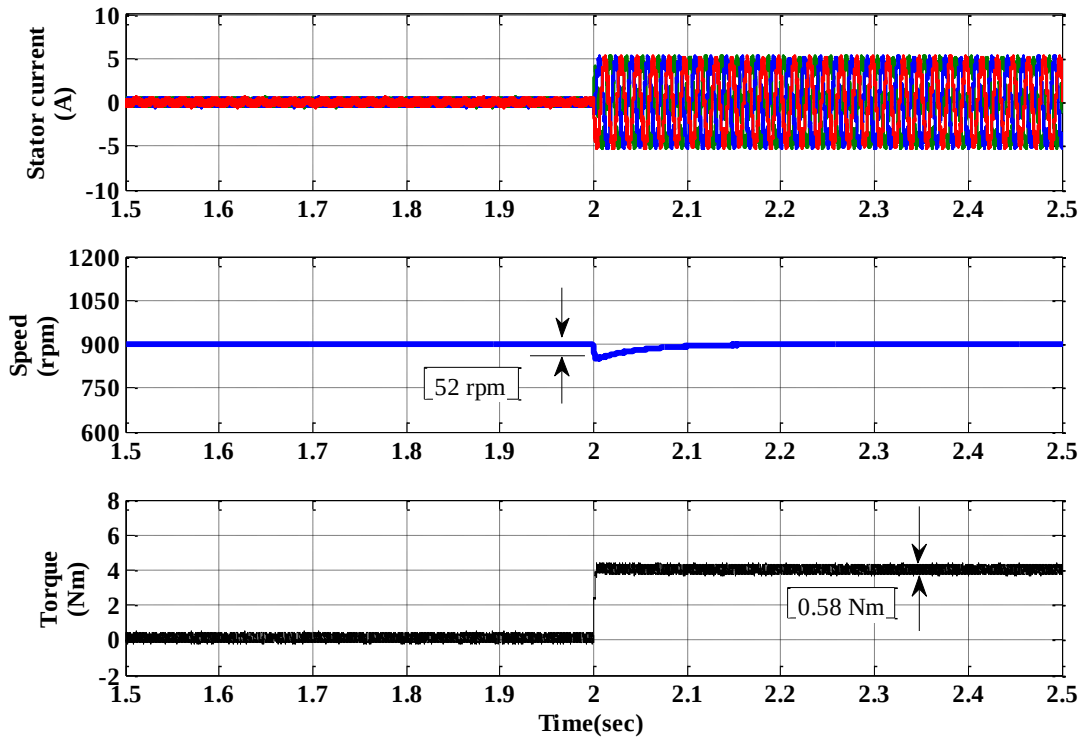

Figure 5.7 Performance of the drive at load changing operation with back-emf based sensorless control

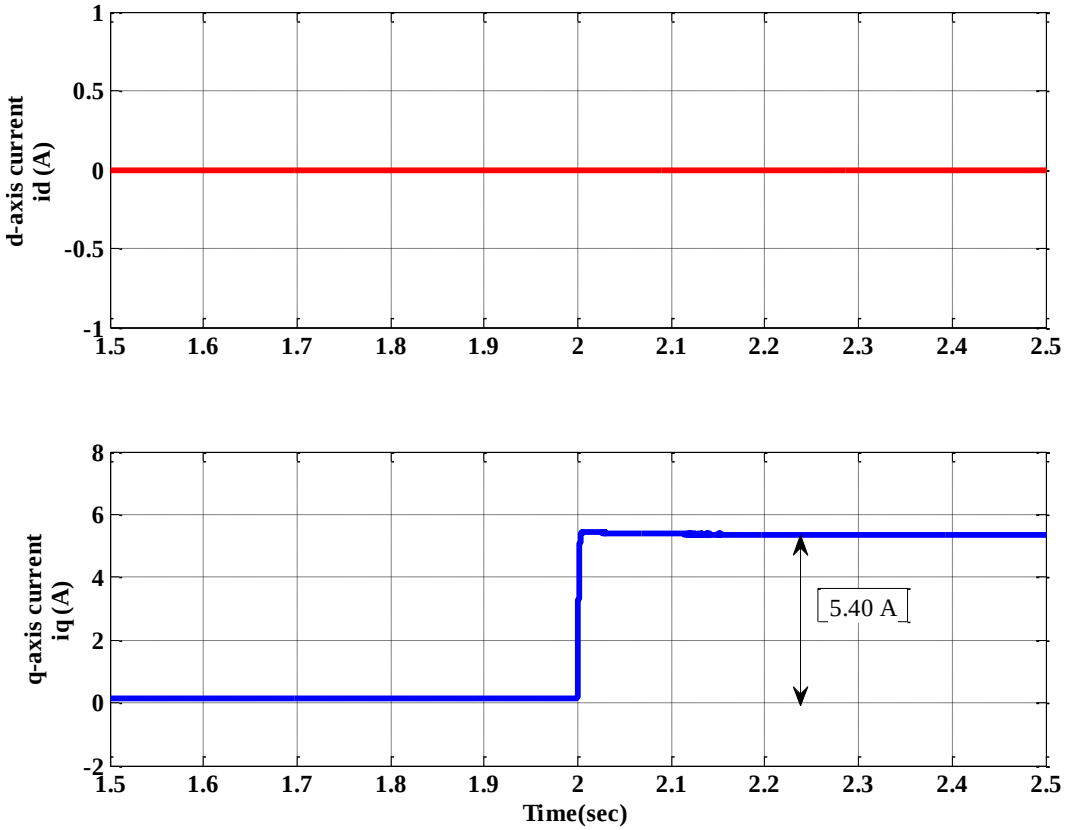

Figure 5.8 d-axis and q-axis current at load changing operation with back-emf based sensorless control

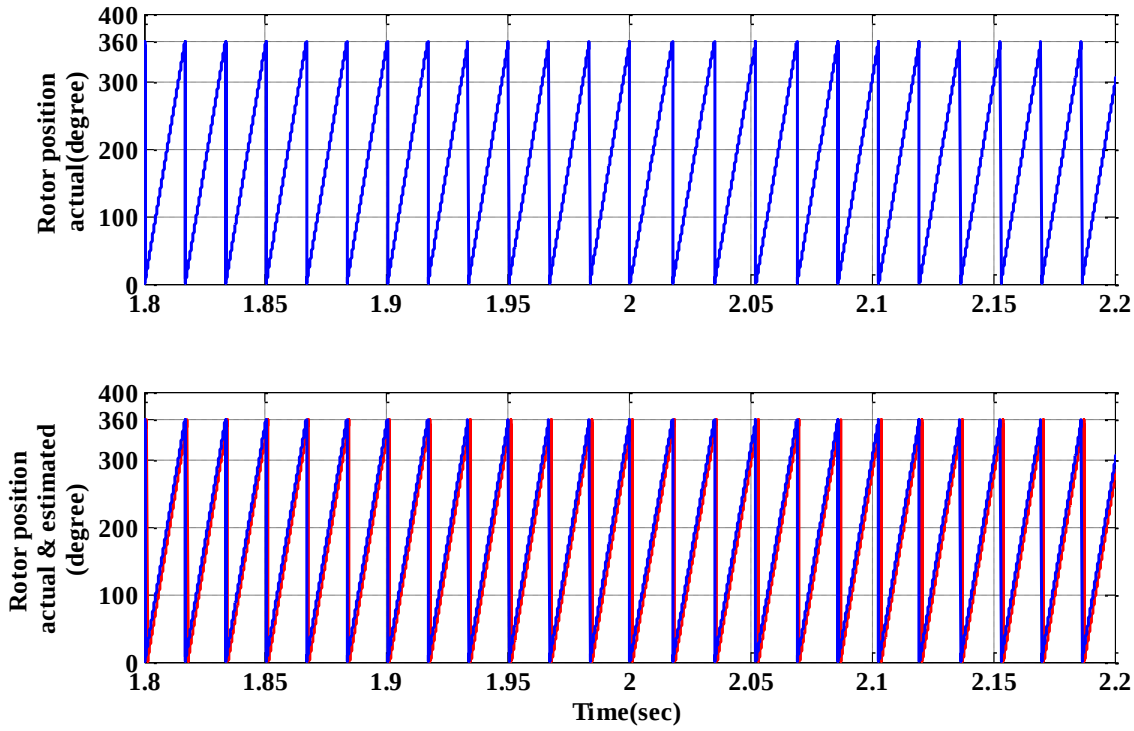

Figure 5.9 Rotor position at load changing operation with back-EMF based sensorless control

5.4 Model Reference Adaptive System (MRAS) Based Estimation

The MRAS algorithm is well-known for the sensorless control of induction machines. The MRAS based estimation for sensorless control of induction motor has been proved to be effective. The MRAS is one of the best available sensorless algorithms for PMSM in high performance application similar to induction motor due to its parameter independency. The performance of most of the observers depends on motor parameters which vary with temperature. In contrast the MRAS based estimation is independent of stator resistance variation. This control is computationally less complex, provides stable operation of the drive and eliminates the integrator problem as back-emf estimation is not necessary. The Model Reference Adaptive System (MRAS) based estimators provide the desired state from two different models, one is reference model and another one is adjustable model. The unknown parameter (speed in this case) is estimated using the error between two models. In MRAS only adjustable model should depend on unknown parameter, the reference model is independent of speed [168]–[174]. The error signal is fed into adaptation mechanism that provides the estimated quantity, which is used to tune the adjustable model. PI controller is used in the adjustable model. This method is simple and requires less computation. In PMSM drive system MRAS is an effective sensorless control method for position and speed estimation.

5.4.1 Structure of MRAS

The structure of MRAS is shown in Figure 5.10. The given performance x is generated by reference model and estimated performance x is generated by adjustable model and the same input u is given to both the models.

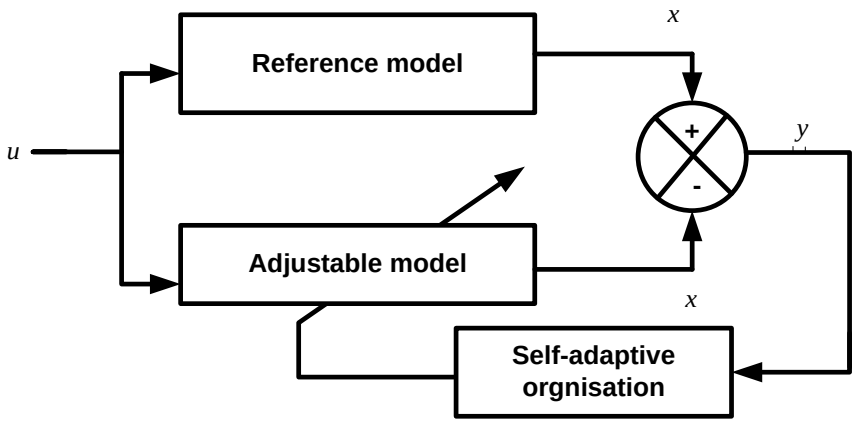

Figure 5.10 Structure of MRAS

x and x are the state variables of reference and adjustable model. The given and estimated performance is compared and generated error y is given to self-adaptive organization which draws the state variable x near to x and the error signal y approaches zero.

5.4.2 Estimator Synthesis for Speed Estimation of PMSM

The design of sensorless algorithm for PMSM drive uses PMSM itself as reference model, and the current equations of PMSM in d-q reference frame as adjustable model, and an adaptation mechanism. A sensorless control algorithm is shown in Figure 5.11. The current model of surface mounted PMSM is obtained by mathematical model presented in chapter 2, is given by-

$$v_d = R_s i_d + L_s \frac{di_d}{dt} - \omega_r L_s i_q \tag{5.6}$$

$$v_q = R_s i_q + L_s \frac{di_q}{dt} - \omega_r L_s i_d + \omega_r \psi_f \tag{5.7}$$

The above equations (5.6) and (5.7) can be re-written in form of

$$\frac{di_d}{dt} = -\frac{R_s}{L_s} i_d + \omega_r i_q + \frac{v_d}{L_s} \tag{5.8}$$

$$\frac{di_q}{dt} = -\frac{R_s}{L_s} i_q - \omega_r i_d - \frac{\psi_f}{L_s} \omega_r + \frac{v_q}{L_s} \tag{5.9}$$

Where v_d, v_q, i_d, i_q are the stator voltages and currents in d-q components; R_s is stator resistance; L_s is stator inductance; ω_r is rotor speed; and ψ_f is rotor flux.

The equations (5.8) and (5.9) can be rearranged and written in matrix form as-

$$p\begin{bmatrix} i_d + \frac{\psi_f}{L_s} \\ i_q \end{bmatrix} = \begin{bmatrix} -\frac{R_s}{L_s} & \omega_r \\ -\omega_r & -\frac{R_s}{L_s} \end{bmatrix} \begin{bmatrix} i_d + \frac{\psi_f}{L_s} \\ i_q \end{bmatrix} + \frac{1}{L_s} \begin{bmatrix} v_d + \frac{R_s \psi_f}{L_s} \\ v_q \end{bmatrix} \tag{5.10}$$

The above equation can be written in simplified form, suppose;

$i_d' = i_d + \frac{\psi_f}{L_s}$,

$$i'_q = i_q$$

$$v'_d = v_d + \frac{R_s \psi_f}{L_s}$$

$$v'_q = v_q$$

Now with these assumptions equation (5.10) becomes in form of-

$$p\begin{bmatrix} i_d^{'} \\ i_q^{'} \end{bmatrix} = \begin{bmatrix} -\frac{R_s}{L_s} & \omega_r \\ -\omega_r & -\frac{R_s}{L_s} \end{bmatrix} \begin{bmatrix} i_d^{'} \\ i_q^{'} \end{bmatrix} + \frac{1}{L_s} \begin{bmatrix} v_d^{'} \\ v_q^{'} \end{bmatrix} \tag{5.11}$$

The equation (5.11) can be written in form of a state equation as-

$$pi^{'} = Ai^{'} + Bv^{'} \tag{5.12}$$

Where,

$$A = \begin{bmatrix} -\frac{R_s}{L_s} & \omega_r \\ -\omega_r & -\frac{R_s}{L_s} \end{bmatrix}$$

$$B = \frac{1}{L_s}$$

It is clear that only matrix A contains the speed information, which is to be estimated, and the PMSM is reference model. In the same way the expression for estimated values to be obtained by adjustable model is expressed as–

$$p\begin{bmatrix} i'_d \\ i'_q \end{bmatrix} = \begin{bmatrix} -\frac{R_s}{L_s} & \omega_r \\ -\omega_r & -\frac{R_s}{L_s} \end{bmatrix} \begin{bmatrix} i'_d \\ i'_q \end{bmatrix} + \frac{1}{L_s} \begin{bmatrix} v'_d \\ v'_q \end{bmatrix} \tag{5.13}$$

The equation (5.13) also can be written in state equation form as–

$$pi' = Ai' + Bv' \tag{5.14}$$

Now subtracting equation (5.13) from equation (5.11)

$$\begin{bmatrix} \frac{de_d}{dt} \\ \frac{de_q}{dt} \end{bmatrix} = \begin{bmatrix} -\frac{R_s}{L_s} & \omega_r \\ -\omega_r & -\frac{R_s}{L_s} \end{bmatrix} \begin{bmatrix} e_d \\ e_q \end{bmatrix} - J\left(\omega_r - \omega_r\right) \begin{bmatrix} i'_d \\ i'_q \end{bmatrix} \tag{5.15}$$

Where,

$$e_d = i'_d - i'_d$$

$$e_q = i'_q - i'_q$$

$$J = \begin{bmatrix} 0 & -1 \\ 1 & 0 \end{bmatrix}$$

In the short form it can be written as–

$$\frac{de}{dt} = A_e e - W \tag{5.16}$$

Where,

$$A_e = \begin{bmatrix} -\frac{R_S}{L_S} & \omega_r \\ -\omega_r & -\frac{R_S}{L_S} \end{bmatrix}$$

$$w = J\left(\omega_r - \omega_r\right) i'_s$$

The adaptation mechanism uses PI controller to process the error and to tune the adjustable model so as to achieve the estimated value of rotor speed. The structure of MRAS for PMSM is shown in Figure 5.11.

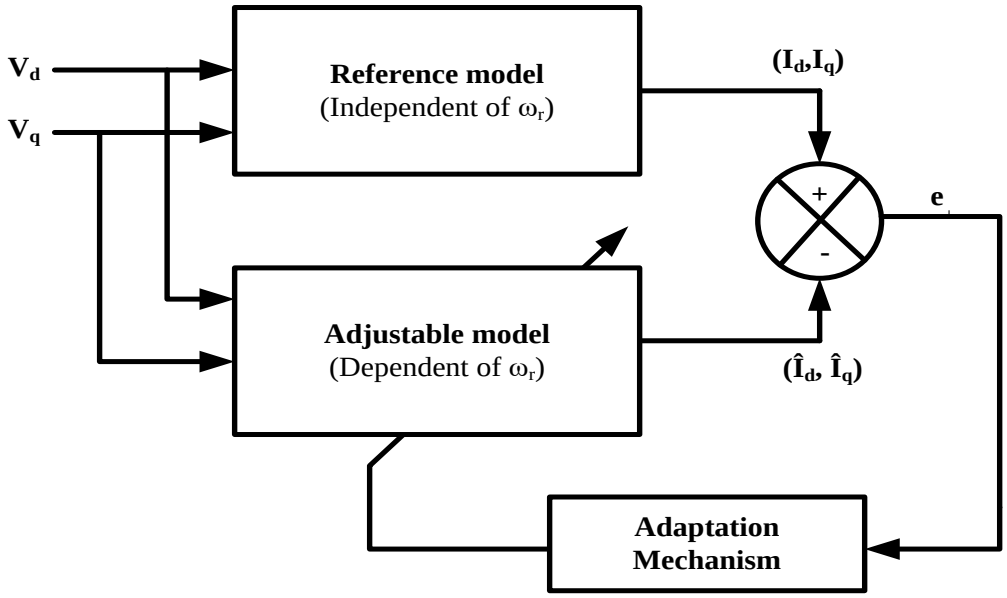

Figure 5.11 Structure of MRAS for PMSM

Using the PI controller the estimated speed using MRAS algorithm is obtained as–

$$\omega_r = \left(K_p + \frac{1}{s} K_i \right) \left[i_d i_q - i_q i_d - \frac{\psi_f}{L_s} \left(i_q - i_q \right) \right] \tag{5.17}$$

The MRAS uses the PI control in adaptation mechanism to process the error. The estimation algorithm used is independent of stator resistance, computationally less complex, free from integrator problem because back-emf estimation is not required and provides stable operation of drive system. MRAS adaptive mechanism based on equation (5.17) is presented in Figure 5.12.

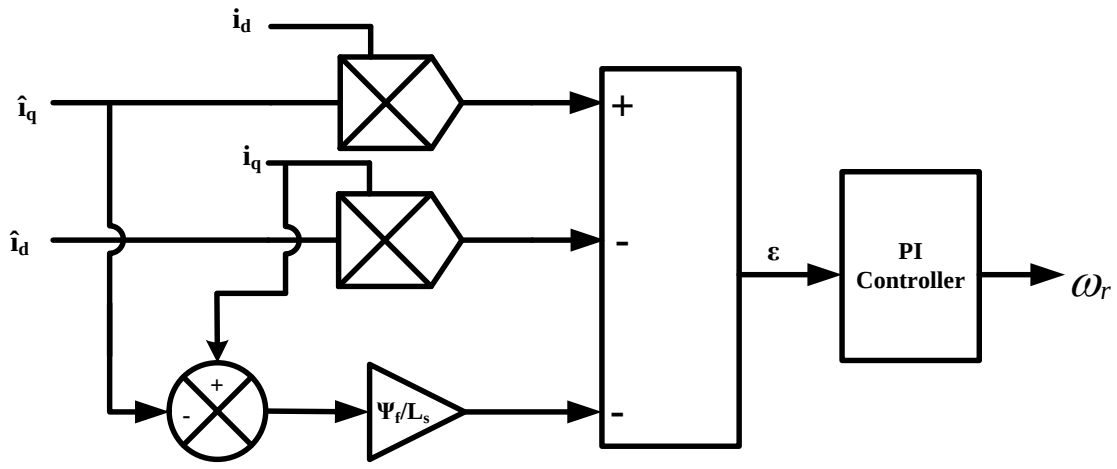

Figure 5.12 MRAS adaptive mechanism

This control methodology solves the problem of nonlinearity and parameter deviations of PMSM drive with application of vector control in terms of zero d-axis current control. Moreover, it achieves high dynamic performance and accurate speed tracking and torque control with superior steady state characteristics.

5.4.3 Implementation of MRAS Based Sensorless Algorithm

A model reference adaptive system technique has been used for speed and position estimation in sensorless vector control of the PMSM driven by three-level NPC inverter. A PI controller is used to process the error between reference model and adjustable model in the adaptation mechanism of MRAS. It provides the robustness in the drive. The estimation algorithm used is independent of stator resistance, computationally less complex, free from integrator problem because back-emf estimation is not required and it provides stable operation of drive.

The MRAS based speed estimator is implemented for three-level NPC inverter fed PMSM drive in MATLAB/Simulink. MRAS used in this system is designed based on the current model of PMSM. The block diagram of PMSM employing MRAS as speed estimator is shown in Figure 5.13. Here the voltages and currents are measured in a−b−c reference and converted to d−q reference frame and given as input to MRAS estimator, which generates the estimated speed. The estimated d−q currents are generated from adjustable model, which is also controlled by output of adaptation mechanism as clearly shown Figure 5.13. In the adjustable model the estimated output is function of (V_s, i_s, ω_{est}).

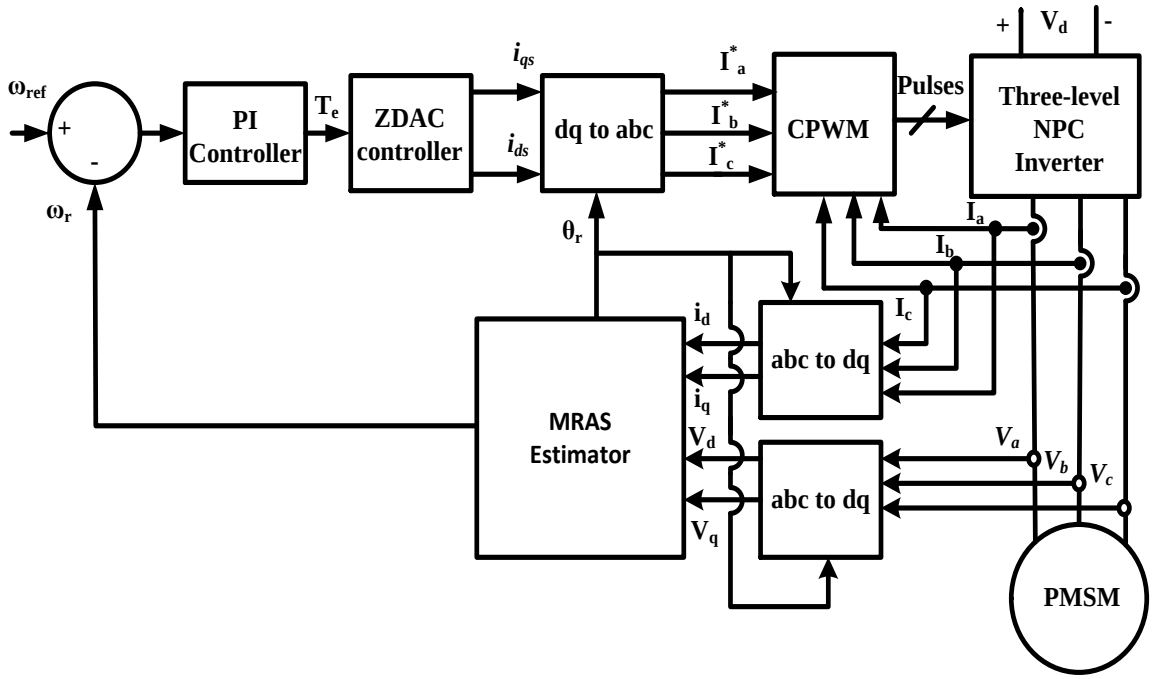

Figure 5.13 Schematic block diagram of MRAS based estimation for PMSM

The measured rotor position is used to compare the estimated value and find out the estimation error. The estimation error is the key point in defining the performance of a sensorless algorithm. The internal processing of estimation algorithm is shown separately in Figure 5.11 and Figure 5.12, which take v_d, v_q, i_d, i_q as combined inputs and gives estimated speed as output as shown in block diagram. Here the controller which processes the error to estimate the speed plays a very important role in performance of sensorless algorithm.

5.4.4 Performance Evaluation of MRAS Estimation Based Sensorless Control of PMSM Drive

To investigate the MRAS estimation based sensorless controlled three-level NPC inverter fed PMSM drive an extensive simulation study is carried out and simulation results are obtain. For the estimation voltages and currents are obtained in d– q reference frame using measured ones. The intermediate current values i_d' , i_q' and the i_d , i_q obtained from reference model (PMSM itself) are used to obtain the estimated speed using a controller. Accuracy of this controller decides the error in the estimated speed. The performance of the complete MRAS based estimation algorithm is observed for various operating conditions.

The starting response of the MRAS estimation based sensorless controlled three-level NPC inverter fed PMSM drive has been shown in the Figure 5.14.

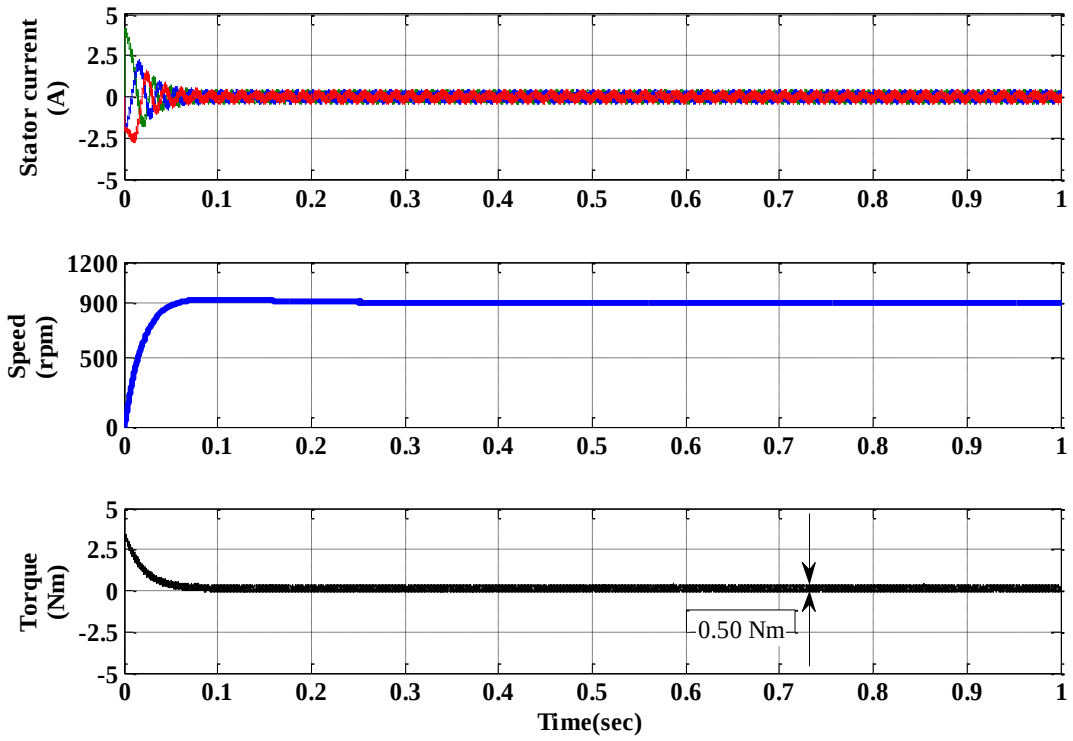

Figure 5.14 Starting response of the drive with MRAS based estimation

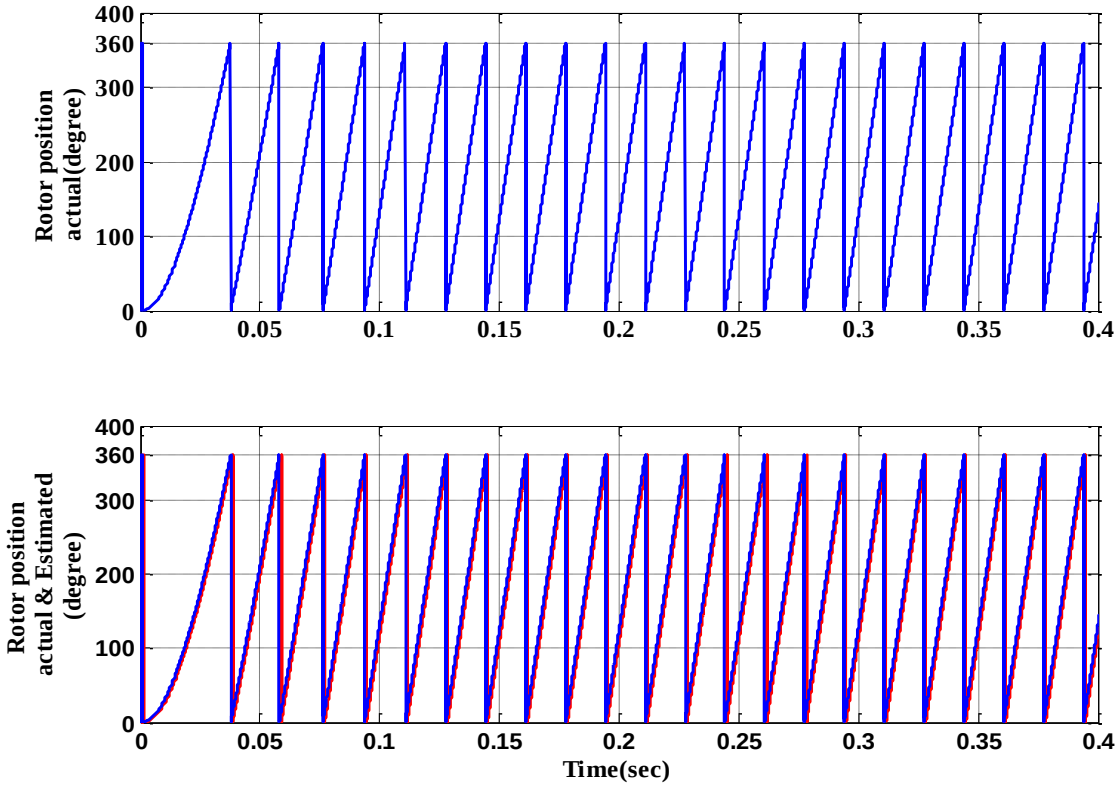

Figure 5.15 Rotor position actual and estimated with MRAS control

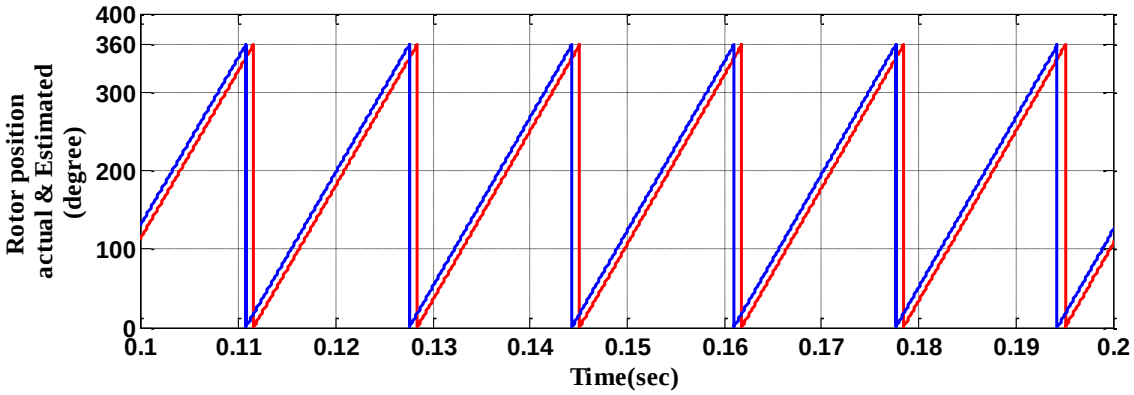

Figure 5.16 Magnified view of actual and estimated rotor position in MRAS control

The reference value of speed is kept 900 rpm and the motor is started with no load. It is observed that the motor reaches its reference speed value as depicted by trace 2. Initial starting torque is high. The stator current is also high at the time. It reduces when the motor reaches its reference speed value. The actual and estimated rotor position is shown in the Figure 5.15 . The Magnified view of actual and estimated rotor position in MRAS control is shown in Figure 5.16. The total no of pole pair in PMSM is 4, hence electrical angle $\theta_e = 4\theta_m$, where θ_m = the mechanical angle. It is observed that the estimated rotor positon follow the actual rotor position with very less error. The results show the effectiveness of the proposed drive.

The performance of the drive at speed changing operation is investigated with MRAS based position estimation. The response of the drive at speed changing operation has been shown in the Figure 5.17.

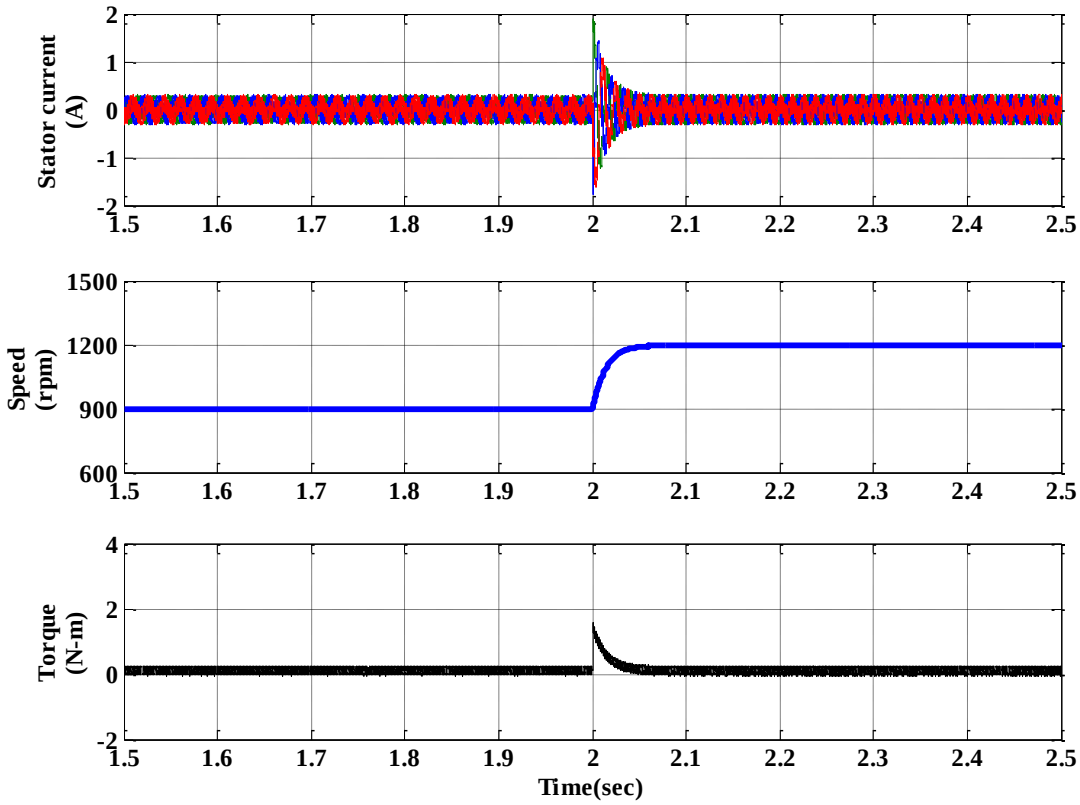

Figure 5.17 Response of the drive with MRAS at speed changing (increasing from 900 rpm to 1200 rpm) operation

The speed reference increased from 900rpm to 1200 rpm. A change in speed reference of 300 rpm has been applied. At 2 second the speed reference command has been increased from 900 rpm to 1200 rpm. At this time the torque is increased by the motor to reach the reference speed. Due to that the stator current is also slightly increased at that time. The torque reduced once the reference speed value reached. The rotor position estimated using MRAS based estimation at speed increasing operation has been shown in Figure 5.18. The torque producing component of stator current is depicted in Figure 5.19. The d-axis current is fixed at zero.

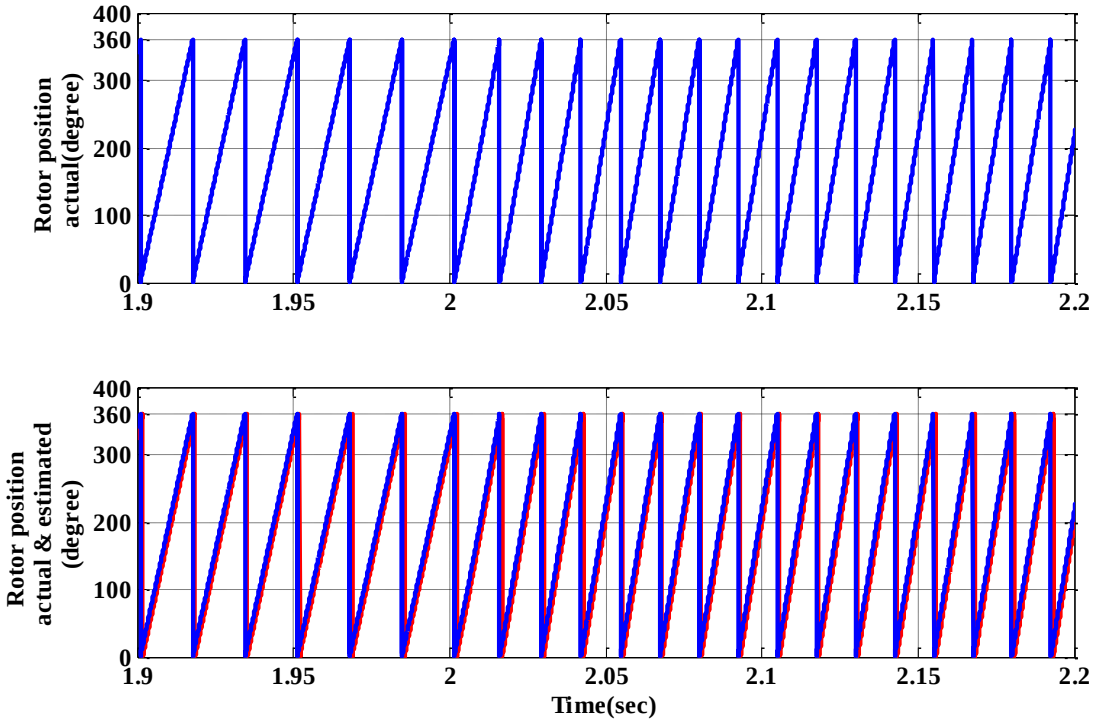

Figure 5.18 Rotor position with MRAS at speed changing (increasing) operation

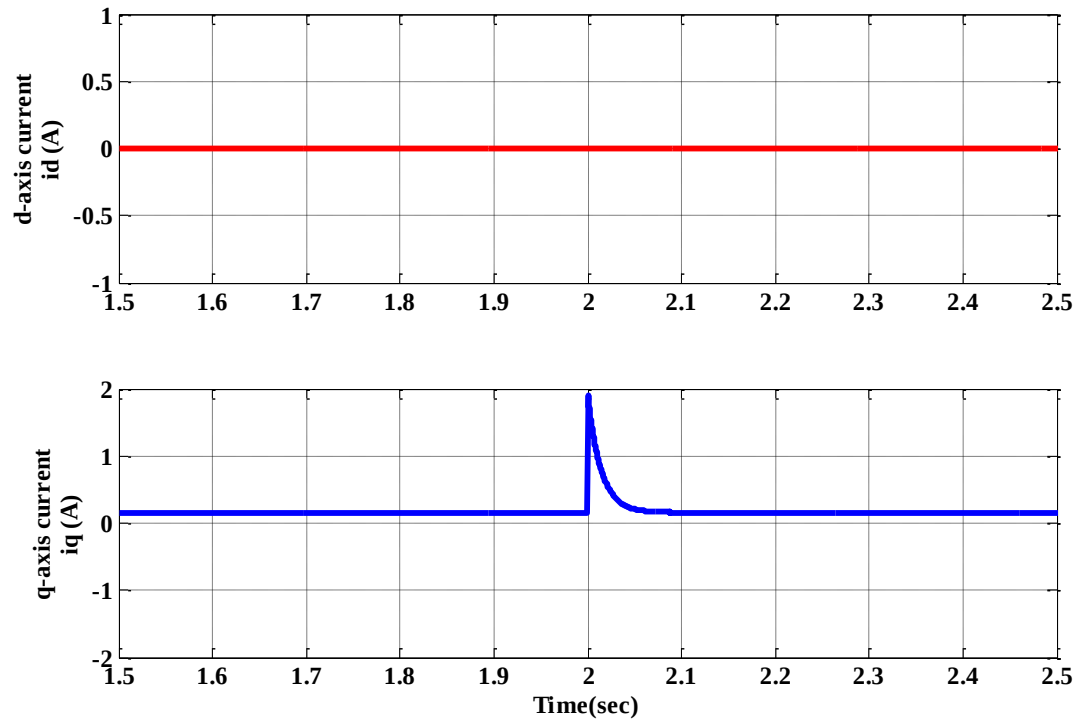

Figure 5.19 d-axis current (id) and q-axis (iq) current in MRAS based estimation of the drive at speed changing (increasing) condition

The performance of the drive at speed decreasing operation is shown in the Figure 5.20.

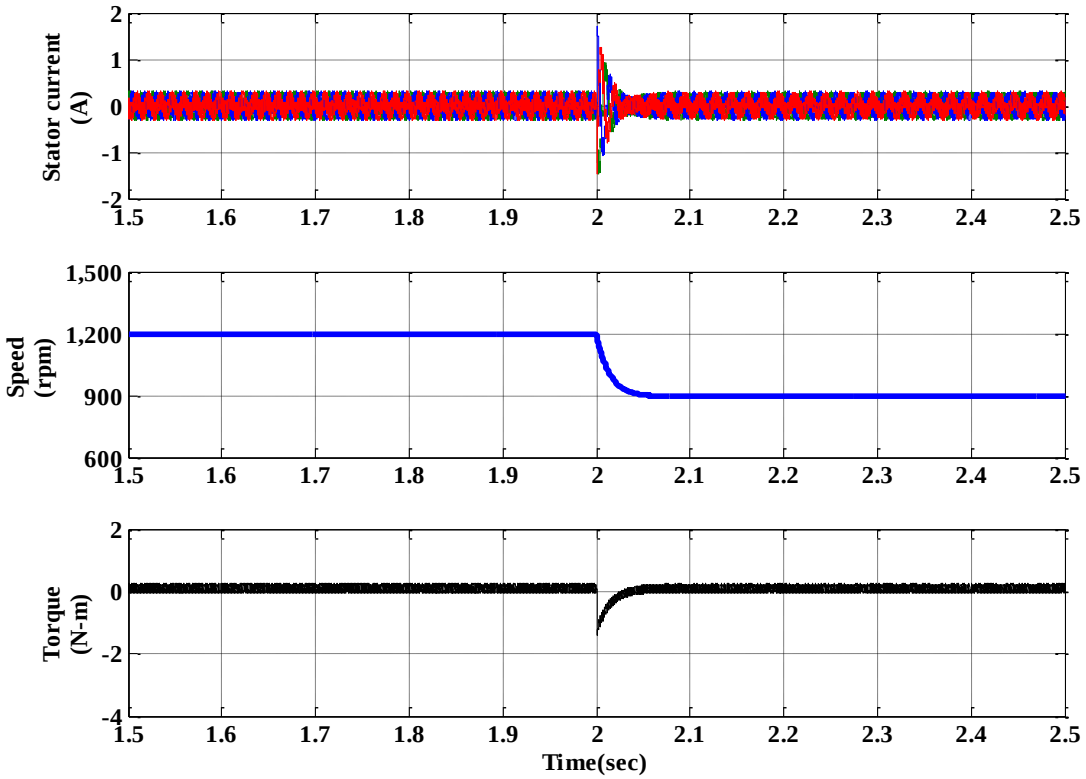

Figure 5.20 Response of the drive with MRAS at speed changing (decreasing from 1200 rpm to 900 rpm) operation

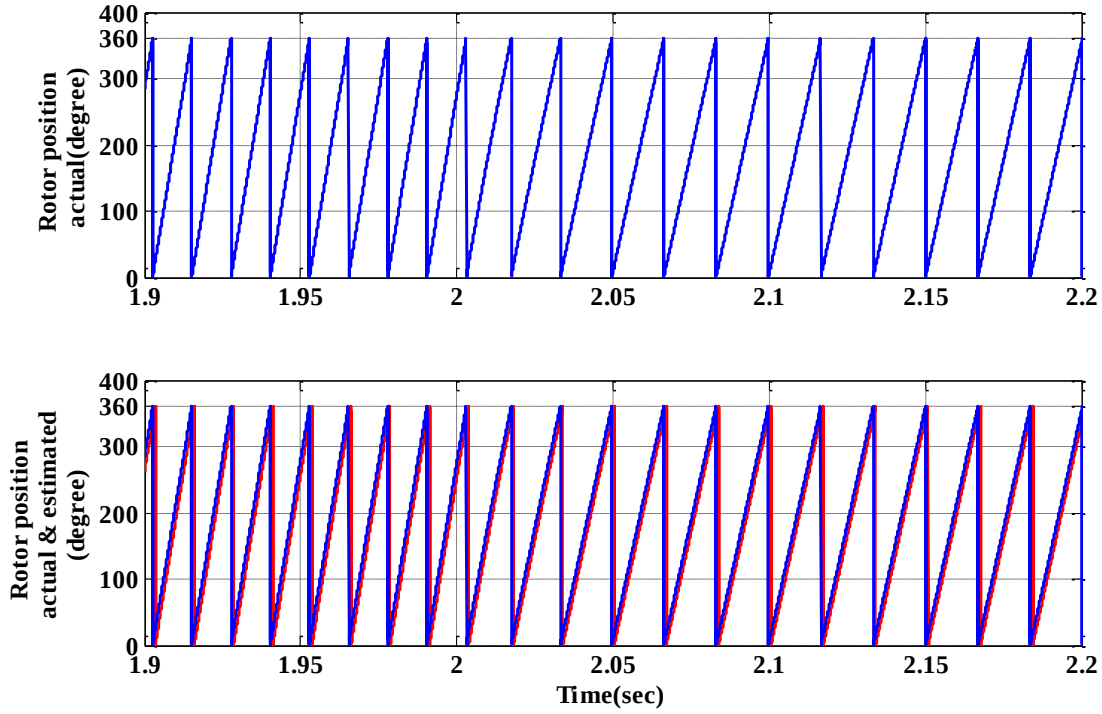

Figure 5.21 Rotor position with MRAS at speed changing (decreasing) operation

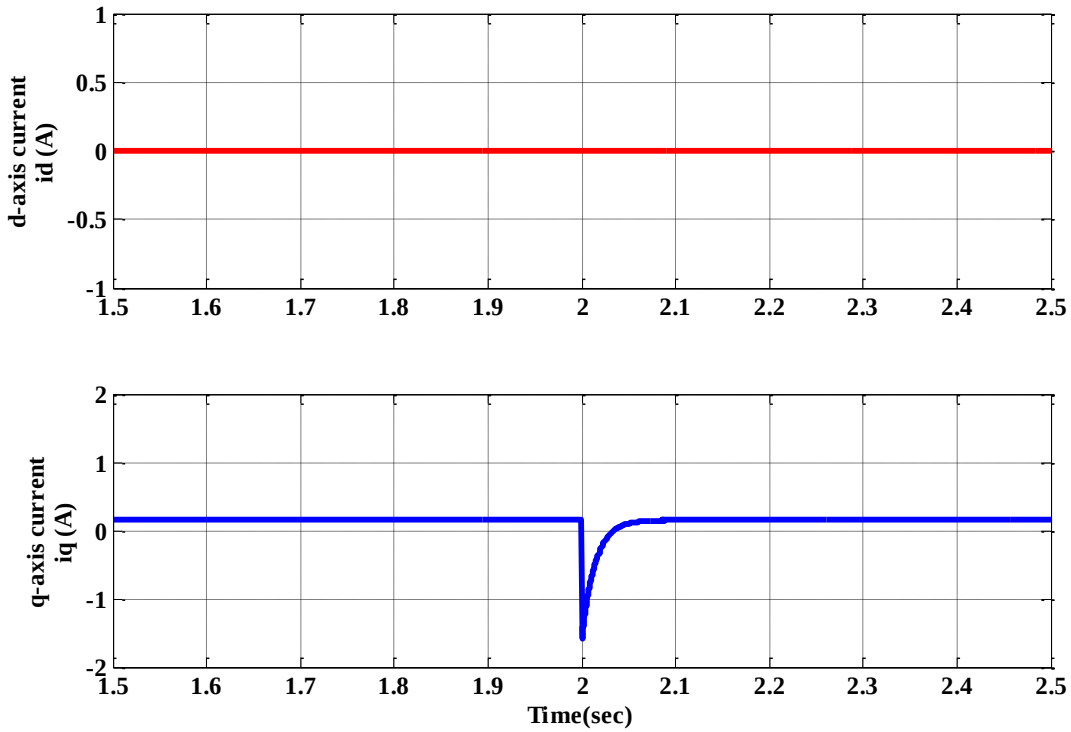

Figure 5.22 d-axis current (id) and q-axis (iq) current in MRAS based estimation of the drive at speed changing (decreasing) operation

A change in speed reference of 300 rpm has been applied. At 2 second the speed reference command has been decreased from 1200 rpm to 900 rpm. At this time the torque is decreased by the motor to reach the reference speed. Due to that the stator current is also slightly increased at that time. The torque reduced once the reference speed value reached. The rotor position estimated using MRAS based estimation at speed decreasing operation has been shown in Figure 5.21. The torque producing component of stator current is depicted in Figure 5.22. The d-axis current is fixed at zero.

Further investigation has been done in three-level NPC inverter fed PMSM drive with MRAS based position estimation. To investigate the performance under loading condition a load of 4Nm is applied to the motor and simulation results are obtained. The response of the drive at increasing load has been shown in the Figure 5.23. A step load of 4 Nm is applied at 2 sec. It is observed that the stator current is increased at the time of loading. It is also observed that the torque producing component of the stator current is also increased due to the loading. This speed response reaches the reference speed command. The estimated rotor position using MRAS estimation method at loading condition is depicted in Figure 5.24. It is observed that the d-axis current is zero and q axis current mainly produce the load torque which has been depicted in Figure 5.25.

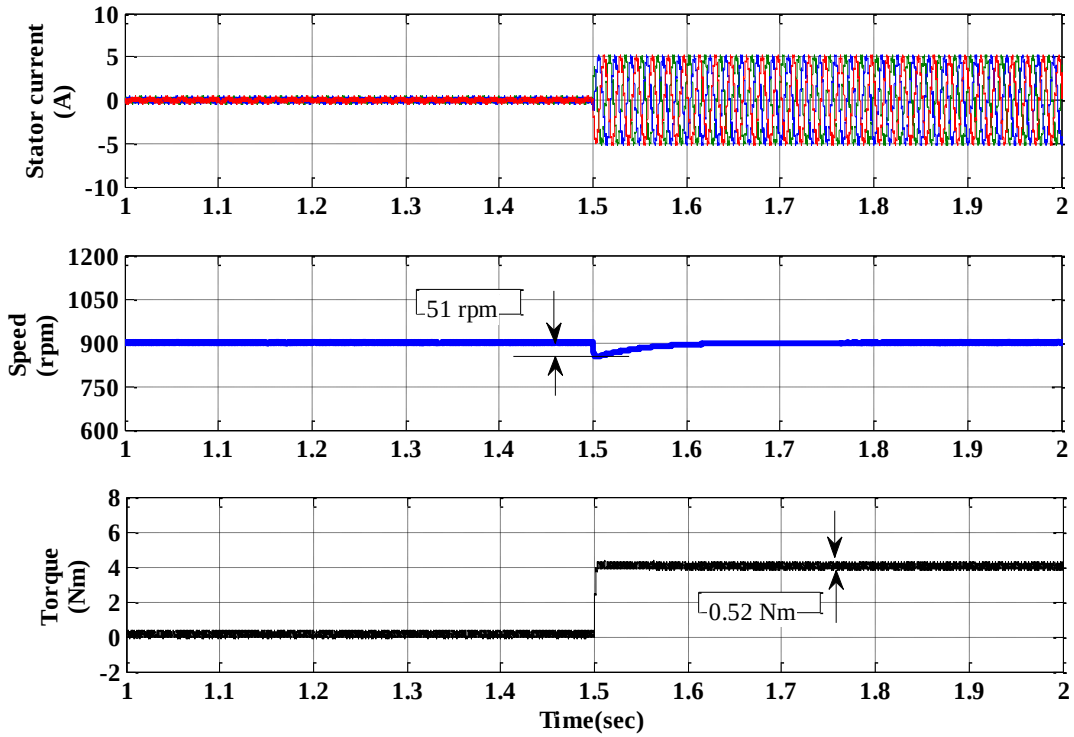

Figure 5.23 Response of the drive with MRAS at load changing operation

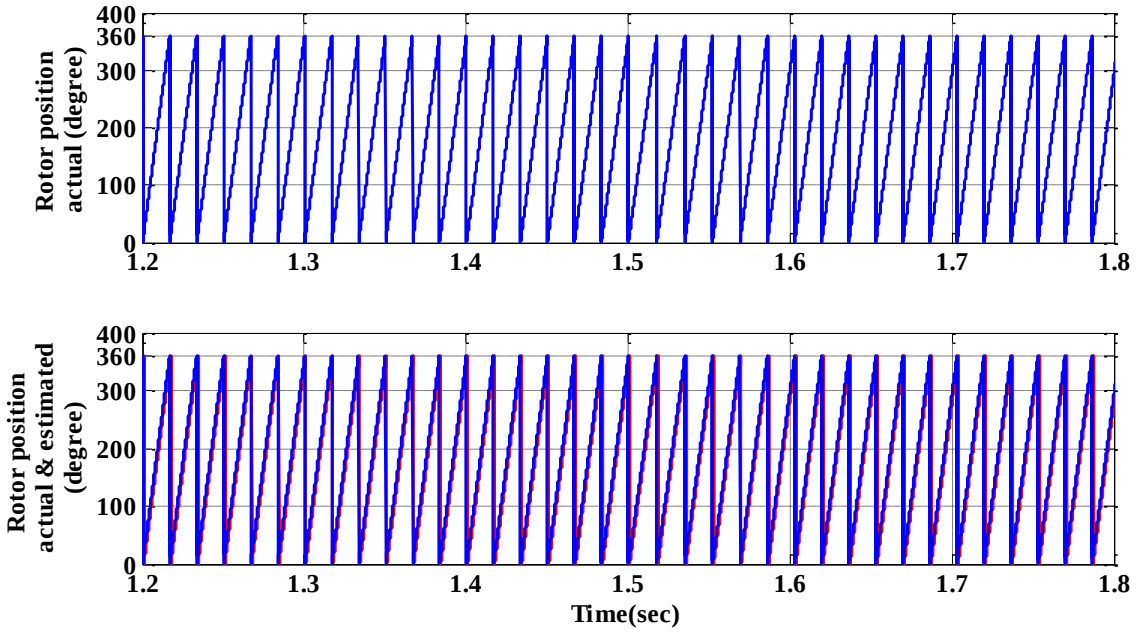

Figure 5.24 Rotor position with MRAS at load changing operation

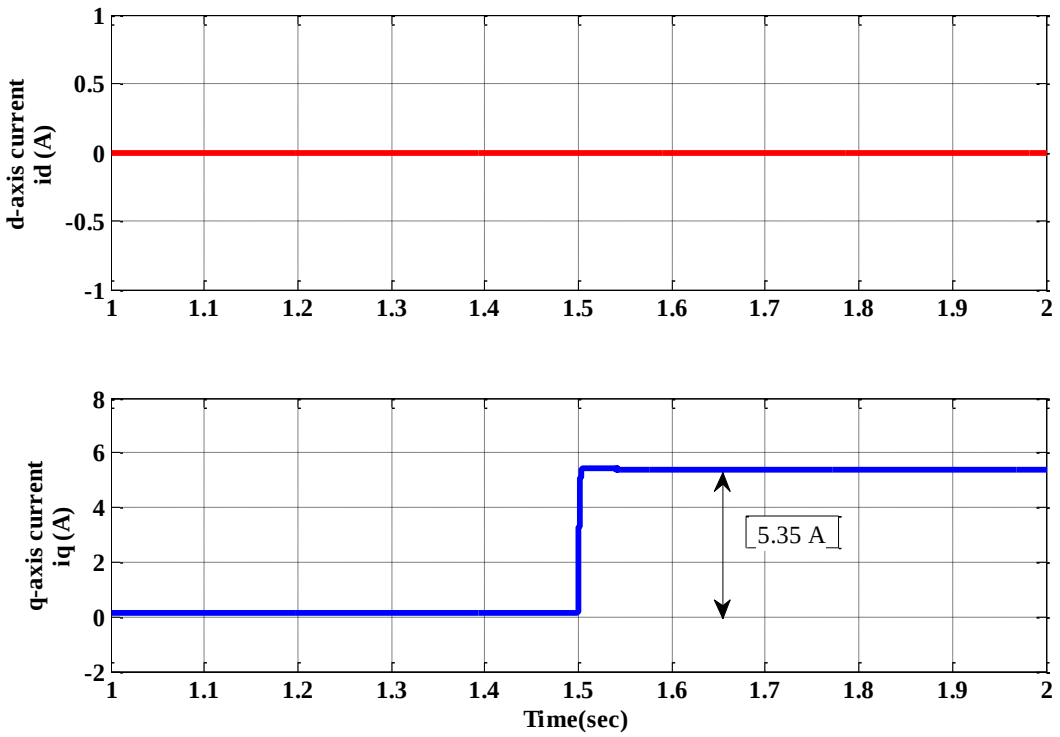

Figure 5.25 d-axis current (id) and q-axis (iq) current in MRAS based estimation of the drive at load changing condition

5.5 Conclusion

The sensorless control of PMSM with zero d-axis current control increases the reliability and robustness of the drive and reduces the cost. The simulation result shows high starting torque which reduces to a smaller value once the speed reach to the commanded speed value. The study also provides useful insight into the concept of removal of traditional shaft-mounted optical encoder, resolver or Hall sensors to obtain the rotor position. Back-EMF based estimation of rotor speed and angular position ensure accurate speed regulation. This method is satisfactory at medium and high-speed. But there are two major deficiencies in the back-emf integration method at low speed are: pure integration problem and sensitivity to the stator resistance. A model reference adaptive system has been investigated to estimate the rotor speed and position, by using PMSM as reference model, PMSM current equations in d-q reference frame as adjustable model and an adaptation mechanism. The estimation algorithm used is independent of stator resistance, computationally less complex, free from integrator problem because back-emf estimation is not required and provides stable operation of drive system. PI controller is used in the adaptation mechanism to process the error, to tune the adjustable model and to achieve the estimated value of rotor speed. The MRAS is simple and easier implementation as compared to the observer based sensorless schemes with reduced

mathematical computation time. The system anti-robustness behavior is improved and also the dynamic and static performance of drive is improved. The simulation results verified the effectiveness and feasibility of the MRAS based estimator in three-level NPC inverter fed PMSM drive system.

CHAPTER 6: SYSTEM DEVELOPMENT AND EXPERIMENTATION

[Prototype hardware system comprising of PMSM, two-level inverter, three-level NPC inverter, dSPACE DS1104 interfacing and related control circuits has been developed for vector controlled PMSM drive system. Software based RDC less position estimation implemented for the proposed drive. MRAS based sensorless control also implemented. The simulation results presented in previous chapters are validated through those hardware systems.]

6.1 Introduction

In order to verify the simulation of two-level voltage source inverter fed and three-level NPC inverter fed PMSM drive the following prototypes have been developed in the laboratory.

a) Two-level voltage source inverter power circuit.
b) Three-level neutral point clamped inverter power circuit.
c) Capacitor voltage balancing circuit with three-level boost converter.
d) The control circuit consisting of the dead-band circuit, the dc power supplies, voltage, and current sensor circuits.

As a first step in hardware development a two-level voltage source inverter has been designed and constructed to fed the surface permanent magnet synchronous motor. The power circuit consists of an auto-transformer, rectifier and a two-level inverter, two mechanically coupled PMSM with resolver manufactured by MOOG motors. One PMSM is working as motor and other as generator. Both the motors have 24 volt DC brake and resolvers. For the experimentation of three-level NPC inverter fed PMSM, a three-level NPC inverter has been designed and constructed. A voltage balancing circuit using three-level boost converter is also designed and constructed. The gate driver circuit for the power electronic switches was designed and various components were mounted on the PCB. For the development of the power circuit, MOSFETs (IRFP460) have been used as the switching devices for realizing the two-level inverter, three-level NPC inverter with three-level boost converter.

The other hardware components required for the operation of the experimental set-up such as pulse amplification circuit, isolation circuit, dead-band circuit, voltage and current sensor circuits have been designed and developed in the laboratory. The complete schematic diagram

for the realization two-level inverter fed PMSM drive and three- level NPC inverter fed PMSM drive system are shown in Figure 6.1 and Figure 6.2 respectively.

A Digital Signal Processor (DSP) DS1104 of dSPACE has been used for the real-time implementation of control algorithms. By using the Real-Time Workshop (RTW) of MATLAB and Real-Time Interface (RTI) feature of dSPACE–DS1104, the simulink models of the various controllers of the prototypes have been implemented. The control algorithm is first designed in the MATLAB/Simulink software. The RTW of MATLAB generates the optimized C-code for real-time implementation. The interface between MATLAB/Simulink and Digital Signal Processor (DSP, DS1104 of dSPACE) allows the control algorithm to be run on the hardware. The master bit I/O is used to generate the required gate pulses and Analog to Digital Converters (ADCs) are used to interface the sensed voltage and current, modulating output signal from the resolver sensor and DC-bus capacitor voltages. The development of different hardware components as required for the operation of the hardware prototypes are discussed in the next section.

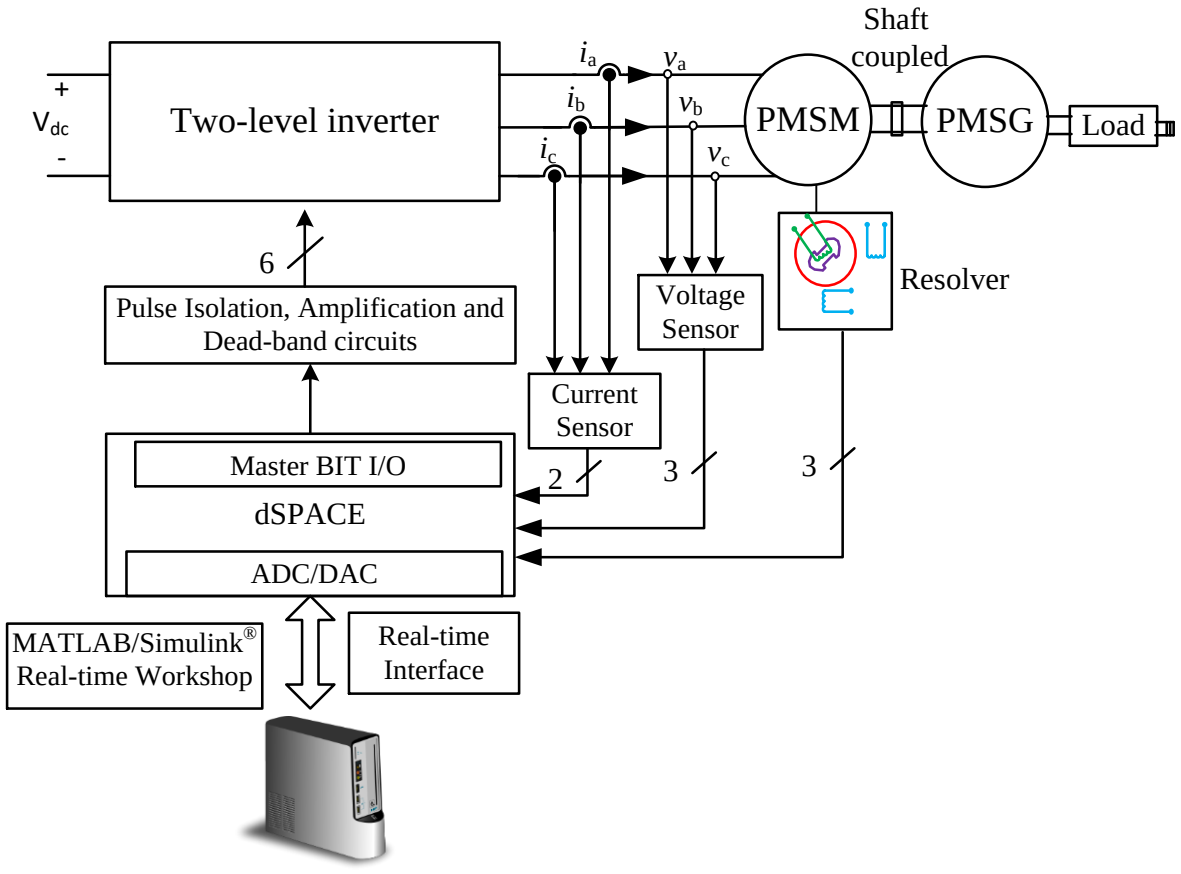

Figure 6.1 Schematic diagram for hardware implementation of two-level inverter fed PMSM drive system.

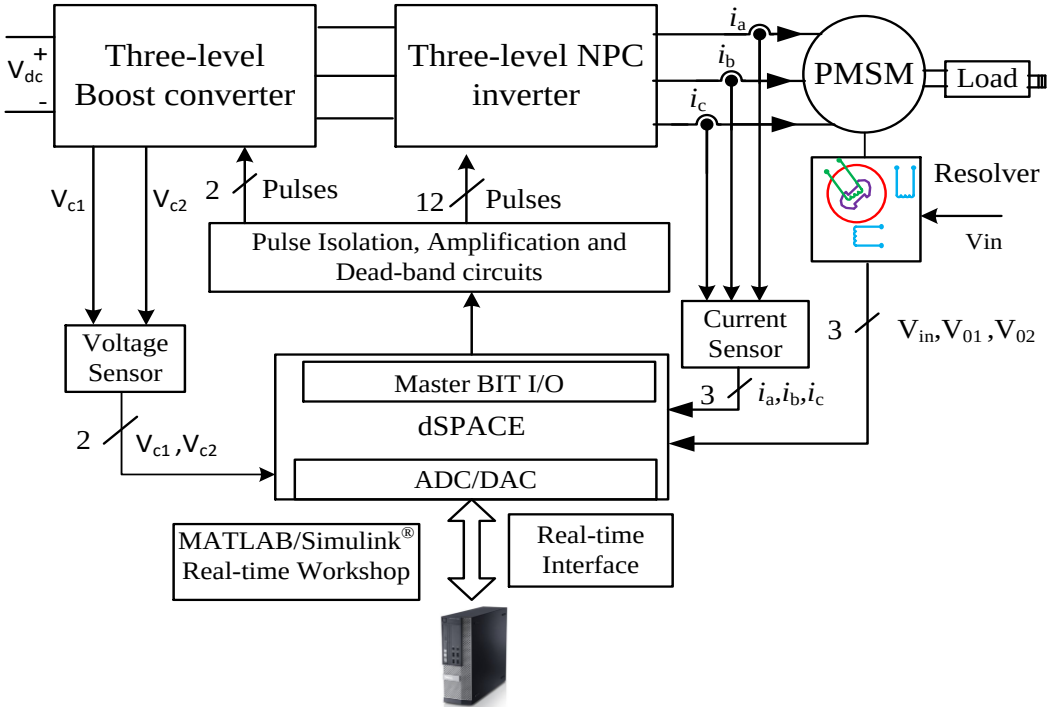

Figure 6.2 Schematic diagram for hardware implementation of three-level NPC inverter fed PMSM drive system

6.2 Development of System Hardware

The developed experimental prototype is comprised of the following parts:

1. Power circuit of 2- level , 3- level inverter
2. Measurement circuits
   - Voltage measurement
   - Current measurement
   - Position measurement from resolver
3. System software
4. Control hardware
   - MOSFET driver circuit for Isolation and Amplification
   - Dead-band circuit

6.2.1 Development of Power Circuit

A single-phase two-level and three-level inverter with suitably designed have been developed in the laboratory. MOSFETs (IRFP460) have been used as switching device for the Inverter. To protect each switching device, a suitably designed snubber circuit is connected across it. The snubber comprises of a parallel combination of a resistor and a capacitor connected

across a Metal-Oxide Varistor (MOV). The devices are mounted on heat sinks to ensure proper heat dissipation.

6.2.2 Measurement Circuits

For the accurate and reliable operation of a system in closed loop, measurement of various system parameters and their conditioning is required. The measurement system must fulfil the following requirements:

- High accuracy
- Galvanic isolation with power circuit
- Linearity and fast response
- Ease of installation and operation

With the availability of Hall-effect current sensors and isolation amplifiers, these requirements are fulfilled to a large extent. In order to implement the control algorithm in closed loop, current and voltage need to be sensed.

6.2.2.1 Sensing of AC Current

The current have been sensed using the PCB-mounted Hall-effect current sensors (TELCON HTP50). The HTP50 is a closed loop Hall effect current transformer suitable for measuring currents up to 50 A. The current sensing circuit is shown in Figure 6.3.

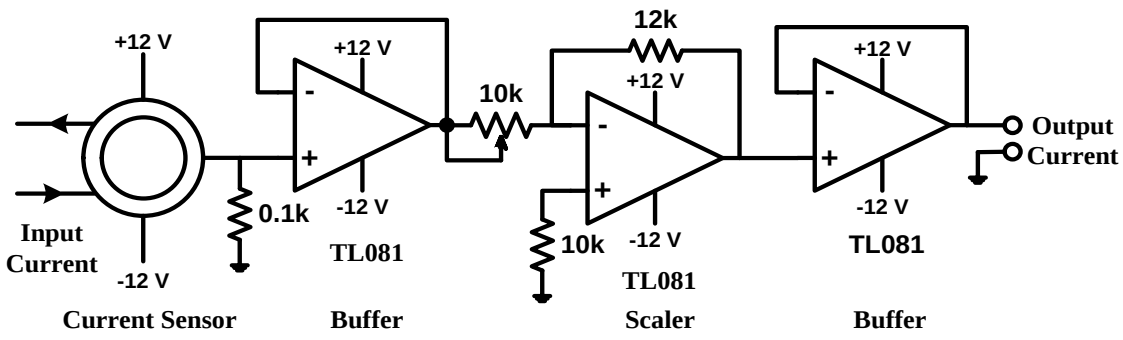

Figure 6.3 Current sensing circuit

This device provides an output current into an external load resistance. These current sensors provide the galvanic isolation between the high voltage power circuit and the low voltage control circuit and require a nominal supply voltage of the range ±12V to ±15V. It has a transformation ratio of 1000:1 and thus, its output is scaled properly to obtain the desired value of measurement.

6.2.2.2 Sensing of Voltage

The voltages are normally sensed using isolation amplifiers and among them, AD202 is a general purpose, two-port, transformer-coupled isolation amplifier that can be used for measuring both AC and DC voltages. The other main features of the AD202 isolation amplifier are:

1. Small physical size
2. High accuracy
3. Low power consumption
4. Wide bandwidth
5. Excellent common-mode performance

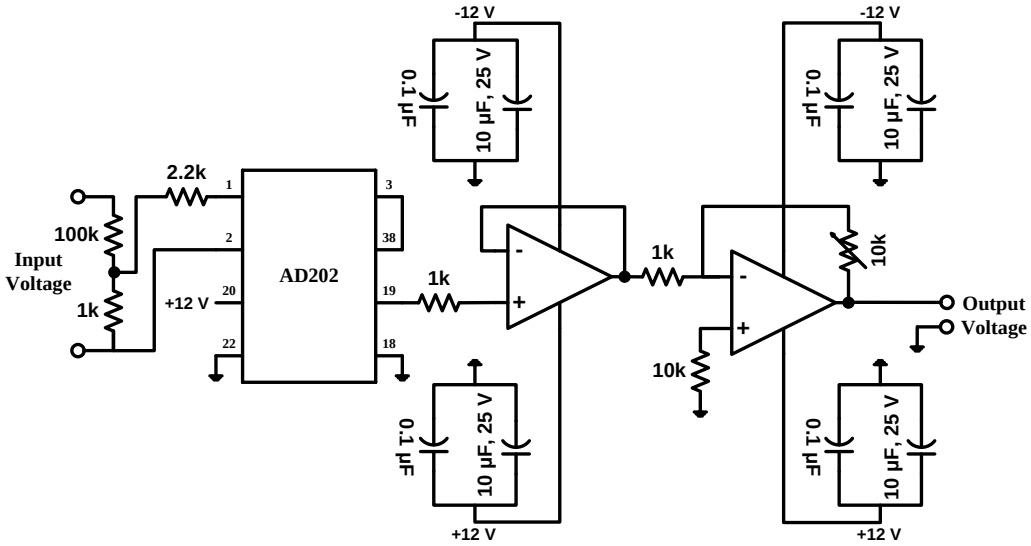

Figure 6.4 AC/DC voltage sensing circuit

This voltage sensor can sense voltages in the range of ±1 kV (peak) and it requires a nominal supply voltage range of ±12V to ±15V. Figure 6.4 shows the circuit diagram for the voltage sensing scheme, which uses AD202 isolation amplifier. The voltage (AC or DC) to be sensed is applied between the terminals 1 and 2 (across a voltage divider comprising of 100 kΩ and 1 kΩ) and the voltage input to the sensor is available at the pins 1 and 2 of AD202 via a resistance of 2.2 kΩ. The isolated sensed voltage is available at the output terminal 19 of AD202. The output of voltage sensor is scaled properly to meet the requirement of the control circuit and is fed to the dSPACE via its ADC channel for further processing.

6.2.2.3 Position Sensing Using Resolver

The PMSM used in this work is in-built with the resolver mounted on the motor shaft.

Figure 6.5 Outer view of PMSM with resolver

A resolver is used to obtain the rotor position of the PMSM. The resolver is mounted on the rotor of the PMSM. The stator of the resolver consists of three windings i.e. one primary winding and two secondary windings. The secondary windings are placed in quadrature to each other in space. The outer view of PMSM with resolver is shown in Figure 6.5. A two pole permanent magnet is mounted on the rotor of the resolver. It induces sinusoidal emf in the stator windings. Since the two secondary windings are in quadrature to each other, if the voltage induced in one is sinusoidal, then the voltage induced in the other will be co-sinusoidal. The details of the resolver connection diagram are shown in Table 6.1.

Table 6.1 Resolver connection details

PIN DETAIL	FUNCTION	SIGNAL	SIGN
1	S1	COSINE (OUTPUT)	+
2	S3		-
3	S2	SINE (OUTPUT)	+
4	S4		-
7	R1	INPUT	+
8	R2		-

The resolver algorithm and the relevant equations are presented in chapter 3. The ±5 V sine signal from function generator is given to the primary winding of resolver and generated voltage of both secondary's are given to dSPACE through ADC channel. The transformation ratio of the resolver is 0.5. The peak voltage induced in the secondary windings is +2.5 V to -2.5 V.

6.2.3 Development of System Software

Historically, control software was developed using assembly language. In recent years, industry began to adopt MATLAB/SIMULINK and Real-Time Workshop (RTW) platform based method, which provides a systematic approach to develop control software. Figure 6.6 shows the Total Development Environment (TDE) of dSPACE and its major component blocks are explained as below.

- MATLAB is widely used as an interactive tool for modeling, analysis and visualization of systems, which itself contains more than 600 mathematical functions and supports additional toolboxes to make it more comprehensive.
- Simulink is a MATLAB add-on software that enables block diagram based modeling and analysis of linear, nonlinear, discrete, and continuous and hybrid systems.
- RTW is Simulink add-on software that enables automatic C-code generation from the Simulink model. The generated optimized code can be executed on PC, microcontrollers, and signal processors.
- Real Time Interface (RTI) is add-on software of dSPACE which provides block libraries for I/O hardware integration of DS1104 R&D controller and generates optimized code for master and slave processors of the board.
- dSPACE's control desk is a software tool interfacing with real-time experimental setup and provides easy and flexible analysis, visualization, data acquisition and automation of the experimental setup. The major feature of real-time simulation is that the simulation has to be carried out as quickly as the real system would actually run, thus allowing to combine the simulation and the inverter (real plant).

The DSP DS1104 R&D controller board of dSPACE is a standard board that can be plugged into Peripheral Component Interconnect (PCI) slot of a desktop computer. The DS1104 is specially designed for the development of high-speed multivariable digital controllers and real-time simulations for various applications. It is a complete real-time control system based on an AMD Opteron™ processor running at 2.6 GHz. It has 256 MB DDR-400 SDRAM local memory for the application and dynamic application data and 128 MB SDR SDRAM global memory for host data exchange. DS1104 R&D controller is a very good platform for the development of dSPACE prototype system for cost-sensitive RCP applications.

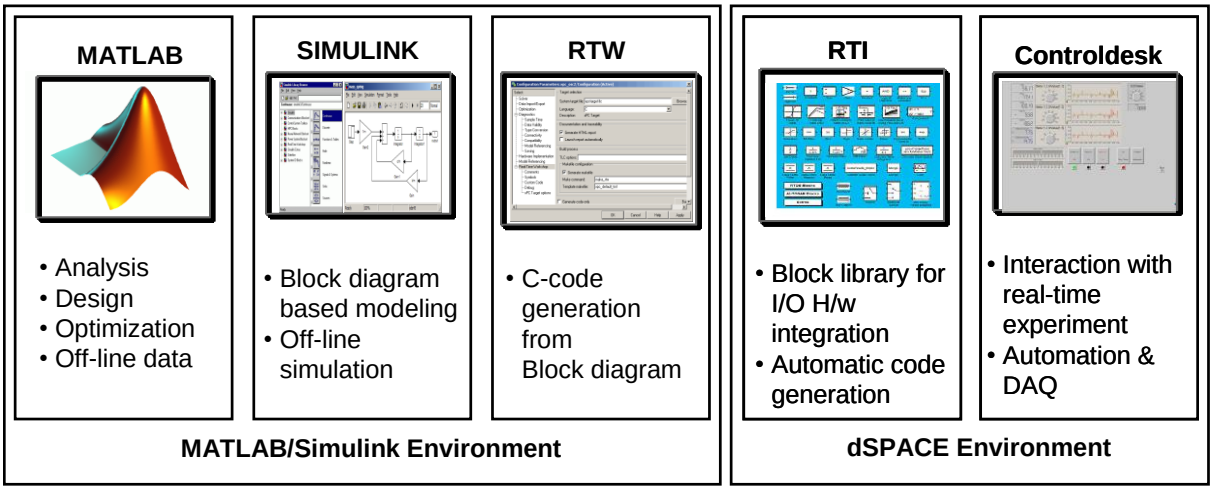

Figure 6.6 Total development environment of dSPACE with MATLAB

It is used for the real-time simulation and implementation of the control algorithm in real-time. The sensed AC and DC voltages are fed to the dSPACE Multi-I/O Board (DS2201) of DS1006 via the available ADC channels on its connector panel. In order to add an I/O block (such as ADCs and master bit I/Os in this case) to the Simulink model, the required block is dragged from the dSPACE I/O library and dropped into the Simulink model of the CHBMLI based PVDG system. In fact, adding a dSPACE I/O block to a Simulink model is almost like adding any Simulink block to the model. The master bit I/Os configured in the output mode, are connected to the model for issuing a gate pulse signal to the MOSFETs. In addition to that ADCs are connected to the model for giving different sensed parameter as input to the DSP hardware. Total development environment of dSPACE with MATLAB is presented in Figure 6.6.

The sensed signals of each topology are used for the processing in the designed control algorithm. The vital aspect for real-time implementation is the generation of real-time code of the controller to link the host computer with the hardware. For dSPACE systems, Real-Time Interface (RTI) carries out this linking function. Together with RTW from the Mathworks®, it automatically generates the real-time code from Simulink models and implements this code on the dSPACE real-time hardware. This saves the time and effort considerably as there is no need to manually convert the Simulink model into another language such as ‘C’. RTI carries out the necessary steps needing only addition of the required dSPACE blocks (I/O interfaces) to the Simulink model. In other words, RTI is the interface between Simulink and various dSPACE platforms. It is basically the implementation software for single-board hardware and connects the Simulink control models to the I/O of the board. In the present case, the optimized C-code of the Simulink model of the control algorithm is automatically generated by the RTW of MATLAB in conjunction with RTI of dSPACE.

The generated code is then automatically downloaded into the dSPACE hardware where it is implemented in real-time and the gating signals are generated. The gating pulses for the power switches of the converter are issued via the Master-bit I/Os available on the dSPACE board. The DS2201 Connector/LED combo panel provides easy-to-use connections between DS1006 board and the devices to be connected to it. The panel also provides an array of LEDs indicating the states of digital signals (gating pulses). The gating pulses are fed to various power devices driver circuits via dead-band and isolation circuits. Figure 6.7 shows the schematic diagram of dSPACE-DS1104 board interfaced with the host computer and the real-world plant (power circuit of PVDG system). Sensed signals are fed to the ADCs and generated gating pulses are given at Master bit I/Os.

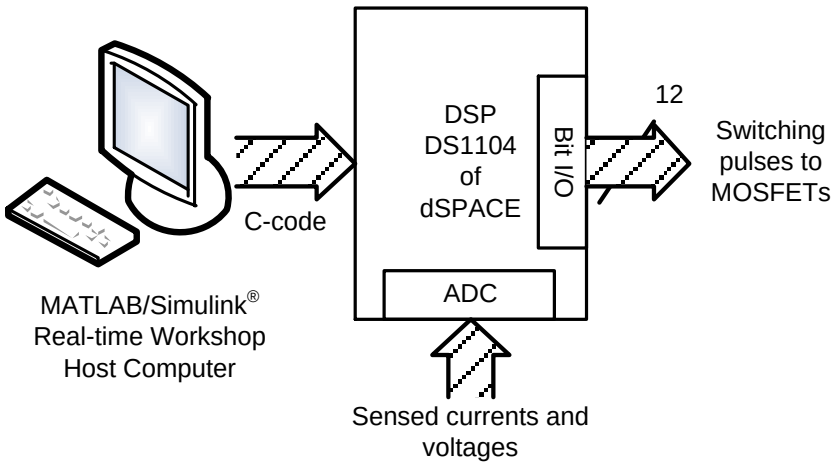

Figure 6.7 DSP (dSPACE-DS1104) circuit board interfacing

6.2.4 Development of Control Hardware

The control algorithm is designed and built into the MATLAB/Simulink software and the control pulses for the power switches of each topology of PMSM drive system are generated by real-time simulation using the DSP of dSPACE. The optimized C-code of the Simulink model of control algorithm is generated with the help of Real-Time Workshop (RTW) of MATLAB. The RTW of MATLAB and the Real-Time Interface (RTI) of dSPACE result in the real-time simulation of the model. The control pulses are generated at the various Master-bit I/Os of the dSPACE which are interfaced with the MOSFET driver circuits through isolation and dead-band circuits. This ensures the necessary isolation of the dSPACE hardware from the power circuit that is required for its protection. Figure 6.8 shows the basic schematic diagram of interfacing firing pulses from the dSPACE board to switching devices of inverter. From Figure 6.8, it can be observed that the following hardware circuits are required for interfacing of inverter with dSPACE board.

1. Dead-band circuit
2. MOSFET driver circuits for isolation and amplification

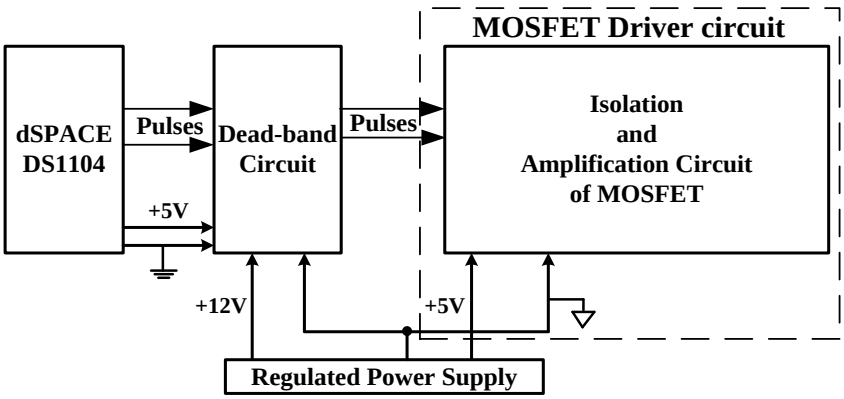

Figure 6.8 Schematic diagram of interfacing firing pulses from dSPACE controller board to switching devices

6.2.4.1 Dead-band Circuit

A dead-band (dead-time or delay) circuit is employed to provide a delay time (of about 1 μs) between the switching pulses to the devices connected in the same output leg of the inverter. This is required to avoid the short circuit of devices in the same leg of the output phase due to simultaneous conduction. The delay time circuit is shown in Figure 6.9.

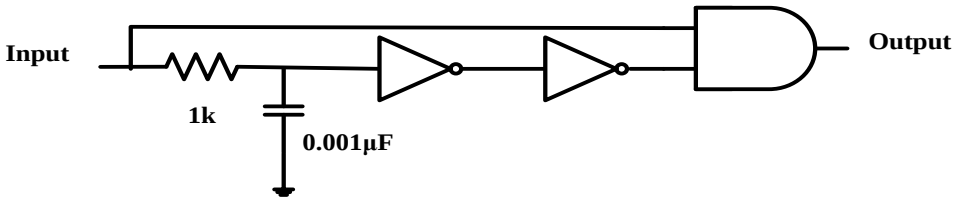

(a)

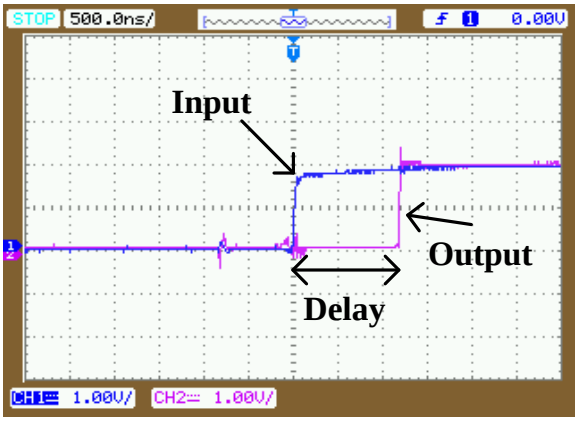

(b)

Figure 6.9(a) Dead-band circuit (b) Input-output waveform

6.2.4.2 MOSFET Driver Circuits

The MOSFET driver circuits are used for pulse amplification and isolation purposes. The control pulses generated from dSPACE unit are not efficient to drive the switching devices. Thus, these signals are further amplified by using proper amplifier circuit. Figure 6.10 (a) shows a circuit diagram of pulse isolation and amplifier circuit for MOSFET driver circuit. For isolation between power circuit and a control circuit, an opto-coupler (MCT2E) is used.

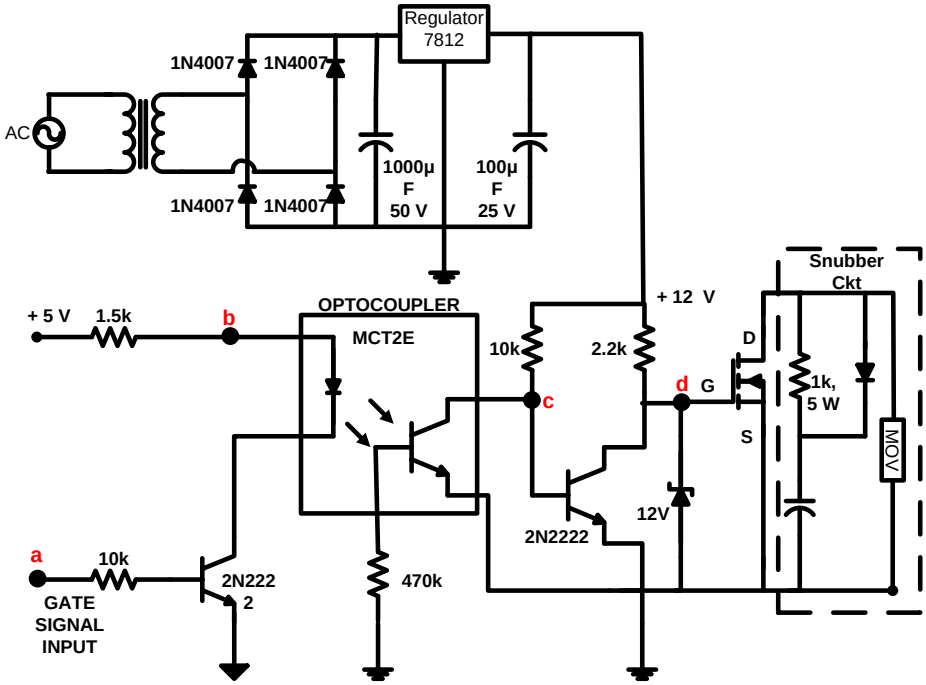

(a)

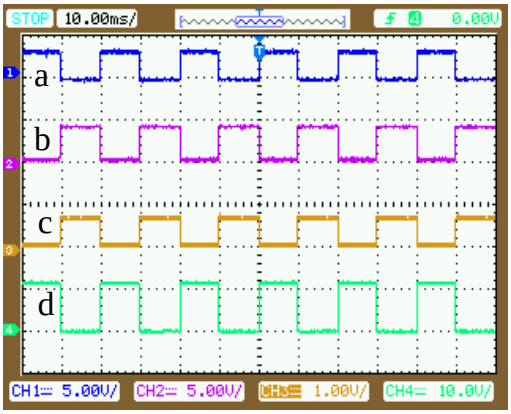

(b)

Figure 6.10 (a) MOSFET driver circuit (b) Waveform at points a (channel 1), b (channel 2), c (channel 3) and d (channel 4)

Although common + 5V, regulated DC power supply is used at the input side of the opto-coupler, but individual regulated DC power supply of +12V is used to connect the output side

of opto-coupler. When the input gating is +5V level, the transistor saturates, the LED conducts and the light emitted by it falls on the base of the phototransistor, thus forming its base drive. The pulse amplification is provided by the output amplifier transistor 2N2222. In order to test the MOSFET driver, a PWM signal is applied at point 'a' of Figure 6.10 (a) and waveforms at different points (a, b, c and d) are recorded as shown in Figure 6.10 (b). It is observed that the waveform at point 'd' is similar to the PWM signal applied at point 'a', but its amplitude is increased to 12 V which is used to drive the MOSFET.

6.3 Prototype Systems Parameter

The system parameter is given in Table 6.2. The control schemes discussed in the simulation is implemented on prototype.

Table 6.2 PMSM Parameters

PMSM Parameter	Value
Make	MOOG G400 series PMSM motor
BRAKE	24 V_{DC} (release)
M_0	3.7
$V_{DC\ max}$	325 V
Power	1.4 kW
Torque Constant	0.75Nm/A
Phase Inductance	5.15 mH
No. of Poles	8
Moment of Inertia 'J'	0.000062 kg-m^2
Total Load Inertia	0.002 kg-m^2
Damping Friction	0.0041N-m/rad
Resolver Parameters	
Input Voltage	5V
Carrier Frequency	1 kHz
Transformation Ratio	0.5

6.4 Experimental Validation of Resolver Based Position Estimation

The prototype models of the two-level inverter and three-level NPC inverter driven PMSM drive have been developed by integrating the power circuit, the control hardware and the dSPACE controller. The view of the experimental test bench with two-level inverter fed PMSM drive is shown in Figure 6.11. The accurate rotor position estimation takes a key role in implementing the vector control. The rotor position of PMSM can be measured by using the resolver without RDC to make cost effective drive.

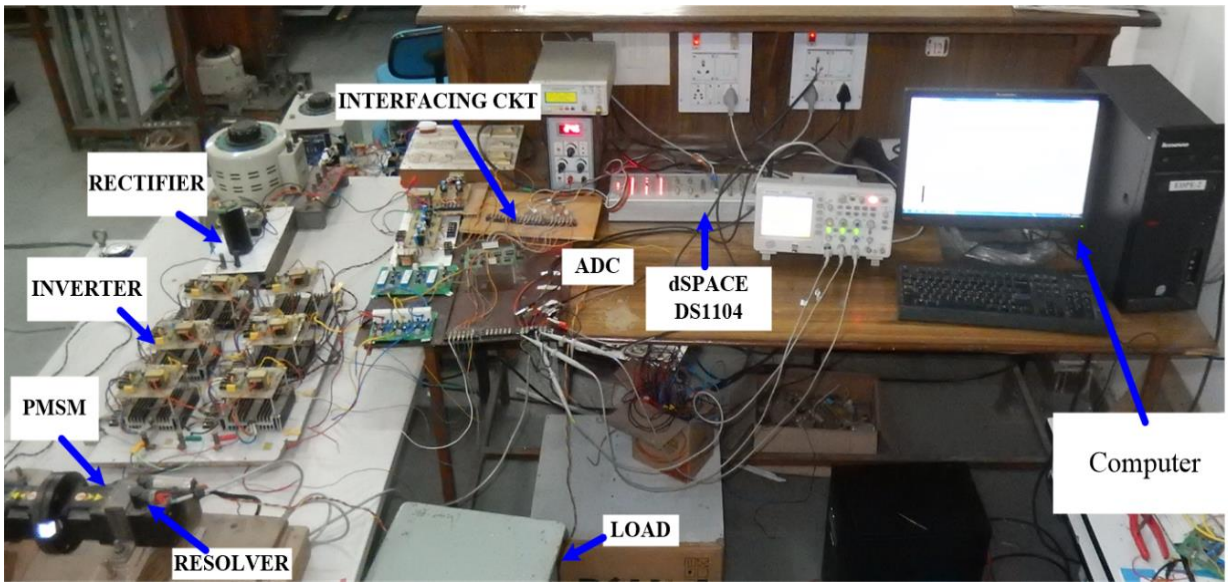

Figure 6.11 Experimental setup with two-level inverter fed PMSM drive

The output signal of resolver at complete 360˚ rotation of the rotor shaft is shown in the Figure 6.12(a). From the experimental results shown in the Figure 6.12(a), it is observed that the sine output signal is zero and the cosine signal is in phase with the input signal at the starting position when the angle is zero. Channel 1 represents the input high frequency excitation signal of the resolver. Channel 2 and 3 represents the sine and cosine output of the resolver. The variation in output signal by 90˚ rotation of the rotor shaft is shown in the Figure 6.12(b). At this position the sine output signal is in phase with the input signal and the cosine signal zero. From Figure 6.12(c) it is observed that the sine output signal is zero and the cosine signal is in opposite phase when the input signal is at 180^{o} rotation of rotor shaft. The cosine output signal is zero and the sine signal is in opposite phase when the input signal is at 270^{o} rotation of rotor shaft as shown in Figure 6.12(d). Further, from Figure 6.12(e) it is observed that the sine output signal is zero and the cosine signal is in phase when the input signal is at 360^{o}.

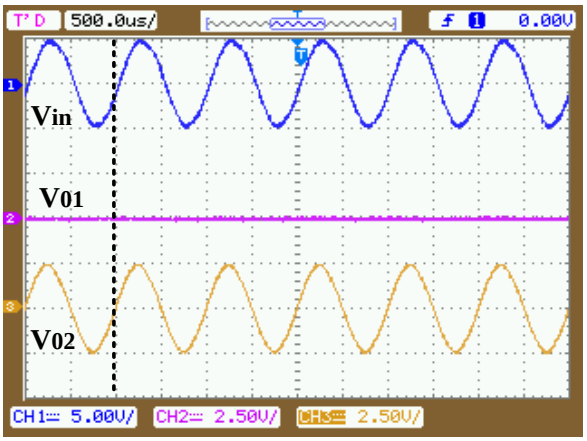

(a)

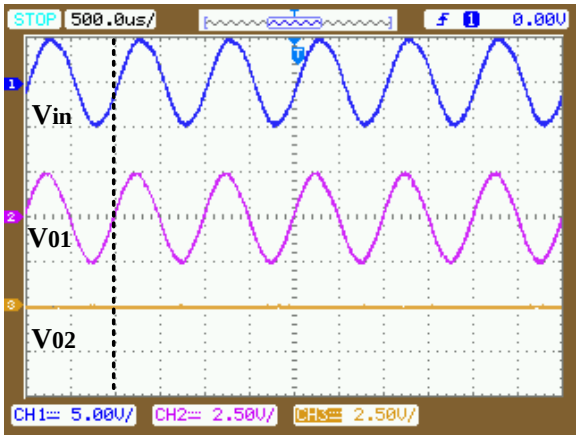

(b)

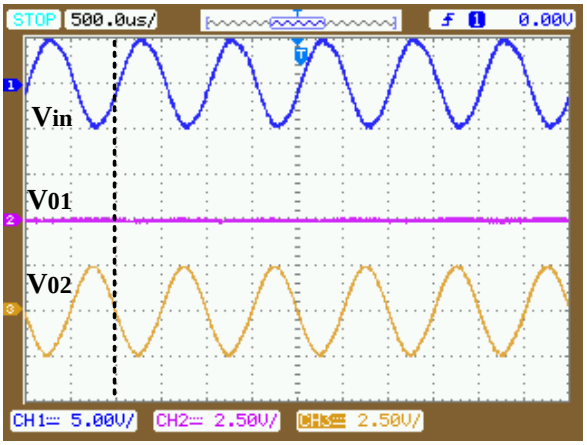

(c)

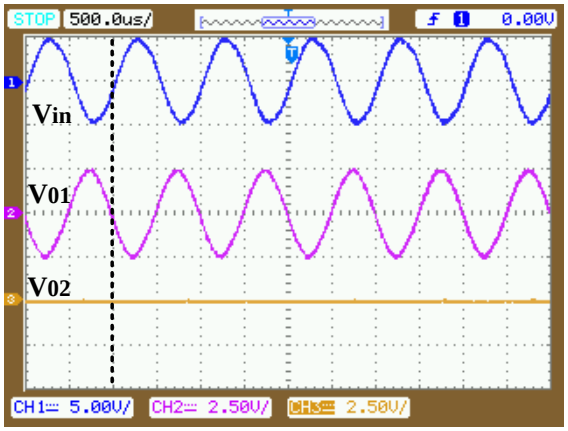

(d)

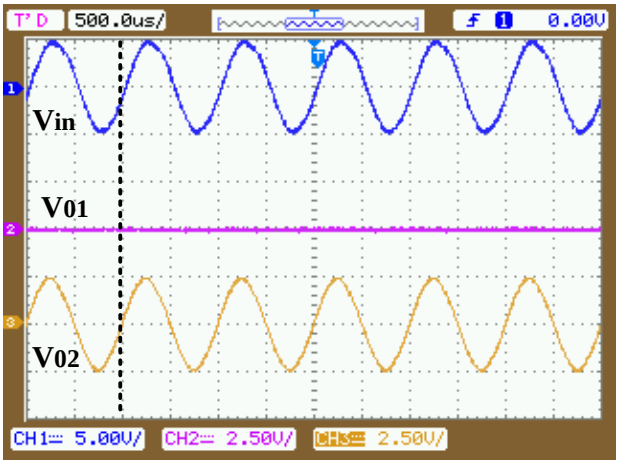

(e)

Figure 6.12 Experimental results of resolver output signal at (a) 0^0 shaft rotation (b) 90^0 shaft rotation (c) 180^0 shaft rotation (d) 270^0 shaft rotation (e) 360^0 shaft rotation

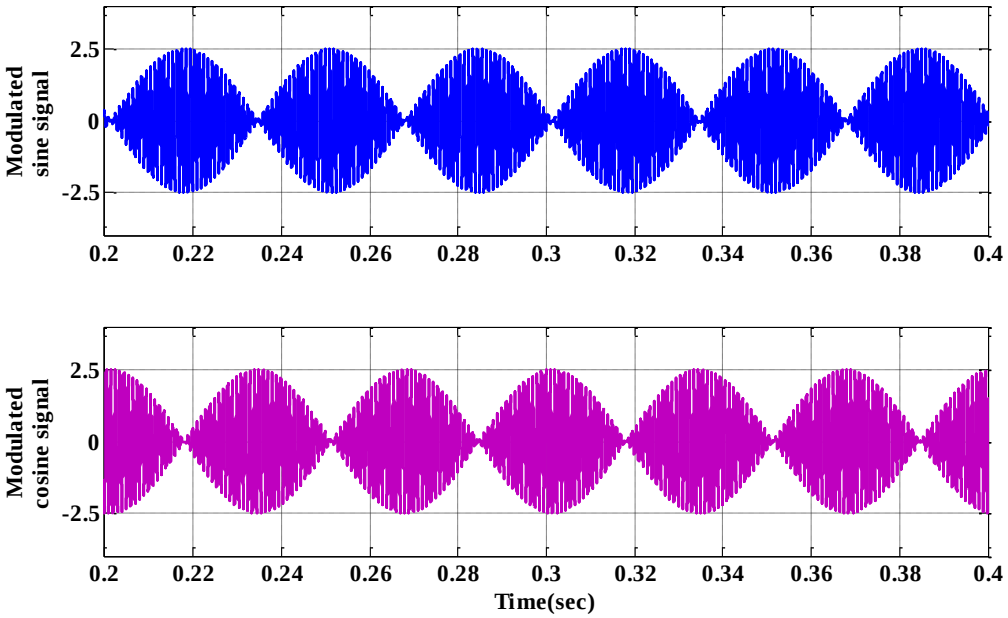

Figure 6.13 Simulation result of modulated sine (2.5V, 1kHz) and cosine output Signal (2.5V, 1kHz)

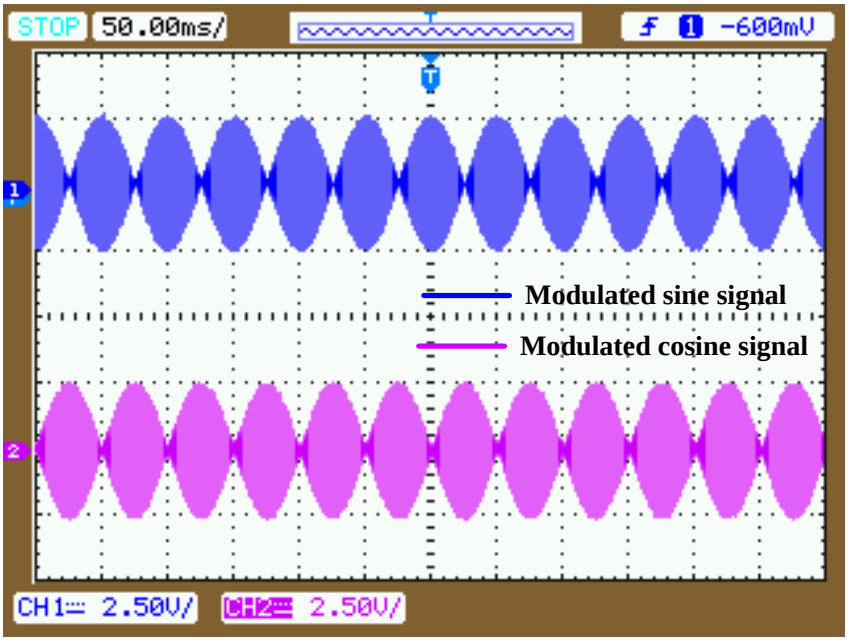

Figure 6.14 Experimental result of modulated sine (2.5V, 1kHz) and cosine output Signal (2.5V, 1kHz)

To excite the primary coil of the resolver high frequency signal is applied. With the rotation of rotor, the resolver induces two modulated signals. These modulated signals are demodulated using the estimation algorithm discussed in chapter 3. The simulation results of modulated sine and cosine are presented in the Figure 6.13. The corresponding experimental results are shown in the Figure 6.14. Trace 1 denotes the modulated output sine signal and the trace 2 denotes the modulated output cosine signal. The simulation results of demodulated

sine and cosine output signal are depicted in the Figure 6.15. The experimental results are shown in the Figure 6.16.

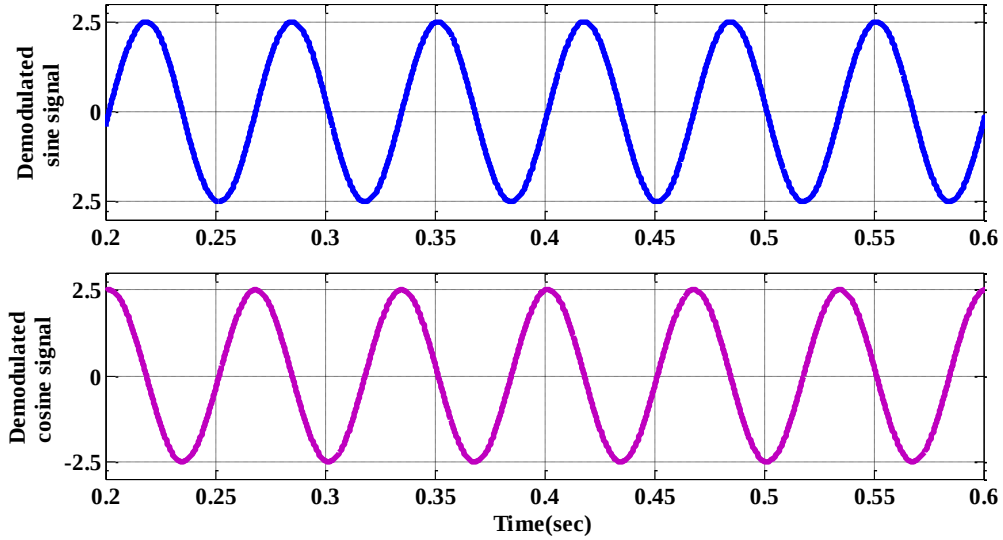

Figure 6.15 Simulation result of demodulated sine signal (2.5V) and cosine signal (2.5V)

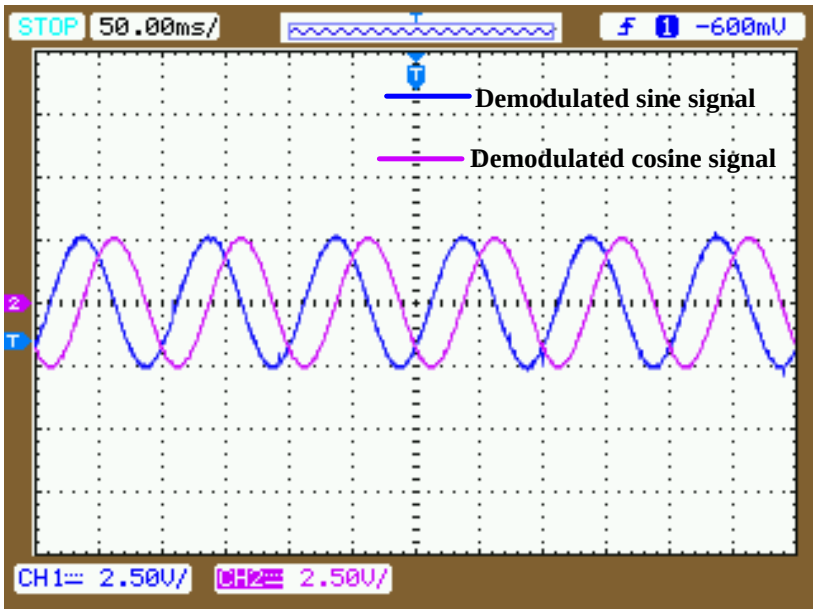

Figure 6.16 Experimental result of demodulated sine signal (2.5V) and cosine signal (2.5V)

The simulation results of the rotor position with respect to demodulated sine signal are shown in the Figure 6.17. The experimental validation of the simulation results is presented in the Figure 6.18. The demodulated sine and cosine output provides θ with the help of resolver algorithm as discussed in chapter 3. The estimated rotor position θ is used in PMSM drive for vector control operation. This estimation eliminates the use of Resolver to Digital Converter (RDC), which in terns reduces the cost of the drive.

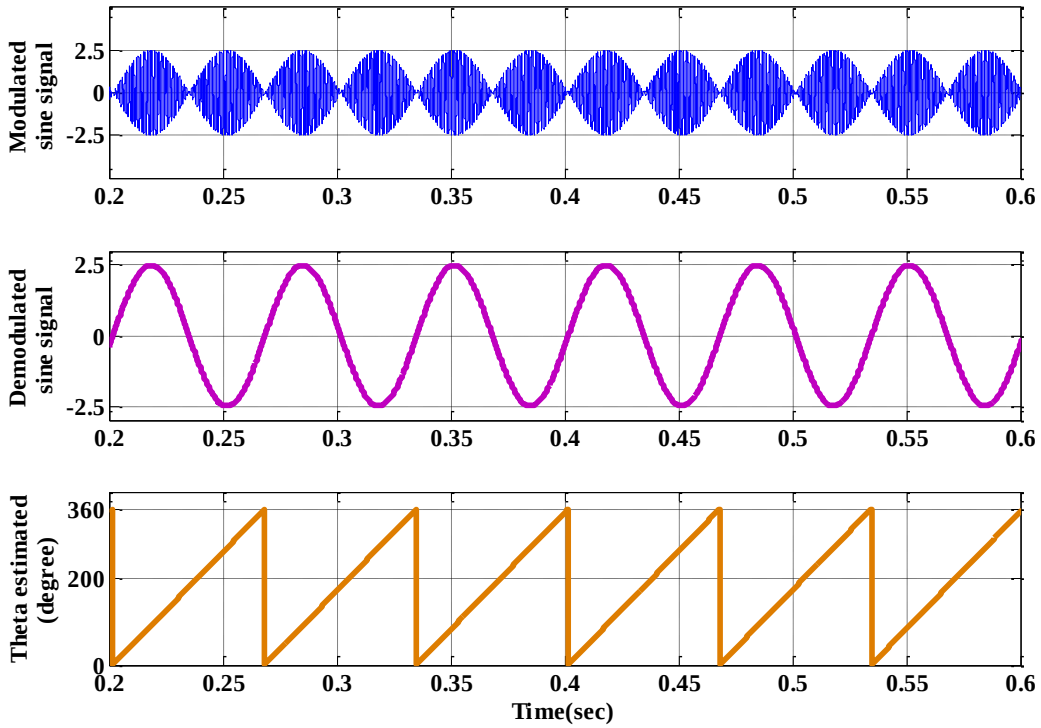

Figure 6.17 Simulation result of demodulated and modulated sine signal (2.5V) and rotor position.

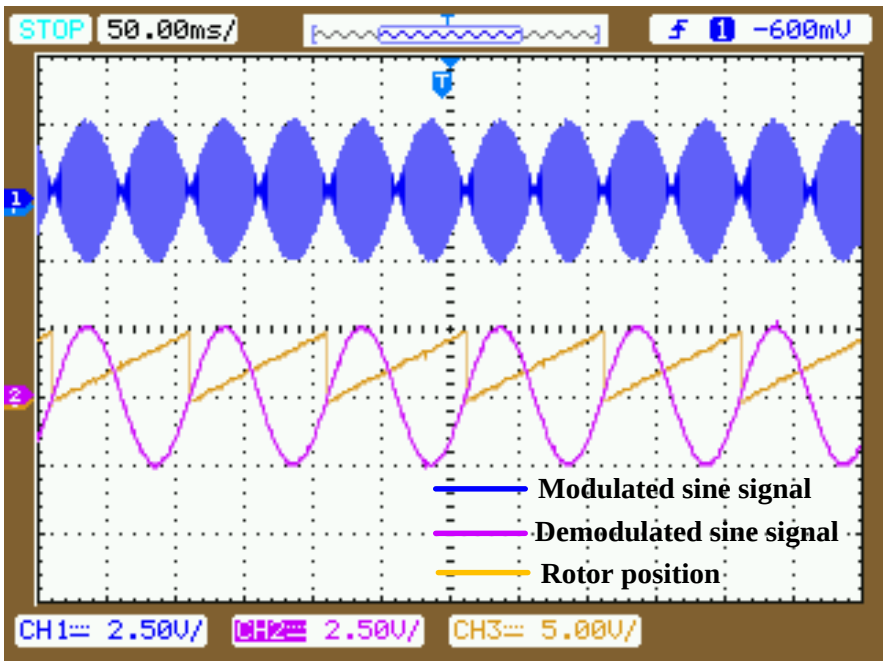

Figure 6.18 Experimental result of demodulated and modulated sine signal (2.5V) and rotor position (360º/div).

6.5 Performance Investigations of ZDAC Control of PMSM Drive

Experiments are performed to investigate the performance of the drive, driven by two-level inverter and validated the simulated results. As the available prototype motor in the laboratory is surface permanent magnet motor. So the vector control in-terms of zero d-axis current control have been implemented. The performance of the drive at different operating condition has been experimentally investigated. The simulated and experimental line to line voltage waveforms of two-level inverter fed drive are shown in the Figure 6.19 and Figure 6.20. The fundamental frequency is kept 100Hz to compare the simulated and experimental results.

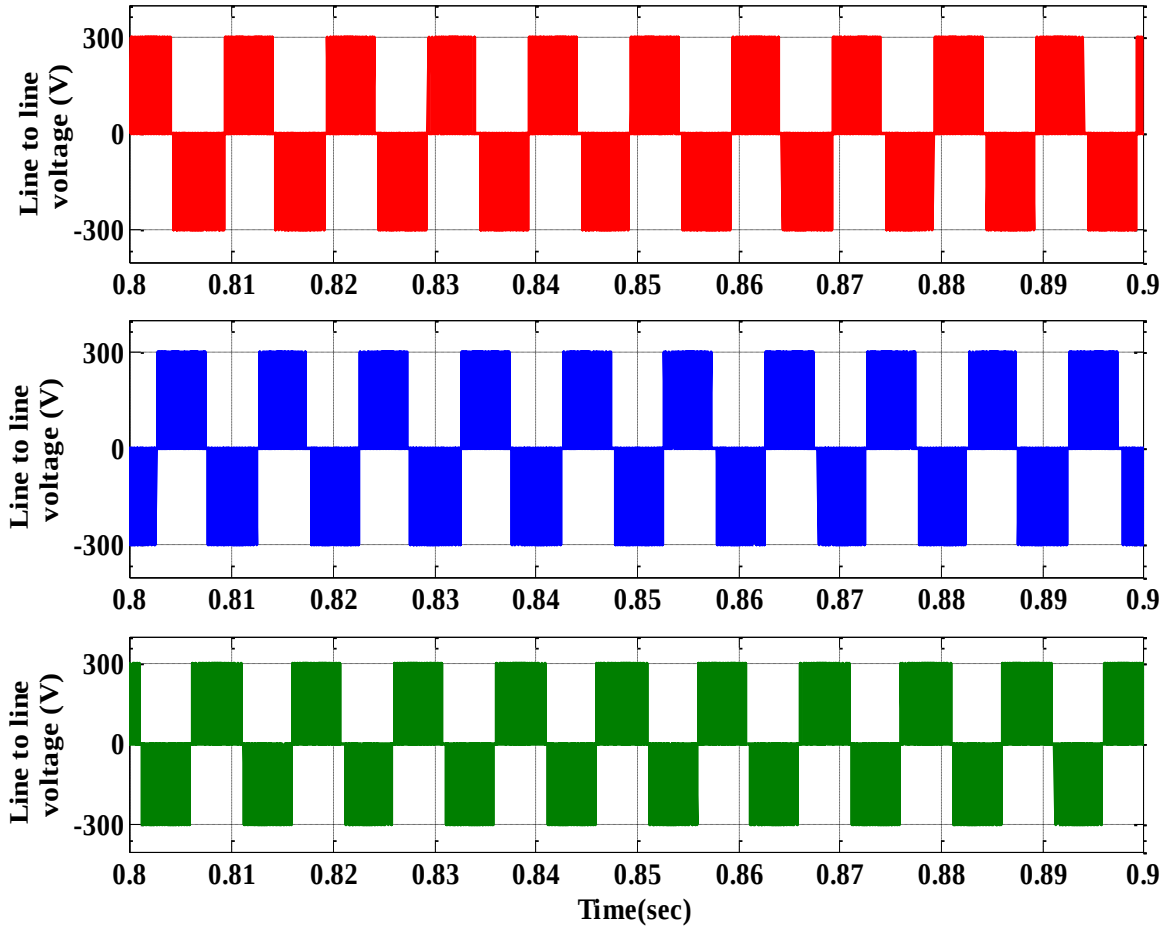

Figure 6.19 Simulation results of line to line voltage (100 Hz) of two- level inverter fed to PMSM drive

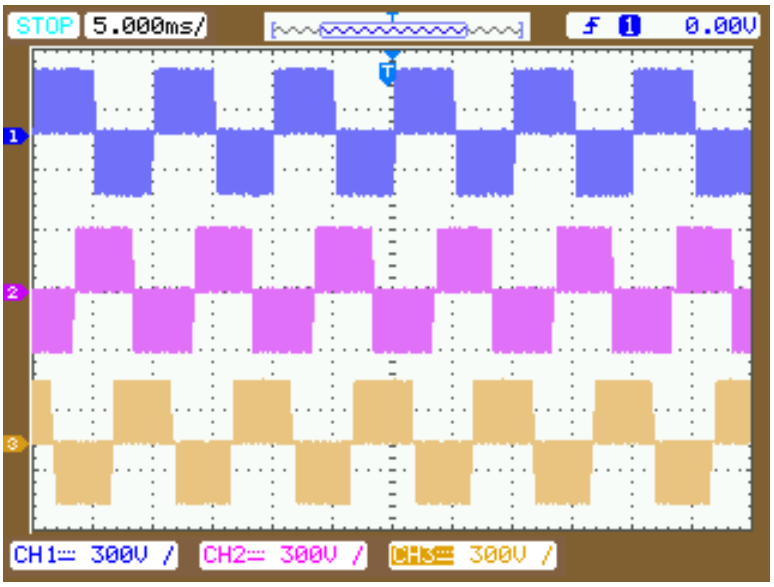

Figure 6.20 Experimental result of line to line voltage (100 Hz) of two-level inverter fed PMSM drive (300V/div)

6.5.1 Starting Response of the Drive

The simulated and experimental results of the starting response of the drive have been shown in Figure 6.21 and Figure 6.22 respectively. Trace 1 in the Figure 6.22 represents the speed of the motor in rpm. Trace 2 shows the stator current. The reference value of speed is kept 900 rpm and the motor is started with no load. It is observed that the motor reaches its reference speed value. Initial starting torque is high. The stator current is also high at the time of starting. The experimental results validate the corresponding simulation results.

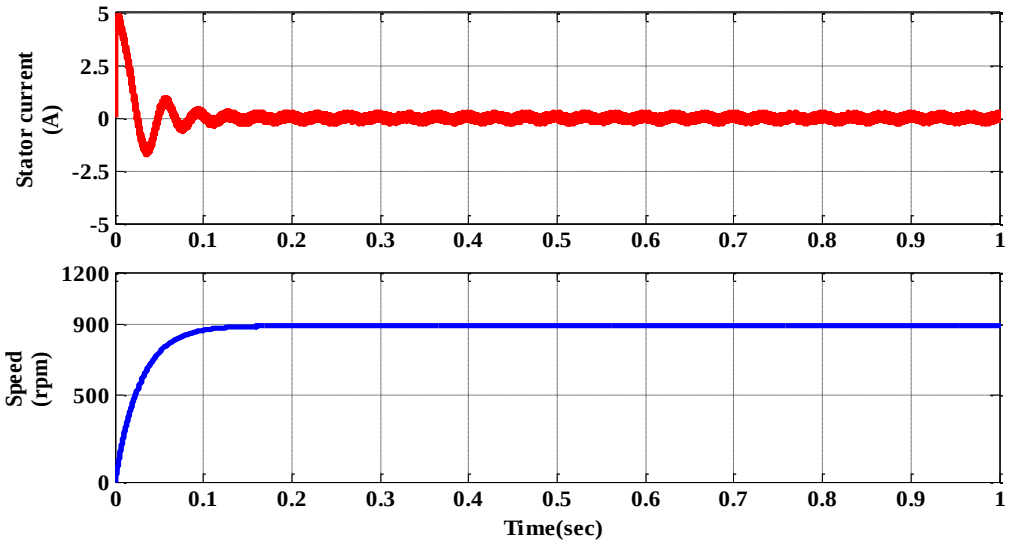

Figure 6.21 Simulation result of starting response of the PMSM drive (speed 900 rpm)

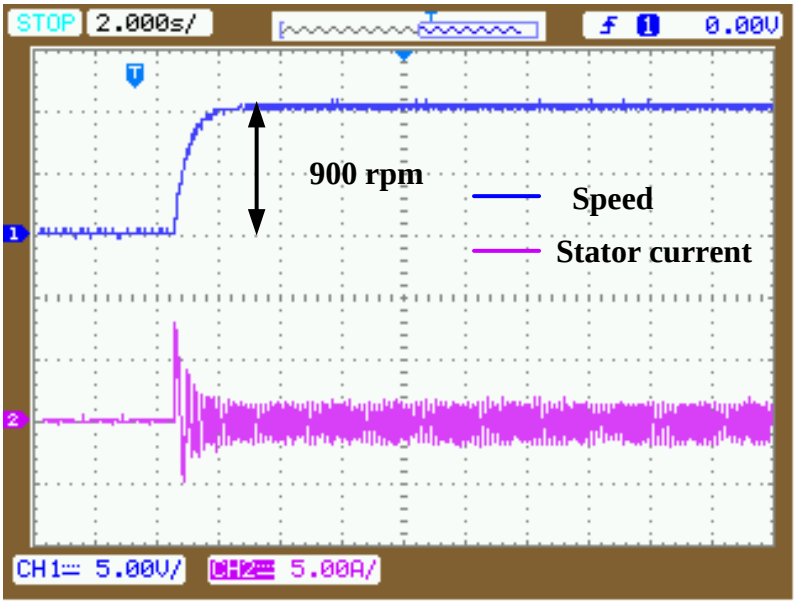

Figure 6.22 Experimental result of starting response of the PMSM drive (speed 450rpm/div, stator current 5A/div)

6.5.2 Performance of the Drive at Loading Condition

To investigate the performance under loading condition a load of 4Nm is applied to the motor and the experimental results are obtained. The corresponding simulation results are shown in Figure 6.23. The experimental result of the drive at increasing load has been shown in the Figure 6.24.

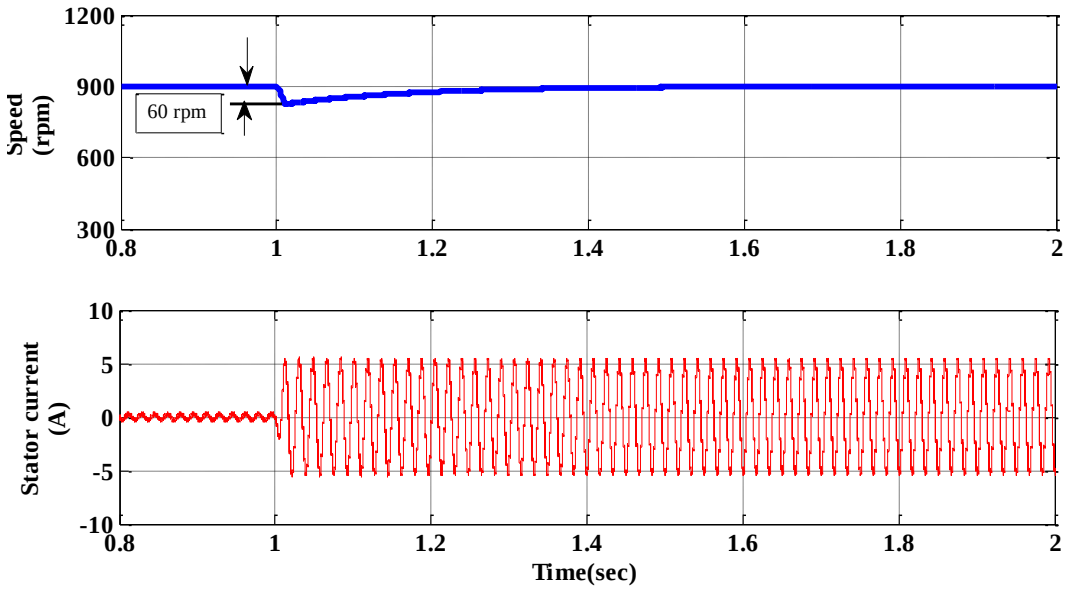

Figure 6.23 Simulation result of the PMSM drive at loading (4Nm) condition

A step load of 4 Nm is applied. It is observed that the stator current is increased at the time of

loading. It is also observed that there is dip in the speed response. This is due to the application of load torque. This speed response reaches the reference value due to the closed loop operation of the drive. Channel 1 represents the speed and channel 2 represents the current response of the drive.

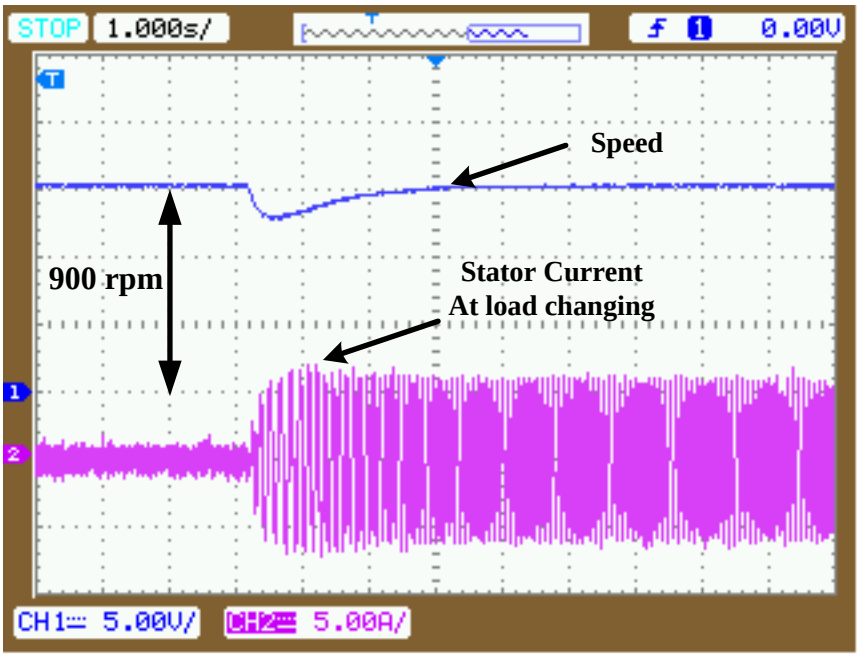

Figure 6.24 Experimental result of the PMSM drive at loading condition (speed 300rpm/div, stator current 5A/div)

6.5.3 Performance of the Drive at Speed Changing Condition

The performance of the drive with two-level inverter at speed changing operation also has been investigated. A change in speed reference of 300 rpm has been applied. The speed reference increased from 900rpm to 1200 rpm. The simulation results are shown in Figure 6.25. The experimental results shown in the Figure 6.26 represents the performance of the drive at speed increasing operation. It is observed that when the speed reference is increased from 900 rpm to 1200 rpm, the torque is increased by the motor to reach the reference speed. Due to that the stator current is also slightly increased at that time. The torque reduced once the reference speed value reached. Furthermore the performance of the drive at speed decreasing condition is investigated and results are obtained which is shown in Figure 6.28 and corresponding simulation results is shown in Figure 6.27. The reference speed command is change from 1200rpm to 900 rpm.

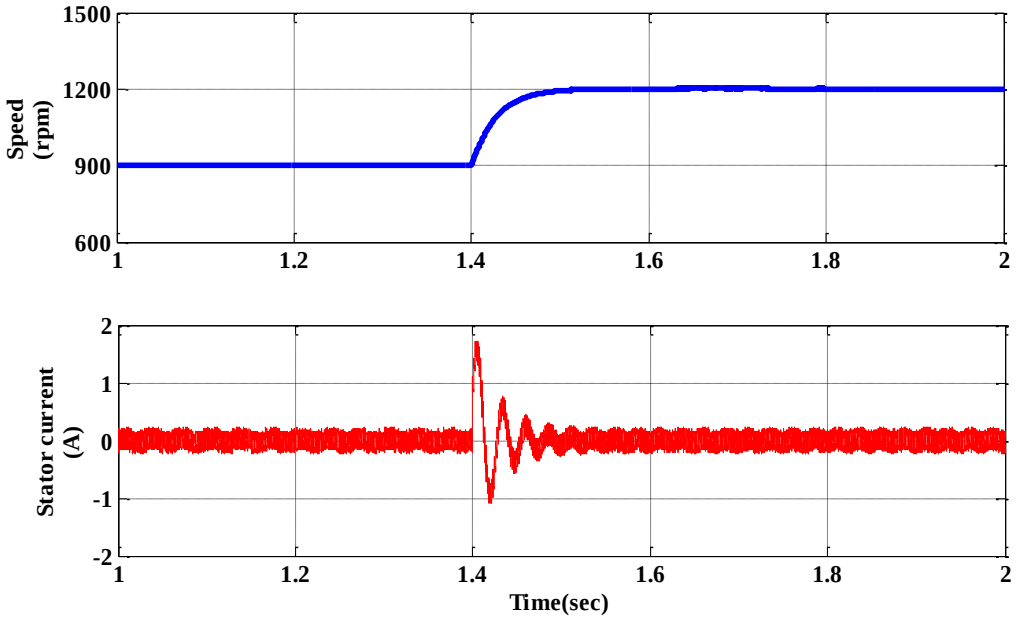

Figure 6.25 Simulation result of the PMSM drive at speed changing (900rpm to 1200 rpm)

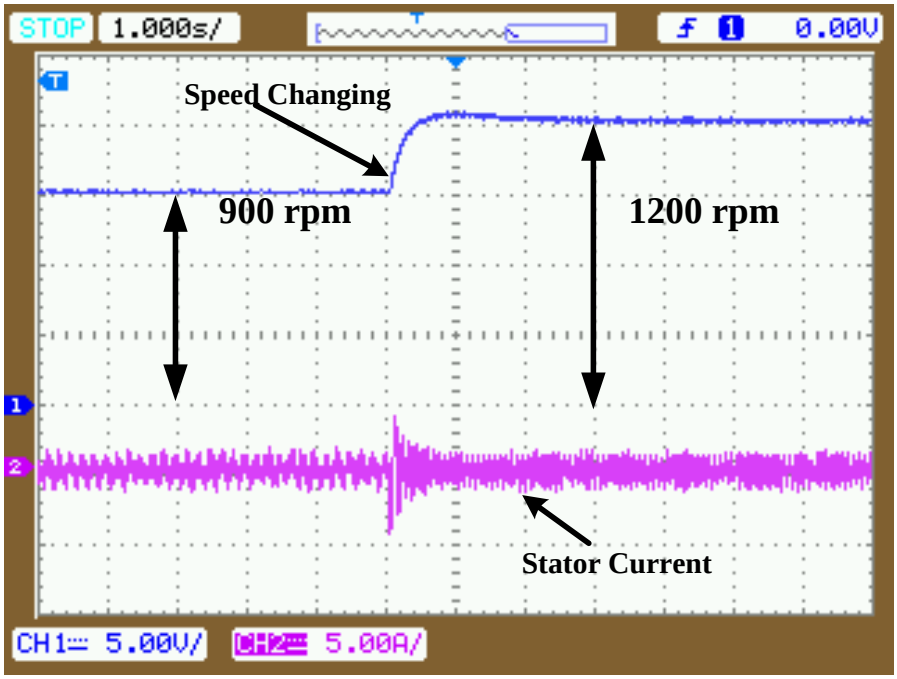

Figure 6.26 Experimental result of the PMSM drive at speed changing (900rpm to 1200 rpm) (speed 300rpm/div, stator current 5A/div)

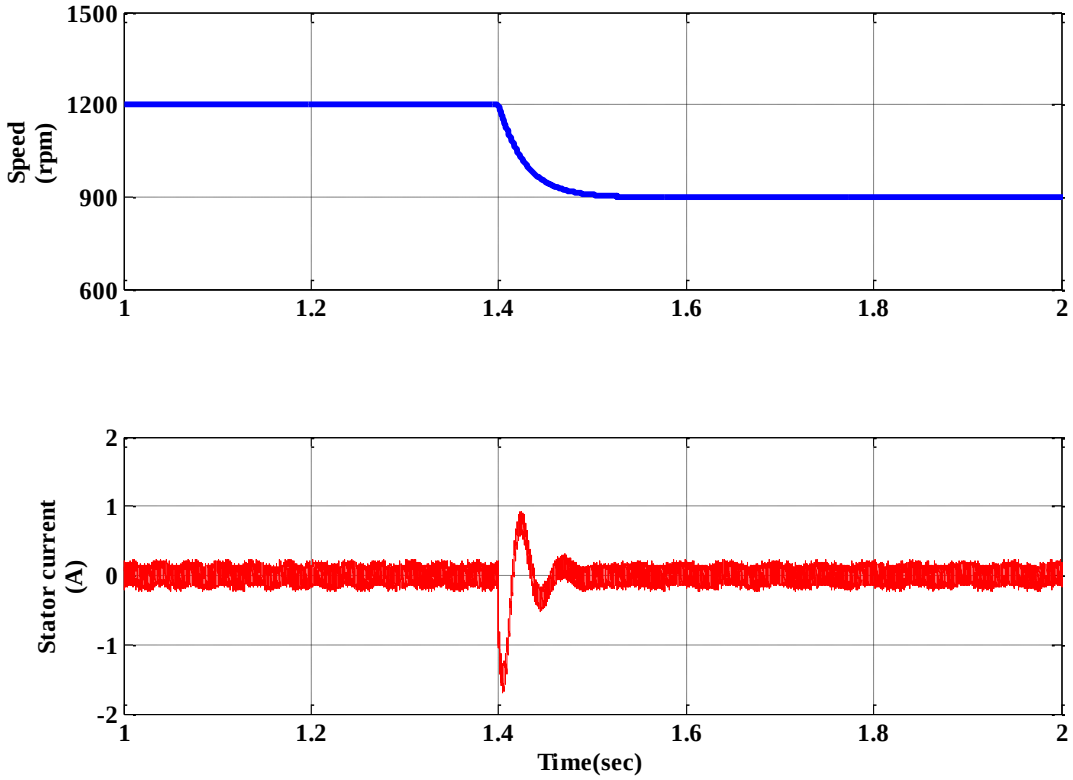

Figure 6.27 Simulation result of the PMSM drive at speed changing (1200rpm to 900 rpm)

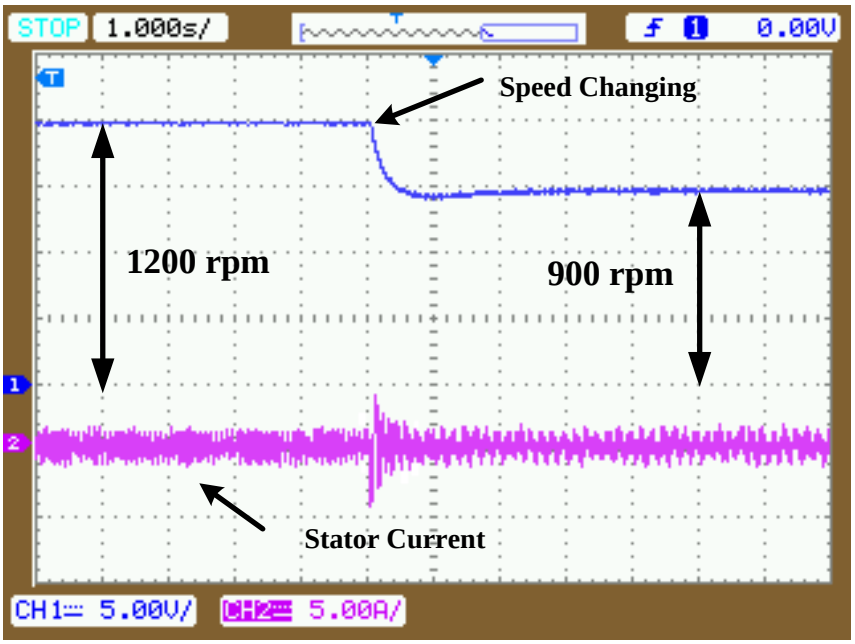

Figure 6.28 Experimental result of the PMSM drive at speed changing (decreasing 1200rpm to 900 rpm) (speed 300rpm/div, stator current 5A/div)

6.6 Performance Investigations of Three-level NPC Inverter Fed Drive with TLBC Circuit

In this experimental study, the developed prototype of three-level neutral point clamped inverter driven PMSM drive are tested with different modes of the controller action, varying speed and load condition to verify their viability and effectiveness. The view of experimental test bench is shown in the Figure 6.29. A voltage balancing strategy, with low switching losses is proposed using three-level boost converter, which keeps the voltage difference between the two dc-link capacitors at a desired level. Moreover, performance of the proposed drive scheme is examined by carrying out extensive simulations and experimental studies on a SPMSM with vector control in terms of zero d-axis current control.

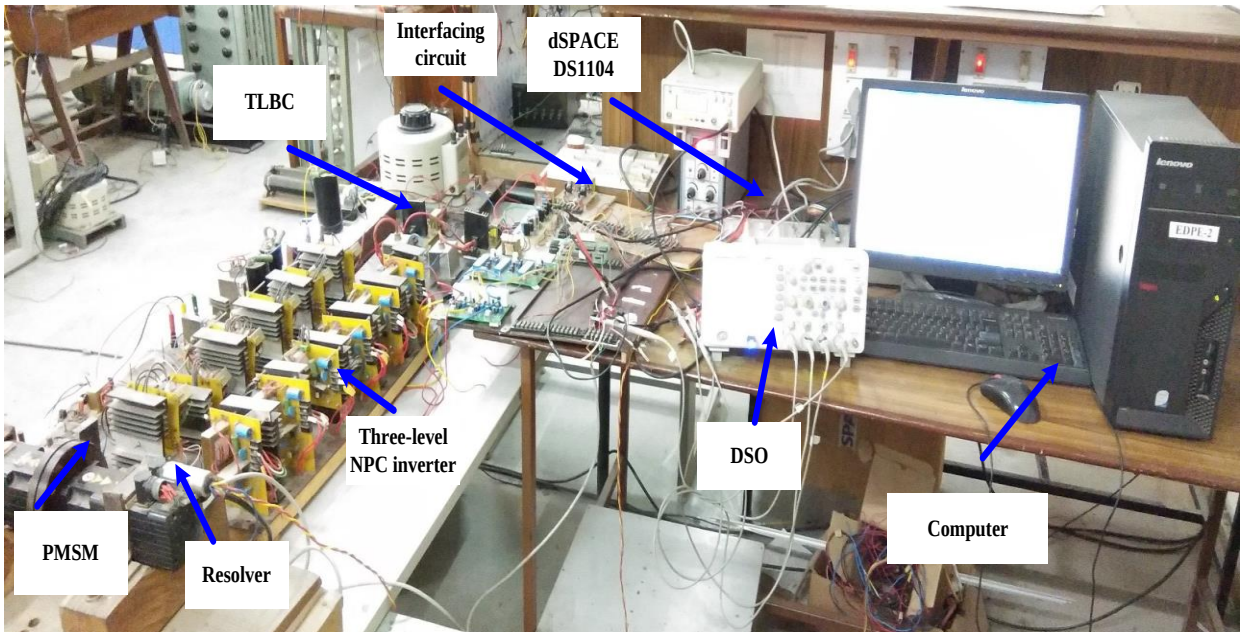

Figure 6.29 Experimental test bench of three-level NPC inverter fed PMSM drive

The simulation results of line to line voltage waveform of three-level NPC inverter fed PMSM drive is shown in the Figure 6.30. The fundamental frequency is kept 100 Hz. The corresponding experimental results are presented in Figure 6.31.

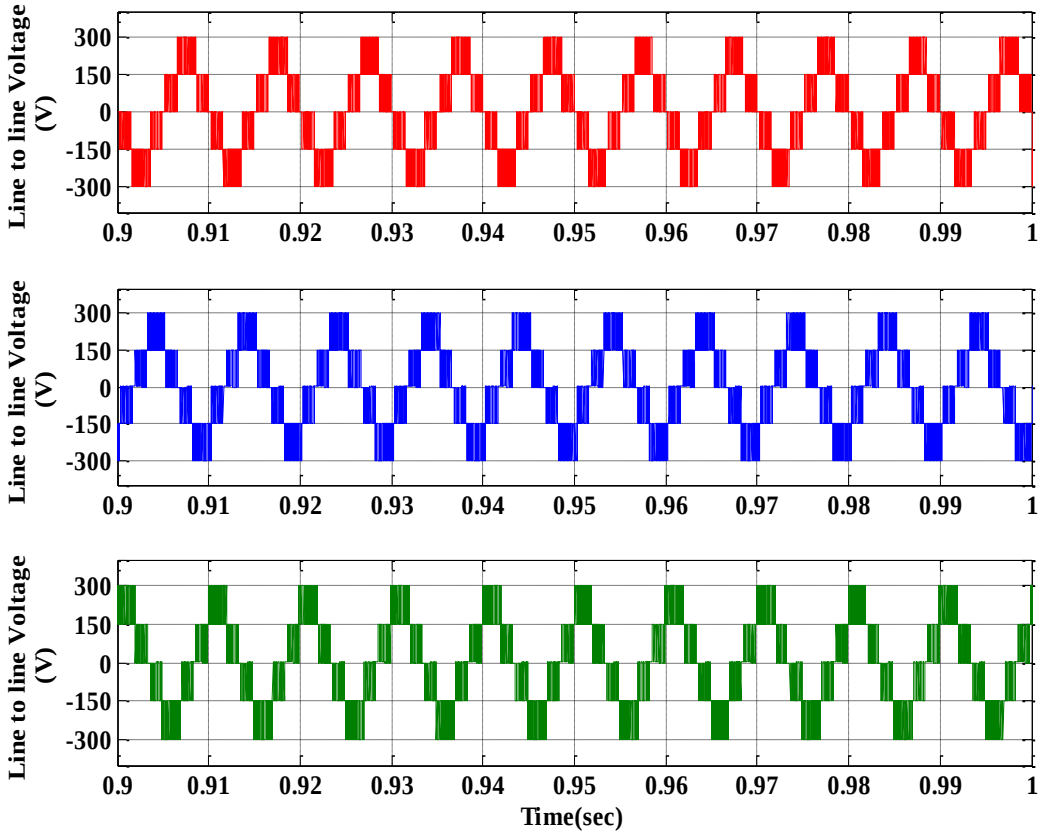

Figure 6.30 Simulation result of line to line voltage (100Hz) of three- level NPC inverter fed to PMSM drive

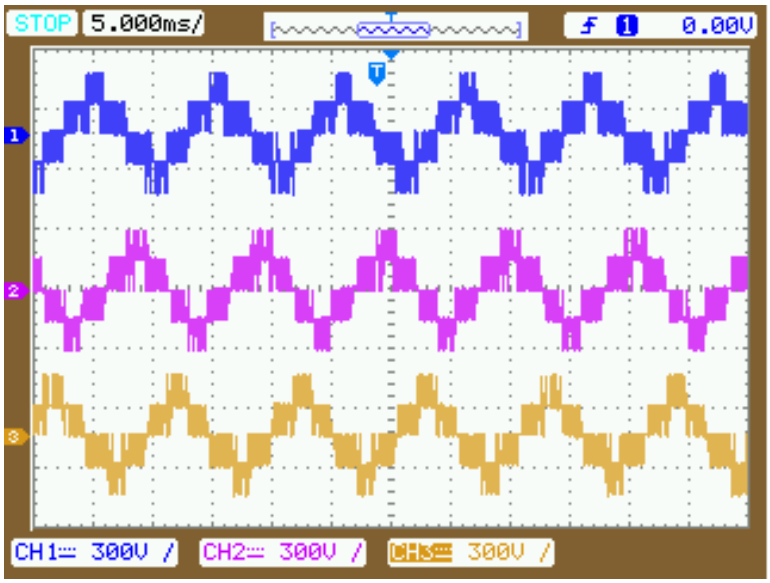

Figure 6.31 Experimental results of line to line voltage (100Hz) of three-level inverter fed to PMSM drive (300V/div)

6.6.1 Capacitor Voltage Balancing and Boosting Using TLBC Circuit

The three-level boost converter (TLBC) is most attracting circuit used for voltage balancing in multi-level NPC inverter. The advantageous feature is reduced switching losses and lower reverse recovery losses of the diode compared with the conventional boost converters. Based on the previously presented simulation studies in the chapter 5, exhaustive experimental study is carried out for the validation. The simulation results of the different capacitor voltage with respect to input dc voltage are shown in the Figure 6.32.

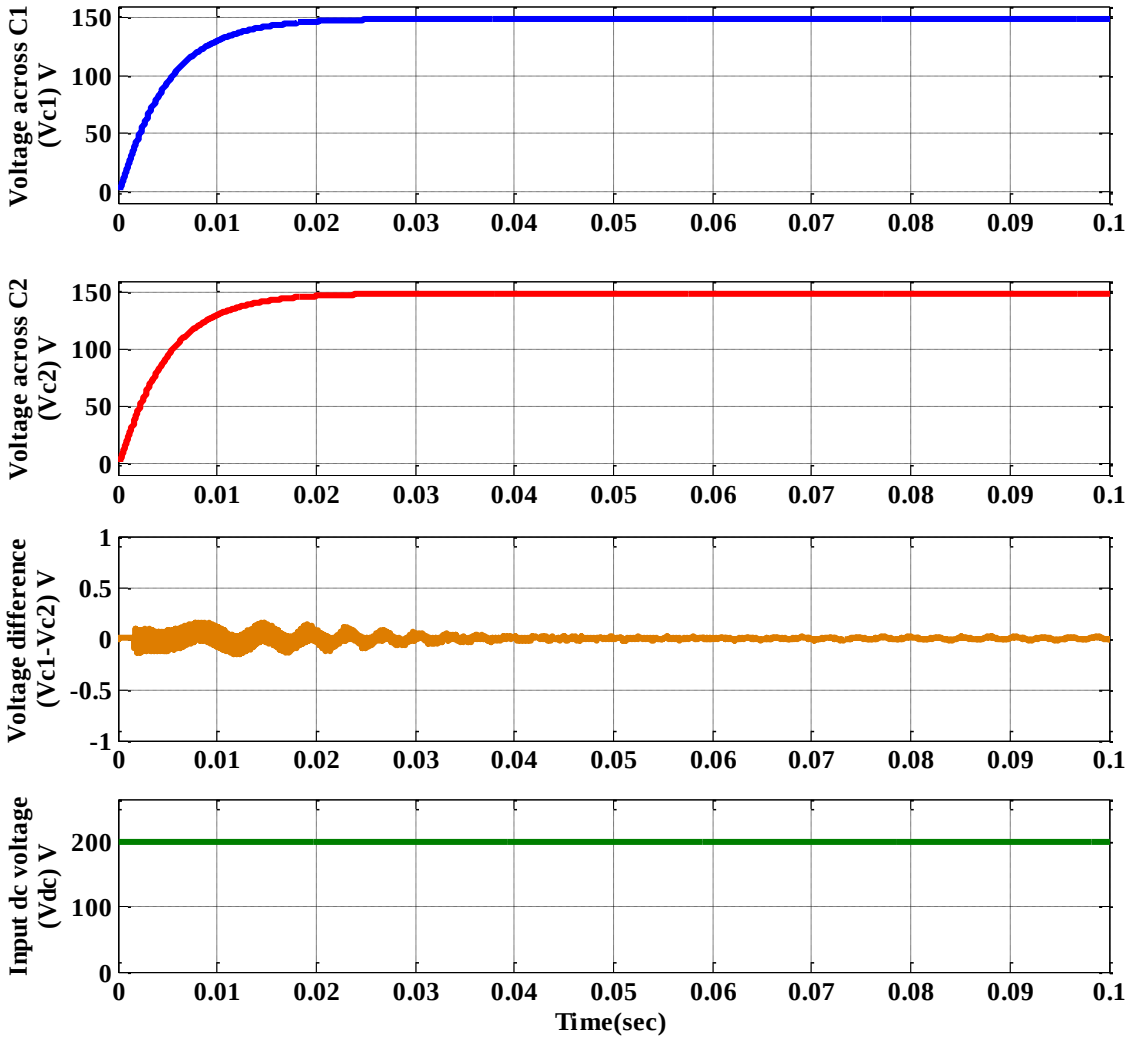

Figure 6.32 Simulation result of capacitor voltage balancing

The experimental results are presented in the Figure 6.33. Channel 1 represents the voltage across the capacitor C_1 and the channel 2 represents the voltage across capacitor C_2. It is observed that with the use of TLBC in three-level NPC inverter the voltage across the capacitors are maintained at desired value 150 V. The voltage difference is shown in channel

3 is quite less. So the dc link voltage is perfectly balanced with the use of TLBC in three-level NPC inverter. The input voltage to the NPC inverter is maintained at 300 V with the help of TLBC by selecting the duty ratio (D) of 0.667, whereas the input dc voltage (V_{dc}) is 200 V. TLBC reduces the computational complexity. The main attraction is the boosting feature of the input voltage along with the balancing of the capacitor voltage.

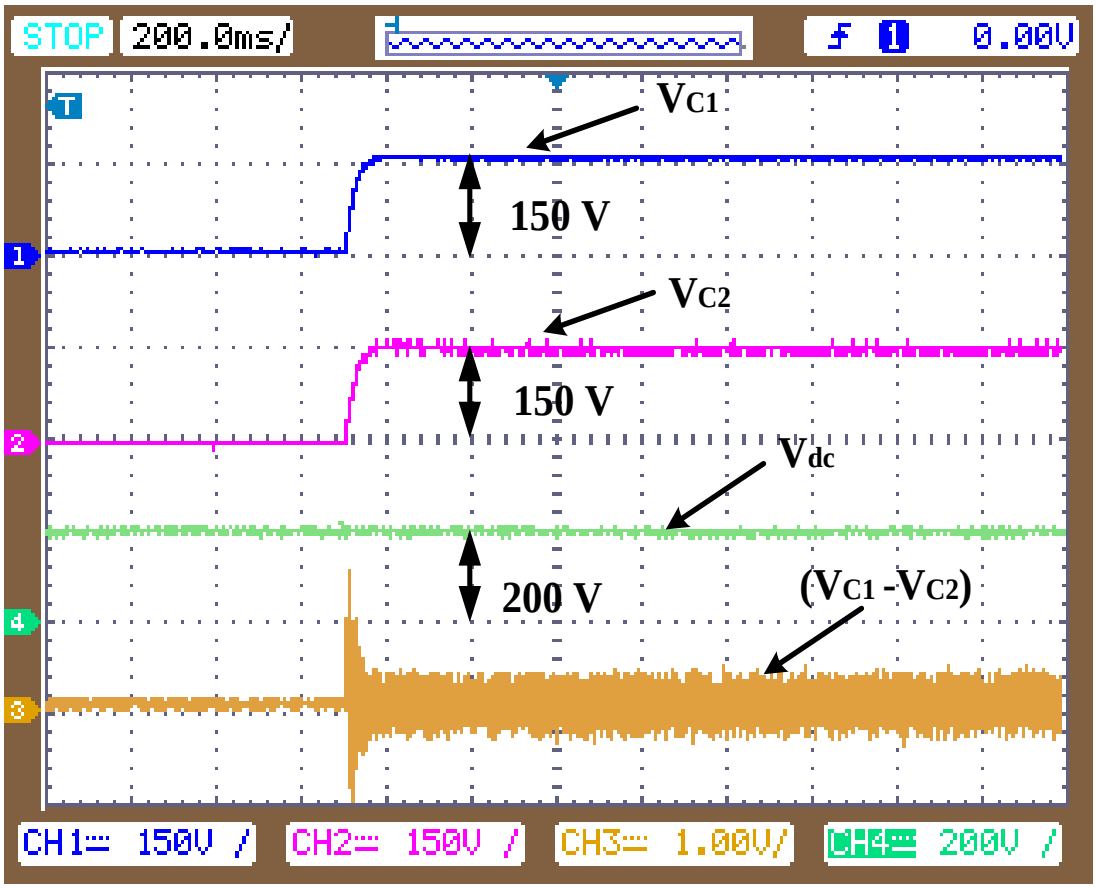

Figure 6.33 Experimental result of capacitor voltage balancing (Capacitor voltage 150V/div, Input dc voltage 200V/div, Capacitor voltage difference 1V/div)

6.6.2 Starting Response of the Proposed Drive

The performance of the proposed there-level NPC inverter fed PMSM drive is experimentally investigated at different operating condition. Initially the starting response of the drive is investigated and the results are presented in the Figure 6.35. The reference value of speed is kept 900 rpm and the motor is started with no load. It is observed that the motor reaches its reference speed value as presented in channel 1. The speed is presented as 450 rpm/div scale. The stator current is shown in channel 2. The stator current is presented as 5 A/div scale. The stator current is high at the time of starting. It reduces when the motor reaches its reference speed value. It is noticed that the simulation results shown in the Figure 6.34 are

experimentally validated and presented in the Figure 6.35.

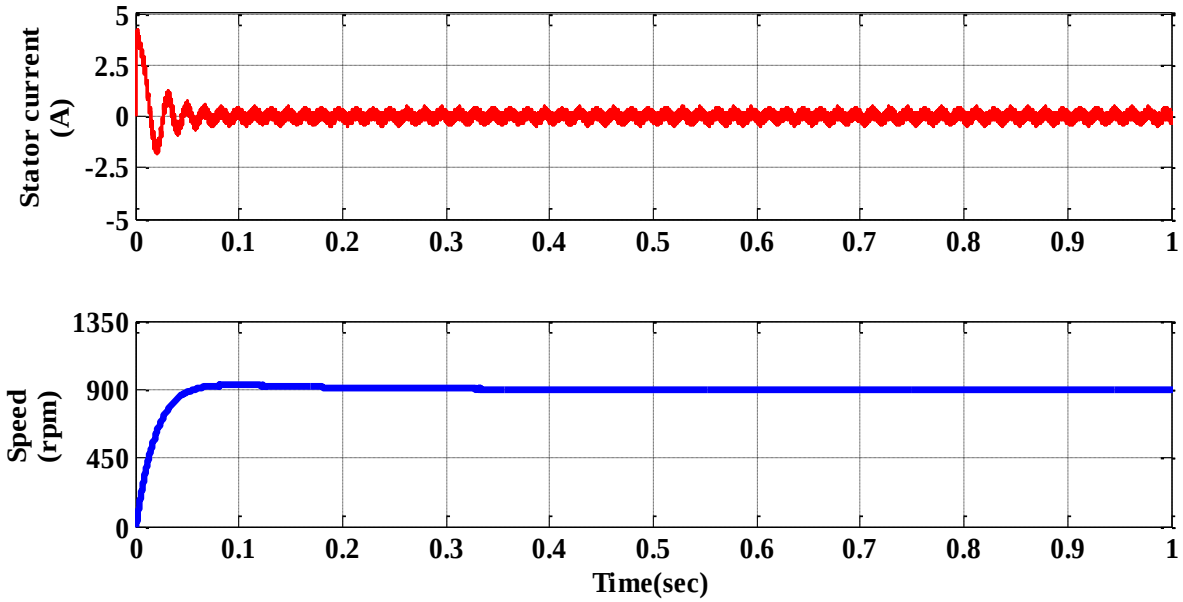

Figure 6.34 Simulation result of starting response of the PMSM drive with three-level inverter

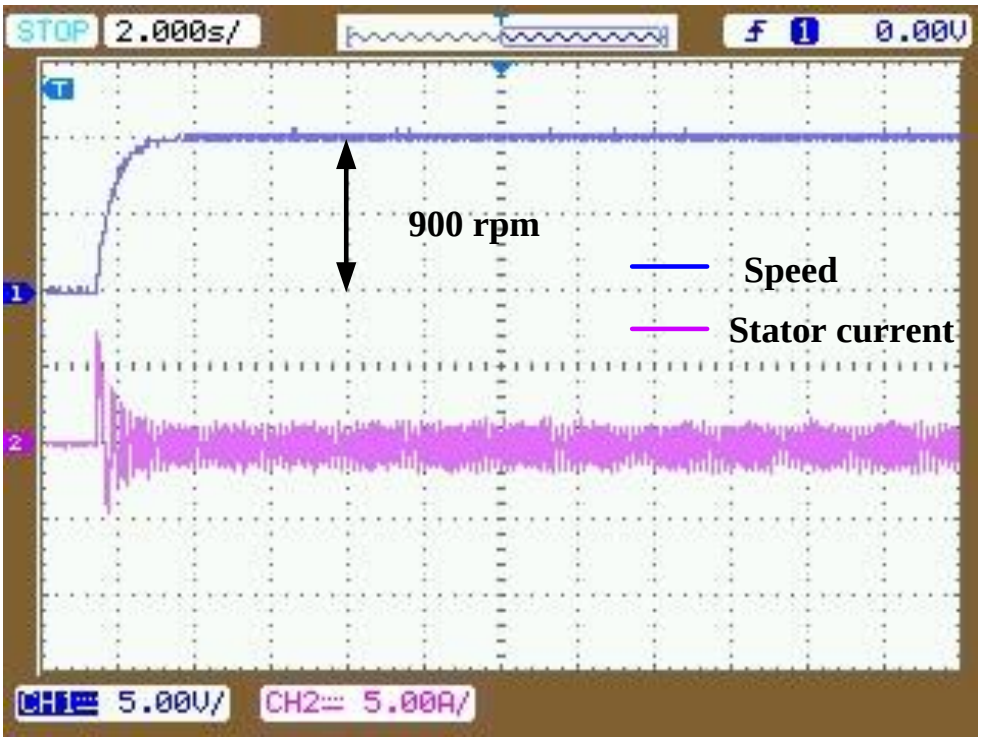

Figure 6.35 Experimental result of starting response (speed 450 rpm/div & stator current 5A/div) of the PMSM drive with three-level inverter

6.6.3 Speed Changing Operation in Proposed Drive

The performance of the proposed drive at speed changing operation also has been experimentally investigated. The speed reference increased from 900rpm to 1200 rpm. A change in speed reference of 300 rpm has been applied. The simulation results are presented in Figure 6.36. The experimental results of the drive at speed increasing operation have been shown in Figure 6.37. The speed of the motor is presented in channel 1 with 600 rpm/div scale. The speed reference has been increased from 900 rpm to 1200 rpm. At this time the torque is increased by the motor to reach the reference speed. Due to that the stator current is also slightly increased at that time which is presented in channel 2 with 5A/div scale. It reduced once the reference speed value reached. The capacitor voltage difference is presented in channel 3 with 1V/div. The experimental results clearly show that the potential difference between the two dc-link capacitors maintained below 1V. The simulation results are presented in Figure 6.38. The experimental result at speed decreasing operation is shown in Figure 6.39. The speed reference has been decreased from 1200 rpm to 900 rpm. The speed of the motor is presented in channel 1 with 600 rpm/div scale whereas channel 2 and 3 presents the stator current and the capacitor voltage difference. It is observed that the proposed drive is maintained the capacitor voltage under speed changing operation.

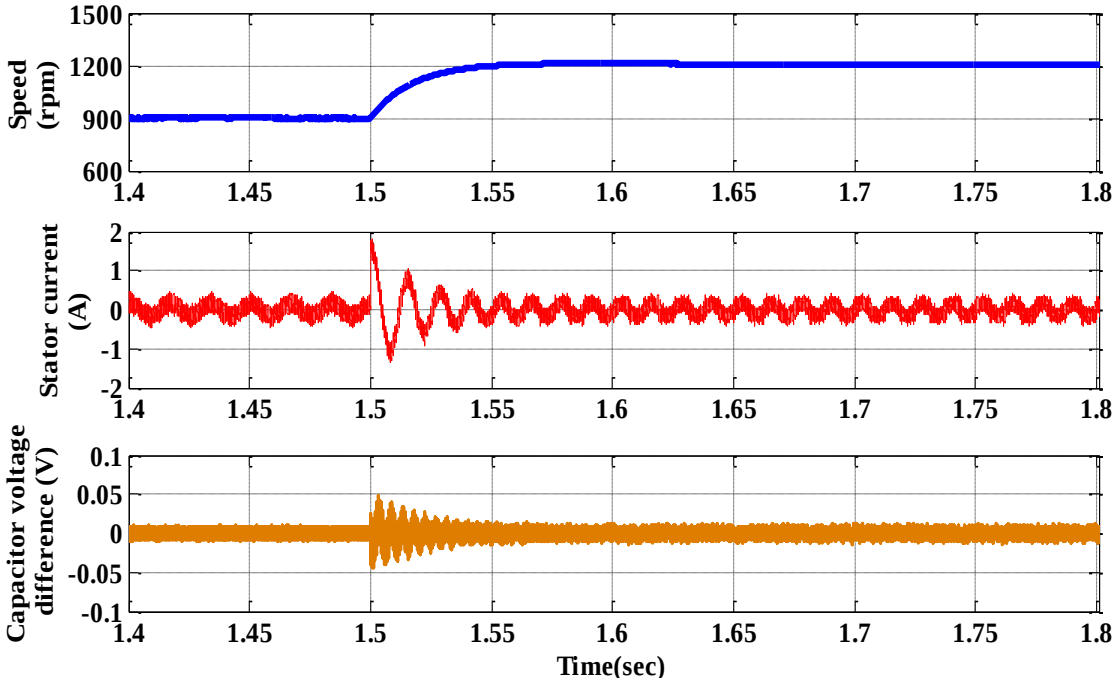

Figure 6.36 Simulation result of the PMSM drive at speed changing (increasing) with three- level inverter

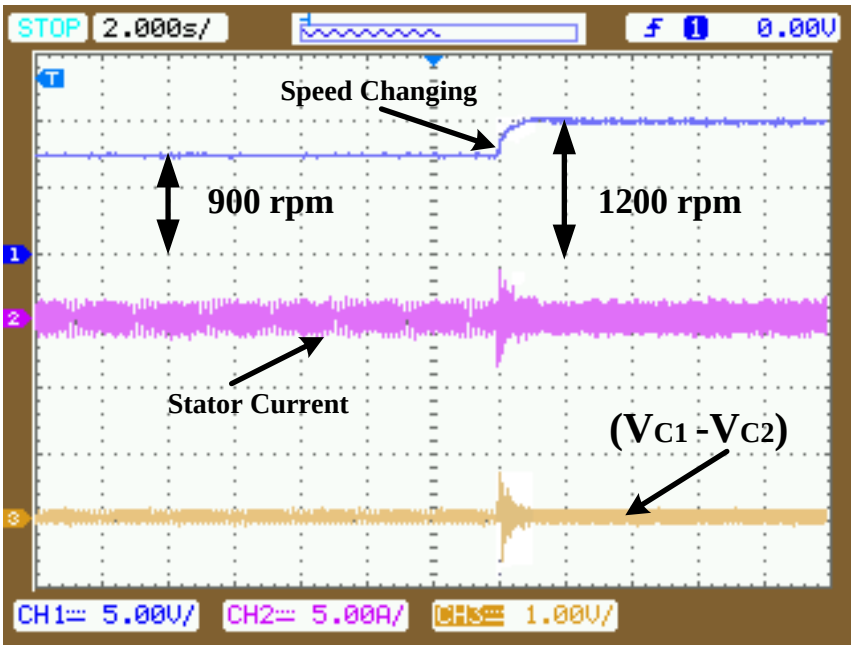

Figure 6.37 Experimental result of the PMSM drive at speed changing (increasing) with three - level inverter (speed 600rpm/div, Stator current 5A/div, Capacitor voltage difference 1V/div)

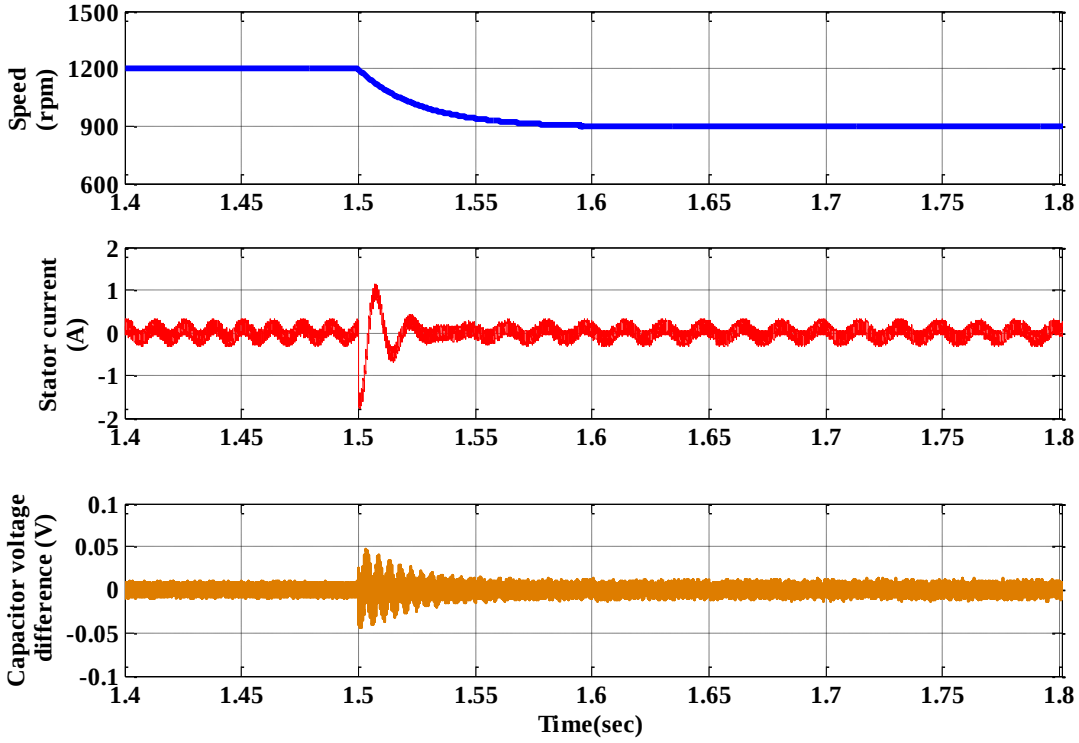

Figure 6.38 Simulation result of the PMSM drive at speed changing (decreasing) with three-level inverter

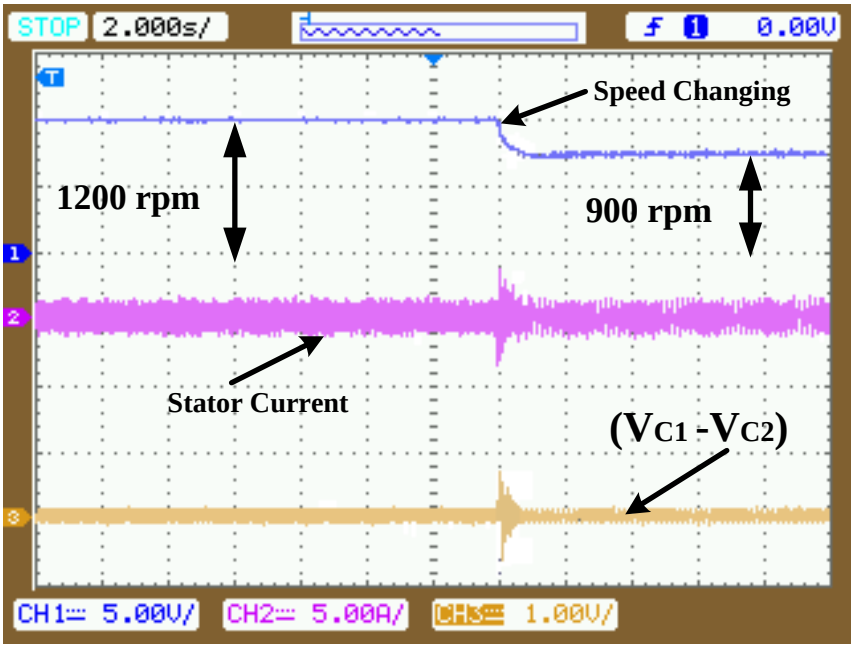

Figure 6.39 Experimental result of the PMSM drive at speed changing (decreasing) with three - level inverter (speed 600rpm/div, stator current 5A/div, capacitor voltage difference 1V/div)

6.6.4 Performance of the Proposed Drive in Load Changing Operation

The neutral point clamed inverter suffers from capacitor voltage balancing problem. It is noticed in the chapter 5 that when the drive is operated without voltage balancing circuit, the capacitor voltages across the two capacitors are unequal. This difference increases at loading operation of the motor. But this problem is eliminated using TLBC circuit. The simulation results of the proposed drive at loading operation are shown in Figure 6.40. The experimental results of the proposed drive at the time of loading are shown in the Figure 6.41. To investigate the performance under loading condition a load of 4Nm is applied to the motor. It is observed that the stator current is increased at the time of loading which is presented in channel 2 with 5A/div. It is also observed that there is dip in the speed response. This dip is due to the loading. This speed response presented in channel 1 with 300 rpm/div reaches the reference due to the closed loop operation of the drive. It is also observed that the proposed drive maintain the capacitor voltage difference within the desired value. The experimental results of voltage difference between the two capacitors are presented in channel 3 with 1V/div.

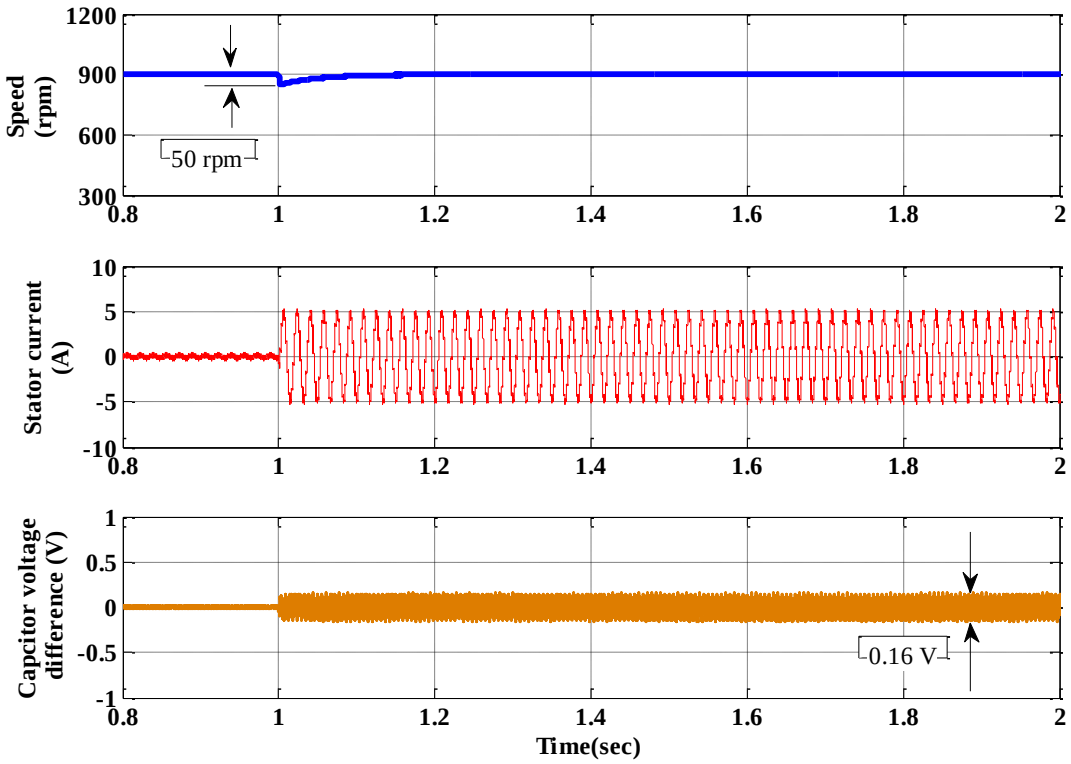

Figure 6.40 Simulation result of the PMSM drive at load changing with three -level inverter

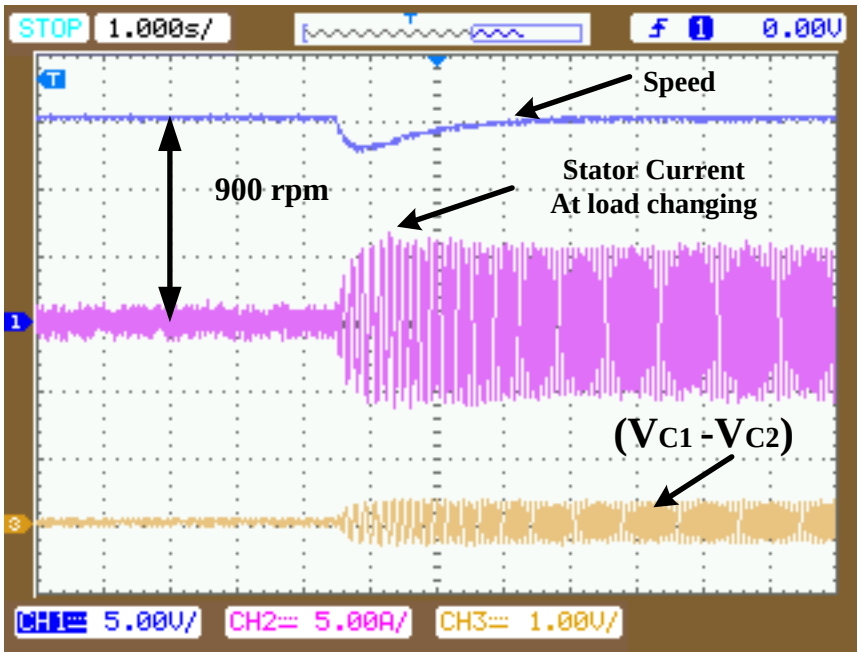

Figure 6.41 Experimental result of the PMSM drive at load changing with three- level inverter (speed 300rpm/div, stator current 5A/div, capacitor voltage difference 1V/div)

6.7 Performance Comparison of Two-level and Three-level NPC Inverter Fed PMSM Drive

The experimentation is carried out for the comparative performance investigation between the two-level inverter and three-level NPC inverter fed PMSM drive at different operating condition. NPC three-level inverter fed PMSM drive draw the key attention to the researchers and technologist due to reduction in total harmonic distortion (THD). The fundamental frequency is kept 100Hz for the analysis. The voltage and current THD for both the inverter in simulation as well as experimental is presented in Table 6.3.

Table 6.3 Comparative analysis of two-level inverter and three-level NPC inverter simulation and experimental study

Different indices	Inverter			
	Two-level inverter		Three-level NPC inverter	
	Simulation	Experimental	Simulation	Experimental
Current THD	4.54%	4.91%	3.41%	3.85%
Voltage THD	74.35.%	76.21%	37.79%	39.62%

Three-level NPC inverter fed PMSM drive promising the better performance in terms of harmonic reduction, high DC link voltage level and lower torque repulsion.

6.8 Performance Investigations on MRAS Based Sensorless Control

The MRAS based sensorless algorithm for PMSM has been implemented. To verify the viability and effectiveness of proposed MRAS for the speed estimation of PMSM, experimental investigations are carried out. Voltage and current sensors are used for sensing of stator terminal voltages and currents. The total no of pole pair in PMSM is 4, hence electrical angle $\theta = 4\theta_m$ where θ_m is the mechanical angle. Experimental studies are carried out in different operating conditions to investigate the performance of drive with proposed sensorless algorithm. The simulation results at speed changing condition are shown in Figure 6.42. Figure 6.43 shows the estimated position and stator current at step change in speed from 900 rpm to 1200 rpm. It is observed that with MRAS based sensorless control the desired performance is achieved.

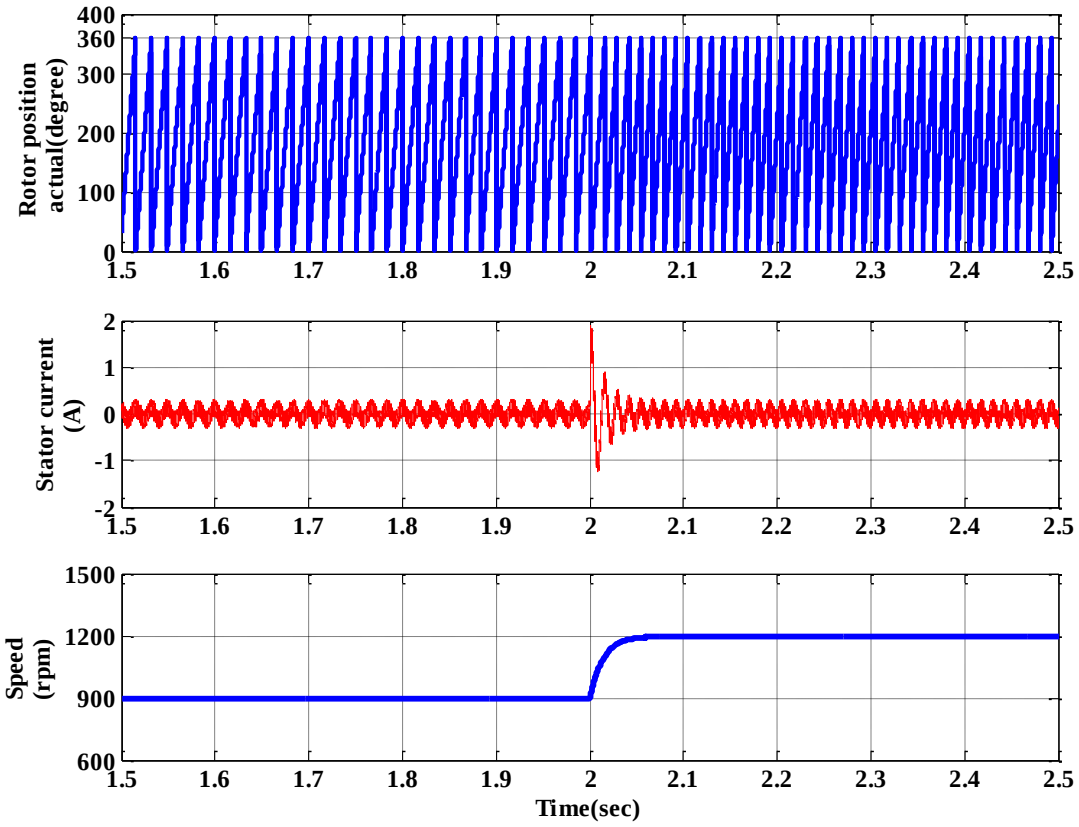

Figure 6.42 Simulation result of the estimated position of PMSM drive at speed changing (increasing from 900 rpm to 1200 rpm)

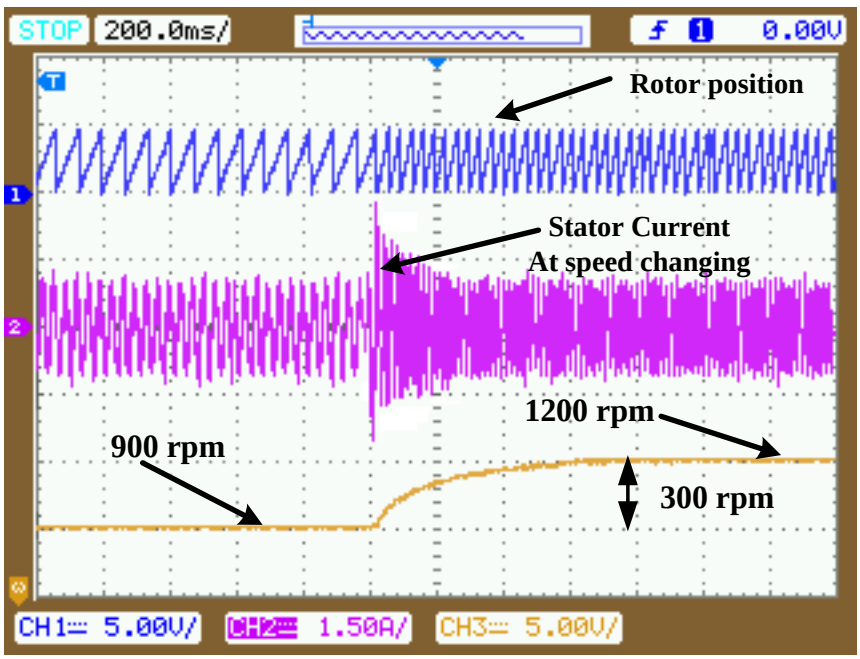

Figure 6.43 Experimental result of the estimated position (360°/div), stator current (5A/div) of PMSM drive at speed (300rpm/div) changing (increasing)

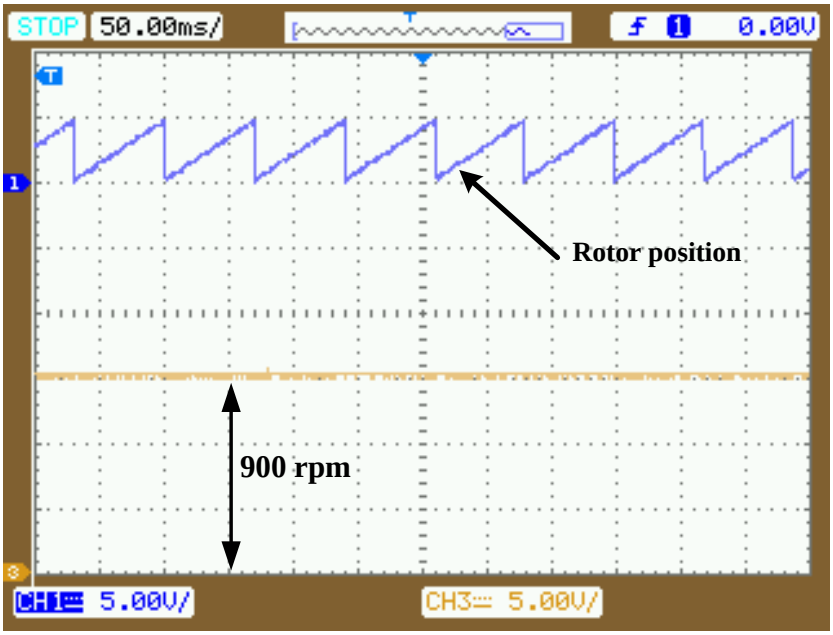

Figure 6.44 Magnified view of the estimated position (360º/div) of PMSM drive at constant speed 900 rpm (300rpm/div)

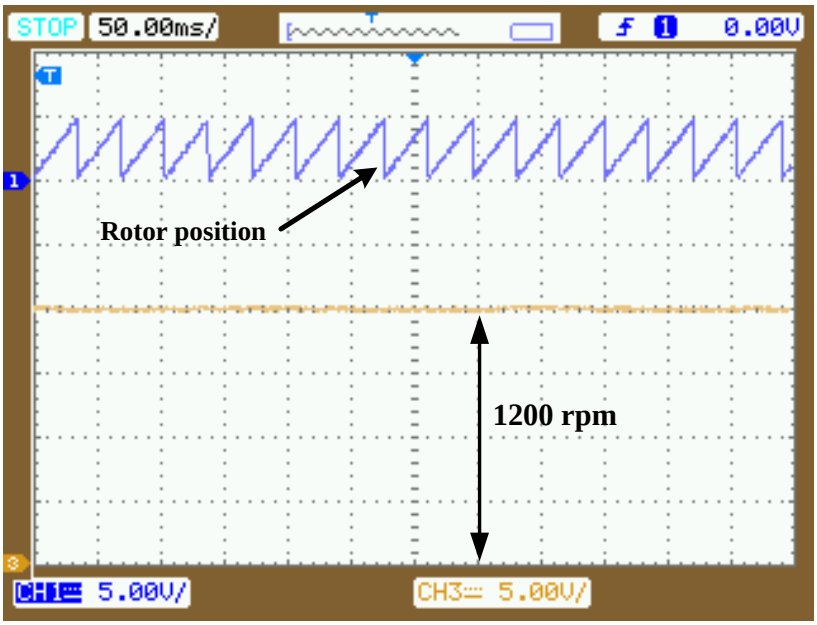

Figure 6.45 Magnified view of the estimated position (360º/div) of PMSM drive at constant speed 1200 rpm (300rpm/div)

The experimental result at constant 900 rpm speed operation is shown in Figure 6.44. The trace 1 shows the rotor position and trace 3 shows the speed of the motor. The Figure 6.45 shows the constant speed operation at 1200 rpm.

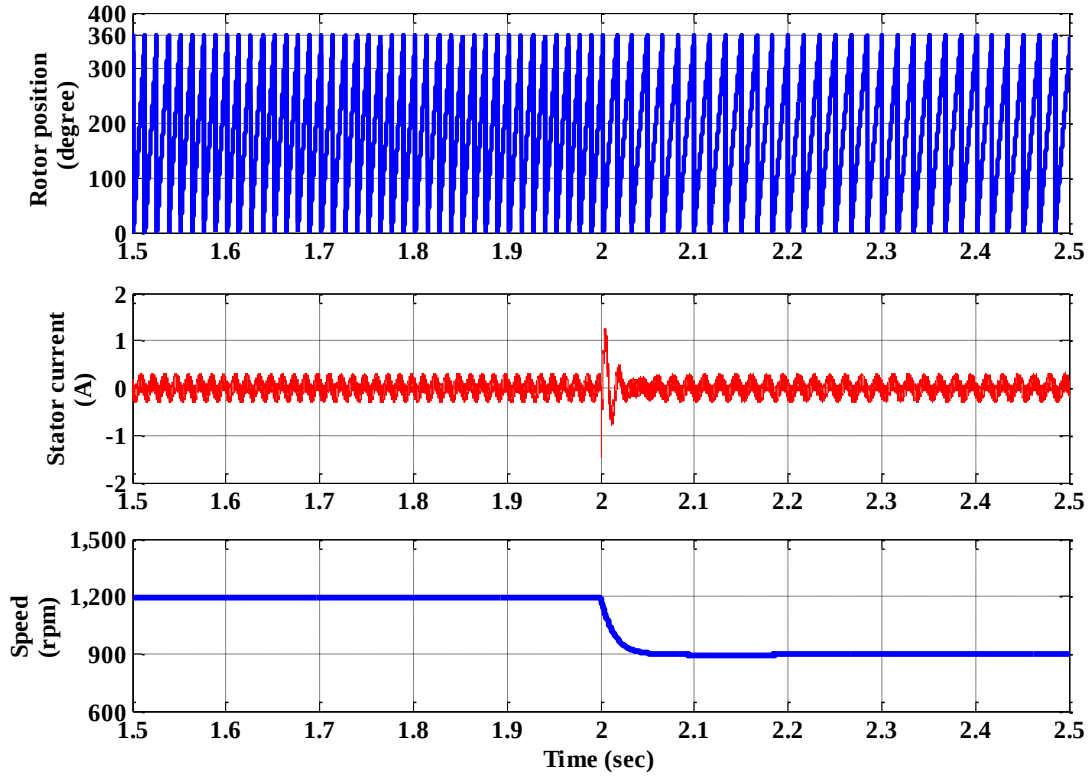

Figure 6.46 Simulation result of the estimated position of PMSM drive at Speed changing (decreasing from 1200rpm to 900 rpm)

The Experimental studies are carried out in speed decreasing operation with the drive system and the results are obtained. The Figure 6.47 shows the estimated position and stator current at step change in speed from 1200 rpm to 900 rpm. The corresponding simulation results are shown in Figure 6.46.

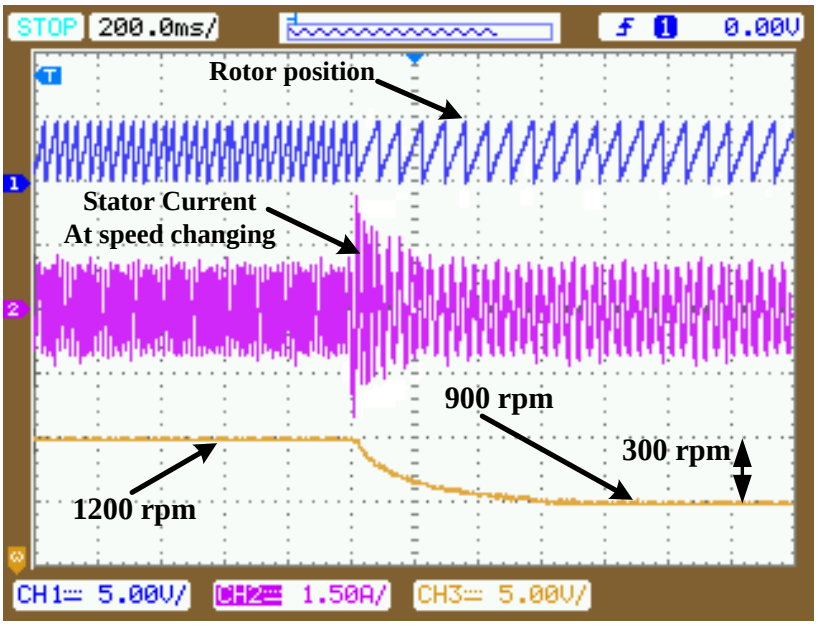

Figure 6.47 Experimental result of the estimated position (3600/div) stator current (5A/div)of PMSM drive at Speed (300rpm/div) changing (decreasing)

6.9 Conclusion

In this chapter, the detailed description of the design and development of laboratory prototype of two-level inverter fed PMSM drive and three-level NPC inverter fed PMSM drive system have been given. A DSP DS1104 of dSPACE has been used for the real-time implementation of control algorithms of two different inverters topology in MATLAB/Simulink environment. The different hardware components as required for the proper operation of experimental set-ups such as pulse amplification, isolation and dead-band circuits, voltage, current and speed sensor circuits have been designed, developed and interfaced using dSPACE. Extensive experimentation has been carried out to investigate the performance of the drive. In the first part of the experimental work the software based RDC less position estimation is implemented using the resolver based position estimation algorithm to estimate the accurate speed and position. The experimental result shows the complete 360^0 rotation of the drive. The accurate position and speed estimation is achieved. In the second part of the experimental work, a two-level inverter fed PMSM drive system is tested in different operating condition. The vector control in terms of zero d-axis current control is implemented. The experimental results validate the simulation results. To improve the performance of the drive further experimentation is carried out in three-level NPC inverter fed PMSM drive. To maintain the voltage across the two dc-link capacitors in three-level NPC inverter a TLBC circuit have been used. The exhaustive experimentation is carried out on the proposed drive in different operating condition. The experimental result shows the validity and effectiveness of the proposed drive in accordance with the simulation results. A comparative analysis is made between two-level inverter and three-level NPC inverter fed PMSM drive and from this it is observed that the voltage THD and current THD is less in three-level inverter fed drive as compared to two-level inverter fed drive. Further, the experimentation is also carried out in sensorless control mode with three-level NPC inverter fed drive. The MRAS based estimation is implemented and the results show the validity of the drive with different operating condition.

CHAPTER 7: CONCLUSIONS AND FUTURE SCOPE

[The main conclusions of the presented work and possible future research have been summarized in this chapter.]

7.1 Conclusions

This thesis presents the research carried out to improve the performance of permanent magnet synchronous motor drive with simplified modeling, control and implementation. The major conclusions derived from this research work are summarized as follows:

- In the first step of the research work a simplified approach of PMSM modelling in stationary and rotating reference frame is presented. The mathematical model is presented for both type of PMSM structure, with saliency (IPMSM) and without saliency (SPMSM). The analytical model of the two-level voltage source inverter is developed. Mathematical models are based on the determination of state equations for dynamic variables. These models are conspicuous by their extreme simplicity in front of other previous analytical models presented in the literature. To obtain a closed loop operation of PMSM drive mathematical model of resolver sensor, speed controller and load is developed.
- The basic idea of the vector control algorithm is to decompose a stator current into a magnetic field-producing component and a torque-producing component. The vector control scheme is developed for PMSM drive in MATLAB/Simulink environment. In usual practice Resolver to Digital Converter (RDC) are used for position and speed estimation from resolver. However, a software based position estimation using the output signal of the resolver has been implemented to eliminate the RDC, which reduce the cost of the drive. In addition, a demodulation based algorithm is implemented to calculate the speed and rotor position. Vector control in terms zero d-axis current control and maximum torque per ampere control is implemented in IPMSM. Comparative analyses have also been presented for both the control techniques. Further for wide speed range of operation a MTPA based flux-weakening control algorithm is developed for IPMSM. SPMSM drive with zero d-axis current control and its performance is investigated. Simulation study is carried out in MATLAB/ Simulink environment. The effects of load variation and speed change on the performance of drive are extensively studied.

- Multi-level inverter fed drive is considered, to achieve the high performance of PMSM drive systems at increased power levels. Cost effective RDC less software based position estimation is implemented for proposed PMSM drive. A detailed study on neutral point clamped (NPC) three-level inverter fed PMSM drive with vector control is presented. But the disadvantage with this inverter is capacitor voltage balancing. To maintain the voltage across the capacitor, a capacitor voltage balancing technique using three-level boost converter (TLBC) is developed. These TLBC successfully maintains the voltage across the capacitor, thus avoiding the capacitor voltage unbalancing in proposed NPC inverter fed drive system. The additional advantage of this balancing circuit as compared to the other carrier based PWM technique or SVM technique is the boosting feature, which is most demanding now a day for the electric vehicle application.
- This proposed MLI fed PMSM drive reduces the voltage THD and torque pulsation. A comparative study between a two-level and a three-level inverter fed PMSM drive shows the better performance of the three-level inverter fed PMSM drive as compared to the conventional two-level VSI fed PMSM drive.
- Furthermore, the proposed drive is investigated for sensorless control operation also. Sensorless controls in terms Back-EMF based position estimation and Model Reference Adaptive System (MRAS) based estimation have been implemented. Back-EMF based estimation of rotor speed and angular position ensure the accuracy and the speed regulation at both medium and high-speed.
- Among the existing sensorless approaches adaptive control seems to be the most promising control strategies. Simple and easier MRAS based estimators provide the desired state from two different models, one is reference and another one is adjustable. Simulation study shows the effectiveness and feasibility under various operating conditions.
- The following prototypes are developed and performed to validate the simulation results: (i) two-level VSI fed PMSM drive system, (ii) three-level NPC inverter fed PMSM drive system and (iii) capacitor voltage balancing circuit with three-level boost converter. A DSP DS1104 of dSPACE is used for the real-time implementation of various control algorithms in the PMSM drive system. Extensive experimentation has been carried out to investigate the performance of the drive. An accurate speed and position is estimated using software based RDC less position estimation algorithm.
- In the second part of the experimental work, a two-level inverter fed PMSM drive system is tested in various operating condition. The vector control in terms of zero d-axis current control is implemented. Further experimentation is carried out in three-level NPC

inverter fed PMSM drive. TLBC circuit successfully maintains the voltage across the capacitors. The exhaustive experimentation is carried out on the proposed drive in various operating condition. The experimental results show the validity and effectiveness of the proposed drive in accordance with the simulation results. The performance comparison shows the better performance of the proposed PMSM drive system as compared to the conventional two level inverter fed PMSM drive system. Further, the experimentation is also carried out in MRAS based sensorless control with three-level NPC inverter fed drive. The experimental results show the validity of the drive under various operating condition.

7.2 Future Prospects

All initial objectives for the thesis work have been fulfilled successfully. This work is presumed to be an important basis for the future research work as briefly pointed below. In light of the work accomplished in this thesis, following aspects are identified for future research work.

- Proposed MLI fed PMSM drive scheme can be further explored with electric vehicle load modeling in MATLAB/Simulink environment and its practical implementation.
- Proposed drive can be further explored for higher level of operation with capacitor voltage balancing and boosting feature.
- The artificial intelligence based techniques like NN, GA, PSO can be used directly as controller or to be used for tuning of classical PI controller.
- The NN based stator resistance estimator can be used with MRAS speed estimator to achieve the high performance drive with high robustness.
- Practical implementation of multilevel inverters for high power drive application is still an active area of research. The development of high power inverters involves a higher number of levels, large number of devices, complex control, large size and higher cost. Intensive research needs to be done on developing new multilevel inverter topology with reduced number of component, low THD and high reliability.
- The proposed drive can be further explored for PV based drive system.

BIBLIOGRAPHY

[1] N. Tesla, “A new system of alternating curents motors and transfomers,” *Trans. Am. Inst. Electr. Eng.*, vol. 5, no. 10, pp. 308–327, 1888.

[2] R. Krishnan, *“Electric Motor drives Modeling Analysis and control.”* Prentice Hall, 2001.

[3] B. K. Bose, *“Modern power electronics and AC drives.”* Prentice Hall, 2002.

[4] F. W. Merrill, “Permanent-Magnet Excited Synchronous Motors,” *Trans. Am. Inst. Electr. Eng. Part III Power Appar. Syst.*, vol. 73, no. 2, pp. 1754–1760, 1954.

[5] J. F. H. Douglas, “Current Loci of Permanent-Magnet Synchronous Motors: An Extension of Blondel Theory,” *Trans. Am. Inst. Electr. Eng. Part III Power Appar. Syst.*, vol. 78, no. 3, pp. 76–78, 1959.

[6] P. Pillay and R. Krishnan, “Modeling of permanent magnet motor drives,” *IEEE Trans. Ind. Electron.*, vol. 35, no. 4, pp. 537–541, 1988.

[7] B. N. Chaudhari and B. G. Fernandes, “Synchronous motor using ferrite magnets for general purpose energy efficient drive,” *TENCON 99. Proc. IEEE Reg. 10 Conf. Cheju Isl.*, vol. 1, pp. 371–374, 1999.

[8] B. Singh, “Recent advances in permanent magnet brushless DC motors,” *Sadhana*, vol. 22, no. 6, pp. 837–853, 1997.

[9] M. A. Rahman and G. R. Slemon, “Promising applications of neodymium boron iron,” *IEEE Trans. Magn.*, vol. MAG-21, no. 5, pp. 1712–1716, 1985.

[10] E. Richter, T. J. E. Miller, T. W. Neumann, and T. L. Hudson, “The Ferrite Permanent Magnet AC Motor-A Technical and Economical Assessment,” *IEEE Trans. Ind. Appl.*, vol. IA-21, no. 4, pp. 644–650, 1985.

[11] H. Weh, H. Mosebach, and M. H, “Design concept and force generation in inverter-fed synchrnous machines with permanent magnet excitation,” *IEEE Trans. Magn.*, vol. MAG 20, no. 5, pp. 1756–1761, 1984.

[12] S. R. Gurumurthy, V. Agarwal, and A. Sharma, “Design Considerations for a PM-BLDC Machine for Flywheel Energy Storage Applications,” *2015 IEEE 6th Int. Symp. Power Electron. Distrib. Gener. Syst. (PEDG), Aachen*, pp. 1–8, 2015.

[13] Y. Liao and T. A. Lipo, “A new doubly salient permanent magnet motor for adjustable speed drives,” *Electr. Mach. Power Syst.*, vol. 22, no. 2, pp. 259–270, 1994.

[14] V. Nedić and T. A. Lipo, “Low-Cost Current-Fed PMSM Drive System With Sinusoidal Input Currents,” *IEEE Trans. Ind. Appl.*, vol. 42, no. 3, pp. 753–762, 2006.

[15] M. Aydin, S. Huang, and T. A. Lipo, “Design, Analysis, and Control of a Hybrid Field-Controlled Axial-Flux Permanent-Magnet motor,” *IEEE Trans. Ind. Electron.*, vol. 57, no. 1, pp. 78–87, 2010.

[16] S. Q. A. Shah, T. A. Lipo, and B. I. Kwon, “Modeling of Novel Permanent Magnet Pole Shape SPM Motor for Reducing Torque Pulsation,” *IEEE Trans. Magn.*, vol. 48, no. 11, pp. 4626–4629, 2012.

[17] S. De, M. Rajne, S. Poosapati, C. Patel, and K. Gopakumar, “Low inductance axial flux BLDC motor drive for more electric aircraft,” *IET Power Electron.*, vol. 5, no. 1, pp. 124–133, 2012.

[18] S. R. Gurumurthy, V. Agarwal, and A. Sharma, “A Novel Dual-Winding BLDC Generator-Buck Converter Combination for Enhancement of the Harvested Energy From a Flywheel,” *IEEE Trans. Ind. Electron.*, vol. 63, no. 12, pp. 7563–7573, 2016.

[19] S. R. Gurumurthy, V. Agarwal, and A. Sharma, “Optimal energy harvesting from a high-speed brushless DC generator-based flywheel energy storage system,” *IET Electr. Power Appl.*, vol. 7, no. 9, pp. 693–700, 2013.

[20] B. N. Chaudhari and B. G. Fernandes, “Steady State Performance of Polyphase Permanent Magnet Synchronous Motor Fed From Single Phase Supply System,” *2001 IEEE Power Eng. Soc. Winter Meet. Conf. Proc. (Cat. No.01CH37194), Columbus, OH*, vol. 3, pp. 1382–1387, 2001.

[21] P. H. Nguyen, E. Hoang, and M. Gabsi, “Performance Synthesis of Permanent-Magnet Synchronous Machines During the Driving Cycle of a Hybrid Electric Vehicle,” *IEEE Trans. Veh. Technol.*, vol. 60, no. 5, pp. 1991–1998, 2011.

[22] B. K. Bose, “A High-Performance Inverter-Fed Drive System of an Interior Permanent Magnet Synchronous Machine,” *IEEE Trans. Ind. Appl.*, vol. 24, no. 6, pp. 987–997, 1988.

[23] T. M. Jahns, G. B. Kliman, and T. W. Neumann, “Interior Permanent-Magnet Synchronous Motors for Adjustable-Speed Drives,” *IEEE Trans. Ind. Appl.*, vol. IA-22, no. 4, pp. 738–747, 1986.

[24] D. Joo, J. H. Cho, K. Woo, B. T. Kim, and D. K. Kim, “Electromagnetic Field and thermal Linked Analysis of Interior Permanent-Magnet Synchronous Motor for Agricultural Electric Vehicle,” *IEEE Trans. Magn.*, vol. 47, no. 10, pp. 4242–4245, 2011.

[25] B. N. Chaudhari, S. K. Pillai, and B. G. Fernandes, “Energy efficient line start permanent magnet synchronous motor,” *TENCON ’98. 1998 IEEE Reg. 10 Int. Conf. Glob. Connect. Energy, Comput. Commun. Control. New Delhi*, vol. 2, pp. 379–382, 1998.

[26] B. A. Welchko, T. M. Jahns, and T. A. Lipo, “Fault Interrupting Methods and Topologies for Interior PM Machine Drives,” *IEEE Power Electron. Lett.*, vol. 2, no. 4, pp. 139–143, 2004.

[27] G. Pellegrino, A. Vagati, P. Guglielmi, and B. Boazzo, “Performance Comparison Between Surface-Mounted and Interior PMMotor Drives for Electric Vehicle Application,” *IEEE Trans. Ind. Electron.*, vol. 59, no. 2, pp. 803–811, 2012.

[28] G. Pellegrino, A. Vagati, B. Boazzo, and P. Guglielmi, “Comparison of Induction and PM Synchronous Motor Drives for EV Application Including Design Examples,” *IEEE Trans. Ind. Appl.*, vol. 48, no. 6, pp. 2322–2332, 2012.

[29] M. N. Uddin and R. S. Rebeiro, “Online efficiency optimization of a fuzzy-logic-controller-based IPMSM drive,” *IEEE Trans. Ind. Appl.*, vol. 47, no. 2, pp. 1043–1050, 2011.

[30] M. N. Uddin, “An adaptive-filter-based torque-ripple minimization of a fuzzy-logic controller for speed control of IPM motor drives,” *IEEE Trans. Ind. Appl.*, vol. 47, no. 1, pp. 350–358, 2011.

[31] S. P. Nikam, V. Rallabandi, and B. G. Fernandes, “A High-Torque-Density Permanent-Magnet Free Motor for in-Wheel Electric Vehicle Application,” *IEEE Trans. Ind. Appl.*, vol. 48, no. 6, pp. 2287–2295, 2012.

[32] R. C. Panaitescu and N. Mohan, “A simple space-vector PWM algorithm for VSI-fed AC motor drives,” *APEC. Seventeenth Annu. IEEE Appl. Power Electron. Conf. Expo. (Cat. No.02CH37335), Dallas, TX*, vol. 1, pp. 72–75, 2002.

[33] R. Dhaouadi and N. Mohan, “Analysis of current-regulated voltage-source inverters for permanenet magnet synchronous motor drives in normal and extended speed ranges,” *IEEE Trans. Energy Convers.*, vol. 5, no. 1, pp. 137–144, 1990.

[34] M. H. Rashid, “Simulation of power electronics circuit. In Modern Electrical Drives,” *Springer Netherlands*, pp. 453–489, 2000.

[35] T. Himei, shigeyuki. Funabiki, Y. Agari, and M. Okada, “Analysis of Voltage Source Inverter-Fed Permanent Magnet Synchronous Motor Taking Account of Converter Performance,” *IEEE Trans. Ind. Appl.*, vol. Ia-21, no. 1, pp. 279–284, 1985.

[36] A. V. Gumaste and G. R. Slemon, “Steady-State Analysis of a Permanent Magnet Synchronous Motor Drive with Voltage-Source Inverter,” *Ind. Appl. IEEE Trans.*, vol. IA-17, no. 2, pp. 143–151, 1981.

[37] H. E. Akhter, V. K. Sharma, A. Chandra, and K. Al-haddad, “Modeling Simulation and Performance Analysis of Switched Reluctance Motor Operating with Optimum Value of Fixed Turn-On and Turn-off Switching Angle,” *Power Electron. Spec. Conf. 2003. PESC ’03. 2003 IEEE 34th Annu.*, vol. 1, pp. 397–402, 2003.

[38] M. P. Kazmierkowski, N. Mohan, and R. Dhaouadi, “Space vector based current controller for transistor PWM-inverter-fed permanent magnet synchronous motor drives,” *Model. Simul. Control A Gen. Phys. MATTER WAVES Electr. Electron. Eng.*, vol. 42, pp. 48–48, 1992.

[39] A. Cheriti, K. Al-Haddad, L. A. Dessaint, T. A. Meynard, and D. Mukhedkar, “A Rugged Soft Commutated PWM Inverter for AC Drives,” *IEEE Trans. Power Electron.*, vol. 7, no. 2, pp. 385–392, 1992.

[40] H. Kanaan, K. Al-Haddad, R. Chaffai, L. Duguay, and F. Fnaiech, “A Comparative Study of Hysteresis and PWM Control Techniques Applied to an Injection-Current-Based Three-Phase Rectifier,” *Can. Conf. Electr. Comput. Eng. 2001. Conf. Proc. (Cat. No.01TH8555), Toronto, Ont*, vol. 2, pp. 785–792, 2001.

[41] R. R. Errabelli and P. Mutschler, “Fault-Tolerant Voltage Source Inverter for Permanent Magnet Drives,” *IEEE Trans. Power Electron.*, vol. 27, no. 2, pp. 500–508, 2012.

[42] S. Kouro *et al.*, “Recent Advances and Industrial Applications of Multilevel Converters,” *IEEE Trans. Ind. Electron.*, vol. 57, no. 8, pp. 2553–2580, 2010.

[43] S. De, D. Banerjee, K. Siva kumar, K. Gopakumar, R. Ramchand, and C. Patel, “Multilevel inverters for low-power application,” *IET Power Electron.*, vol. 4, no. 4, pp. 384–392, 2011.

[44] H. Vahedi, K. Al-Haddad, P. A. Labbe, and S. Rahmani, “Cascaded Multilevel Inverter

with Multicarrier PWM Technique and Voltage Balancing Feature," *2014 IEEE 23rd Int. Symp. Ind. Electron. (ISIE), Istanbul*, pp. 2155–2160, 2014.

[45] M. Hamdi, M. Hamouda, F. Fnaiech, and K. Al-haddad, "Space vector pulse width modulation of multilevel inverters: A new method for selecting the appropriate small hexagon," *ECON 2012 - 38th Annu. Conf. IEEE Ind. Electron. Soc. Montr. QC*, pp. 774–779, 2012.

[46] V. K. Gupta and R. Mahanty, "Optimized switching scheme of cascaded H-bridge multilevel inverter using PSO," *Int. J. Electr. Power Energy Syst.*, vol. 64, pp. 699–707, 2015.

[47] R. Mahanty and A. K. Kapoor, "Quasi-passive filter for harmonic filtering," *Electr. Power Syst. Res.*, vol. 78, no. 8, pp. 1456–1465, 2008.

[48] K. Chatterjee and A. A. Ghodke, "Three-phase three-level one-cycle controlled bidirectional ac–dc neutral-point-clamped converter without having voltage sensors," *IET Power Electron.*, vol. 7, no. 8, pp. 2161–2172, 2014.

[49] G. Bhuvaneswari and Nagaraju, "Multi-Level Inverters—A Comparative Study," *IETE J. Res.*, vol. 51, no. 2, pp. 141–153, 2005.

[50] J. Rodriguez, S. Bernet, P. K. Steimer, and I. E. Lizama, "A Survey on Neutral-Point-Clamped Inverters," *IEEE Trans. Ind. Electron.*, vol. 57, no. 7, pp. 2219–2230, 2010.

[51] Y. Jiao, F. C. Lee, and S. Lu, "Space VectorModulation for Three-Level NPC ConverterWith Neutral Point Voltage Balance and Switching Loss Reduction," *IEEE Trans. Power Electron.*, vol. 29, no. 10, pp. 5579–5591, 2014.

[52] T. Brückner and D. G. Holmes, "Optimal Pulse-Width Modulation for Three-Level Inverters," *IEEE Trans. Power Electron.*, vol. 20, no. 1, pp. 82–89, 2005.

[53] R. José *et al.*, "Multilevel Converters: An Enabling Technology for High-Power Applications," *Proc. IEEE*, vol. 97, no. 11, pp. 1786–1817, 2009.

[54] K. Yamanaka, A. M. Hava, H. Kirino, Y. Tanaka, N. Koga, and T. Kume, "A Novel Neutral Point Potential Stabilization Technique Using the Information of Output Current Polarities and Voltage Vector," *IEEE Trans. Ind. Appl.*, vol. 38, no. 6, pp. 1572–1580, 2002.

[55] N. Celanovic and D. Boroyevich, "A Fast Space-Vector Modulation Algorithm for Multilevel Three-Phase Converters," *IEEE Trans. Ind. Appl.*, vol. 37, no. 2, pp. 637–641, 2001.

[56] R. Teichmann and S. Bernet, “A Comparison of Three-Level Converters Versus Two-Level Converters for Low-Voltage Drives, Traction, and Utility Applications,” *IEEE Trans. Ind. Appl.*, vol. 41, no. 3, pp. 855–865, 2005.

[57] J. Rodríguez, J. Lai, and F. Z. Peng, “Multilevel Inverters: A Survey of Topologies, Controls, and Applications,” *IEEE Trans. Ind. Electron.*, vol. 49, no. 4, pp. 724–738, 2002.

[58] H. Abu-Rub, J. Holtz, J. Rodriguez, and Ge Baoming, “Medium-Voltage Multilevel Converters-State of the Art, Challenges, and Requirements in Industrial Applications,” *IEEE Trans. Ind. Electron.*, vol. 57, no. 8, pp. 2581–2596, 2010.

[59] S. Kincic, A. Chandra, and S. Babic, “Five level diode clamped voltage source inverter and its application in reactive power compensation,” *Power Eng. 2002 Large Eng. Syst. Conf. on, LESCOPE 02*, pp. 86–92, 2002.

[60] J. Rodríguez, S. Bernet, B. Wu, J. O. Pontt, and S. Kouro, “Multilevel Voltage-Source-Converter Topologies for Industrial Medium-Voltage Drives,” *IEEE Trans. Ind. Electron.*, vol. 54, no. 6, pp. 2930–2945, 2007.

[61] L. G. Franquelo *et al.*, “Three-Dimensional Space-VectorModulation Algorithm for Four-Leg Multilevel Converters Using abc Coordinates,” *IEEE Trans. Ind. Electron.*, vol. 53, no. 2, pp. 458–466, 2006.

[62] B. Wu, *High Power Converters and AC Drives*. IEEE press/Wiley A John Wiley & Sons,: Inc., Hoboken, New Jersey, 2006.

[63] A. Nabae, I. Takahashi, and H. Akagi, “A New Neutral-Point-Clamped PWM Inverter,” *IEEE Trans. Ind. Appl.*, vol. IA-17, no. 5, pp. 518–523, 1981.

[64] A. Choudhury, P. Pillay, and S. S. Williamson, “Comparative Analysis Between Two-Level and Three-Level DC / AC Electric Vehicle Traction Inverters Using a Novel DC-Link,” *IEEE J. Emerg. Sel. Top. POWER Electron.*, vol. 2, no. 3, pp. 529–540, 2014.

[65] A. Choudhury, P. Pillay, and S. S. Williamson, “DC-Link Voltage Balancing for a Three-Level Electric Vehicle Traction Inverter Using an Innovative Switching Sequence Control Scheme,” *IEEE J. Emerg. Sel. Top. Power Electron.*, vol. 2, no. 2, pp. 296–307, 2014.

[66] V. Yaramasu and B. Wu, “Predictive Control of a Three-Level Boost Converter,” *IEEE Trans. Power Electron.*, vol. 29, no. 10, pp. 5308–5322, 2014.

[67] V. Yaramasu and B. Wu, “Predictive Control of Three-Level Boost Converter and NPC

Inverter for High Power PMSG-Based Medium Voltage Wind Energy Conversion Systems," *IEEE Trans. Power Electron.*, vol. PP, no. 99, pp. 1–1, 2014.

[68] M. Marchesoni, M. Mazzucchelli, and S. Tencon, "A Nonconventional Power Converter for Plasma Stabilization," *IEEE Trans. POWER Electron.*, vol. 5, no. 2, pp. 212–219, 1990.

[69] P. W. Hammond, "A New Approach to Enhance Power Quality for Medium Voltage AC Drives," *IEEE Trans. Ind. Appl.*, vol. 33, no. 1, pp. 202–208, 1997.

[70] F. Z. Peng, J. Lai, J. W. Mckeever, and J. Vancoevering, "A Multilevel Voltage-Source Inverter with Separate DC Sources for Static Var Generation," *IEEE Trans. Ind. Appl.*, vol. 32, no. 5, pp. 1130–1138, 1996.

[71] A. Lesnicar and R. Marquardt, "An Innovative Modular Multilevel Converter Topology Suitable for a Wide Power Range," *IEEE Bol. PowerTech Conf. June 23-26, Bol. Italy*, pp. 1–6, 2003.

[72] M. H. Rashid, *"Power electronics handbook."* Academic Press, 2001.

[73] D. Grahame, Holmes and T. A. Lipo, *Pulse Width Modulation for Power Converters:Principles and Practice*. , Piscataway, NJ, Wiley-IEEE Press, 2003.

[74] A. Cataliotti, F. Genduso, A. Raciti, and G. R. Galluzzo, "Generalized PWM–VSI Control Algorithm Based on a Universal Duty-Cycle Expression: Theoretical Analysis, Simulation Results, and Experimental Validations," *IEEE Trans. Ind. Electron.*, vol. 54, no. 3, pp. 1569–1580, 2007.

[75] J. Holtz, "Pulsewidth Modulation—A Survey," *IEEE Trans. Ind. Electron.*, vol. 39, no. 5, pp. 410–420, 1992.

[76] Z. Pan and F. Z. Peng, "A Sinusoidal PWMMethodWith Voltage Balancing Capability for Diode-Clamped Five-Level Converters," *IEEE Trans. Ind. Appl.*, vol. 45, no. 3, pp. 1028–1034, 2009.

[77] J. R. Rodríguez, J. W. Dixon, J. R. Espinoza, J. Pontt, and P. Lezana, "PWM regenerative rectifiers: State of the art," *IEEE Trans. Ind. Electron.*, vol. 52, no. 1, pp. 5–22, 2005.

[78] J. Rodriguez, S. Member, S. Bernet, P. K. Steimer, and I. E. Lizama, "A Survey on Neutral-Point-Clamped Inverters," vol. 57, no. 7, pp. 2219–2230, 2010.

[79] H. Vahedi, K. Al-Haddad, and H. Y. Kanaan, "A New Voltage Balancing Controller

Applied on 7-Level PUC Inverter," *IECON 2014 - 40th Annu. Conf. IEEE Ind. Electron. Soc. Dallas, TX*, pp. 5082–5087, 2014.

[80] B. P. Mcgrath and D. G. Holmes, "Multicarrier PWM Strategies for Multilevel Inverters," *IEEE Trans. Ind. Electron.*, vol. 49, no. 4, pp. 858–867, 2002.

[81] L. Li, D. Czarkowski, Y. Liu, and P. Pillay, "Multilevel Selective Harmonic Elimination PWM Technique in Series-Connected Voltage Inverters," *IEEE Trans. Ind. Appl.*, vol. 36, no. 1, pp. 160–170, 2000.

[82] L. G. Franquelo, J. Nápoles, R. C. P. Guisado, J. I. León, and M. A. Aguirre, "A Flexible Selective HarmonicMitigation Technique to Meet Grid Codes in Three-Level PWMConverters," *IEEE Trans. Ind. Electron.*, vol. 54, no. 6, pp. 3022–3029, 2007.

[83] Y. Ounejjar and K. Al-Haddad, "New line currents and neutral point balancing technique of three-level three-phase NPC converter," *2006 IEEE Int. Symp. Ind. Electron. Montr. Que.*, pp. 1436–1441, 2006.

[84] N. Celanovic and D. Boroyevich, "A Comprehensive Study of Neutral-Point Voltage Balancing Problem in Three-Level Neutral-Point-Clamped Voltage Source PWM Inverters," *IEEE Trans. POWER Electron.*, vol. 15, no. 2, pp. 242–249, 2000.

[85] R. Abdullah, N. A. Rahim, S. R. Sheikh Raihan, and A. Z. Ahmad, "Five-Level Diode-Clamped InverterWith Three-Level Boost Converter," *IEEE Trans. Ind. Electron.*, vol. 61, no. 10, pp. 5155–5163, 2014.

[86] K. Corzine, G. Mondal, K. Siva kumar, K. Gopakumar, and Sukumar de, "Neutral-point balancing of neutral-point- clamped three-level inverter with a front end switched rectifier DC source for the full modulation range," *IET Power Electron.*, vol. 2, no. 5, pp. 527–534, 2009.

[87] T. Naik, R. G. Wandhare, and V. Agarwal, "Three-Level NPC Inverter with Novel Voltage Equalization for PV Grid Interface Suitable for Partially Shaded Conditions," *2013 IEEE Power Energy Conf. Illinois (PECI), Champaign, IL*, pp. 186–193, 2013.

[88] J. Shen, S. Schr¨ oder, R. R¨ osner, and S. E.-B. El-Barbari, "A Comprehensive Study of Neutral-Point Self-Balancing Effect in Neutral-Point-Clamped Three-Level Inverters," *IEEE Trans. POWER Electron.*, vol. 26, no. 11, pp. 3084–3095, 2011.

[89] A. Bendre, G. Venkataramanan, D. Rosene, and V. Srinivasan, "Modeling and Design of a Neutral-Point Voltage Regulator for a Three-Level Diode-Clamped Inverter UsingMultiple-Carrier Modulation," *IEEE Trans. Ind. Electron.*, vol. 53, no. 3, pp.

718–726, 2006.

[90] A. K. Gupta and A. M. Khambadkone, “A Simple Space Vector PWMScheme to Operate a Three-Level NPC Inverter at High Modulation Index Including Overmodulation Region, With Neutral Point Balancing,” *IEEE Trans. Ind. Appl.*, vol. 43, no. 3, pp. 751–760, 2007.

[91] W. Jiang, S. Du, L. Chang, Y. Zhang, and Q. Zhao, “Hybrid PWM Strategy of SVPWM and VSVPWM for NPC Three-Level Voltage-Source Inverter,” *IEEE Trans. POWER Electron.*, vol. 25, no. 10, pp. 2607–2619, 2010.

[92] J. Pou, J. Zaragoza, S. Ceballos, M. Saeedifard, and D. Boroyevich, “A carrier-based PWM strategy with zero-sequence voltage injection for a three-level neutral-point-clamped converter,” *IEEE Trans. Power Electron.*, vol. 27, no. 2, pp. 642–651, 2012.

[93] R. M. Tallam, R. Naik, and T. A. Nondahl, “A Carrier-Based PWM Scheme for Neutral-Point Voltage Balancing in Three-Level Inverters,” *IEEE Trans. Ind. Appl.*, vol. 41, no. 6, pp. 1734–1743, 2005.

[94] J. Zaragoza, J. Pou, S. Ceballos, E. Robles, C. Jaen, and M. Corbalán, “Voltage-Balance Compensator for a Carrier-Based Modulation in the Neutral-Point-Clamped Converter,” *IEEE Trans. Ind. Electron.*, vol. 56, no. 2, pp. 305–314, 2009.

[95] J. Zaragoza, J. Pou, S. Ceballos, E. Robles, P. Ibáñez, and J. L. Villate, “A Comprehensive Study of a Hybrid Modulation Technique for the Neutral-Point-Clamped Converter,” *IEEE Trans. Ind. Electron.*, vol. 56, no. 2, pp. 294–304, 2009.

[96] H. Zhang, S. J. Finney, A. Massoud, and B. W. Williams, “An SVM Algorithm to Balance the Capacitor Voltages of the Three-Level NPC Active Power Filter,” *IEEE Trans. POWER Electron.*, vol. 23, no. 6, pp. 2694–2702, 2008.

[97] J. Kim, S. Sul, and P. N. Enjeti, “A Carrier-Based PWMMethodWith Optimal Switching Sequence for aMultilevel Four-Leg Voltage-Source Inverter,” *IEEE Trans. Ind. Appl.*, vol. 44, no. 4, pp. 1239–1248, 2008.

[98] A. Lewicki, Z. Krzeminski, and H. Abu-Rub, “Space-vector pulsewidth modulation for three-level NPC converter with the neutral point voltage control,” *IEEE Trans. Ind. Electron.*, vol. 58, no. 11, pp. 5076–5086, 2011.

[99] A. Choudhury, P. Pillay, and S. S. Williamson, “Modified DC-Bus Voltage-Balancing Algorithm Based Three-Level Neutral-Point-Clamped IPMSM Drive for Electric Vehicle Applications,” *EEE Trans. Ind. Electron.*, vol. 63, no. 2, pp. 761–772, 2016.

[100] J. Pou, R. Pindado, D. Boroyevich, and P. Rodríguez, “Limits of the Neutral-Point Balance in Back-to-Back-Connected Three-Level Converters,” *IEEE Trans. Power Electron.*, vol. 19, no. 3, pp. 722–731, 2004.

[101] H. Chen and J. Liao, “Design and Implementation of Sensorless Capacitor Voltage Balancing Control for Three-Level Boosting PFC,” *IEEE Trans. POWER Electron.*, vol. 29, no. 7, pp. 3808–3817, 2014.

[102] R. Krishna, D. E. Soman, S. K. Kottayil, and M. Leijon, “Pulse delay control for capacitor voltage balancing in a three-level boost neutral point clamped inverter,” *IET Power Electron.*, vol. 8, no. 2, pp. 268–277, 2015.

[103] J. Kwon, B.-H. Kwon, and K.-H. Nam, “Three-Phase Photovoltaic SystemWith Three-Level Boosting MPPT Control,” *IEEE Trans. POWER Electron.*, vol. 23, no. 5, pp. 2319–2327, 2008.

[104] M. Sahoo and S. Keerthipati, “A Three-Level LC-Switching-Based Voltage Boost NPC Inverter,” *IEEE Trans. Ind. Electron.*, vol. 64, no. 4, pp. 2876–2883, 2017.

[105] R. Mahanty, “A novel large value ac capacitor using two dc capacitors,” *Int. J. Circuit Theory Appl.*, vol. 36, no. 8, pp. 967–973, 2008.

[106] P. Alemi, Y. Jeung, and D.-C. Lee, “DC-Link Capacitance Minimization in T-Type Three-Level AC/DC/AC PWM Converters,” *IEEE Trans. Ind. Electron.*, vol. 62, no. 3, pp. 1382–1391, 2015.

[107] B. Singh, A. Chandra, and K. Al-haddad, “Performance Analysis of a Low Cost Vector Controlled Induction Motor Drive: A Philosophy for Sensor Reduction B.N.Singh’,” *1997 IEEE Int. Electr. Mach. Drives Conf. Rec. Milwaukee, WI*, p. TB3/1.1-TB3/1.3, 1997.

[108] B. Singh and S. Singh, “Single-phase power factor controller topologies for permanent magnet brushless DC motor drives,” *IET Power Electron.*, vol. 3, no. 2, pp. 147–175, 2010.

[109] B. Singh, B. P. Singh, and S. Dwivedi, “DSP Based Implementation of Sliding Mode Speed Controller for Vector Controlled Permanent Magnet Synchronous Motor Drive,” *2006 IEEE India Int. Conf. Power Electron.*, pp. 22–27, 2006.

[110] B. Singh, G. Bhuvaneswari, and V. Garg, “Harmonic Mitigation in AC – DC Converters for Vector Controlled Induction Motor Drives,” *IEEE Trans. Energy Convers.*, vol. 22, no. 3, pp. 637–646, 2007.

[111] H. Ahuja, G. Bhuvaneswari, and R. Balasubramanian, “Performance comparison of DFIG and PMSG based WECS,” *IET Conf. Renew. Power Gener. (RPG 2011)*, pp. 1–6, 2011.

[112] M. Singh and A. Chandra, “Control of PMSG Based Variable Speed Wind- Battery Hybrid System in an Isolated Network,” *2009 IEEE Power Energy Soc. Gen. Meet. Calgary, AB*, pp. 1–6, 2009.

[113] R. Dhaouadi and N. Mohan, “DSP-based control of a permanent magnet synchronous motor with estimated speed and rotor position,” *Eur. Conf. POWER Electron. Appl.*, vol. 1, pp. 596–596, 1992.

[114] B. Singh, G. Bhuvaneswari, V. Garg, and S. Gairola, “Pulse Multiplication in AC–DC Converters for HarmonicMitigation in Vector-Controlled InductionMotor Drives,” *IEEE Trans. Energy Convers.*, vol. 21, no. 2, pp. 342–352, 2006.

[115] V. B. Honsinger, “Performance of Polyphase Permanent Magnet Machines,” *IEEE Trans. Power Appar. Syst.*, vol. PAS-99, no. 4, pp. 1510–1518, 1980.

[116] N. S. Kumar and K. Saravanan, “Speed control of PMSM drive using VSI,” *30th Annu. Conf. IEEE Ind. Electron. Soc. 2004. IECON 2004*, vol. 1, pp. 888–895, 2004.

[117] P. Pillay and R. Krishnan, “Modeling, simulation, and analysis of permanent-magnet motor drives. I. The permanent-magnet synchronous motor drive,” *IEEE Trans. Ind. Appl.*, vol. 25, no. 2, pp. 265–273, 1989.

[118] S. Bouchiker, G. A. Capolino, and M. Poloujadoff, “Vector Control of a Permanent-Magnet Synchronous Motor Using AC–AC Matrix Converter,” *IEEE Trans. Power Electron.*, vol. 13, no. 6, pp. 1089–1099, 1998.

[119] P. Enjeti, P. D. Ziogas, J. F. Lindsay, and M. H. Rashid, “‘A novel current controlled PWM inverter for variable speed AC drives.,’” *Conf. Rec. IEEE-IAS Annu. Meet.*, pp. 235–243, 1986.

[120] P. I.-H. Lin and M. Rashid, “A PC-based measurement and control system for DC motors,” *Conf. Rec. 1990 IEEE Ind. Appl. Soc. Annu. Meet. Seattle, WA, USA, 1990*, vol. 2, pp. 1829–1834, 1990.

[121] P. Enjeti, P. D. Ziogas, J. F. Lindsay, and M. H. Rashid., “A New Current Control Scheme for ac Motor Drives,” *IEEE Trans. Ind. Appl.*, vol. 28, no. 4, pp. 842–849, 1992.

[122] S. Morimoto, Y. Takeda, T. Hirasa, and K. Taniguchi, “Expansion of Operating Limits

for Permanent Magnet Motor by Current Vector Control Considering Inverter Capacity," *IEEE Trans. Ind. Appl.*, vol. 26, no. 5, pp. 866–871, 1990.

[123] N. Imai, S. Morimoto, M. Sanada, and Y. Takeda, "Influence of rotor configuration on sensorless control for permanent-magnet synchronous motors," *IEEE Trans. Ind. Appl.*, vol. 44, no. 1, pp. 93–100, 2008.

[124] S. Huang, Z. Chen, K. Huang, and J. Gao, "Maximum Torque Per Ampere and Flux-weakening Control for PMSM Based on Curve Fitting," *2010 IEEE Veh. Power Propuls. Conf. Lille*, pp. 1–5, 2010.

[125] K. Baoquan, L. Chunyan, and C. Shukang, "Flux-Weakening-Characteristic Analysis of a New Permanent-Magnet Synchronous Motor Used for Electric Vehicles," *IEEE Trans. Plasma Sci.*, vol. 39, no. 1, pp. 511–515, 2011.

[126] K.-C. Kim, "A Novel Magnetic Flux Weakening Method of Permanent Magnet Synchronous Motor for Electric Vehicles," *IEEE Trans. Magn.*, vol. 48, no. 11, pp. 4042–4045, 2012.

[127] T. J. E. Miller, M. Popescu, C. Cossar, M. McGilp, and J. A. Walker, "Calculating the interior permanent-magnet motor," *IEMDC 2003 - IEEE Int. Electr. Mach. Drives Conf.*, vol. 2, pp. 1181–1187, 2003.

[128] A. Kumar, B. G. Fernandes, and K. Chatterjee, "'Direct Torque Control of Three - Phase Induction Motor Using SVPWM Without Sector and Angle Determination,'" *EPE -PEMC 04, Riga, Latv.*, 2004.

[129] A. Choudhury and K. Chateerjee, "Modified stator flux estimation-based direct torque controlled induction motor drive with constant switching frequency operation," *Int. J. Power Electron.*, vol. 4, no. 6, pp. 566–579, 2012.

[130] M. F. Rahman, L. Zhong, and K. W. Lim, "A Direct Torque-Controlled Interior Permanent Magnet Synchronous Motor Drive Incorporating Field Weakening," *IEEE Trans. Ind. Appl.*, vol. 34, no. 6, pp. 1246–1253, 1998.

[131] M. Preindl and S. Bolognani, "Model Predictive Direct Torque ControlWith Finite Control Set for PMSM Drive Systems, Part 2: Field Weakening Operation," *IEEE Trans. Ind. INFORMATICS*, vol. 9, no. 2, pp. 648–657, 2013.

[132] M. Preindl and S. Bolognani, "Model Predictive Direct Torque ControlWith Finite Control Set for PMSM Drive Systems, Part 1: Maximum Torque Per Ampere Operation," *IEEE Trans. Ind. INFORMATICS*, vol. 9, no. 4, pp. 1912–1921, 2013.

[133] M. N. Uddin and M. A. Rahman, “High-Speed Control of IPMSM Drives Using Improved Fuzzy Logic Algorithms,” *IEEE Trans. Ind. Electron.*, vol. 54, no. 1, pp. 190–199, 2007.

[134] G. Foo and M. F. Rahman, “Sensorless Sliding-Mode MTPA Control of an IPM Synchronous Motor Drive Using a Sliding-Mode Observer and HF Signal Injection,” *IEEE Trans. Ind. Electron.*, vol. 57, no. 4, pp. 1270–1278, 2010.

[135] S. Kim, Y. Yoon, S. Sul, and K. Ide, “Maximum Torque per Ampere (MTPA) Control of an IPM Machine Based on Signal Injection Considering Inductance Saturation,” *IEEE Trans. POWER Electron.*, vol. 28, no. 1, pp. 488–497, 2013.

[136] M. A. Khan, M. N. Uddin, and M. A. Rahman, “A NovelWavelet-Neural-Network-Based Robust Controller for IPM Motor Drives,” *IEEE Trans. Ind. Appl.*, vol. 49, no. 5, pp. 2341–2351, 2013.

[137] R. Ni, D. Xu, G. Wang, L. Ding, G. Zhang, and L. Qu, “Maximum Efficiency Per Ampere Control of Permanent-Magnet Synchronous Machines,” *IEEE Trans. Ind. Electron.*, vol. 62, no. 4, pp. 2135–2143, 2015.

[138] T. Inoue, Y. Inoue, S. Morimoto, and M. Sanada, “Mathematical Model for MTPA Control of Permanent-Magnet Synchronous Motor in Stator Flux Linkage Synchronous Frame,” *IEEE Trans. Ind. Appl.*, vol. 51, no. 5, pp. 3620–3628, 2015.

[139] M. Naidu and B. K. Bose, “Rotor position estimation scheme of a permanent magnet synchronous machine for high performance variable speed drive,” *Conf. Rec. 1992 IEEE Ind. Appl. Soc. Annu. Meet. Houston, TX*, vol. 1, pp. 48–53, 1992.

[140] M. S. Zaky, M. a Morsi, and S. S. Shokrallah, “High Dynamic Performance of Interior Permanent Magnet Synchronous Motor Drives Based on Feed-forward Load Torque Compensator,” *Electr. Power Components Syst.*, vol. 41, no. November 2014, pp. 235–251, 2013.

[141] S. Wekhande and V. Agarwal, “High-Resolution Absolute Position Vernier Shaft Encoder Suitable for High-Performance PMSM Servo Drives,” *IEEE Trans. Instrum. Meas.*, vol. 55, no. 1, pp. 357–364, 2006.

[142] S. Sarma, V. K. Agrawal, and S. Udupa, “Software-Based Resolver-to-Digital Conversion Using a DSP,” *IEEE Trans. Ind. Electron.*, vol. 55, no. 1, pp. 371–379, 2008.

[143] S. Wekhande and V. Agarwal, “High resolution absolute position Vernier shaft encoder

suitable for high performance PMSM servo drives," *PESC Rec. - IEEE Annu. Power Electron. Spec. Conf.*, vol. 1, no. 2, pp. 119–124, 1998.

[144] C. Hou, Y. Chiang, and C. Lo, "DSP-based resolver-to-digital conversion system designed in time domain," *IET Power Electron.*, vol. 7, no. 9, pp. 2227–2232, 2014.

[145] D. C. Hanselman, "Techniques for improving resolver-to-digital conversion accuracy," *IEEE Trans. Ind. Appl.*, vol. 38, no. 6, pp. 501–504, 1991.

[146] C. H. Yim, I. J. Ha, and M. S. Ko, "A Resolver-to-Digital Conversion Method for Fast Tracking," *IEEE Trans. Ind. Electron.*, vol. 39, no. 5, pp. 369–378, 1992.

[147] M. Benammar, L. Ben-Brahim, and M. a. Alhamadi, "A Novel Resolver-to-360 Linearized Converter," *IEEE Sens. J.*, vol. 4, no. 1, pp. 96–101, 2004.

[148] R. Hoseinnezhad, "Position sensing in brake-by-wire callipers using resolvers," *IEEE Trans. Veh. Technol.*, vol. 55, no. 3, pp. 924–932, 2006.

[149] C. Attaianese and G. Tomasso, "Position Measurement in Industrial Drives by Means of Low-Cost Resolver-to-Digital Converter," *IEEE Trans. Instrum. Meas.*, vol. 56, no. 6, pp. 2155–2159, 2007.

[150] S. Murakami, T. Shiota, M. Ohto, K. Ide, and M. Hisatsune, "Encoderless Servo Drive With Adequately Designed IPMSM for Pulse-Voltage-Injection-Based Position Detection," *IEEE Trans. Ind. Appl.*, vol. 48, no. 6, pp. 1922–1930, 2012.

[151] F. Alonge, A. O. D. Tommaso, R. Miceli, and C. Rando, "Sensorless Control of Permanent Magnet Synchronous Motors for Wide Speed Range Applications," *Int. Symp. Power Electron. Electr. Drives, Autom. Motion, 2006. SPEEDAM 2006., Taormina*, pp. 1008–1013, 2006.

[152] M. Rashed, P. F. A. MacConnell, A. F. Stronach, and P. Acarnley, "Sensorless indirect-rotor-field-orientation speed control of a permanent-magnet synchronous motor with stator-resistance estimation," *IEEE Trans. Ind. Electron.*, vol. 54, no. 3, pp. 1664–1675, 2007.

[153] G. Bhuvaneswari, S. G. Thakurata, P. S. Rao, and S. S. Murthy, "Modeling of switch reluctance motor in sensorless and 'with sensor' Modes," *J. Power Electron.*, vol. 6, no. 4, pp. 315–321, 2006.

[154] P. Vas, *Sensorless Vector and Direct Torque Control*. Oxford university press Oxford, UK, 1998., 1998.

[155] J. Hu and B. Wu, “New Integration Algorithms for Estimating Motor Flux over a Wide Speed Range,” *IEEE Trans. Power Electron.*, vol. 13, no. 5, pp. 969–977, 1998.

[156] A. V. Stanković, E. L. Benedict, V. John, and T. A. Lipo, “A novel method for measuring induction machine magnetizing inductance,” *IEEE Trans. Ind. Appl.*, vol. 39, no. 5, pp. 1257–1263, 2003.

[157] M. Schroedl, “Sensorless Control of AC Machines at Low Speed and Standstill Based on the "INFORM’’ Method,” *IAS ’96. Conf. Rec. 1996 IEEE Ind. Appl. Conf. Thirty-First IAS Annu. Meet.*, vol. 1, pp. 270–277, 1996.

[158] S. Bolognani, L. Tubiana, and M. Zigliotto, “Extended Kalman filter tuning in sensorless PMSM drives,” *Proc. Power Convers. Conf. 2002, PCC-Osaka 2002*, vol. 1, no. 6, pp. 276–281, 2002.

[159] S. Bolognani, R. Oboe, and M. Zigliotto, “Sensorless full-digital PMSM drive with EKF estimation of speed and\nrotor position,” *IEEE Trans. Ind. Electron.*, vol. 46, no. 1, pp. 184–191, 1999.

[160] S. Bolognani, M. Zigliotto, and M. Zordan, “Extended-range PMSM sensorless speed drive based on stochastic filtering,” *IEEE Trans. Power Electron.*, vol. 16, no. 1, pp. 110–117, 2001.

[161] F. Genduso, R. Miceli, C. Rando, and G. R. Galluzzo, “Back EMF sensorless-control algorithm for high-dynamic performance PMSM,” *IEEE Trans. Ind. Electron.*, vol. 57, no. 6, pp. 2092–2100, 2010.

[162] A. Girolkar and G. Bhuvaneswari, “Control of PMBLDC Motor Using Back EMF Sensing with Adaptive Filtering,” *2013 Int. Conf. Comput. Commun. Informatics, Coimbatore*, pp. 1–5, 2013.

[163] F. Genduso, R. Miceli, C. Rando, and G. R. Galluzzo, “A Novel Correction Method for a Low Cost Sensorless Control System of IPMSM Electrical Drives,” *2008 IEEE Int. Symp. Ind. Electron. Cambridge*, pp. 509–514, 2008.

[164] S. Chi, Z. Zhang, and L. Xu, “Sliding-mode sensorless control of direct-drive PM synchronous motors for washing machine applications,” *IEEE Trans. Ind. Appl.*, vol. 45, no. 2, pp. 582–590, 2009.

[165] H. Kim, J. Son, and J. Lee, “A high-speed sliding-mode observer for the sensorless speed control of a PMSM,” *IEEE Trans. Ind. Electron.*, vol. 58, no. 9, pp. 4069–4077, 2011.

[166] Y. S. Han, J. S. Choi, and Y. S. Kim, “Sensorless PMSM drive with a sliding mode control based adaptive speed and stator resistance estimator,” *IEEE Trans. Magn.*, vol. 36, no. 5 I, pp. 3588–3591, 2000.

[167] M. Elbuluk, “A sliding mode observer for sensorless control of permanent magnet synchronous motors,” *Conf. Rec. 2001 IEEE Ind. Appl. Conf. 36th IAS Annu. Meet. (Cat. No.01CH37248)*, vol. 2, no. C, pp. 1273–1278, 2001.

[168] C. Schauder, “Adaptive Speed Identification for Vector Control of Induction Motors Without Rotational Transducers,” *IEEE Trans. Ind. Appl.*, vol. 28, no. 5, pp. 1054–1061, 1992.

[169] V. Verma, C. Chakraborty, S. Maiti, and Y. Hori, “Speed sensorless vector controlled induction motor drive using single current sensor,” *IEEE Trans. Energy Convers.*, vol. 28, no. 4, pp. 938–950, 2013.

[170] S. Maiti, C. Chakraborty, and S. Sengupta, “Simulation studies on model reference adaptive controller based speed estimation technique for the vector controlled permanent magnet synchronous motor drive,” *Simul. Model. Pract. Theory*, vol. 17, no. 4, pp. 585–596, 2009.

[171] S. Maiti and C. Chakraborty, “Reactive Power Based Speed Sensorless Controller for Permanent Magnet Synchronous Motor Drive,” *2006 IEEE Int. Conf. Ind. Technol. Mumbai*, pp. 247–252, 2006.

[172] K. Jinsong, Z. Xiangyun, W. Ying, and H. Dabing, “Study of position sensorless control of PMSM based on MRAS,” *Proc. IEEE Int. Conf. Ind. Technol.*, no. 3, pp. 3–6, 2009.

[173] S. Maiti and C. Chakraborty, “A new instantaneous reactive power based MRAS for sensorless induction motor drive,” *Simul. Model. Pract. Theory*, vol. 18, no. 9, pp. 1314–1326, 2010.

[174] Q. An and L. Sun, “On-line parameter identification for vector controlled PMSM drives using adaptive algorithm,” *Veh. Power Propuls. Conf. 2008. VPPC ’08. IEEE*, vol. 0, no. 2, pp. 1–6, 2008.

[175] R. Guclu and K. Gulez, “Neural network control of seat vibrations of a non-linear full vehicle model using PMSM,” *Math. Comput. Model.*, vol. 47, no. 11–12, pp. 1356–1371, 2008.

[176] T. D. Batzel and K. Y. Lee, “An approach to sensorless operation of the permanent-

magnet synchronous motor using diagonally recurrent neural networks," *IEEE Trans. Energy Convers.*, vol. 18, no. 1, pp. 100–106, 2003.

[177] M. Singh, A. Chandra, and B. Singh, "Sensorless Power Maximization of PMSG based Isolated Wind-Battery Hybrid System Using Adaptive Neuro-Fuzzy Controller," *2010 IEEE Ind. Appl. Soc. Annu. Meet. Houston, TX*, pp. 1–6, 2010.

[178] M. Singh and A. Chandra, "Comparative Study of Sliding Mode and ANFIS Based Observers for Speed & Position Sensor- less Control of Variable Speed PMSG," *Can. Conf. Electr. Comput. Eng. (CCECE)2010, Calgary, AB*, pp. 1–4, 2010.

[179] M. Singh and A. Chandra, "Power Maximization and Voltage Sag/Swell Ride-Through Capability of PMSG based Variable Speed Wind Energy Conversion System," *2008 34th Annu. Conf. IEEE Ind. Electron. Orlando, FL*, pp. 2206–2211, 2008.

[180] M. J. Corley and R. D. Lorenz, "Rotor position and velocity estimation for a salient-pole permanent magnet synchronous machine at standstill and high speeds," *IEEE Trans. Ind. Appl.*, vol. 34, no. 4, pp. 784–789, 1998.

[181] S. Y. Kim and I. J. Ha, "A New Observer DesignMethod for HF Signal Injection Sensorless Control of IPMSMs," *IEEE Trans. Ind. Electron.*, vol. 55, no. 6, pp. 2525–2529, 2008.

APPENDIX

Specification of simulated Interior permanent magnet motor

stator phase resistance	0.9585Ω
Torque Constant	1.092
d-axis inductance (L_d)	0.004987 H
q-axis inductance (L_q)	0.005513 H
Moment of inertia (J)	0.0006329kg-m2
No of poles	8
DC link voltage	300 V

Specification of simulated surface permanent magnet motor

d-axis inductance (Ld)	5.15mH
q-axis inductance (Lq)	5.15mH
Torque Constant	0.75 Nm/A
No of poles (p)	8
DC link voltage	300 V
Moment of inertia (J)	0.000062kg-m^2
Total load inertia	0.001914 kg-m^2
Damping friction	0.0041N-m/rad

Prototype system parameters

PMSM Parameter	Value
Make	MOOG G400 series PMSM motor
BRAKE	24 V_{DC} (release)
M_0	3.7
$V_{DC\ max}$	325 V
Power	1.4 kW
Torque Constant	0.75Nm/A
Phase Inductance	5.15 mH
No. of Poles	8
Moment of Inertia 'J'	0.000062 kg-m^2
Total Load Inertia	0.001914 kg-m^2
Damping Friction	0.0041N-m/rad
Resolver Parameters	
Input Voltage	5V
Carrier Frequency	1 kHz
Transformation Ratio	0.5

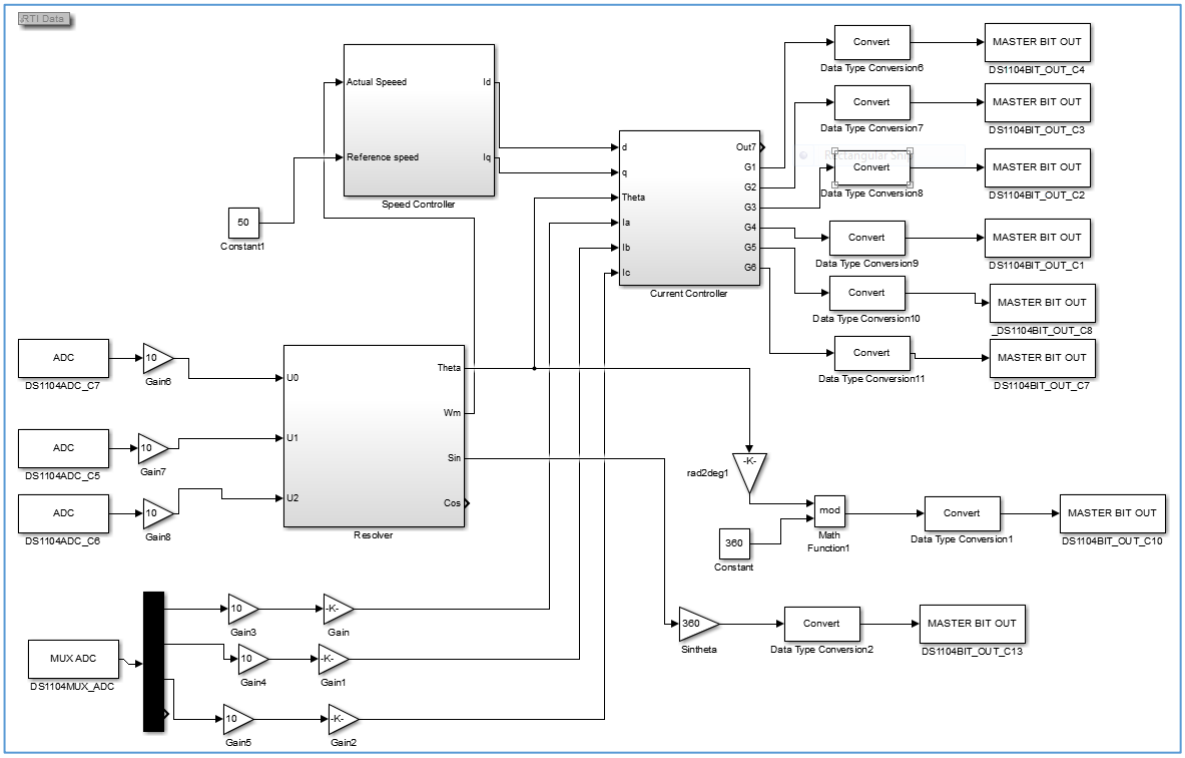

Figure A. Closed loop control of PMSM with resolver based RDC less position estimation implemented in MATLAB Simulink.

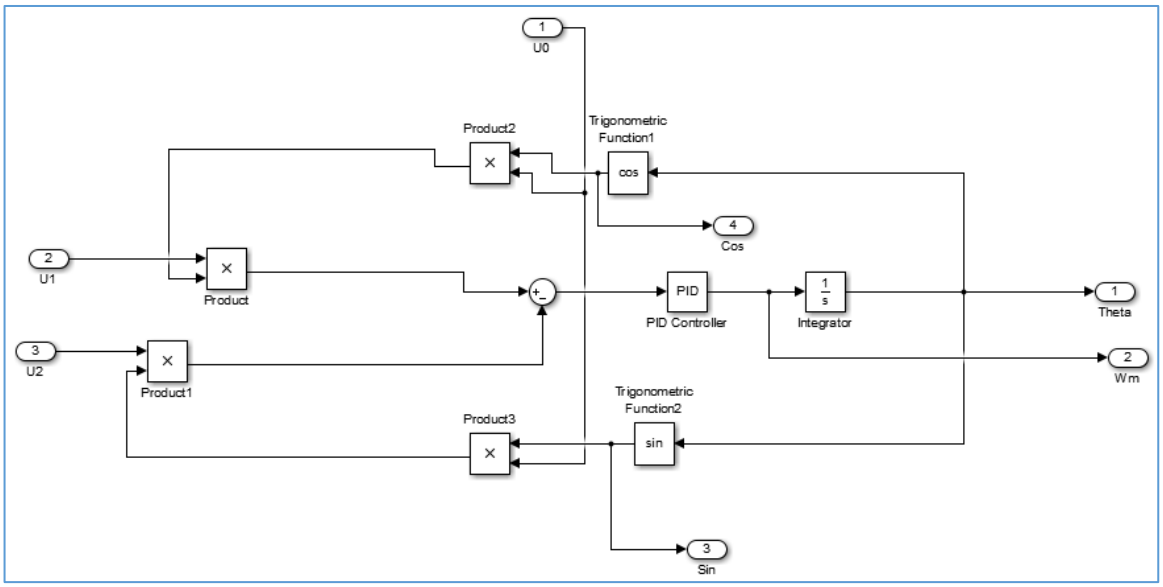

Figure B. Internal diagram of resolver implemented in MATLAB Simulink

LIST OF PUBLICATIONS

List of Journal Papers

1. **Sukanta Halder**, Pramod Agarwal, S.P. Srivastava. “A capacitor voltage Boosting and Balancing using TLBC for three-level NPC inverter fed RDC less PMSM drive”, Journal of Power Electronics, (Accepted for Publication).
2. **Sukanta Halder**, Pramod Agarwal, S.P. Srivastava. “A RDC less software based position estimation using dSPACE DS1104 for ZDAC Control of PMSM Drive” Electric Power Components and Systems (EPCS). (Under review).
3. **Sukanta Halder**, Pramod Agarwal, S.P. Srivastava “A Novel Design and Parametric Analysis of Spoke Type Permanent Magnet Synchronous Motor” Turkish journal of electrical engineering & computer sciences, (Under review).
4. **Sukanta Halder**, Janardhana Kotturu, Pramod Agarwal, S.P. Srivastava, "Three-level NPC inverter fed SPMSM drive with position and speed estimation by Model Reference Adaptive System”, International Journal of Pure and Applied Mathematics (Accepted for Publication).
5. **Sukanta Halder**, Pramod Agarwal, S.P. Srivastava. “A comparative performance analysis of two-level and three-level NPC inverter fed vector controlled PMSM drive”, Journal of Electrical Engineering & Technology, (Under review).

Conference Publications

6. **Sukanta Halder**, S.P. Srivastava, Pramod Agarwal, "Flux weakening control algorithm with MTPA control of PMSM drive," in Power Electronics (IICPE), 2014 IEEE 6th India International Conference on , vol., no., pp.1-5, 8-10 Dec. 2014.
7. **Sukanta Halder**, Pramod Agarwal, S.P. Srivastava, " Comparative analysis of MTPA and ZDAC control in PMSM drive," 2015 Annual IEEE India Conference (INDICON), New Delhi, pp. 1-5., 17-20 Dec. 2015.
8. **Sukanta Halder**, Pramod Agarwal, S.P. Srivastava, "Permanent magnet synchronous motor drive with wheel slip control in traction application," 2015 2nd International IEEE Conference on Recent Advances in Engineering & Computational Sciences (RAECS), Chandigarh, 2015, pp. 1-4.

9. **Sukanta Halder**, Pramod Agarwal, S.P. Srivastava, "MTPA based Sensorless Control of PMSM using position and speed estimation by Back-EMF method," 2016 IEEE 6th International Conference on Power Systems (ICPS), New Delhi, India, 2016, pp. 1-4.

10. **Sukanta Halder**, S.P. Srivastava, Pramod Agarwal, , "Maximum torque per ampere control for interior permanent magnet synchronous motor drive.," in Recent advances in science and technology (NCRAST-2015), 2015 National Conference on, 22-23 Aug. 2015.

11. **Sukanta Halder**, Pramod Agarwal, S.P. Srivastava, " Resolver based Zero d-axis Current control of PMSM.," in Recent advances in science and technology (NCRAST-2016), 2016 National Conference on, 29-30 Aug. 2016.

12. **Sukanta Halder**, Janardhana Kotturu, Pramod Agarwal, S.P. Srivastava, "Three-level NPC inverter fed SPMSM drive with position and speed estimation by Model Reference Adaptive System", Recent Trends in Electrical and Electronics Engineering RTEEE 2017 National Conference on, 14-15 April,2017